US Army Corps of Engineers
Waterways Experiment Station

Final Report
CPAR-GL-98-2
July 1998

CONSTRUCTION PRODUCTIVITY ADVANCEMENT RESEARCH (CPAR) PROGRAM

Estimating Bearing Capacity of Piles Installed with Vibratory Drivers

by

Peter J. Bosscher, Eva Menclova, Jeffrey S. Russell, Ronald E. Wahl

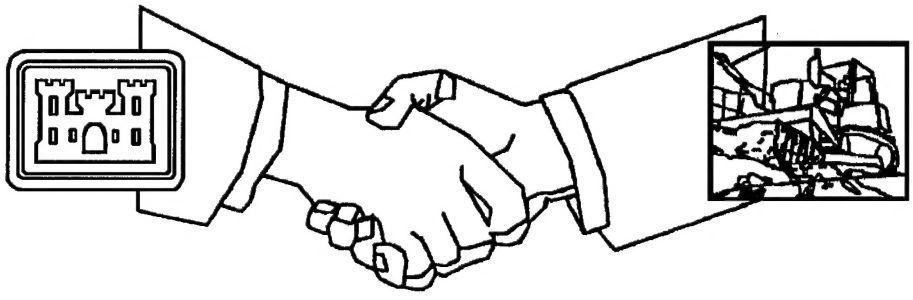

A Corps/Industry Partnership to Advance Construction Productivity and Reduce Costs

The contents of this report are not to be used for advertising, publication, or promotional purposes. Citation of trade names does not constitute an official endorsement or approval of the use of such commercial products.

The findings of this report are not to be construed as an official Department of the Army position, unless so designated by other authorized documents.

Construction Productivity Advancement Research (CPAR) Program

Technical Report
CPAR-GL-98-2
July 1998

Estimating Bearing Capacity of Piles Installed with Vibratory Drivers

by Peter J. Bosscher, Eva Menclova, Jeffrey S. Russell

University of Wisconsin-Madison
Department of Civil and Environmental Engineering
Madison, WI 53714

Ronald E. Wahl

U.S. Army Corps of Engineers
Waterways Experiment Station
3909 Halls Ferry Road
Vicksburg, MS 39180-6199

Final report

Prepared for U.S. Army Corps of Engineers
Washington, DC 20314-1000

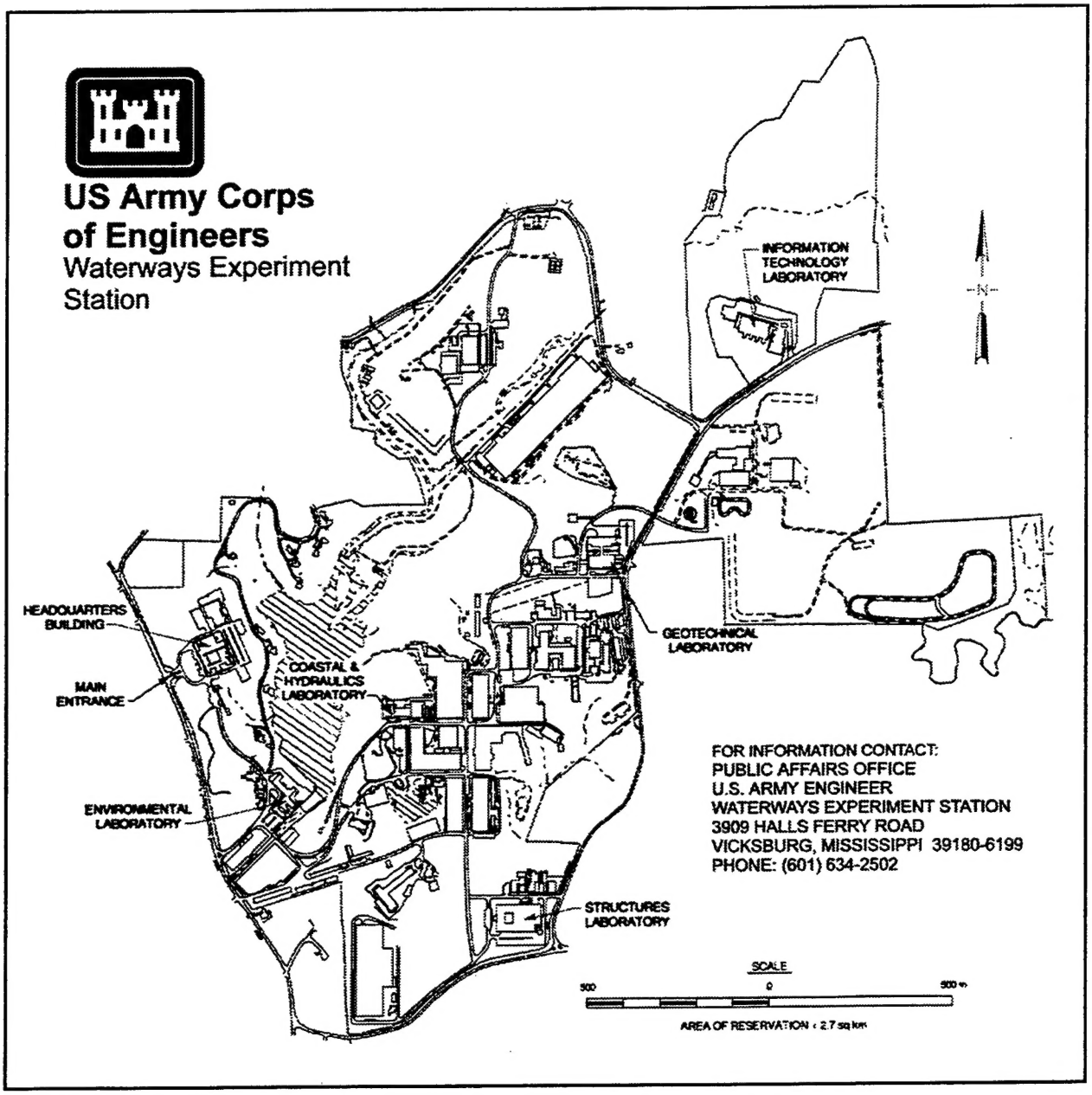

Waterways Experiment Station Cataloging-in-Publication Data

Estimating bearing capacity of piles installed with vibratory drivers / by Peter J. Bosscher ... [et al.] ;
prepared for U.S. Army Corps of Engineers.
171 p. : ill. ; 28 cm. — (Technical report ; CPAR-GL-98-2)
Includes bibliographical references.
1. Piling (Civil engineering) 2. Soils — Vibration. 3. Pile drivers. 4. Soil dynamics. I. Bosscher, Peter J. II. United States. Army. Corps of Engineers. III. U.S. Army Engineer Waterways Experiment Station. IV. Geotechnical Laboratory (U.S. Army Engineer Waterways Experiment Station) V. Construction Productivity Advancement Research Program (U.S.) VI. Series: Technical report (U.S. Army Engineer Waterways Experiment Station) ; CPAR-GL-98-2.
TA7 W34 no.CPAR-GL-98-2

Contents

List of Figures

List of Tables

Preface

The study reported herein was conducted as a part of the Construction Productivity Advancement Research (CPAR) Program. This report is the final report for a project entitled "Predicting the Bearing Capacity of Piles Installed with Vibratory Drivers." The study was conducted by the Geotechnical Laboratory (GL), U.S. Army Engineer Waterways Experiment Station (WES), Vicksburg, MS, for Headquarters, U.S. Army Corps of Engineers (HQUSACE), in conjunction with the industry partner, the University of Wisconsin (UW), Madison, WI. The HQUSACE Technical Monitors were Messrs. J. Chang, C. Harris, and D. Chen.

The study was performed under the general supervision of Dr. W. F. Marcuson III, Director, GL, and Dr. D. C. Banks, former Chief, Soil and Rock Mechanics Division (SRMD), GL. Mr. William F. McCleese was the manager of the CPAR Program at WES. The report was performed under the direct supervision of Mr. R. D. Bennett, Chief, Soil Research Center (SRC), SRMD. The report was written and prepared by Dr. Peter J. Bosscher, Dr. Jeffrey S. Russell, and Ms. Eva Menclova, UW, and Mr. Ronald E. Wahl, SRC. The following contributors provided time, interest, money, and technical support: Mr. John Jennings, Hercules Machinery Corporation; Mr. Don Warrington, Vulcan Pile Driving Corporation, Steding Pile Driving, McMahon and Associates, Handpipe Structural Steel Pipes, Rick Nebel II, Engineering and International Equipment Corporation; and Mr. John W. Rogers, Ray's Crane Service, and Edward Kraemer and Sons.

During the publication of this report, Dr. Robert W. Whalin was Director of WES, and COL Robin R. Cababa, EN, was Commander.

Executive Summary

A new method for estimating the bearing capacity of structural piles installed with vibratory drivers is proposed in this research report. The method is based on measurements of dynamic properties of the soil-pile system during driving. The method is verified by evaluating field data collected during the driving of 24 experimental piles at the National Geotechnical Experimental Site near College Station, Texas.

Vibratory drivers are commonly used to install sheet-pile walls, nonbearing piles, and some load-bearing piling, though restrikes with impact hammers often are employed to increase pile capacity. In comparison to traditional impact hammers, vibratory drivers have several advantages: (a) require less energy, (b) have higher rates of penetration in cohesionless soils, (c) produce less noise, and (d) result in less structural damage to the pile during driving (Gardner 1987, O'Neill and Vipulanandan 1989). Presently there are no reliable methods for estimating the bearing capacity of the piling during the driving operation. The most common method for estimating the capacity of a vibratory driven pile is by restriking it with an impact hammer. For impact hammers, the relationship between number of blows per meter (foot) and the static bearing capacity is well established. However, the need to restrike the vibratory driven pile limits the economic viability of the driving operation. The goal of this project is to establish a sound method for estimating the bearing capacity of vibratory driven structural piles during the driving operation. Because sheet piling is usually not designed to carry structural bearing loads, it was not investigated.

In a previous study by Moulai-Khatir, O'Neill, and Vipulanandan (1994), the computer program, Vibratory Pile Driving Analyzer (VPDA), was developed. VPDA correlates the rate of penetration of the pile to its bearing capacity. Parameters input into the computer program include the dynamic properties of the vibrator and indices characterizing the soil-pile interaction. The computer program was calibrated with results from laboratory tests.

To verify the performance of VPDA and to gain more information about the characteristics of the soil-pile system, field data have been collected from 24 instrumented experimental piles. The experimental piles range in size from 152.4-mm (6-in.) to 254-mm (10-in.) diameters, lengths of 6.1 m (20 ft) and 9.14 m (30 ft). Both H and pipe pile were tested for all dimensions. Accelerations, stresses, and rates of penetration for the piles were recorded during

driving using an electronic data acquisition system. Static load tests were performed about 5 months after driving to measure the ultimate static bearing capacity.

The records collected during vibratory driving were analyzed to obtain profiles of frequency and amplitude of driving as well as static and dynamic stresses. Power and energy delivered to the top of the pile were calculated from measurements made during driving. Trends between measured parameters and the ultimate bearing capacity determined by load tests were investigated and the significant parameters were identified as:

a. Perimeter of pile.

b. Cross section of pile.

c. Frequency of driving.

d. Power delivered to top of pile.

e. Amplitude of vibration measured as peak acceleration.

For the experimental piles driven, the results from VPDA based on published soil-structure interaction parameters did not correlate well with results from the field. This is likely due to the loss of soil-structure stress transfer during the vibratory driving.

This research provided two end products which could be commercialized.

The first product is a computer hardware-software combination (WiscVPDA) designed to employ a regression model developed from field testing results. Similar to the Pile Driver Analyzer, this hardware records and analyzes dynamic input information and predicts the ultimate bearing capacity of individual piles driven by vibratory drivers in given soil conditions. The instrumentation needed consists of only measurements of frequency and amplitude of vibration at the driver and acceleration and strain at the top of the pile. The WiscVPDA may be useful as a tool for determining and optimizing construction of deep foundations.

The second product, an offshoot of the first product, is a suggested tool to be employed by the vibratory driving industry to investigate a site for the potential of successful use of vibratory driving. Initially, the tool would be used only to determine site suitability. Eventually, as a data set was gathered and correlated to measured pile capacities, the tool may be used to estimate the bearing capacity of vibratory driven piles on any site. Thus, vibratory hammers could be used for driving bearing piles for foundations and used on sites with a great deal of confidence in the predicted capacities.

Neither of these products were fully developed and tested. Each would require additional industry input and support to implement successfully. Similar efforts are already underway in Europe.

1 Project Objective

The objective of this project was to develop the capability for predicting the ultimate bearing capacity of structural piling from the response of the piling during installation with vibratory driving systems. A capability already exists for impact driven piling where the capacity can be assessed from data gathered about the pile-soil dynamics during the driving operation. The commercial product to do this is called a Pile Driving Analyzer (PDA) which consists of a hardware-software package. A similar device for vibratory driven piles would meet needs in the pile-driving industry. Other testing devices may also be considered.

2 Research Plan

The objective was accomplished through four tasks:

Task 1: Information was collected on vibratory driving and load testing. Requirements for any additional data needed to accomplish the objective were determined as described in the paragraph entitled "Literature and Data Review."

Task 2: The field testing program for vibratory driven piles, including static load testing, was designed and implemented. In situ soil tests such as standard penetration, cone penetration, and laboratory tests on disturbed and undisturbed boring samples were obtained to properly characterize the soil as described in the paragraph entitled "Materials and Methods."

Task 3: Data were compiled and analyzed. This task included comparisons between predictive tools and actual performance. Correlations were also obtained to predict bearing capacity during pile driving as described in the paragraph entitled "Results and Discussions."

Task 4: Products were prepared for commercialization. This is described in Chapter 5.

These tasks are individually described and reported in the following paragraphs.

Literature and Data Review

In Appendix A, the principles of vibratory driving are explained and examples of applications of vibratory driving in construction are examined. The latter portion of Appendix A is devoted to methods of evaluating bearing capacity and computer models developed for this purpose. The computer model Vibratory Pile Driving Analyzer (VPDA), which was used for analyzing the data collected in this study, is described in detail. A brief summary of methods for evaluating the load testing of piles and methods of calculating static bearing capacity are also presented in Appendix A.

Materials and Methods

This subject is divided into three parts: (a) prediction of static-bearing capacity prior to pile driving, (b) field testing of vibratory driven piles, and (c) analysis of data collected during field testing. Bearing capacity was estimated using both empirical equations and the VPDA software. The text regarding field testing includes descriptions of soil conditions, pile instrumentation, pile driving procedures, and the data acquisition system used during field experiments. Finally, there is an outline of methods used for analyzing data records collected during vibratory driving and load testing.

Predictions of static-bearing capacity and VPDA

Prior to the experimental portion of this project, predictions of bearing capacity of the piles were made using common static-bearing capacity formulas. Also, a series of computations were made using VPDA to estimate the bearing capacity as a function of the rate of penetration.

Static-bearing capacity. The static-bearing capacity of the piles was calculated using three methods developed by Meyerhof (1976), Vesic (1977), and Briaud et al. (1985). The Meyerhof and Vesic methods are described by Das (1990), and the Briaud et al. method is described by Coduto (1994). These formulas were developed from correlation of Standard Penetration Test blow counts of the soil (N_{SPT}) and dimensional properties of the pile with bearing capacity.

The ultimate bearing capacity of a pile, Q, is:

$$Q = Q_t + Q_s \tag{1}$$

where

Q_t = load carried by the tip of the pile

Q_s = resistance due to friction on the side of the pile

Meyerhof Method. For piles in sand, the load carried by the tip of the pile in units of kN can be estimated based on N_{SPT} near the pile tip from (Das 1990):

$$Q_t = 40 \frac{L}{D} N_{SPT} A_t \tag{2}$$

where

L = length of the pile in meters

D = diameter of the pile in meters

A_t = area of the tip including the soil plug in square meters

For undrained conditions in saturated clays, the load carried by the pile tip in units of kN can be estimated from (Das 1990):

$$Q_t = 9c_u A_t \tag{3}$$

where

c_u = unconfined compressive strength in kN/m^2

A_t = as defined in Equation 2

As shown in Table 1, the unconfined compressive strength can be estimated using N_{SPT} for clay.

Table 1
Unconfined Compressive Strength and Approximate Correlation to Standard Penetration Test Blow Counts (after Das 1990)

Standard Penetration N-Value N_{SPT}	Unconfined Compressive Strength, c_u kN/m^2
0-2	0-25
2-5	25-50
5-10	50-100
10-20	100-200
20-30	200-400
>30	>400

The frictional resistance along the side of the pile can be calculated from (Das 1990):

$$Q_s = f_s P_p L \tag{4}$$

where

f_s = unit side friction

P_p = perimeter of the pile (including the soil plug for H-piles)

L = embedded length of the pile inserted in consistent units

In sand, the unit side friction in units of kN/m^2 can be estimated as (Das 1990):

$$f_s = 2N_{SPT} \tag{5}$$

In clay, the unit side friction in units of kN/m^2 can be estimated as:

$$f_s = 38.3\sqrt{c_u \gamma h} \tag{6}$$

where

γ = unit weight in kN/m^3

h = depth of the clay layer in meters

Vesic Method. The pile capacity at the tip can be calculated as:

$$Q_t = A_t (cN_c^* + \sigma_0' N_s^*) \tag{7}$$

where

c = cohesion of the soil

σ_o' = mean normal effective horizontal soil pressure at the tip of the pile

N_c^* and N_s^* = bearing-capacity factors for the piles (Das 1990)

The mean normal effective horizontal soil pressure is calculated as:

$$\sigma_o = \left(\frac{1 + 2K_o}{3} \right) q \tag{8}$$

where

K_o = coefficient of earth pressure at rest

q = effective vertical soil pressure

The coefficient K_o can be estimated for sand as:

$$K_o = 1 - \sin\phi \tag{9}$$

where

ϕ, shown in Table 2, = angle of internal friction estimated using N_{SPT}

Table 2
Relation between N_{SPT} and ϕ (after Das 1990)

Standard Penetration N-Value N_{SPT}	Angle of Friction ϕ (deg)
0 - 5	26 - 30
5 - 10	28 - 35
10 - 30	35 - 42
30 - 50	38 - 46

Method after Briaud et al. (Coduto 1994). The end-bearing capacity Q_t (kN) can be calculated as:

$$Q_t = 1.97 \times 10_3 (N_{SPT})^{0.36} A_t \tag{10}$$

where N_{SPT} and A_t are as defined above. The unit side friction in units of kN/m^2 can be estimated as:

$$f_s = 22.4 (N_{SPT})^{0.29} \tag{11}$$

where N_{SPT} is as defined above.

Vibratory Pile Driver Analyzer (VPDA). The computer program VPDA was used for predicting the bearing capacity as a function of the rate of penetration. VPDA requires that all input parameters are input in English units. Thus, both SI and English unit systems are used in the following text. A vibratory driver manufactured by International Construction Equipment, ICE 416L, was used to drive the piles in the field. Data input into the program to characterize the driver including eccentric moment, frequency of driving, total weight of vibrator, weight of bias mass, vibrating mass, and efficiency of vibrator were obtained from manufacturer's literature or estimated based on recommendations made in the VPDA Manual (Moulai-Khatir, O'Neill, and Vipulanandan 1994). Parameters characterizing the stiffness and damping of the connection between the vibrator and pile were specified according to the VPDA Manual and are listed in Table 3.

Parameters characterizing the pile including pile size, cross section of steel area of the pile, cross section of pile including soil plug, weight per unit length of pile, external perimeter, radius of pile, and pile damping were input into VPDA. For pipe piles, the pile radius, r, was half of the diameter of the pile. For H-piles, the pile radius was calculated as:

$$r = \sqrt{\frac{h*w}{\pi}} \tag{12}$$

Table 3
VPDA Input Parameters for Model ICE 416L Vibratory Driver and Clamp

Specification of Vibratory Driver and Clamp	SI Units	English Units
Eccentric moment	2,304 kg-cm	2,000 lb-in.
Frequency	1,600 vpm 26.7 Hz	1,600 vpm 26.7 Hz
Amplitude	6 to 19 mm	1/4 to 3/4 in.
Total weight of vibrator with clamp	4,490 kg	9,900 lb
Weight of bias mass	1,483 kg	3,270 lb
Vibrating weight	2,871 kg	6,330 lb
Vibrator efficiency	20 %	20 %
Stiffness of connection between clamp and pile	27×10^6 kg/m	15×10^5 lb/in.
Viscous damping of connection	744 kg-sec/m	500 lb-sec/ft
Hysteric damping of connection	1%	1%

where

h = height of web

w = width of flange according to the VPDA Manual

The remaining parameters characterizing the piles were determined from the characteristics of experimental piles used during field testing (Table 4).

The unit weight of soil was estimated using the results of laboratory testing on soil samples collected at the site. Soil conditions at the site are discussed in the following text. The type of side shear distribution and inclusion of side shear on the first element were input as well (Table 4).

Either the Smith or the hyperbolic models can be chosen to represent the soil resistance in the VPDA program (Table 5). The Smith and hyperbolic models are discussed in Appendix A. Calculation using the Smith model of soil resistance required the specification of quake and damping at the tip and side of a pile. The parameters for the hyperbolic soil model require a stiffness and exponent for the side and tip of a pile in both loading and unloading modes of the sinusoidal wave.

The specification of parameters controlling temporal discretization and driving time is also required. Values recommended in the VPDA Manual were used for these parameters. The computational time increment was 0.01 msec and driving time was 1,000 msec.

Input files for VPDA were generated using an MS Excel® macro. The macro was designed such that variable inputs were selected from tables in the spreadsheet and the macro combined all of the input data into the data file.

Table 4
VPDA Input Parameters for Specifications of Piles and Soil

Input Parameter		SI Units	English
Pile size	for H-pile (depth)	152 mm 203 mm 254 mm	6 in. 8 in. 10 in.
	for Pipe (O.D.)	168 mm 219 mm 273 mm	6.63 in. 8.63 in. 10.75 in.
Cross section (excluding plug)	for H-pile	4,770 mm^2 6,840 mm^2 8,000 mm^2	7.4 $in.^2$ 10.6 $in.^2$ 12.4 $in.^2$
	for Pipe	3,610 mm^2 5,420 mm^2 7,680 mm^2	5.6 $in.^2$ 8.4 $in.^2$ 11.9 $in.^2$
Weight per unit length of pile	for H-pile	0.363 kN/m 0.520 kN/m 0.608 kN/m	25 lb/ft 36 lb/ft 42 lb/ft
	for Pipe	0.275 kN/m 0.422 kN/m 0.579 kN/m	19 lb/ft 29 lb/ft 40 lb/ft
Pile radius	for H-pile	90 mm 117 mm 145 mm	3.5 in. 4.6 in. 5.7 in.
	for Pipe	84 mm 109 mm 137 mm	3.3 in. 4.3 in. 5.4 in.
Cross Section (including plug)	for H-pile	25,000 mm^2 42,200 mm^2 65,900 mm^2	38.7 $in.^2$ 65.4 $in.^2$ 102.2 $in.^2$
	for Pipe	22,300 mm^2 37,700 mm^2 58,600 mm^2	34.5 $in.^2$ 58.4 $in.^2$ 90.8 $in.^2$
External perimeter	for H-pile	632 mm 823 mm 1,030 mm	24.9 in. 32.4 in. 40.4 in.
	for Pipe	528 mm 688 mm 858 mm	20.8 in. 27.1 in. 33.8 in.
Unit weight of soil		18.9 kN/m^3	120 pcf
Side shear distribution		Triangular Rectangular	Triangular Rectangular
Side shear on first pile element		Yes No	Yes No
Pile damping		0 kg-sec/m	0 lb-sec/in.
Shear wave velocity		210 m/sec	690 ft/sec
Young's Modulus		200 GPa	2.90×10^7 psi

Table 5
VPDA Input Parameters for Soil Models (Moulai-Khatir, O'Neill, and Vipulanandan 1994)

Input Parameter		SI Units	English Units
Smith Model of Soil Resistance			
Tip quake	for H-pile	2.8 mm	0.11 in.
	for Pipe	3.0 mm	0.12 in.
Tip damping	for H-pile	1.35 sec/m	0.41 sec/ft
	for Pipe	1.48 sec/m	0.45 sec/ft
Side quake		2.5 mm	0.1 in.
Side damping		6.4 mm	0.25 in.
Hyperbolic Soil Model: Loading			
Side stiffness	for H-pile	167 kN/m^3	6.57 lb/in.^{3}
	for Pipe	164 kN/m^3	6.45 lb/in.^{3}
Tip stiffness	for H-pile	195 × 10^3 kN/m^3	7,670 lb/in.^{3}
	for Pipe	188 × 10^3 kN/m^3	7,390 lb/in.^{3}
Side exponent	for H-pile	2.46	2.46
	for Pipe	2.53	2.53
Tip exponent	for H-pile	2.32	2.32
	for Pipe	2.31	2.31
Hyperbolic Soil Model: Unloading			
Side stiffness	for H-pile	170 kN/m^3	6.70 lb/in.^{3}
	for Pipe	165 kN/m^3	6.50 lb/in.^{3}
Tip stiffness	for H-pile	198 × 10^3 kN/m^3	7,780 lb/in.^{3}
	for Pipe	203 × 10^3 kN/m^3	7,990 lb/in.^{3}
Side exponent	for H-pile	2.41	2.41
	for Pipe	2.34	2.34
Tip exponent	for H-pile	2.35	2.35
	for Pipe	2.30	2.30

Field testing of vibratory driven piles

Soil conditions. The field portion of the project was conducted at the National Geotechnical Experimental Site, located at the Riverside Campus of Texas A&M University near College Station, Texas. The field testing was performed at the sandy portion of the experimental site, where the soil consists of sediments deposited in horizontal layers having grain sizes ranging from sand to clay.

To characterize the soil profile at the experiment site, three boreholes were drilled with a hollow-stem auger. Soil samples were collected from the boreholes with a standard split spoon sampler, and standard penetration blowcounts were recorded. A representative profile was constructed from the exploration data as shown in Figure 1. The top layer of the soil profile consists of very stiff red sandy clay about 2.1 m thick. Underneath, there is a firm reddish-brown sand down to a depth of 6.7 m. The groundwater level is within the

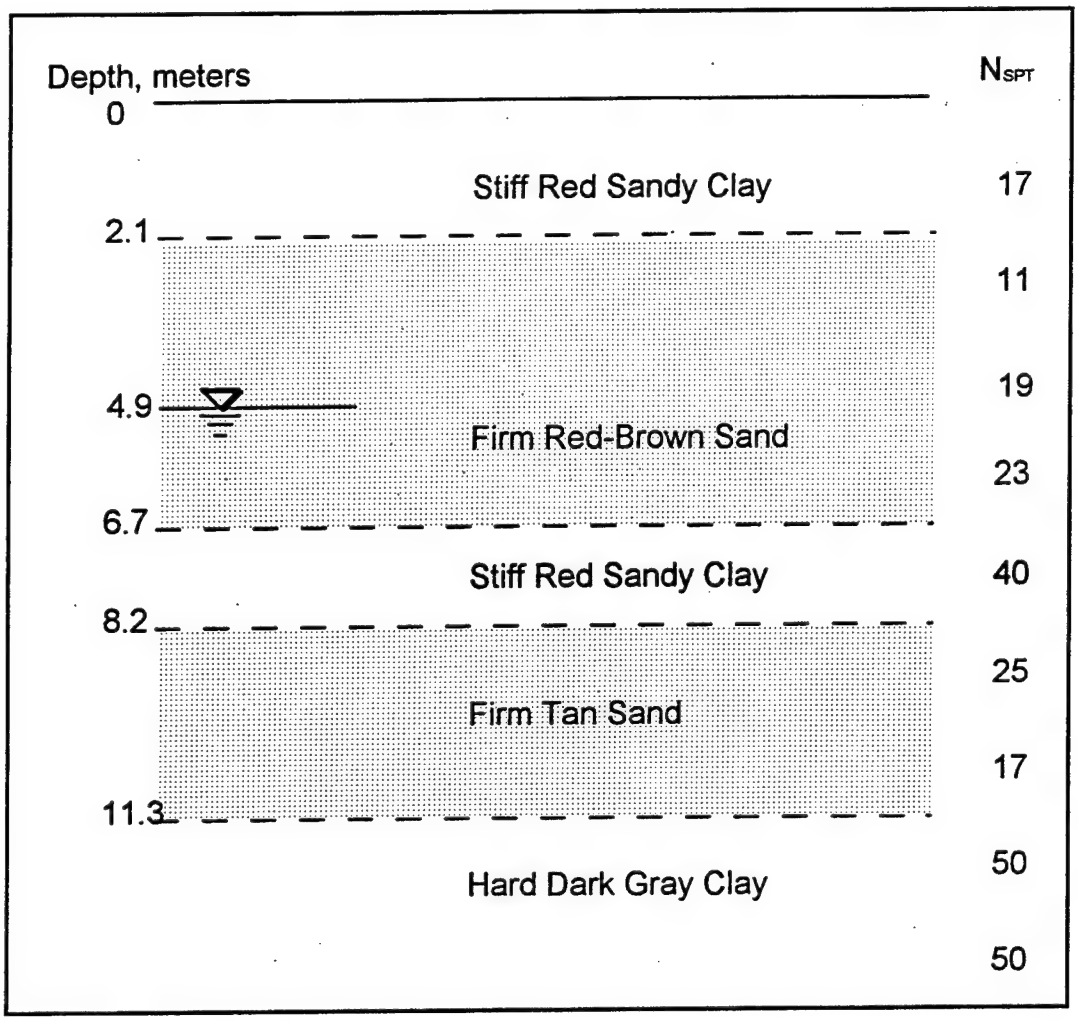

Figure 1. Representative soil profile at National Geotechnical Testing Site near College Station, Texas

second layer at depth of about 4.9 m. Underlying the reddish-brown sand is a 1.5-m-thick layer of clay mixed with red sand from 6.7 to 8.2 m. This layer is underlain by a 3.1-m-thick layer of firm tan sand (depth of 8.2 to 11.3 m). All three boreholes reached a depth of about 11.3 m before encountering a layer of hard gray clay. The boreholes were terminated at a depth of about 12.2 m.

Soil samples were taken at 1.5-m intervals and were tested for the grain size distribution and Atterberg limits. Representative grain size distribution curve for the layer of firm red-brown sand is presented in Figure 2. The curves were developed following procedures outlined in American Society for Testing and Materials (ASTM) D-2217-85 (ASTM 1993c). The sand has a coefficient of uniformity C_u of about 1.5 and coefficient of curvature C_c of about 1.0. According to the Unified Soil Classification System (USCS), the material is classified as poorly graded sand (SP).

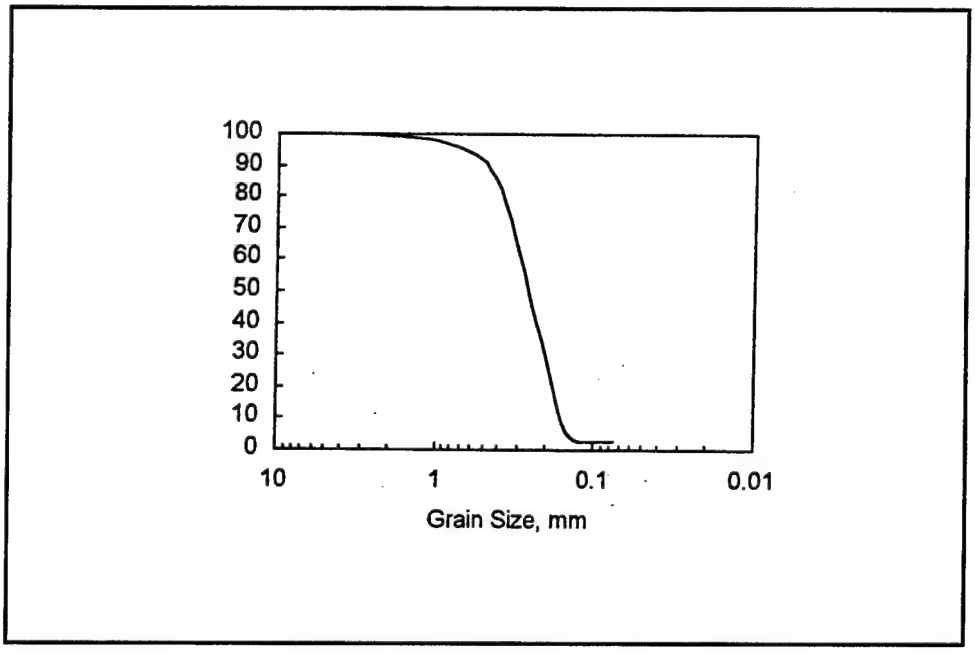

Figure 2. Grain size distribution curve for firm red sand

Atterberg limits of soil from the clay layer sampled at a depth of 7.5 m were measured according to ASTM D-4318-84 (Table 6). Under the USCS, red sandy clay is classified as inorganic clay having high plasticity (CH). The natural water content of the sample was tested in the laboratory following procedures outlined in ASTM D-2216-90 (ASTM 1993d) on the soil samples transported from field to the laboratory in sealed glass jars. The natural water content was 28 percent, only 1 percent higher than the plastic limit. At this water content, the clay has a hard consistency, which corresponds to observations made in the field during pile driving that the driving conditions were more difficult through this layer of soil. In some instances, piles could not be driven through this layer. In a single case, driving was terminated and the pile was lifted out of the soil. The soil attached to the pile was observed to be the hard clayey soil.

Table 6
Results of Laboratory Tests for Atterberg Limits

Soil Property	Moisture Content
Plastic limit	27 percent
Liquid limit	80 percent
Plasticity index	53 percent
Natural water content	28 percent

Calibration of instruments. Electronic instruments were used for instrumentation of piles during field testing. Prior to driving, calibrations of the instruments were made to determine the relation between input and output from

the devices. The readings from the devices were compared to standard known calibrations.

Calibration of hydraulic cylinder. The RC 5013 EnerPac™ hydraulic cylinder was calibrated using a Southwark hydraulic press in the testing laboratory of University of Wisconsin-Madison. Loads up to 900 kN were applied and measured with accuracy of 0.5 kN. The relationship between the readings of a dial gauge on the hydraulic cylinder and the hydraulic press are linear as shown in Figure 3 and can be expressed as:

$$P = 0.049X_{hc} \tag{13}$$

where

P = load in kN

X_{hc} = reading from the dial gauge of the hydraulic cylinder (psi)

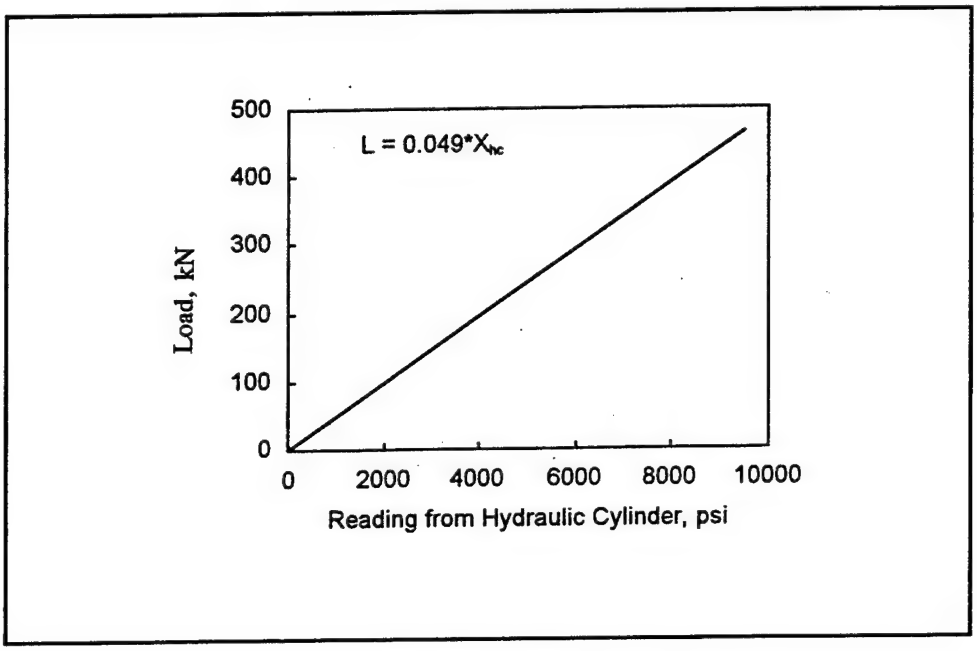

Figure 3. Calibration curve of RC 5013 Hydraulic Cylinder

Calibration of Strain Gauges. Strain gauges used in the field instrumentation were Omega™ precision resistive strain gauges with a single element. The strain gauges mounted on each of the 24 experimental piles required calibration before the piles were driven into the ground. The piles with strain gauges were loaded and the changes in the resistance of the strain gauges were determined.

The calibration setup was designed to meet a criterion for easy hand assembly without the use of a crane and for testing of piles of all types, length, and

diameters included in the testing program. During calibration, an experimental pile was loaded at one end by a hydraulic cylinder and held between end plates connected by four rods to prevent movement. A schematic of the assembly is shown in Figure 4. The rods were Dywidag™ rods having a length of 4.5 m connected with couplers and attached to the end plates by anchor plates and nuts. The load was applied for about 2 min, while the readings from the strain gauges were taken and recorded using an automatic data acquisition system.

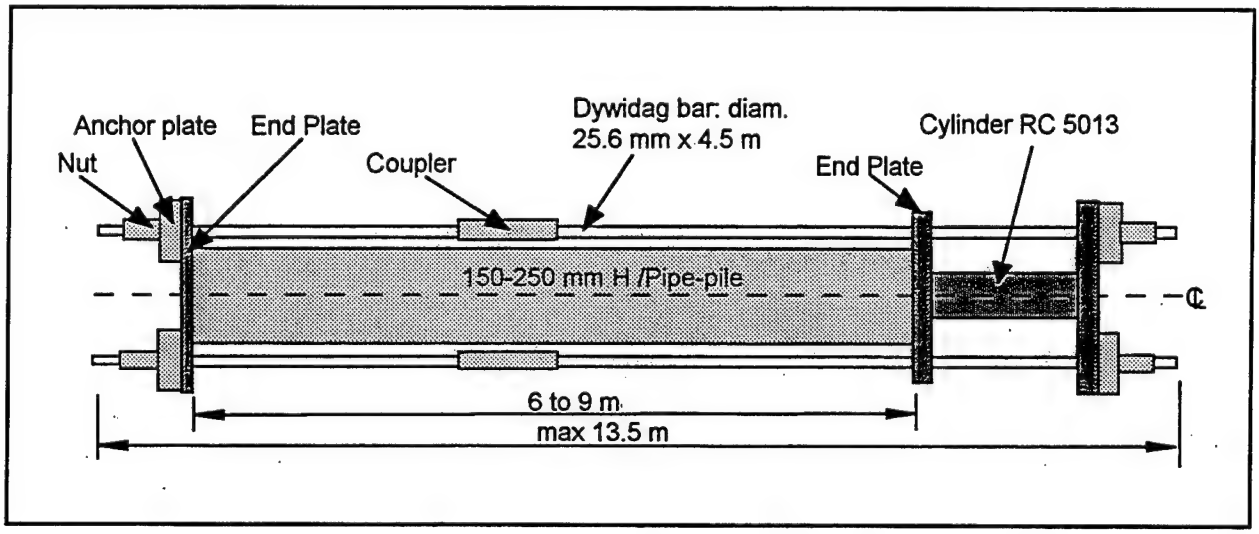

Figure 4. Calibration equipment schematic

The resistance of the single-element gauge depends on placement of the gauge in relation to the direction of applied load and the quality of bond of the gauge to the pile surface. These factors vary with each pile, thus unique calibration relations had to be determined for the top and bottom strain gauges. Loads up to 450 kN were applied during calibration in increments of about 45 kN. Several cycles of loading and unloading were repeated during calibration of each pile to exercise the strain gauges. The RC 5013 Enerpac™ hydraulic cylinder was used for applying the load and the magnitude of the load was read from a pressure gauge on the pump.

The readings from the strain gauges during calibration were analyzed to obtain a relation between the load applied to the pile and the change in resistance of the strain gauge. Two readings were taken for every load applied. The relation between the load and resistance was linear in the range of loads applied. The increases of strain for the increase in load of 45 kN were calculated and averaged to obtain a slope s or calibration factor in terms of kN per mV/V for each strain gauge (Figure 5). The uncertainty in calibration factor of each strain gauge was calculated as:

$$U_s = \frac{1}{s} t_{0.025,n} \frac{S_s}{\sqrt{n}} \tag{14}$$

where

$t_{0.025,n}$ = t-statistic for 95 percent confidence interval of n measurements

S_s = standard deviation of data set with a mean of s

n = number of measurements (Beckwith, Marangoni, and Lienhard 1993).

Table 7 presents the calibration data and uncertainties for all piles.

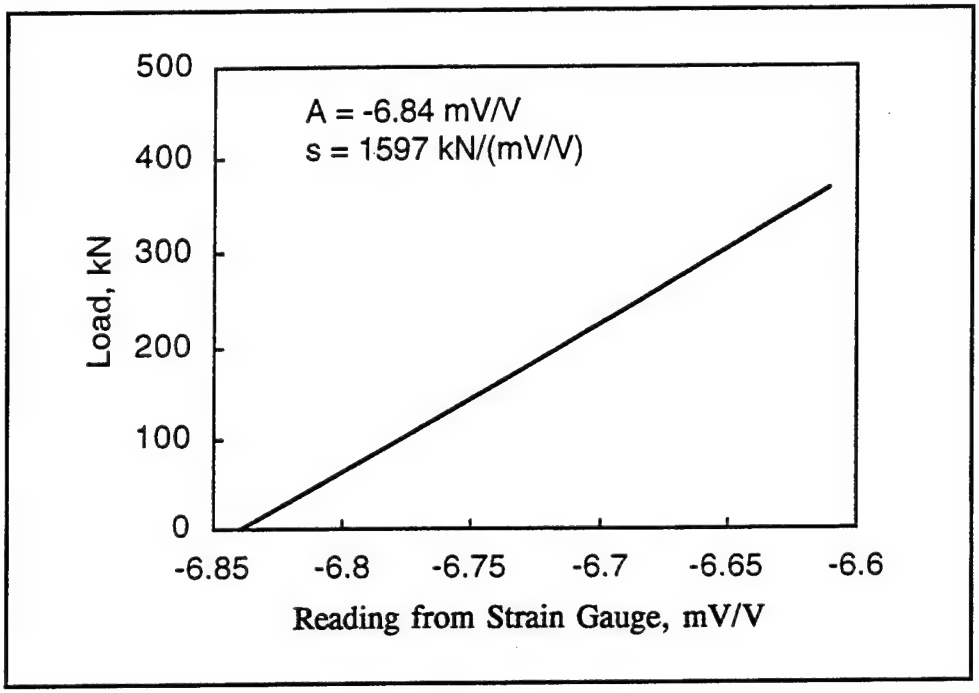

Figure 5. Example of calibration curve for strain gauge at top of pile 10-30-H-A

Calibration of accelerometers. The Analog Devices™ ADXL 50AH accelerometer was calibrated by comparison to a PCB™ 302A SV5570 ICP accelerometer used for reference in the laboratory. Both accelerometers were subjected to the same sinusoidal vibration motion and their voltage outputs were collected and analyzed using Data 6000 Analogic™ digital oscilloscope.

A fast Fourier transform (FFT) analysis was performed on signals from the calibrated and reference accelerometers. Peaks in amplitudes of their signals were recorded over a range of frequency from 15 to 90 Hz. The reference PCB™ 302A SV5570 ICP accelerometer had voltage sensitivity of 9.94 mV/g (PCB™ piezotronic Calibration Certificate Project No. 822/255630).

To obtain voltage sensitivity for the calibrated accelerometer, the voltage outputs were measured for both reference and calibrated accelerometers. The voltage output from the reference accelerometer was transferred to acceleration

Table 7
Calibration Relations of Strain Gauges

Pile	Top Strain Gauge			Bottom Strain Gauge		
	Slope			Slope		
	kN/ (mV/V)	Uncert. percent	Intercept mV/V	kN/ (mV/V)	Uncert. percent	Intercept mV/V
10-30-H-A	1,597	4.0	-6.84	2,275	26.8	-9.30
10-30-H-B	1,600	2.4	-6.95	1,632	7.4	-9.07
10-20-H-A	1,647	2.0	-5.95	2,424	7.0	-7.50
10-20-H-B	1,714	2.1	-6.07	598	9.5	-7.84
8 -30-H-A	1,293	27.7	-6.72	926	39.0	-8.63
8 -30-H-B	-	-	-6.15	979	15.0	-8.39
8-20-H-A	1,641	3.4	-5.55	2,424	5.3	-6.13
8-20-H-B	1,444	3.6	-5.39	956	5.7	-6.76
6-30-H-A	1,865[1]	5.4	3.83[1]	1,276	11.8	-9.30
6-30-H-B	950	2.5	-6.79	846	8.8	-8.95
6-20-H-A	1,148	2.1	-5.69	1,234	5.7	-7.14
6-20-H-B	1,014	2.5	-5.48	1,219	5.0	-7.09
10-30-P-A	1,417	36.5	-6.15	1,526	11.6	-8.19
10-30-P-B	3,047	13.3	-6.05	2,737	23.0	-8.47
10-20-P-A	1,360	9.7	-5.49	2,197	10.0	-6.84
10-20-P-B	1,340	2.6	-5.14	1,786	3.5	-6.32
8-30-P-A	1,230	16.8	-6.36	951	7.4	-8.63
8-30-P-B	1,375	10.2	-6.53	1,073	12.9	-8.06
8-20-P-A	997	5.0	-4.93	1,067	4.4	-6.54
8-20-P-B	1,017	5.4	-5.70	1,412	6.2	-7.02
6-30-P-A	569	11.7	-6.09	629	10.3	-8.91
6-30-P-B	711	4.1	-7.24	828	4.7	-9.04
6-20-P-A	888	2.5	-5.59	759	2.9	-6.52
6-20-P-B	626	11.6	-4.55	608	2.5	-6.37

[1] The strain gauges were connected in a quarter bridge arrangement with only one active gauge.

through the known voltage sensitivity of the reference accelerometer. The measured voltage output of the calibrated accelerometer was compared to the acceleration determined from the reference accelerometer and expressed in terms of voltage sensitivity, as shown in Figure 6.

The calibration determined that the voltage sensitivity of the Analog Devices™ ADXL 50AH accelerometer was 19.95 mV/g over the range of frequencies from 15 to 30 Hz.

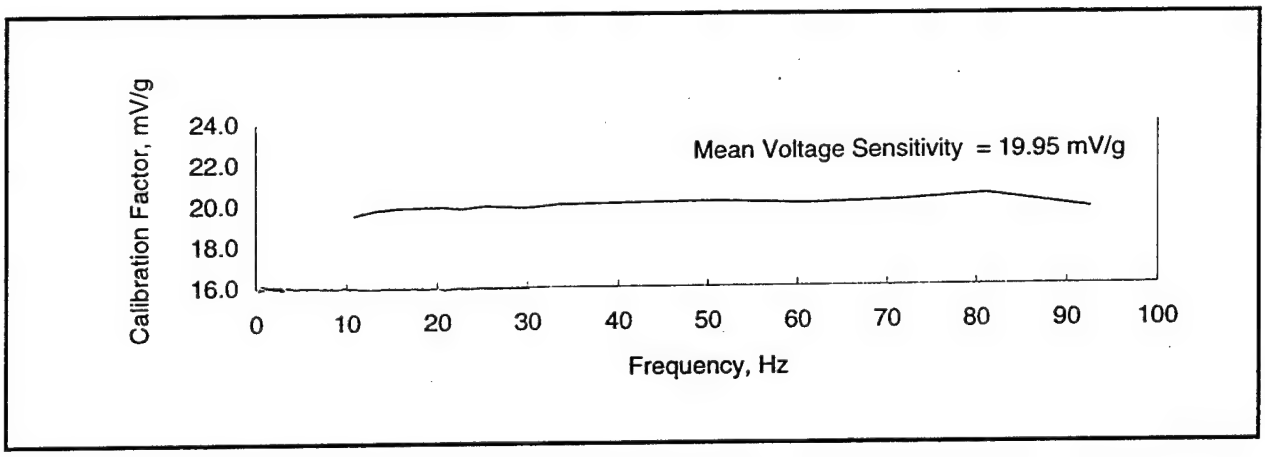

Figure 6. Calibration curve for Analog Devices™ ADXL 50AH Accelerometer

Calibration of load cell. The load cell was also calibrated using the Southwark hydraulic press in the testing laboratory at the University of Wisconsin-Madison. Loads up to 1,420 kN were applied to the load cell and measured with an accuracy of 0.5 kN. The calibration relationship was linear, shown in Figure 7, and can be expressed as:

$$P = 444.54\,(X_{lc} - B_{lc}) \tag{15}$$

where

P = load in kN

X_{lc} = reading from the load cell in mV

B_{lc} = reading from the load cell when a load of zero is applied

Calibration of displacement transducers. Displacement transducers were used to measure movement of the pile during load testing. Two displacement transducers, which were custom made by SpaceAge Control, Inc., were calibrated against a measuring tape in the laboratory. Readings in increments of 10 mm were taken and averaged. The calibration relationship was:

$$D = \frac{X_{dl}}{8.03} - B_{dl} \tag{16}$$

where

D = displacement in millimeters

X_{dl} = reading from the displacement transducer in mV when supplied with a 5-V excitation

B_{dl} = reading of the transducer when the displacement equals zero

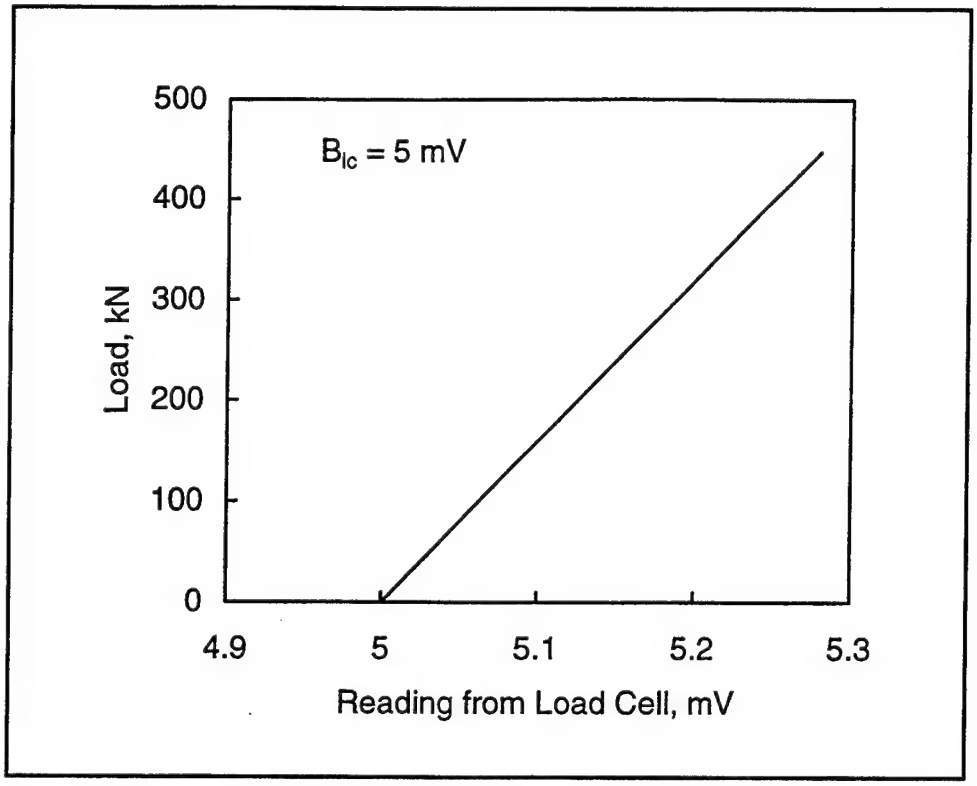

Figure 7. Example of calibration curve for load cell

This relationship is graphically shown in Figure 8. The uncertainty was found to be 1 percent using the method of evaluation of uncertainty described in the text describing the calibration of the strain gauges.

Description of piles. Characterization of piles. The design of the field experiment consisted of a full factorial design with two replicates of two factors in two levels and one factor in three levels. Based on the soil profile, the pile length and dimensions were selected such that the behavior of the piles driven with the vibratory driver into sandy soil could be monitored. The sandy portions of the strata reached down to a depth of about 11 m. The length of the experimental piles was limited to 9 m to avoid penetrating into the underlying hard gray clay layer. To identify the influence of pile length on the behavior of vibratory driven piles, shorter piles of 6 m were also included in the testing program. Additionally, pile diameter and pile cross-sectional type were varied to determine these influences.

Forty-one driven piles were divided into two groups: 24 test piles and 17 anchor piles. The experimental piles were instrumented with accelerometers and strain gauges. The anchor piles were not instrumented and served as reaction piles during load testing.

Twelve different combinations of pile type, length, and diameter for the experimental piles were tested. There were two replicate piles for each combination distinguished by the symbols A or B. Replicates were tested to provide

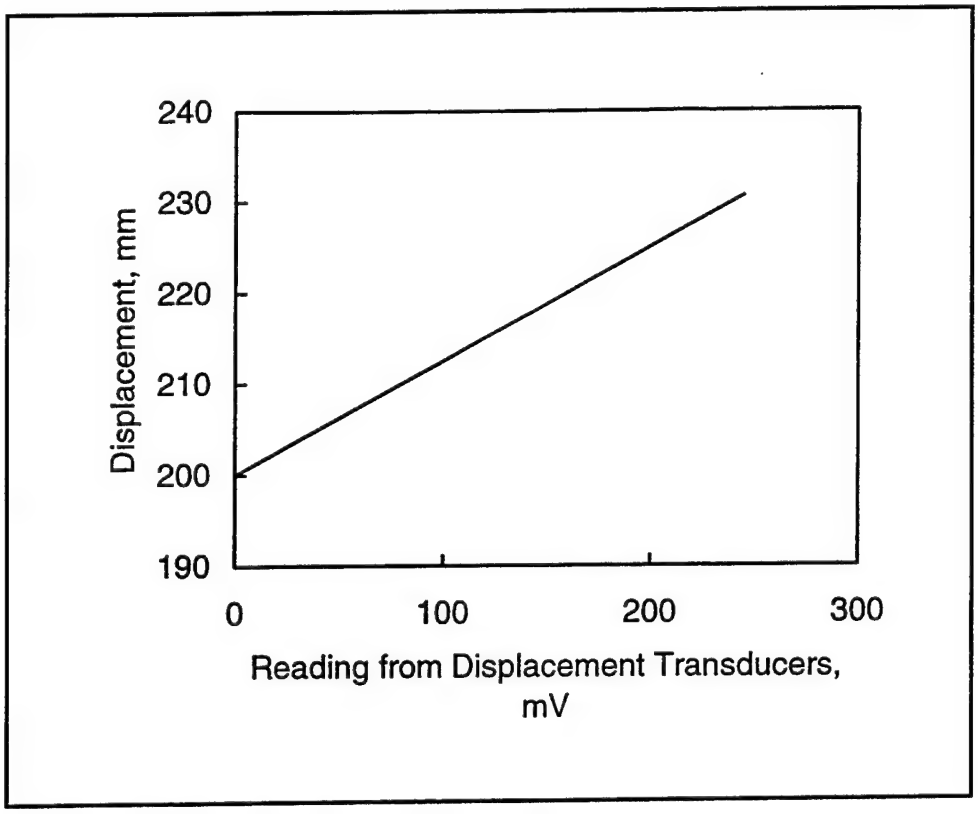

Figure 8. Example of calibration curve for displacement transducer

a control set in case of instrumentation problems or a significantly nonhomogeneous soil profile. The types of cross sections used for the test piles were H-piles and pipe piles, having pile diameters ranging from 150 to 250 mm and lengths of 6.10 or 9.14 m. For the anchor piles, H-piles having diameters of 150 or 200 mm and length of 13.8 m were used. Table 8 presents the description of the piles. The notation for the fourth column of the table, Pile Identification, is as follows:

WW-XX-Y-Z

where

WW = pile dimension in millimeters (inches) (section depth or diameter)

XX = pile length in meters (feet)

Y = pile type (H=H-pile or P=pipe pile)

Z = replicate designator (A or B).

The anchor piles (H-piles) were individually labeled with sequential letters from A to Q.

Table 8
Specifications of Piles

Type of Pile	Diameter mm	Length m	Pile Identification
Experimental piles H-pile		9.14	10-30-H-A
	254		10-30-H-B
		6.10	10-20-H-A
			10-20-H-B
		9.14	8 -30-H-A
	203		8 -30-H-B
		6.10	8-20-H-A
			8-20-H-B
		9.14	6-30-H-A
	152		6-30-H-B
		6.10	6-20-H-A
			6-20-H-B
Experimental piles Pipe-pile		9.63	10-30-P-A
	273	9.36	10-30-P-B
		6.31	10-20-P-A
		6.31	10-20-P-B
		9.20	8-30-P-A
	219	9.51	8-30-P-B
		6.40	8-20-P-A
		6.06	8-20-P-B
		9.60	6-30-P-A
	168	9.63	6-30-P-B
		6.40	6-20-P-A
		6.40	6-20-P-B
Anchor piles H-pile	203	13.8	A, B, D, E, F, H, I, K, L, M, P
	152		C, G, J, N, O, Q

Instrumentation of piles. Instrumentation of the experimental piles consisted of accelerometers and strain gauges attached at the top and bottom of the piles. The accelerometer evaluation board ADXLEB, made by Analog Devices™, was used for instrumenting the accelerometers. To measure accelerations up to 50 g, an Analog Devices™ ADXL 50AH accelerometer with appropriate capacitors and resistors was soldered onto the evaluation board. When fully assembled, the evaluation board was 20 mm square and 7 mm thick. A total of 50 accelerometer boards were used for instrumentation of piles and none of the accelerometer boards were reused.

To attach the accelerometers to the pile, four holes were drilled through the pile and accelerometers were mounted with nuts and bolts to the pile. A plastic washer having thickness about 10 mm was used to isolate the board from the pile. The accelerometer was secured to the pile so that the measured signal was not affected by additional vibration of the acceleration board. A 5V power

supply, ground, self-test, and signal wires were attached to each of the boards. Cables were led to the top of pile and extended approximately 20 m to reach the data acquisition system.

On the H-piles, accelerometers were attached at the flange, 533 mm from the top and 76 mm from the bottom of the pile. The placement of the accelerometers and strain gauges is shown in Figure 9. Specific dimensions of the

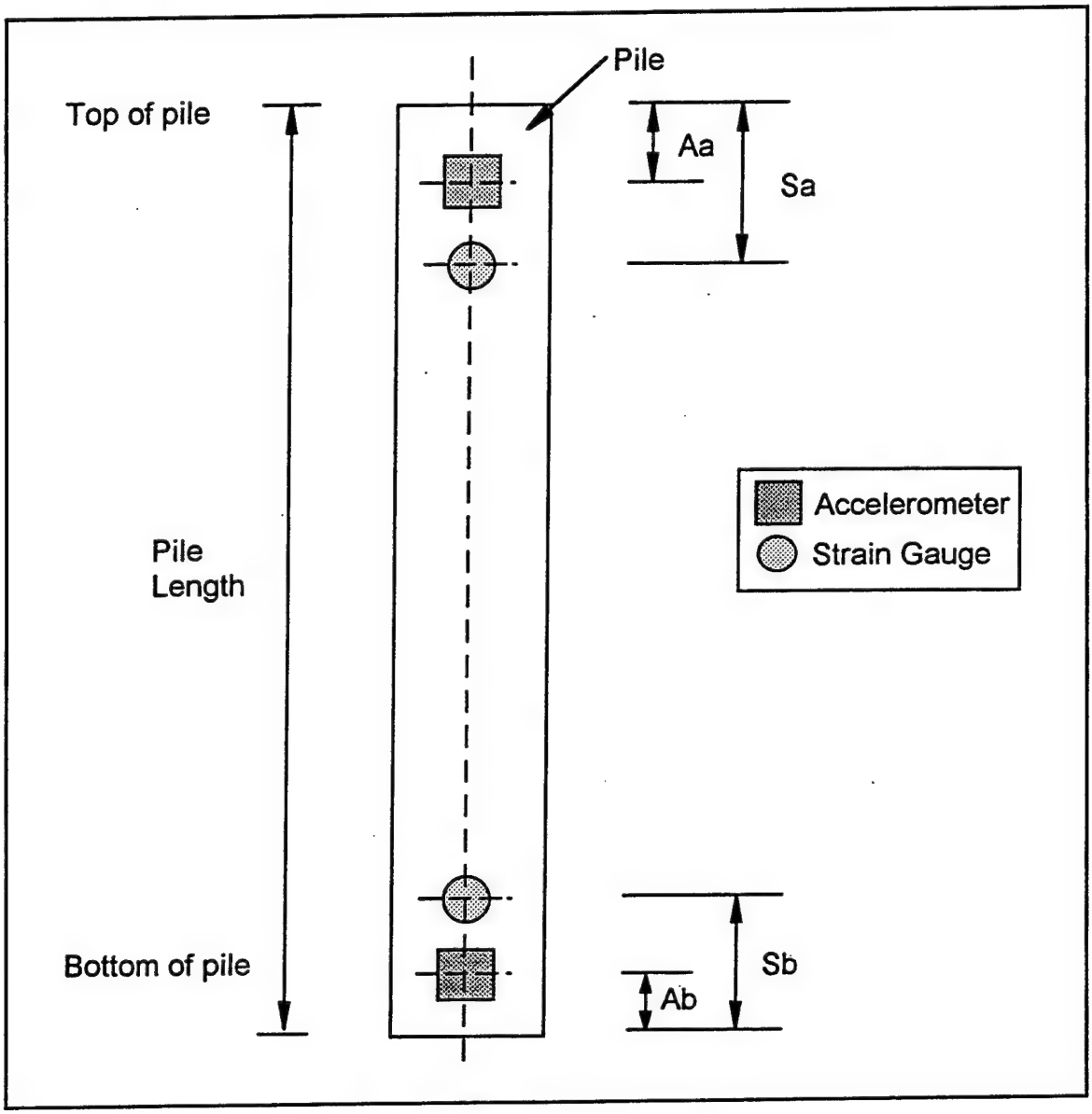

Figure 9. Placement of devices

locations are given in Table 9. The extra length at the top of the pile permitted the hydraulic clamp of the vibratory driver to attach without damaging the instruments and wires. For the pipe piles, accelerometers were placed 305 mm from the top and bottom of the pile on the outside. After the wires were

attached, accelerometers on both H-piles and pipe piles were covered with a silicon coating to guard against moisture and damage. All instruments and connecting wires were protected against damage during driving with steel angles welded on the piles.

Table 9
Placement of Devices

Pile	Distance from the Edge, mm			
	Accelerometer		Strain Gauge	
	Top of Pile Aa	Bottom of Pile Ab	Top of Pile Sa	Bottom of Pile Sb
Pipe pile	305	305	305	305
H-pile	533	76	610	152

Omega™ precision resistive strain gauges with single elements were used for instrumentation of the experimental piles. The gauges were mounted on the pile with M-Bond 200 adhesive (Measurements Group™), soldered to the wires, and protected against damage and moisture by a silicon coating. The strain gauges were placed at the top and bottom of the pile. To compensate for bending, two strain gauges were placed at each location on opposite sides of the pile (Figure 10). The strain gauges, as well as the connecting wires, were protected against damage during the driving with protective steel angles which

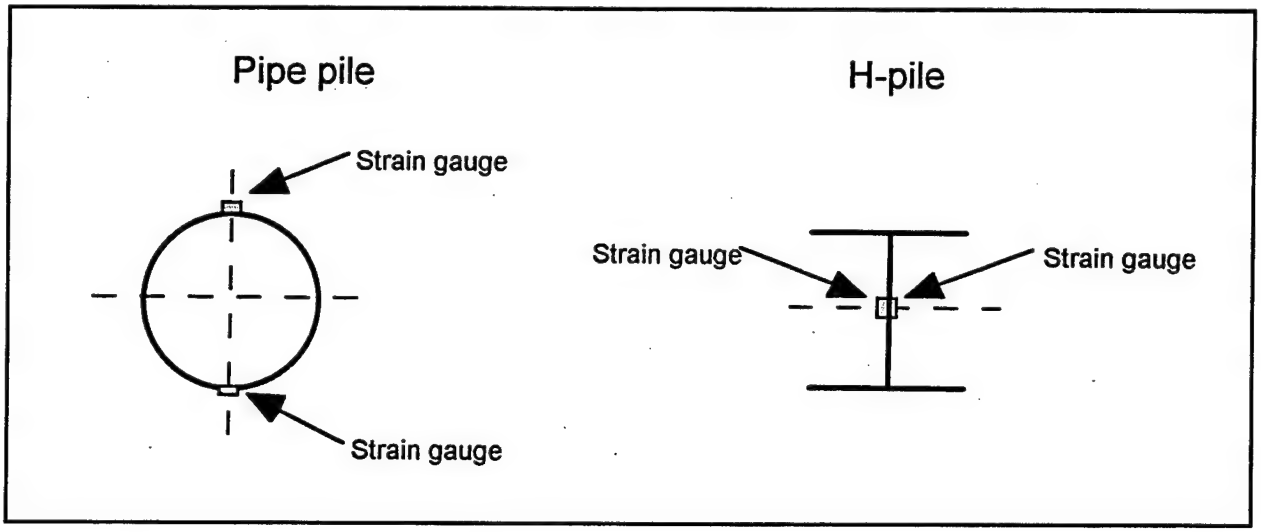

Figure 10. Placement of strain gauges

were welded onto the piles. At the bottom of the pile, a small plate was added to prevent soil intrusion inside of the protective angle which would damage the instruments.

Vibratory driving. In this section, the instrumentation of the vibratory driver, the construction process used to drive piles using the vibratory driver, and the final layout of the piles including measurements of embedded length and plug are described.

Instrumentation of vibratory driver. The vibratory driver was instrumented with two accelerometers placed on the bias mass and on the eccentric mass housing. The accelerometers were attached to pieces of steel angle that were welded to the vibrator and were protected against damage during driving by another steel angle attached at the top. The readings from these accelerometers were recorded during driving of both the experimental and anchor piles.

Vibratory driving scheme. All of the piles were driven using a International Construction Equipment (ICE) Model 416L vibratory driver. The anchor piles were driven first and then the experimental piles were added between the anchor piles. Placement of the piles was crucial to ensure a uniform spacing required to simplify the load testing. A driving template was fabricated and used to layout the location of the anchor piles and experimental piles. The template, shown in Figure 11, helped maintain the desired spacing and supported the piles during vibratory driving. The piles were driven through the loops in the template. The template was supported about 1.5 m above the ground for the driving of the anchor piles.

Referring to Figure 12, the anchor piles were driven so that about 2 m of their length were above the ground. The length of about 2 m was needed to attach the frame during load testing, when the anchor piles were used as reaction piles. For one placement of the template, up to four anchor piles could be driven. Then, the template was lifted with the aid of a crane and relocated to drive another set of piles.

After all of the anchor piles were driven, the template was adjusted for driving the test piles. The support legs were lowered to a height of 0.5 m to allow for the test piles to be driven such that their length above ground was about 1 m. For each placement of the template, up to three experimental piles could be driven between anchor piles, as shown in Figure 13. Then the template was relocated and placed on another set of anchor piles.

Final layout of piles. The total of 17 anchor piles and 24 experimental piles were driven using the vibratory driver in an area of about 100 m^2 (Figure 14). The layout of the test and anchor piles was designed to require a minimum number of anchor piles for load testing. Effectively, at certain locations, one anchor pile could be used as a reaction pile for load tests on four experimental piles.

After the driving of piles was completed, the elevations of the experimental piles were surveyed. The embedded length as well as the length of the plug are presented in Table 10. A tape had a weight attached to the end and was lowered inside the pipe to measure the length of the plug. The measured length was subtracted from the length of pile to obtain length of plug. Only the pipe piles developed a soil plug.

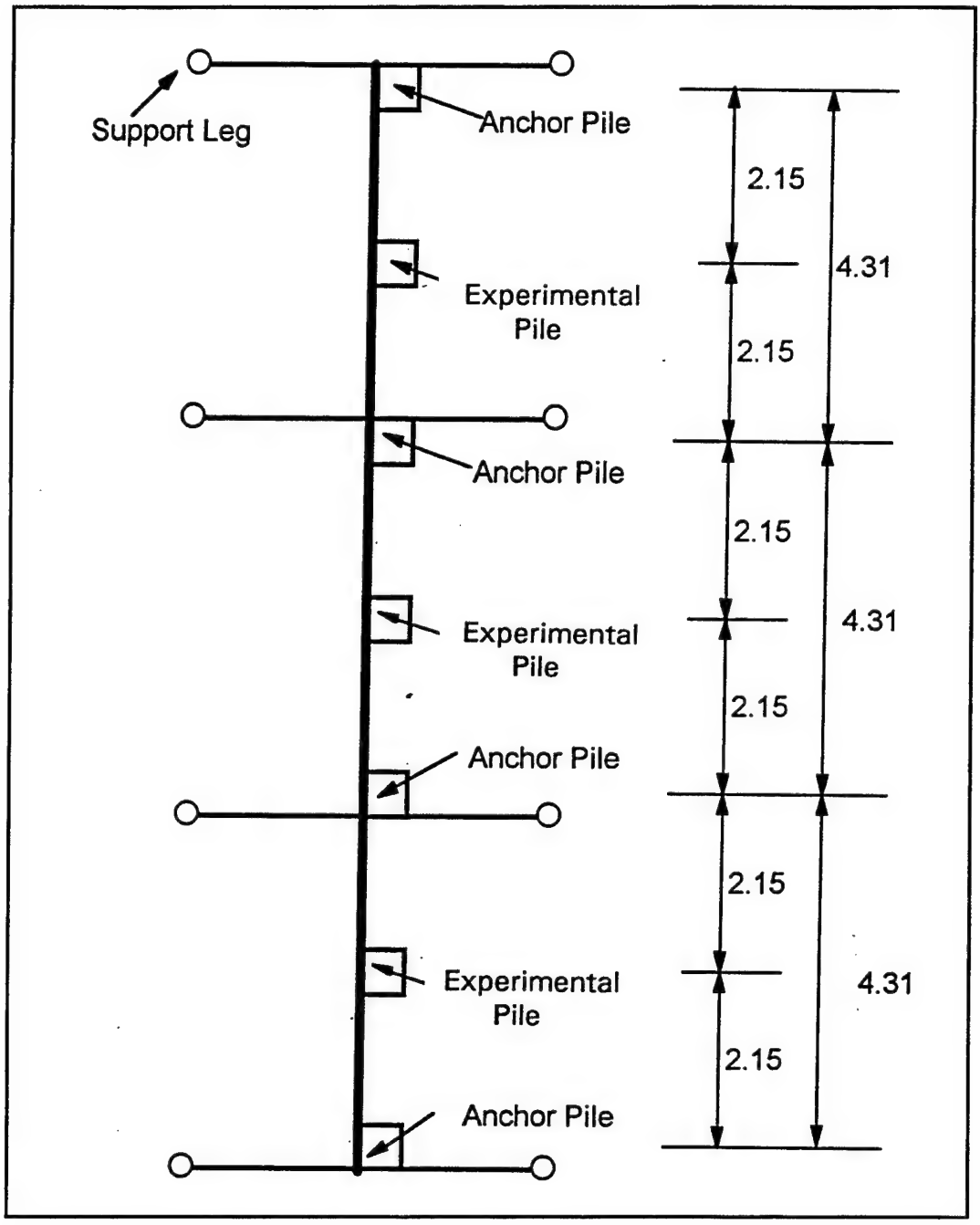

Figure 11. Plan view of driving template

Data acquisition system. Data from the accelerometers and strain gauges on the pile and driver were recorded using an electronic data acquisition system. The system consisted of Campbell Scientific, Inc.™, CR9000 system for real-time data acquisition and a portable PC computer for data recording and storage. Wires connected to the accelerometers and strain gauges on the pile and driver were wrapped into a bundle and routed to the data acquisition

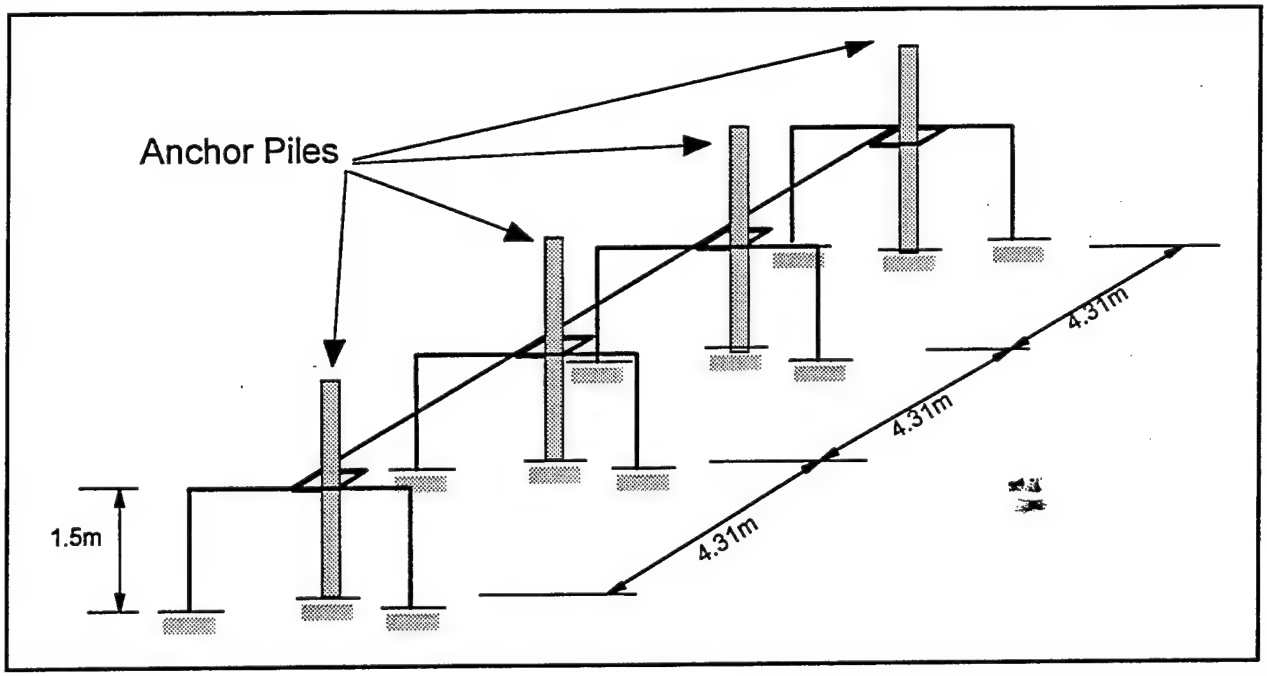

Figure 12. Schematic of template for driving anchor piles

system (Figure 15). Special care was taken to protect the wires against damage during driving by securing them to the hydraulic hose of the vibratory driver.

During driving of the experimental piles, seven channels of information were recorded. Table 11 presents the content of records obtained during driving. Readings of the measurement devices were taken at a rate of 200 times per second. This rate was selected to obtain approximately 10 readings for each cycle of vibratory driving with an estimated frequency of about 20 Hz.

Four conductors were connected to the data acquisition system from each of the accelerometers. Voltage output (V_{out}) and ground conductors were used to collect the acceleration signal. The 5V power supply was the excitation. The fourth conductor was the self-test of the accelerometer that measured constant voltage of 3.4V when the accelerometer functioned properly. The pairs of strain gauges mounted on top and bottom of the pile were connected to the data acquisition system in a Wheatstone bridge arrangement (Figure 16). The active gauges 1 and 4 were the strain gauges mounted on the pile and subjected to the loading during the driving of the piles. The dummy gauges 2 and 3 had the same characteristics as the active gauges but were not loaded. The active gauges were on the opposite sides of the bridge to provide compensation for bending of the pile.

To measure the rate of penetration, piles were marked in 0.3-m intervals and visually inspected during vibratory driving. A remote control device was used to send a signal to the data acquisition system to record the time, when a mark at the pile passed a reference point on the ground.

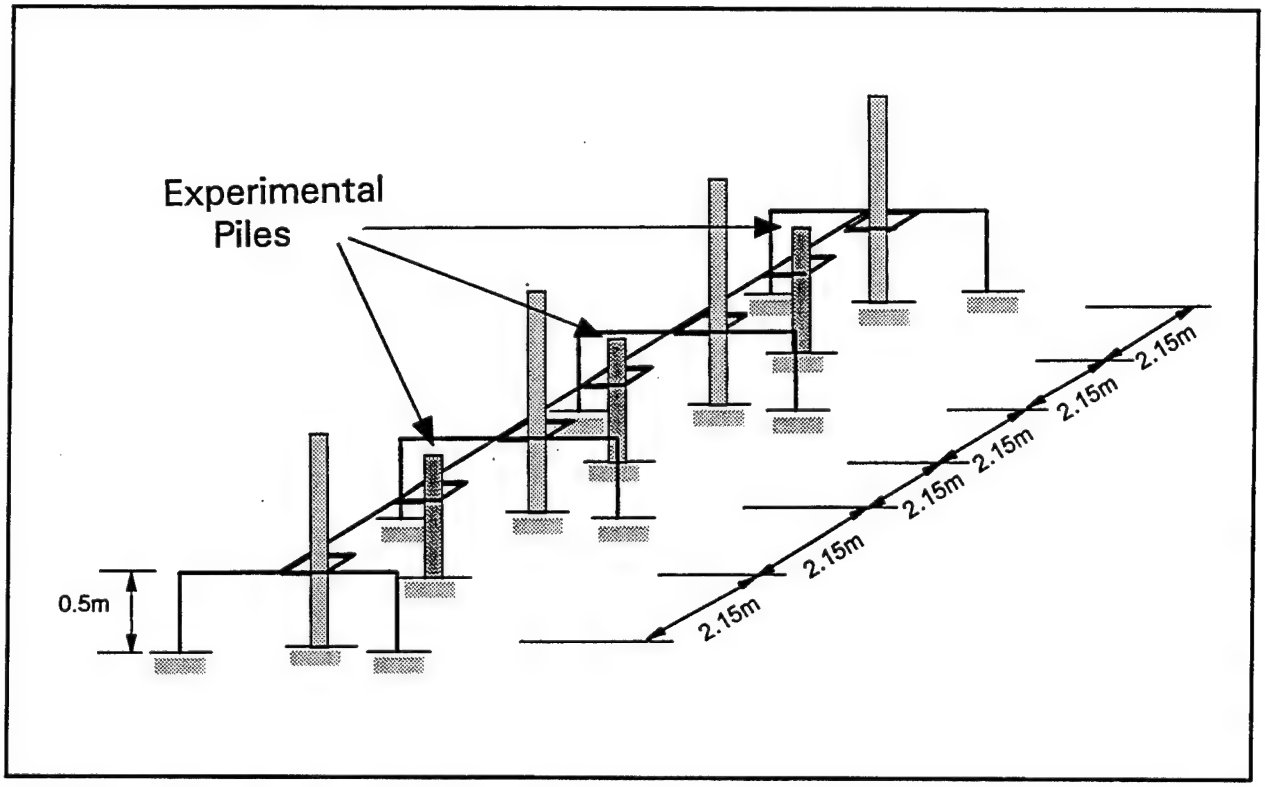

Figure 13. Schematic of template for driving experimental piles

Load Testing. All 24 experimental piles were load tested 4 months after they were driven with the vibratory driver. The load tests were performed according to ASTM D-1143-81, "Standard test method for piles under static axial compressive load," (ASTM 1993d).

Load testing setup. The load test setup consisted of a load beam, load cell, hydraulic cylinder with a pump, and displacement transducers, as shown in Figure 17. The load beam and the attached load cell were placed between two anchor piles and set on a clip angle welded onto the anchor piles. During the actual loading, the load beam was pushing against the upper angles welded to the anchor piles. The hydraulic cylinder RC 5013 was placed on the experimental pile and aligned with the load cell. The reference frames (having length about 4 m) were placed perpendicular to the load beam and founded on small stakes driven near the ends of the reference frames. The displacement transducers were attached to the reference frames and their cables were attached to the experimental pile.

Load testing procedure. A series of 11 steps were performed for load testing each of the 24 experimental piles. The procedure consisted of the following steps:

a. Weld the reaction angles and supports to the anchor piles.

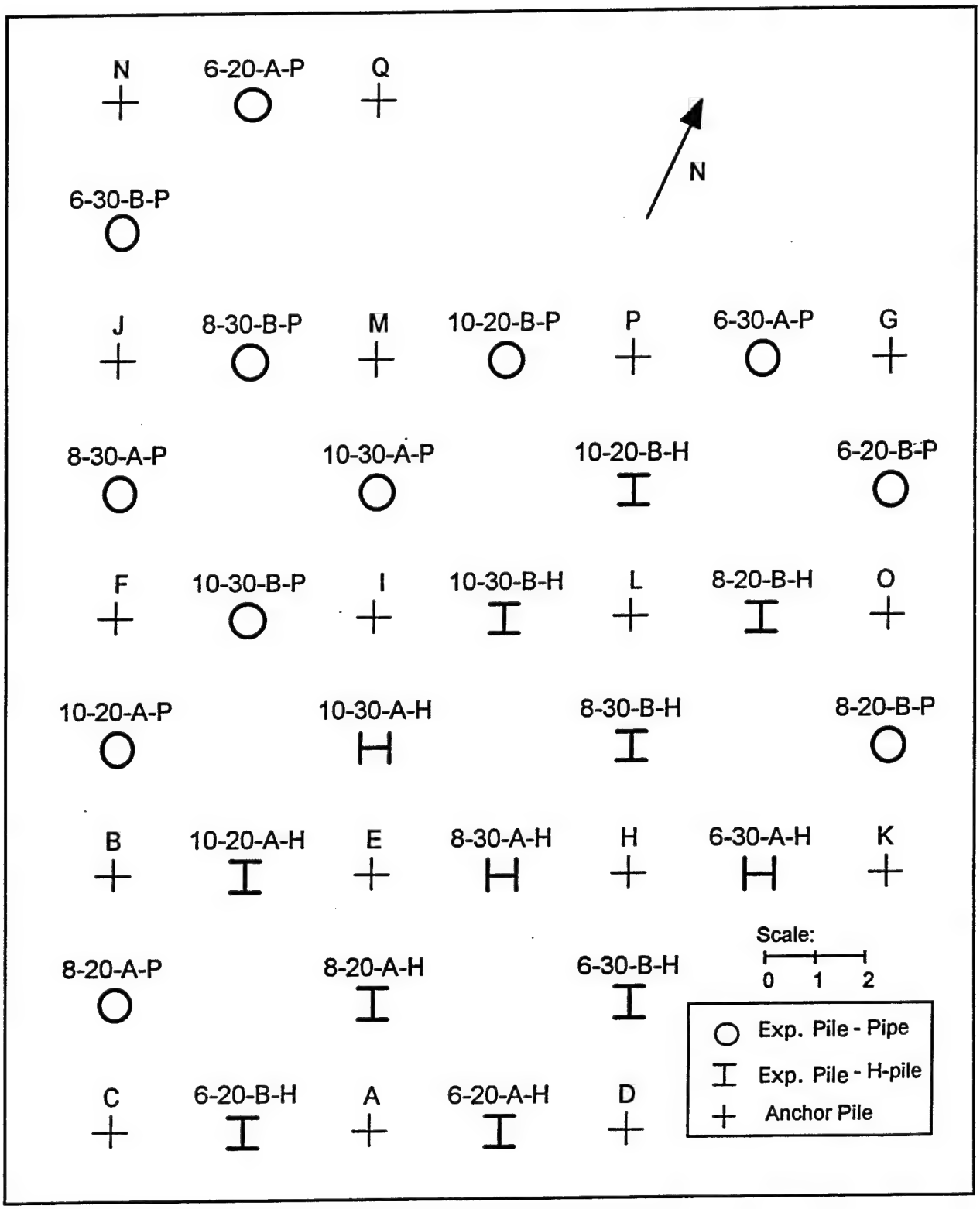

Figure 14. Final layout of piles

Table 10
Embedded Length and Length of Plug for Experimental Piles

Pile	Embedded Length m	Plug Length m
10-30-H-A	8.23	-
10-30-H-B	8.06	-
10-20-H-A	5.15	-
10-20-H-B	5.17	-
8 -30-H-A	8.39	-
8 -30-H-B	8.16	-
8-20-H-A	5.19	-
8-20-H-B	5.02	-
6-30-H-A	8.07	-
6-30-H-B	8.02	-
6-20-H-A	5.09	-
6-20-H-B	5.12	-
10-30-P-A	8.03	1.82
10-30-P-B	8.21	1.64
10-20-P-A	5.10	1.43
10-20-P-B	5.13	1.58
8-30-P-A	8.16	1.30
8-30-P-B	8.14	1.25
8-20-P-A	5.03	1.52
8-20-P-B	5.02	2.55
6-30-P-A	8.11	1.83
6-30-P-B	8.23	1.43
6-20-P-A	5.12	1.46
6-20-P-B	5.06	1.34

b. Move the load beam between the anchor piles with a small Bobcat and slide the load beam between reaction and support angles on the supports.

c. Secure load beam with a safety chain while the load beam is still attached to Bobcat.

d. Place hydraulic cylinder on the experimental pile and align the cylinder with the load beam.

e. Disconnect and remove the Bobcat from the area of the load test.

f. Place the reference beams and attach the displacement transducers to the reference beams and the experimental pile.

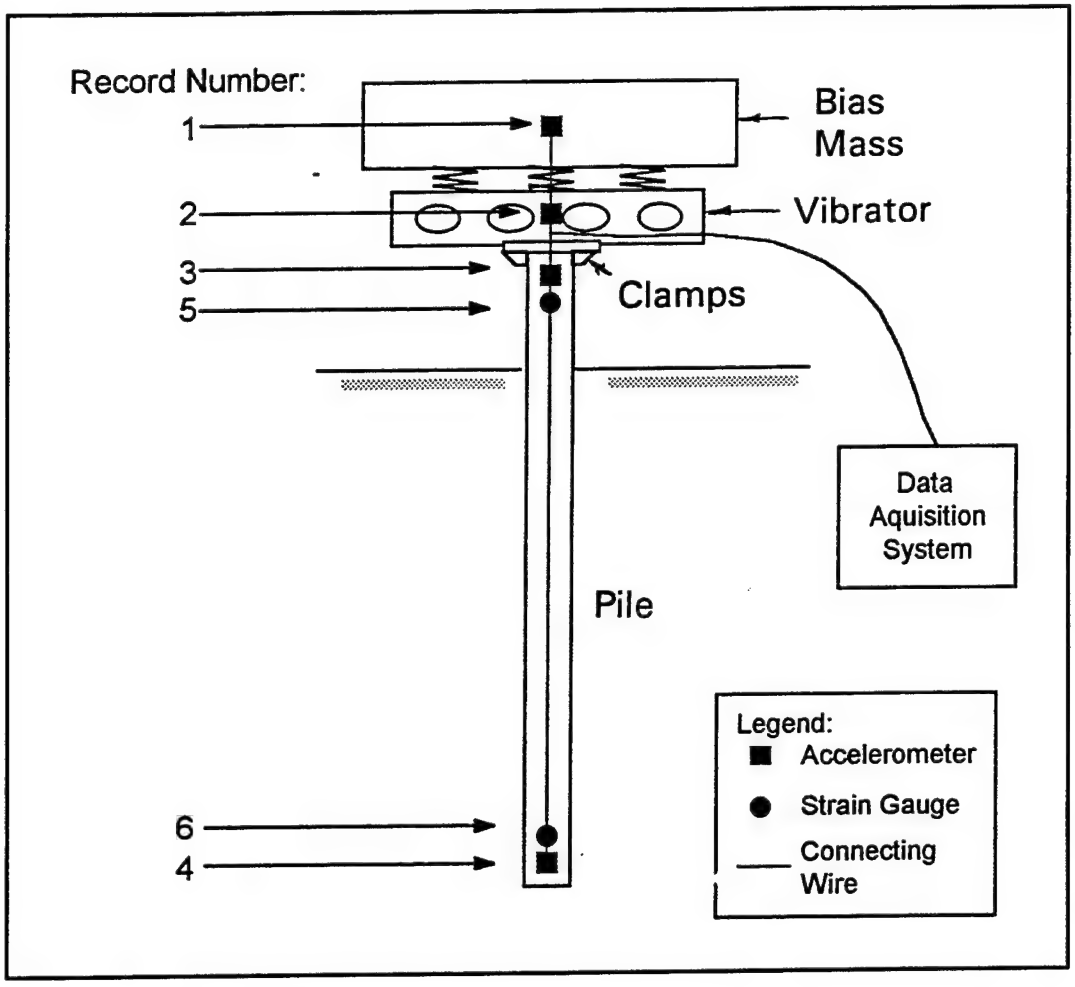

Figure 15. Instrumentation and data acquisition system

Table 11
Records during Vibratory Driving

Record Number	Record
1	Acceleration at the bias mass of the vibratory driver
2	Acceleration at the eccentrics of vibratory driver
3	Acceleration at the top of the pile
4	Acceleration at the bottom of the pile
5	Strain at the top of the pile
6	Strain at the bottom of the pile
7	Pulse at each 0.3 m of pile penetration into the ground

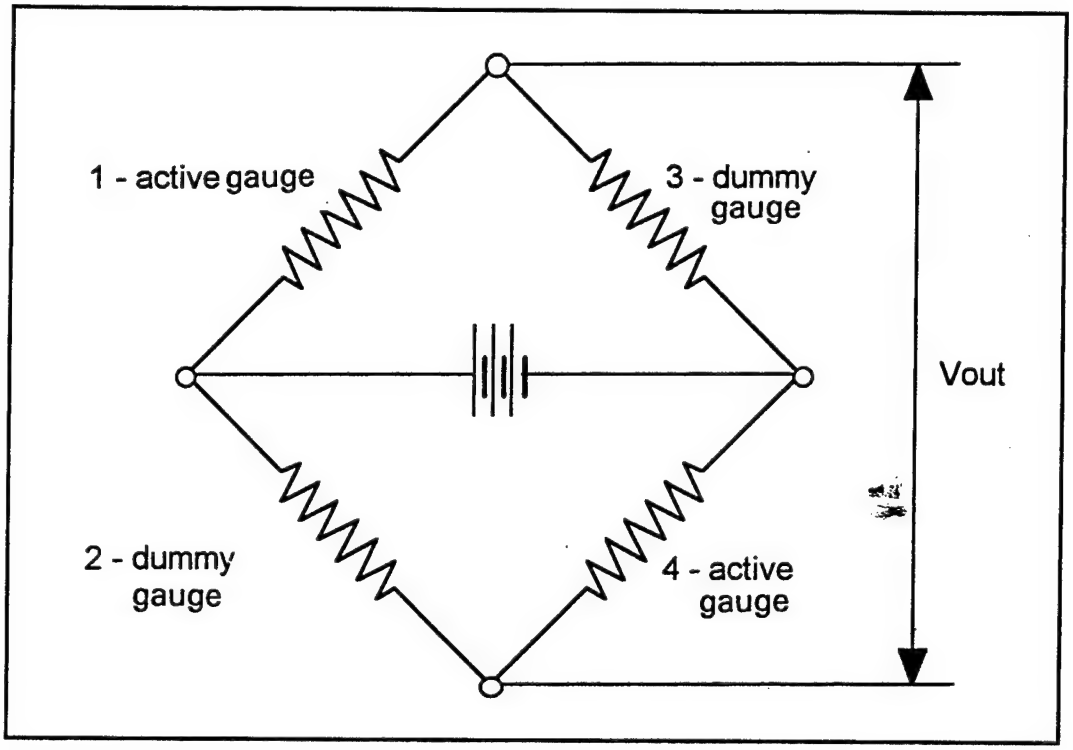

Figure 16. Wiring diagram for strain gauges in Wheatstone Bridge arrangement

g. Connect the wires from the load cell, displacement transducers, and strain gauges on the experimental pile to data acquisition system.

h. Load test the pile while the data are collected by the automatic data acquisition system, and manually record readings taken for maximum pressure on the dial gauge of the cylinder and maximum displacement against reference marks in 25-mm increments on the test piles.

i. Disconnect the load cell and strain gauges and remove the displacement transducers and reference frame.

j. Support the load beam with the Bobcat and remove the hydraulic cylinder.

k. Remove the safety chain and move the load beam to the next experimental pile.

Methods of analysis of data collected in field testing

Driving records from accelerometers and strain gauges were analyzed using a computer program entitled TAMU developed using the computer language, Borland C++. The records were analyzed to obtain frequencies and amplitudes of driving forces in the pile and rates of penetration. Readings taken

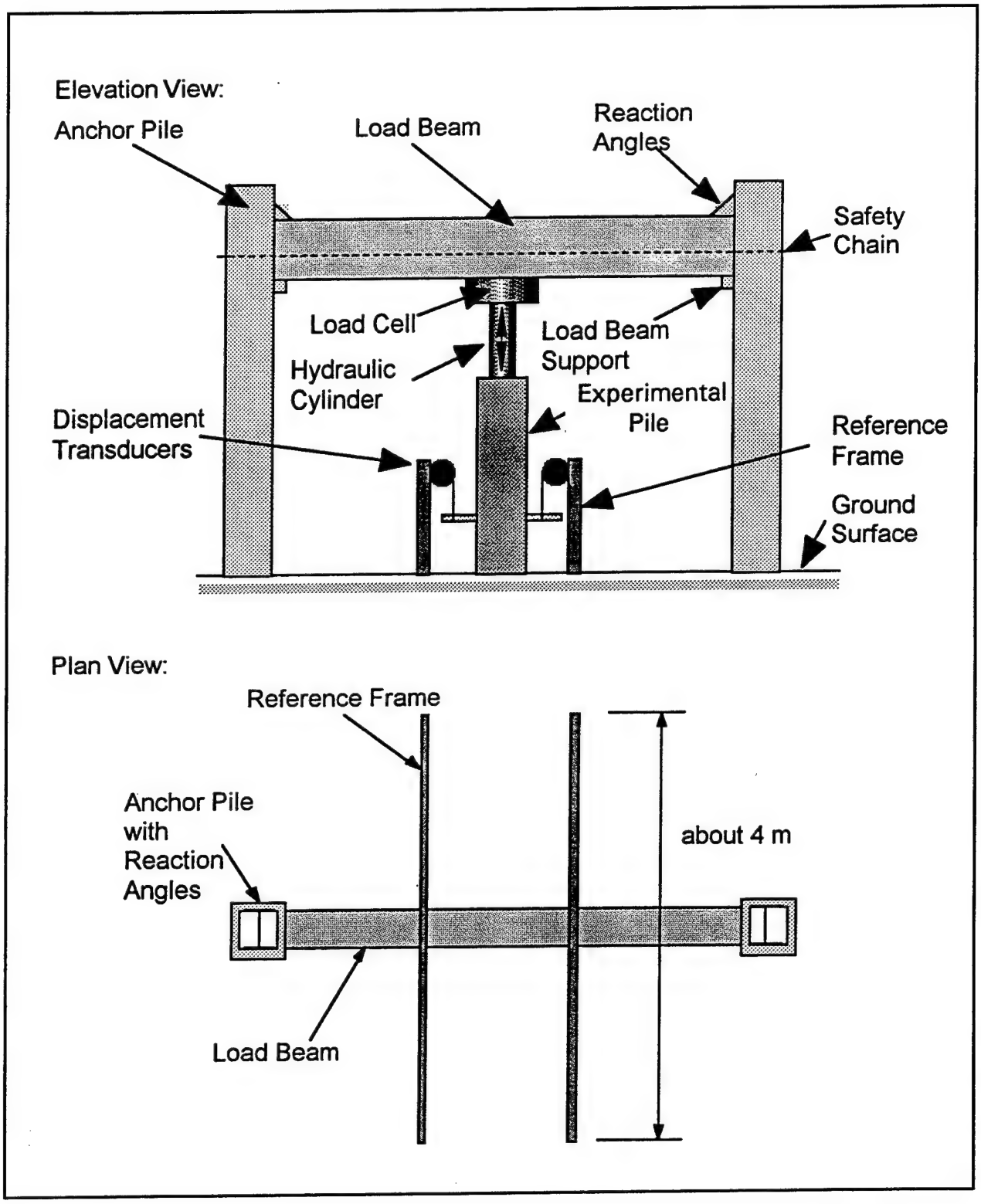

Figure 17. Load test setup

during load testing were analyzed using an MS Excel™ Macro to obtain the loads and settlements of piles.

Rate of penetration. The rate of penetration was calculated from the data extracted from the driving records by the program TAMU. The program created a data file of the times when the signal from the rate penetration device indicated that the reference mark on the pile was aligned with the reference point. The rate of penetration *RP* was calculated as:

$$RP = \frac{d}{\Delta t} \tag{17}$$

where

d = distance between the reference marks on the pile

Δt = time interval between the two readings

The distance d of the reference marks on the pile used in the field was 300 mm.

Frequency and amplitude of vibratory driving. Data collected during vibratory driving from the accelerometers and strain gauges attached to the piles were analyzed using an FFT analysis, which transfers the record from the time domain to the frequency domain. The analysis was automated in the program TAMU.

In the analysis, TAMU first locates the beginning of the driving record and disregards the initial part of the record that was taken before the vibratory driver was started. Referring to Figure 18, the point that had an amplitude of at least 25 percent of the maximum amplitude reached during driving was considered as the beginning of the record.

The FFT analysis was performed on the remaining record. The FFT analysis required a signal oscillating around zero. Thus, the mean of the record was subtracted from all of the readings. The record was then divided into sections of N data points, where N is a number that can be expressed as a power of 2. The selection of N is important, because the frequency can be determined more accurately (smaller Δf) with a larger N as shown:

$$\Delta f = \frac{1}{N\Delta t} \tag{18}$$

Smaller N values provide more detailed information and less averaging as the pile penetration progresses. The smallest N value based upon the sampling frequency of 200 samples/sec and a desire for frequency resolution of 0.4 Hz is 512 points. For most records, a frequency resolution of 0.2 Hz (1,024 points) was used.

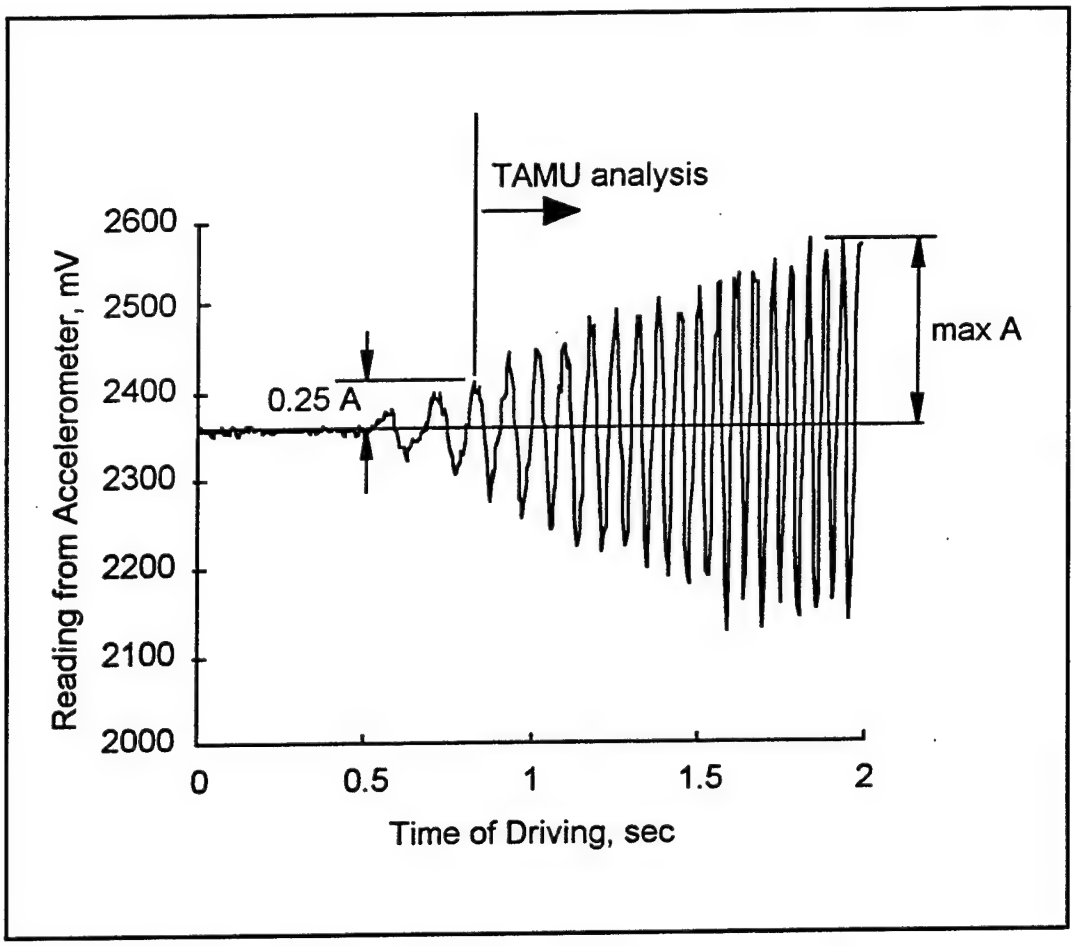

Figure 18. Driving record analysis using Program TAMU

The analysis of the records from accelerometers and strain gauges were slightly different. For the accelerometers, N was chosen considering, on one hand, resolution in determination of frequency (large N), and on the other hand, having enough sections to create a profile of frequency with embedded length of pile (small N). For most of the records, N was equal to 1,024 data points (equals 2^{10}). In some special cases of short driving record, N was equal to 512 data points (equals 2^9), as seen in Table 12. For accelerometers, the mean of all readings in the record was calculated and subtracted prior to the analysis. This was necessary because of the +2.5V signal offset from the Analog Devices™ ADXL 50AH accelerometer.

For the strain gauges, the record was divided into sections of 128 data points (equals 2^7). The smaller number, N, was chosen to ensure that the signal oscillates around zero as required for FFT analysis. The static portion of strain in the pile was increasing as the pile penetrated deeper into the ground and the mean was calculated and subtracted in sections of 128 points.

One of the sections of N data points was analyzed at a time. The beginning and end points were at the random location in a cycle. Thus, a mean of N

Table 12
Value of N for Analysis of Records from Driving Experimental Piles

Pile Identification	N, Data Points
10-30-H-A	1,024
10-30-H-B	1,024
10-20-H-A	512
10-20-H-B	512
8-30-H-A	512
8-30-H-B	1,024
8-20-H-A	512
8-20-H-B	512
6-30-H-A	512
6-30-H-B	1,024
6-20-H-A	512
6-20-H-B	--
10-30-P-A	1,024
10-30-P-B	1,024
10-20-P-A	1,024
10-20-P-B	1,024
8-30-P-A	1,024
8-30-P-B	1,024
8-20-P-A	1,024
8-20-P-B	1,024
6-30-P-A	1,024
6-30-P-B	1,024
6-20-P-A	1,024
6-20-P-B	1,024

Note: Driving record for 6-20-H-B is missing.

points was affected by the location of these points (Figure 19a). For example, a generated sine wave of 128 points oscillating around zero having incomplete cycles at the ends has a mean of -0.05. This inaccuracy causes an inaccuracy in determination of frequency using FFT analysis. This effect could be eliminated using a windowing technique, demonstrated in Figure 19b. The value of each data point is multiplied by a weighting factor that reduces the amplitude of signal at the ends. In this analysis, a Hanning window was used and the weighting factor was calculated as:

$$w_j = \frac{1}{2}\left[1 - \cos\left(\frac{2\pi j}{N}\right)\right] \tag{19}$$

where j = sequence number of the data point in section of N data points.

The FFT analysis was performed on a windowed signal of N data points (Figure 20a). The FFT analysis transformed the signal from the time domain

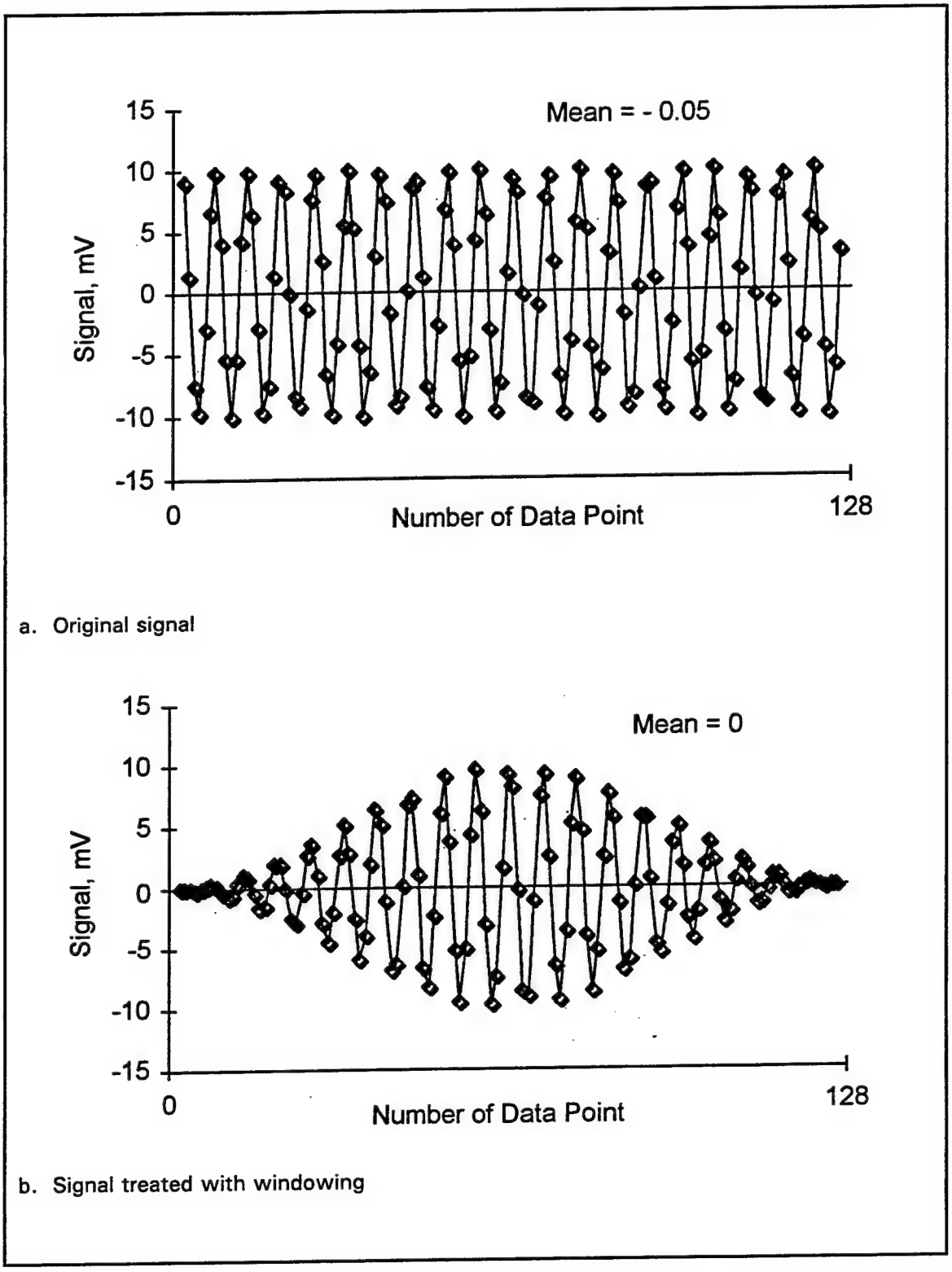

Figure 19. Signals with and without windowing

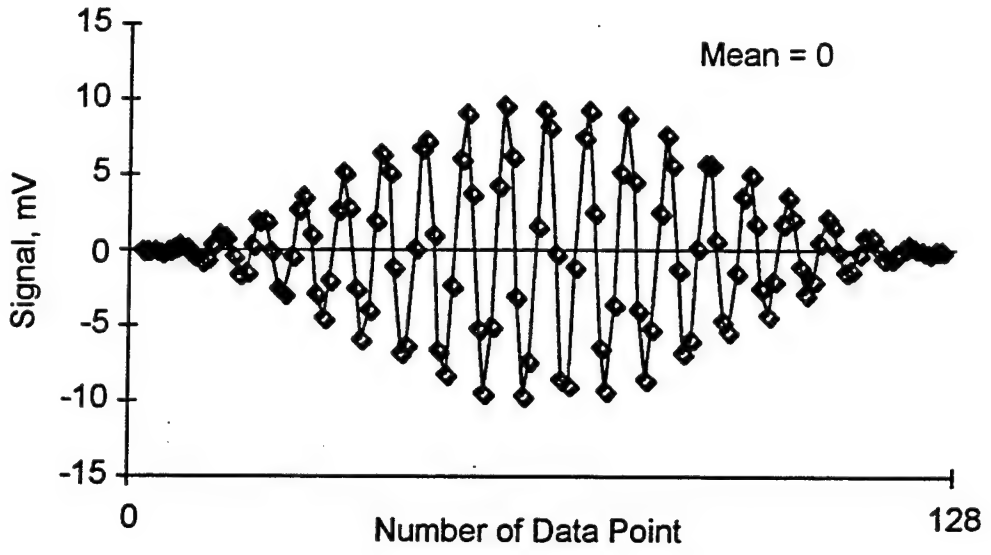

a. Signal in time domain

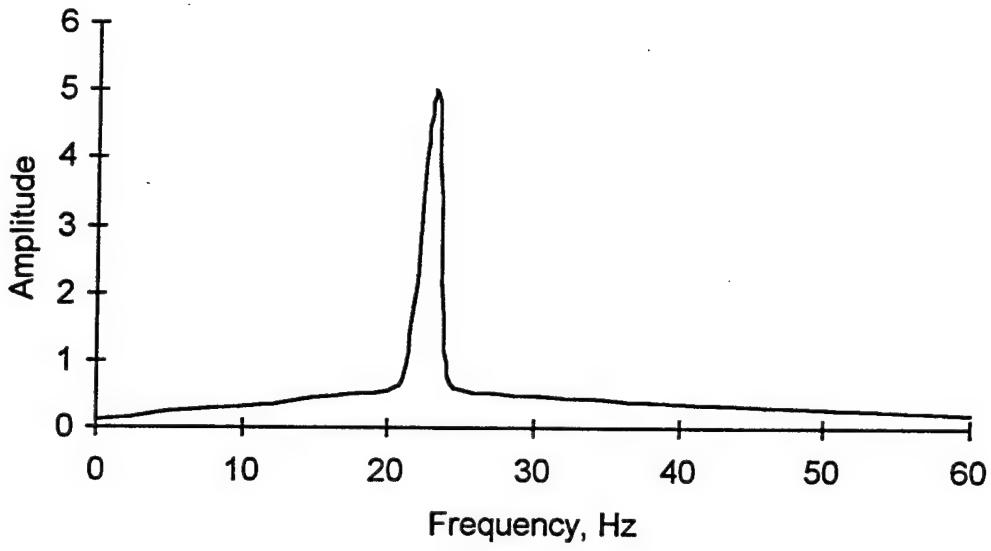

b. Signal in frequency domain after FFT analysis

Figure 20. FTT analysis

to the frequency domain using the program TAMU. The program TAMU was developed in computer language C++ using routine 'realft' developed by Press et al. (1992), which performed the Fourier transform of a single real-valued data array. In the program TAMU, the routine was called several times to perform FFT on six signals collected from accelerometers and strain gauges and repeated for each section of N data points. The results of the FFT were *N*/2 new data points in the frequency domain (Figure 20b). The amplitude in the frequency domain due to use of the Hanning window corresponded to the half of the amplitude of the signal in the time domain.

The results of FFT analysis performed by TAMU were stored in separate data files for each accelerometer and pair of strain gauges. The data files were transformed to MS Excel™ spreadsheets and analyzed using an MS Excel™ macro. The corresponding frequency, f, of each of the new data points was calculated as:

$$f = i \frac{f_{sampling}}{N} \tag{20}$$

where

I = sequence number of the new data point from FFT

$f_{sampling}$ = sampling frequency of data collection

In this testing, the sampling frequency was 200 Hz.

The amplitude of vibration and dynamic strain were transformed from the voltage reading using the calibration relations. The analysis was performed for all four accelerometers and two pairs of strain gauges were attached to the experimental piles. From the acceleration record, the frequency corresponding to maximum amplitude of vibration was determined for each of the sections of N data points. The profile of maximum frequency of vibration and corresponding amplitude was made for the driving record of every pile. Frequency and amplitude were plotted against the depth of penetration of the tip of the pile that was calculated using records of rate of penetration and driving time. For a strain record, the amplitude obtained from the FFT analysis represented a dynamic part of strain. The strain results were transformed to force for each pile using the calibration relation unique to each individual pile.

Analysis of static strain. The static strain due to the penetration of the pile during the driving was also analyzed using the program TAMU. The record from the strain gauges was divided to sections of 128 (2^7) elements used for the FFT analysis, and the mean value of strain was calculated for each section. This mean value represented an average level of static strain of pile for the time period of 0.64 sec (128 data points collected at rate of 200 times/sec). The value of strain was transformed to force in the pile using the calibration factor and point of zero strain determined during calibration. The force F was transformed to the strain, ϵ, using Hooke's Law:

$$\varepsilon = \frac{F}{AE} \tag{21}$$

where

A = cross-sectional area of steel of the pile

E = Young's Modulus

The mean value of strain can be related to recorded time and subsequently to the depth of penetration of the pile from the measured rate of penetration.

Evaluation of energy and power delivered to pile. The energy and power delivered to top and bottom of pile were evaluated using the program TAMU developed in computer language Borland C++. The record was divided to the sections of N data points. The value of N was consistent with the value used in the FFT analysis of the acceleration record, paragraph entitled "Frequency and amplitude of vibratory driving." For each section j, power P_j was evaluated as:

$$P_j = \frac{1}{T}\sum_{i=1}^{N} abs(F_i)\,abs(V_i)\,\Delta t \tag{22}$$

where

T = driving time needed for recording of N data points (equals N*0.005 sec for this data recording)

F = force for i point in section

v = velocity for i point in section

Δt = time period between the readings (equals 0.005 sec for this data recording)

The velocity can be calculated by integration of acceleration with respect to time. For discrete readings of acceleration, the trapezoidal rule was applied and velocity was calculated as:

$$v_i = \frac{a_i + a_{i+1}}{2}\Delta t \tag{23}$$

where a_i and a_{i+1} are accelerations of two consecutive points.

Total energy delivered to top and bottom of pile was calculated as:

$$E = T * \sum_{j=1}^{m} P_j \tag{24}$$

where m is number of sections in the record.

In Figure 21, the calculation of power and energy is shown in graphically.

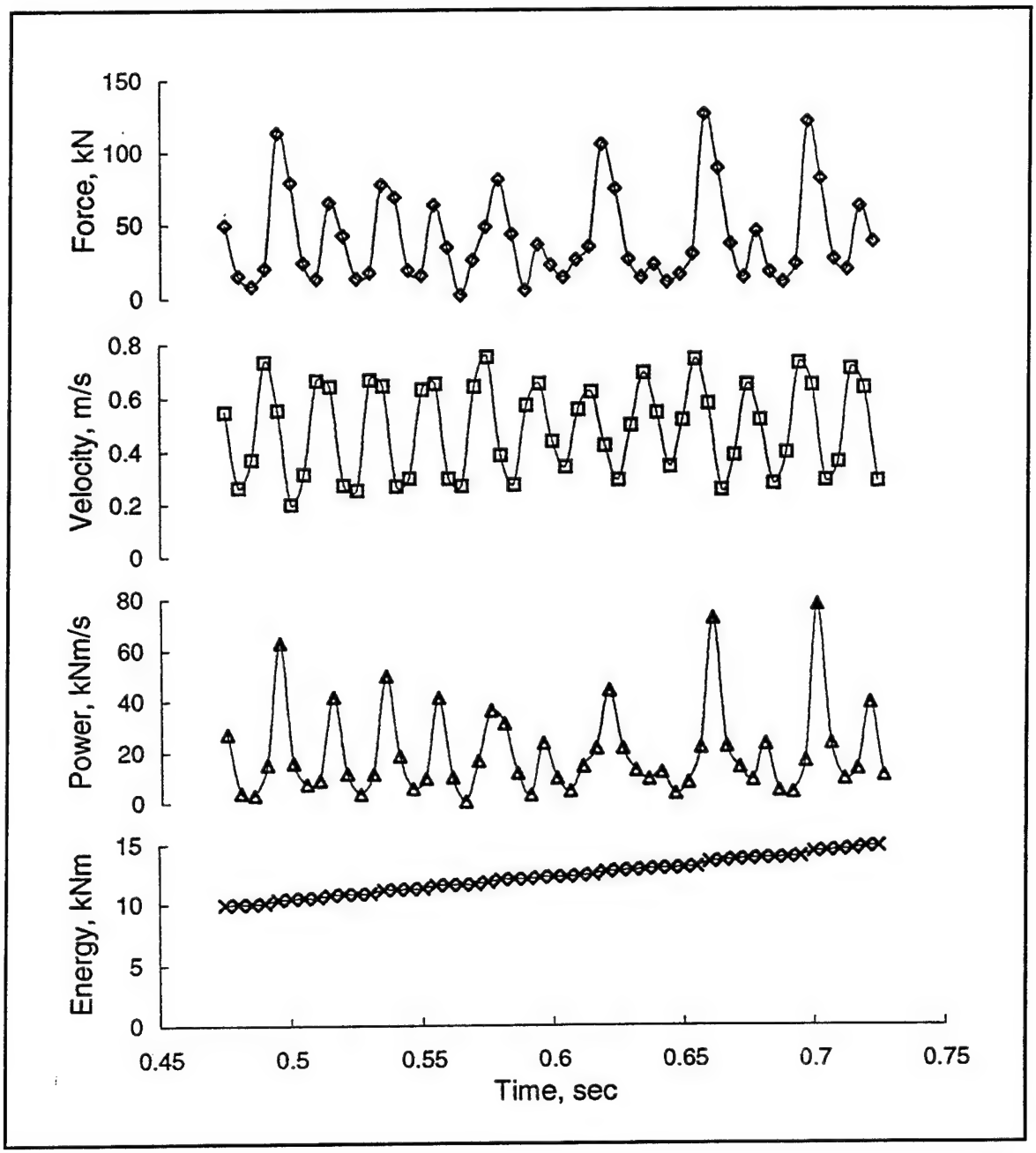

Figure 21. Principle for calculation of power and energy

To obtain the force, the voltage reading of the strain gauge was referenced to a voltage reading of zero strain and transformed to force using the calibration factor. First, a zero strain obtained during the calibration, when the pile was lying on the ground, was used as a reference. This approach resulted in variable levels of strain ranging from 0.8 to -0.2 percent. These levels of strain could not be explained by loading of the pile due to its self-weight or the weight of vibrator. The increase in static strain due to the weight of vibratory driver was on the order of 0.003 percent. The increase in strain at the bottom of the pile due to self-weight of the pile was on the order of 0.0004 percent. Rather, an additional unknown factor in the time between calibration and actual driving seemed to produce an unpredictable bias in the zero readings of the strain gauges. Thus, a mean of the first 100 data points at the beginning of driving was used as reference point of zero strain.

The acceleration was calculated from voltage readings from the accelerometer referenced to a reading of zero acceleration. The point of zero acceleration could be obtained through known displacement of the pile at the end of driving. Displacement of the pile can be obtained through double integration of acceleration with respect to time. Total displacement had to equal the embedded length of the pile. The point of zero acceleration can be estimated through an interactive process of calculation of displacement, comparison to the embedded length, and correction in estimation of zero acceleration. The true point of zero acceleration was calculated for two piles using MS Excel™. The corrected zero acceleration was used for calculation of energy and in both cases the change of energy due to correction in zero acceleration was less than 0.1 percent. Such an error was considered acceptable considering the uncertainty in evaluation of calibration factors for strain gauges. In the analysis, the point of zero acceleration was evaluated as a mean of the record and used for calculation of power and energy.

Analysis of load tests. Readings from the load cell and the displacement transducers were transformed from voltage readings into values for load and displacement, respectively, using calibration relations. Readings from the two displacement transducers were averaged to compensate for bending of the experimental pile. Load versus displacement curves were plotted and the maximum displacement, maximum load reached, and final plastic displacement was recorded. The ultimate load, or bearing capacity of the pile, was analyzed using the Davisson limit load method, Brinch-Hansen method, and Chin-Kondner method.

Results and Discussions

In this section, the results of an analysis on the VPDA program, vibratory driving records, and bearing capacity estimates are presented. A sensitivity analysis of VPDA was conducted to determine the most significant input parameters. The performance of the piles during driving was analyzed in terms of frequency, dynamic and static strains, and rates of penetration. Stepwise linear regression was performed on the results of analysis of the driving

records to determine if there was any correlation between the parameters measured during driving and the bearing capacity.

Results of VPDA analysis

A sensitivity analysis was conducted on VPDA to identify the most significant input parameters to the program. Initially, 15 input parameters were studied using a fractional factorial design. After the vibratory driver was selected, an additional sensitivity analyses was performed using a fractional factorial design.

Sensitivity analysis of VPDA input parameters. A sensitivity analysis of the input parameters to the program VPDA was performed using a fractional factorial design. The goal was to determine input parameters that significantly influence predictions of the rate of penetration for the required bearing capacity using VPDA. Since VPDA has a large number of input parameters, a fractional factorial design with large number of factors and small number of runs was selected. A two-level 2^{15-10} fractional factorial design with four central points and 15 input parameters was used for analysis of 36 runs of VPDA. The input parameters studied were: (a) characteristics of the driver, (b) characteristics of the connector between the driver and pile, (c) characteristics of the pile, and (d) characteristics of the soil, as presented in Table 13. For each input parameter, reasonable estimates of high and low levels under field conditions were made.

The measured response from VPDA was rate of penetration (millimeters per second) for required bearing capacity (kN). Results were collected for seven levels of bearing capacity, ranging from 67 to 200 kN in increments of 22.2 kN.

The fractional factorial design used in this analysis had a resolution of four (IV). The main effects were aliased with three-factor interactions and two-factor interactions were confounded (Box, Hunter, and Hunter 1978). It is assumed that the three-factor interactions were not significant, thus the significance of the main effects could be estimated. The central points were generated using the qualitative factors, type of soil model, and type of side friction, which were considered at both levels, as in full factorial design with those two factors. For those four runs, the quantitative factors were equal to their midvalue between low and high levels. The design with levels of each factor for each run is provided in Appendix B.

The fractional factorial analysis was performed using the MINITAB statistical software package. The significance of factors was evaluated at the 95 percent confidence level corresponding to p-values of less than 0.05. The confidence level of 95 percent represents a probability of 5 percent that a parameter is erroneously identified as statistically significant.

Based on the results of the analysis, the significant input parameters were: (a) the eccentric moment of driver, (b) weight of driver, and (c) unit weight of the soil, as shown in Table 14. These results are to be expected in that the

Table 13
List of Factors and Levels for Initial Sensitivity Analysis

Factor	Description	Level -	Level +
1	Eccentric moment of the driver, kN-cm (lbf-in.)	22.6 (2,000)	113.0 (10,000)
2	Bias mass of the driver, kg (lb)	1,133.98 (2,500)	2,267.96 (5,000)
3	Weight of vibrator, kg (lb)	2,267.96 (5,000)	5,443.1 (12,000)
4	Frequency of driving, Hz	20	25
5	Type of pile profile	pipe	H-pile
6	Size of pile, mm (in.)	152.4 (6)	254.0 (10)
7	Length of pile, m (ft)	3,048 (10)	9.14 (30)
8	Type of soil model	Hyperbolic	Smith
9	Efficiency of vibrator, %	20	25
10	Stiffness of connector, kN/m (lb/in.)	2.28×10^5 (1,300,000)	2.63×10^5 (1,500,000)
11	Viscous damping of connector, N-sec/m (lb-sec/ft)	7,297.0 (500)	8,756.3 (600)
12	Pile capacity at tip, %	20	40
13	Unit weight of soil, kN/m^3 (pcf)	17.3 (110)	20.4 (130)
14	Damping of pile, N-sec/m (lb-sec/in.)	15,761 (90)	19,264 (110)
15	Velocity of shear wave, m/sec (ft/sec)	198.1 (650)	228.6 (750)

Table 14
Results of First-Stage Sensitivity Analysis

Significant Input Parameters	p-value for Estimated Bearing Capacity						
(95% Significance Level)	67 kN	89 kN	111 kN	133 kN	156 kN	178 kN	200 kN
Eccentric moment of driver	0.007	0.013	0.006	0.000	0.006	0.011	0.024
Weight of vibrator	0.011	0.019	0.012	0.001	0.021	0.046	ns
Unit weight of soil	ns	ns	0.011	0.003	ns	ns	ns

Note: ns = not significant.

increase in the eccentric moment of the driver and/or weight of driver tends to increase the rate of penetration, because the driver with higher eccentric moment and/or weight of driver produces more power and results in higher rates of penetration. The significance of unit weight of soil is identified only at certain bearing capacities. In those bearing capacities, the increase in unit weight of soil tends to increase the rate of penetration. That is counter to what would be expected because soils with lower unit weights have lower lateral stresses and generate poorer resistance, and thus, higher rates of penetration could be expected. Also, the significance of the factors decreases with increasing required bearing capacity. The full listings of results are included in Appendix B. This part of the analysis suggested that the driver is the most important input parameter for VPDA.

Second stage sensitivity analysis of VPDA input parameters. The driver to be used in the field experiments was selected based on the estimates of rates of penetrations predicted using VPDA and on recommendations from the equipment manufacturer. The vibratory driver selected was the ICE 416L vibratory driver. An additional sensitivity analysis was conducted using another fractional factorial design with a smaller number of factors. The analysis was conducted to determine if any additional significant parameters existed when using a known vibratory driver. Results of the initial investigation were strongly influenced by the driver and the effects of the driver may have masked sensitivity of other parameters.

The input parameters included in this analysis were characteristics of piles, soil, and frequency of vibration. The low and high level of the factors were estimated based on reasonable values of parameters that could be expected in the field. In most cases, these parameters were kept at the same level as in the fractional factorial design described in the paragraph entitled "Sensitivity analyses of VPDA input parameters" and are shown in Table 15. A fractional factorial design 2^{12-7} was applied with 12 factors in 32 runs and the measured response was the rate of penetration for a required bearing capacity.

As in the initial investigation, the resolution of the design was four (IV), and main effects were aliased with three-factor interactions and two-factor interactions were confounded. It was again assumed that the three-factor interactions were not significant. The design with levels of each factor for each run is included in Appendix B.

The rate of penetration was calculated for four levels of bearing capacity: 45, 111, 178, and 245 kN. The factors were considered at the 95 percent significance level corresponding to a p-value equal to 0.05. For the measured response of the rate of penetration required for a bearing capacity of 45 kN, the following factors were identified as shown in Table 16:

a. Percentage of bearing capacity that is assigned to the tip of pile.

b. Type of soil model.

Table 15
List of Factors and Levels for Second Sensitivity Analysis

Factor	Description	Level -	Level +
1	Frequency of driving, Hz	22.5	25
2	Type of pile profile	pipe-pile	H-pile
3	Size of pile, mm (in.)	152.4 (6)	254.0 (10)
4	Length of pile, m (ft)	6.096 (20)	9.144 (30)
5	Type of soil model	Hyperbolic	Smith
6	Efficiency of vibrator, %	20	25
7	Stiffness of connector, kN/m (lb/in.)	227,665 (1,300,000)	262,690 (1,500,000)
8	Viscous damping of connector, N-sec/m (lb-sec/ft)	7,296 (500)	8,756 (600)
9	Pile capacity at tip, %	30	60
10	Unit weight of soil, kN/m^3 (pcf)	17.3 (110)	20.4 (130)
11	Damping of pile, N-sec/m (lb-sec/in.)	15,761 (90)	19,263 (110)
12	Velocity of shear wave, m/sec (ft/sec)	198.1 (650)	228.6 (750)

Table 16
Results of Second-Stage Sensitivity Analysis

Significant Input Parameters	p-value for Estimated Bearing Capacity			
(95% Significance Level)	45 kN	111 kN	178 kN	245 kN
Percentage of bearing capacity on tip of pile	0.000	0.001	0.008	0.045
Type of soil model	0.000	ns	0.013	ns
Efficiency	0.001	0.015	ns	ns
Size of pile	0.012	ns	ns	ns
Length of pile	0.026	ns	ns	ns
Frequency	0.027	ns	ns	ns

Note: ns = not significant (p>5).

c. Efficiency of vibratory driver.

d. Size of the pile.

e. Length of the pile.

f. Frequency of driving.

However, for increasing bearing capacities, the only input parameter that was significant at all levels of the measured response was percentage of bearing capacity at the tip of pile. The full listings of results are included in Appendix B.

Important input parameters to VPDA. VPDA was developed as a tool to predict bearing capacity based on the measured rate of penetration. The output of the program is the relationship between rate of penetration and bearing capacity. The effects of input parameters can be evaluated by studying graphs of rate of penetration versus bearing capacity for simulations having only one input parameter varied for a particular set of runs.

The relationship between the rate of penetration and bearing capacity is shown in Figure 22. In general, increased predicted bearing capacity occurred for piles having lower rates of penetration. The eccentric moment of the driver was also varied to observe the effect of this parameter. The greater the eccentric moment, the greater the predicted bearing capacity that can be reached for a given rate of penetration. This can be explained as the greater eccentric moment, the greater force is applied to the pile that results in higher bearing capacity.

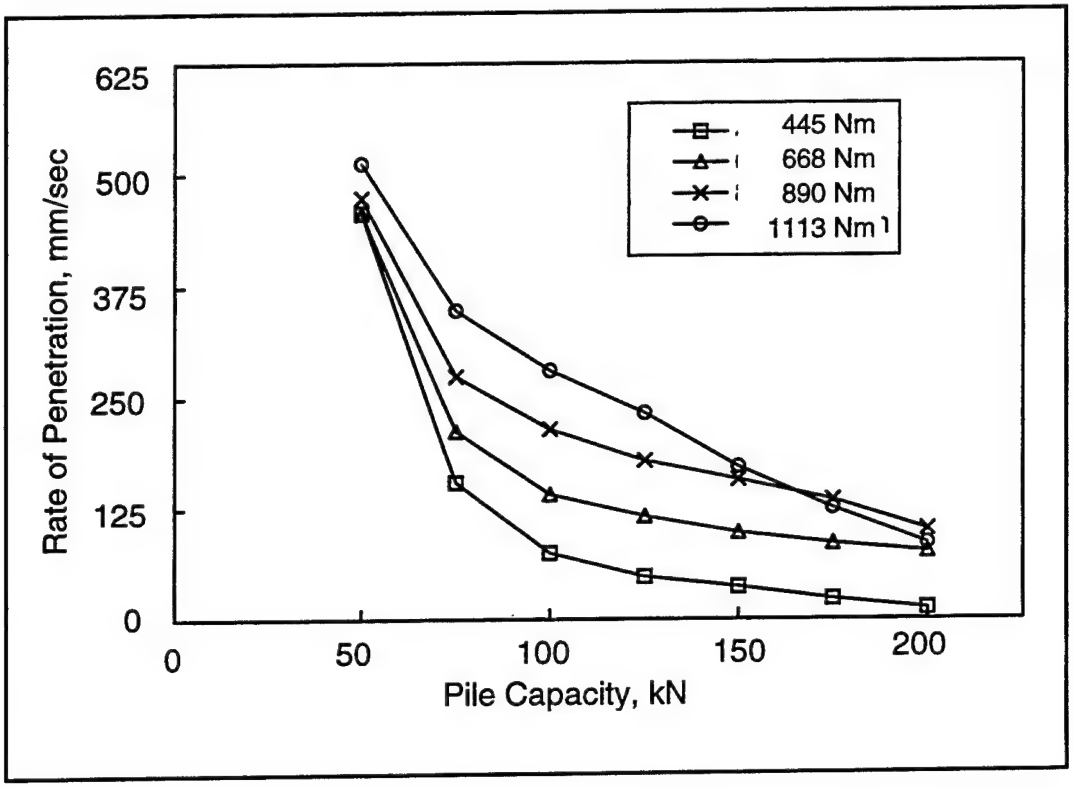

Figure 22. VPDA prediction rate of penetration versus pile-bearing capacity with variable eccentric moment (Smith Soil Model, H-pile length of 9 m, frequency of 25 Hz)

The percentage of load carried by the tip of the pile was varied and the results are shown in Figure 23. For a given predicted bearing capacity, the higher rates of penetration are predicted for piles in which less load is carried by the tip of the pile. The percentage of load carried by the tip of pile is an indicator of the ratio between bearing capacity of the tip and skin friction resistance. The higher the loads carried by the tip, the stronger the soil has to be under the tip of the pile. Thus, the vibrator would not be able to penetrate the soil when higher percentage of load carried by the tip of the pile is specified.

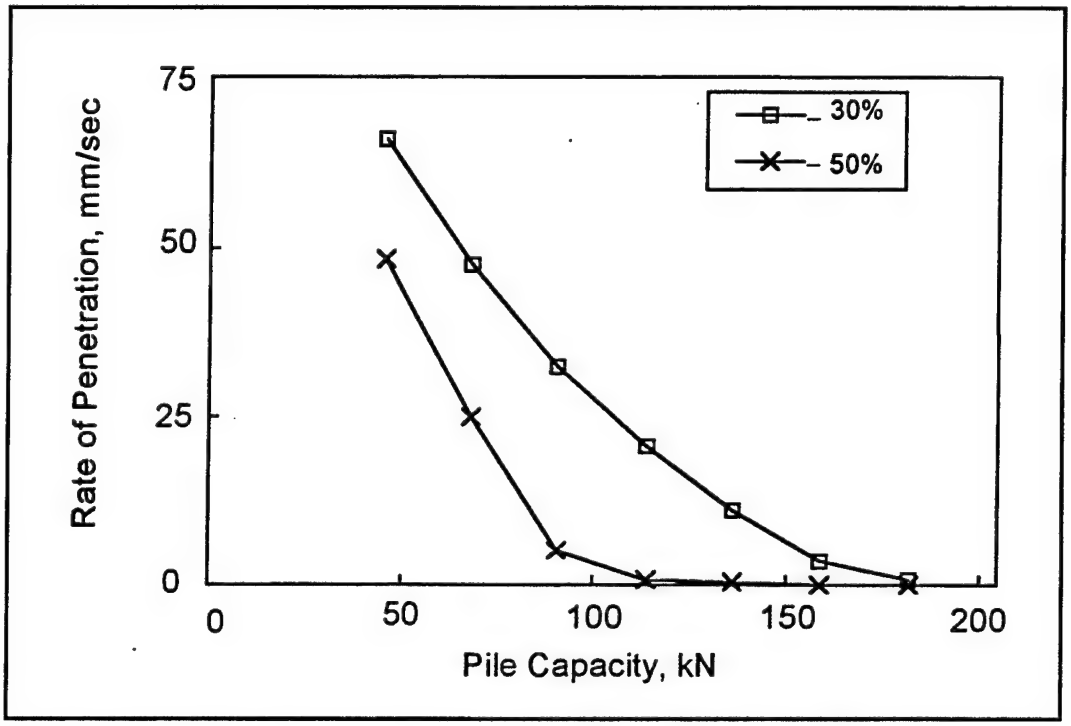

Figure 23. VPDA predictions of rate of penetration versus pile-bearing capacity for variable percentage of capacity on pile tip (hyperbolic soil model, 9-m H-pile length, 25-Hz frequency)

The type of soil model and length of pile were also varied and results are presented in Figure 24. The effect of the type of soil model is dramatic particularly for lower capacities. Using the Smith soil model, VPDA predicts higher rates of penetration at lower capacities for all pile lengths studied compared to predictions using the hyperbolic model. For the hyperbolic soil model, longer piles penetrate slower than the shorter piles of the same capacity according to VPDA.

The effect of frequency of the driver on the predicted rate of penetration for a fixed bearing capacity of 111 kN is shown in Figure 25. The VPDA predictions using Smith and hyperbolic soil models were studied for a range of frequency from 5 to 50 Hz. For the hyperbolic soil model, the rate of penetration has a peak at frequency about 14 Hz and again increases for frequencies higher than 30 Hz. For the Smith soil model, the rate of penetration increases up to a

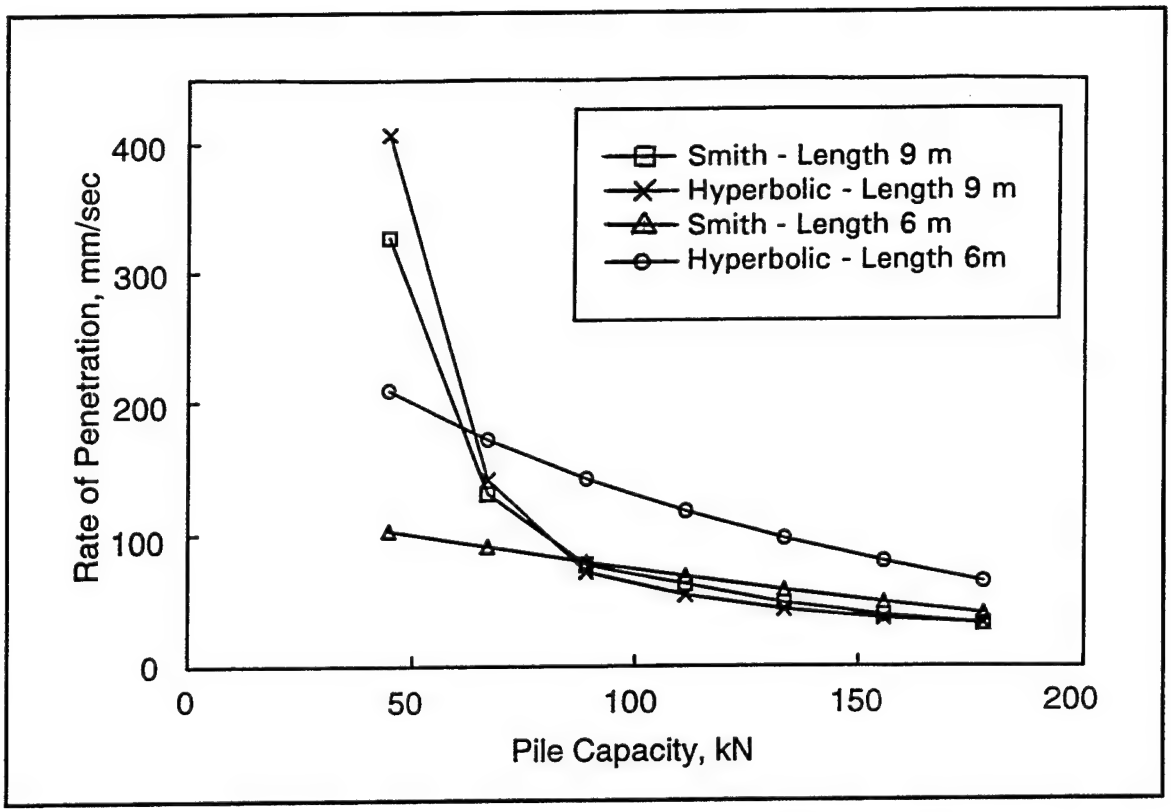

Figure 24. VPDA prediction of rate of penetration versus pile-bearing capacity with variable length of pile for both hyperbolic and Smith soil models (H-pile - 200-mm diam, 25-Hz frequency)

frequency of about 30 Hz and then begins to decrease. For the common range of frequencies, between 20 to 25 Hz, both soil models give similar results.

Results of experimental data analyses

Results of analyses of records collected during the field experiment on vibratory driven piles are presented in this section. The data collected in the field included the rate of penetration, frequency, amplitude, and dynamic and static strains on the pile. The measured response was a bearing capacity of piles evaluated by load testing. Results of analyses of the driving data are synthesized in this section and will be used to fit a stepwise linear regression in the paragraph entitled "Regression between bearing capacity and measured parameters."

The analysis was performed for all piles with four exceptions. The driving record of pile 6-20-B-H was lost due to transfer of the data. Portions of the driving records of piles 10-20-A-H, 8-30-A-H, and 6-30-A-H were damaged during transition from the field data acquisition system to the final storage system and are not included in the analysis.

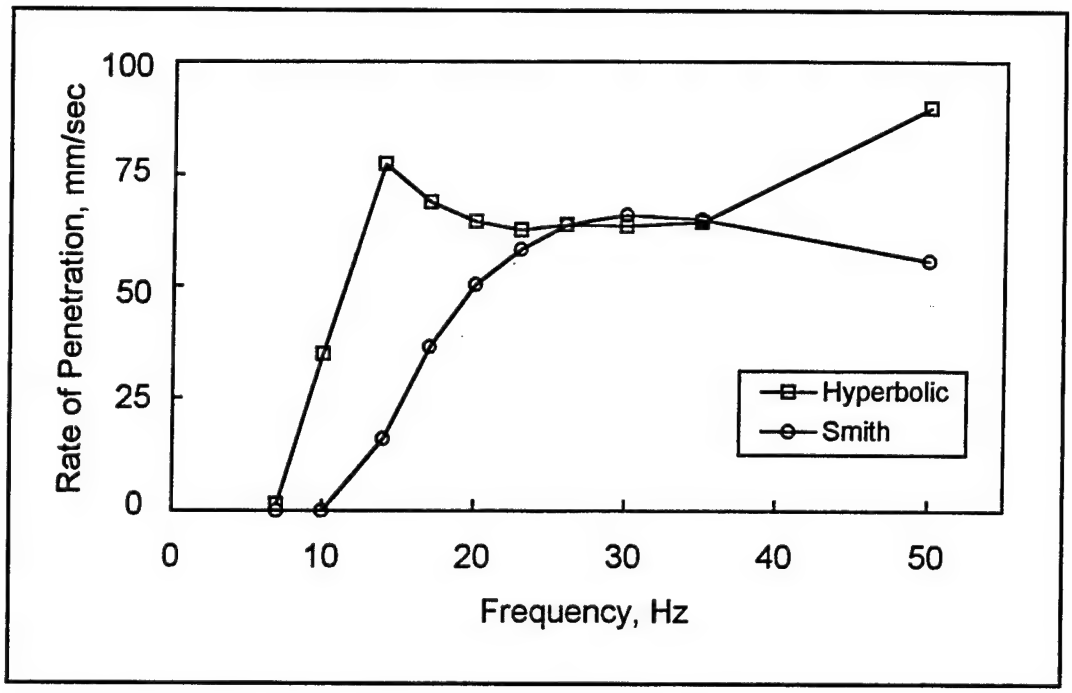

Figure 25. VPDA prediction of rate of penetration versus driving frequency for bearing capacity of 111kN

Rate of penetration. Rates of penetration were evaluated for all piles. The rates ranged from as low as 10 mm/sec to as high as 400 mm/sec. The measured rates of penetration in part were affected by construction practice during vibratory driving. The crane was supporting the vibratory driver to prevent lateral movement of the driver. To an embedded length of pile of about 3 m, the rate of penetration corresponded to the rate of release of the crane support rather than to the resistance of soil to penetration. For the initial 3 m of driving, the rate of penetration was about 50 mm/sec. After 3 m of driving, the crane support was intentionally released and the rate of penetration increased up to about 150 mm/sec (Figure 26). Graphs of rates of penetrations versus depth of pile tip for all experimental piles are included in Appendix C.

Due to the uncertainty regarding how much the crane influenced the measured rate of penetration, the relationship between the rate of penetration and the resistance of the soil is difficult to interpret. However, it was assumed, that the influence of the crane was smallest during the last portion of driving. Thus, for the regression analysis, the average rate of penetration (shown in Table 17) was estimated for the last part of driving (see Figure 26).

Frequency and acceleration amplitude of vibratory driving. The frequency and acceleration amplitude of vibratory driving were analyzed for 20 experimental piles. The amplitude of vibratory driving was measured in terms of peak acceleration. The characteristics that were common to all 20 piles were: (a) the frequency of the vibratory driver ranged from 23 to 25 Hz, and the variability of this measurement did not correlate to the

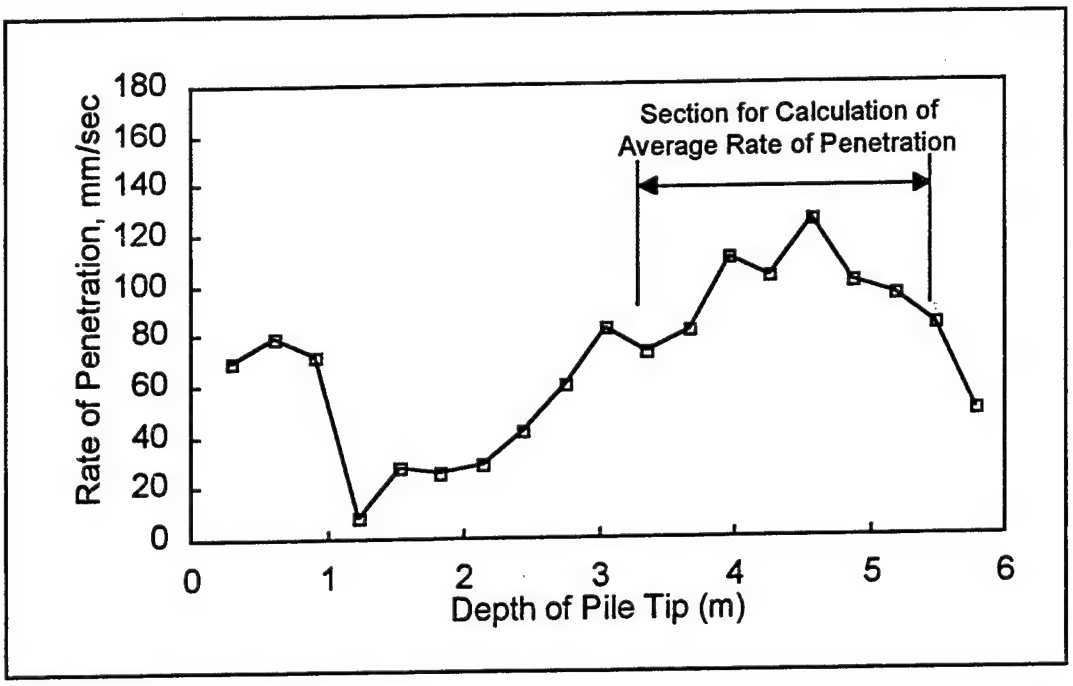

Figure 26. Typical record of rate of penetration (pile 8-20-P-A)

embedded length of pile, (b) the accelerations measured on the eccentric masses were in the range of 10 to 15 g, and (c) the acceleration at the bias mass was about 15 to 20 percent of the acceleration measured at the eccentric masses.

The results of analyses of the 20 piles were divided into three groups based on profiles of frequency and acceleration, as shown in Table 18. The first group was represented by 12 piles, 7 H-piles, and 5 pipe piles with variable lengths and diameters. This group of piles was characterized by the same frequency of vibration measured on the bias mass, the eccentric masses, at the top of the pile, and at the bottom of the pile. The accelerations at the top and bottom of the pile ranged from 95 to 110 percent of the accelerations measured at the eccentric masses. The piles in this group can be considered to vibrate as a rigid body with a stiff connection to the vibrator (Figure 27). These results are representative of results reported in the literature by Berhard (1968), Rodger and Littlejohn (1980), and Smith and To (1988). Since the majority of the piles behaved in this manner, they were labeled as "typical."

The second group of piles was represented by five pipe piles. The defining characteristic of these piles was that they had lower accelerations at the bottom of pile ranging between 5 to 25 percent of the accelerations measured at the eccentric masses as shown in Figure 28. Also, the frequency measured at the bottom of the piles decreased to about 16 Hz in parts of record. This kind of behavior developed for pipe piles having large diameters of 200 and 250 mm. A possible reason for this trend is increased damping on the tip of the pile due to plugging that developed during driving of pipe piles that resulted in wave behavior of the pile. For large-diameter pipe piles, the weight of the soil plug

Table 17
Rate of Penetration

Pile	Rate of Penetration, mm/sec
10-30-H-A	120
10-30-H-B	150
10-20-H-A	na
10-20-H-B	110
8 -30-H-A	na
8 -30-H-B	150
8-20-H-A	140
8-20-H-B	165
6-30-H-A	na
6-30-H-B	90
6-20-H-A	180
6-20-H-B	na
10-30-P-A	250
10-30-P-B	190
10-20-P-A	50
10-20-P-B	115
8-30-P-A	480
8-30-P-B	100
8-20-P-A	115
8-20-P-B	50
6-30-P-A	380
6-30-P-B	152
6-20-P-A	75
6-20-P-B	80

Note: na = not available.

Table 18
Groups of Piles Based on Frequency and Acceleration Profiles

Type of Behavior	Piles	
Typical	10-30-H-A	8-20-H-B
	10-30-H-B	6-30-H-B
	10-20-H-B	6-30-P-B
	10-20-P-A	6-20-H-A
	10-20-P-B	6-20-P-A
	8-20-H-A	6-20-P-B
Plugging	10-30-P-A	8-20-P-A
	10-30-P-B	8-20-P-B
	8-30-P-A	
Atypical	8-30-H-B	6-30-P-A
	8-30-P-B	

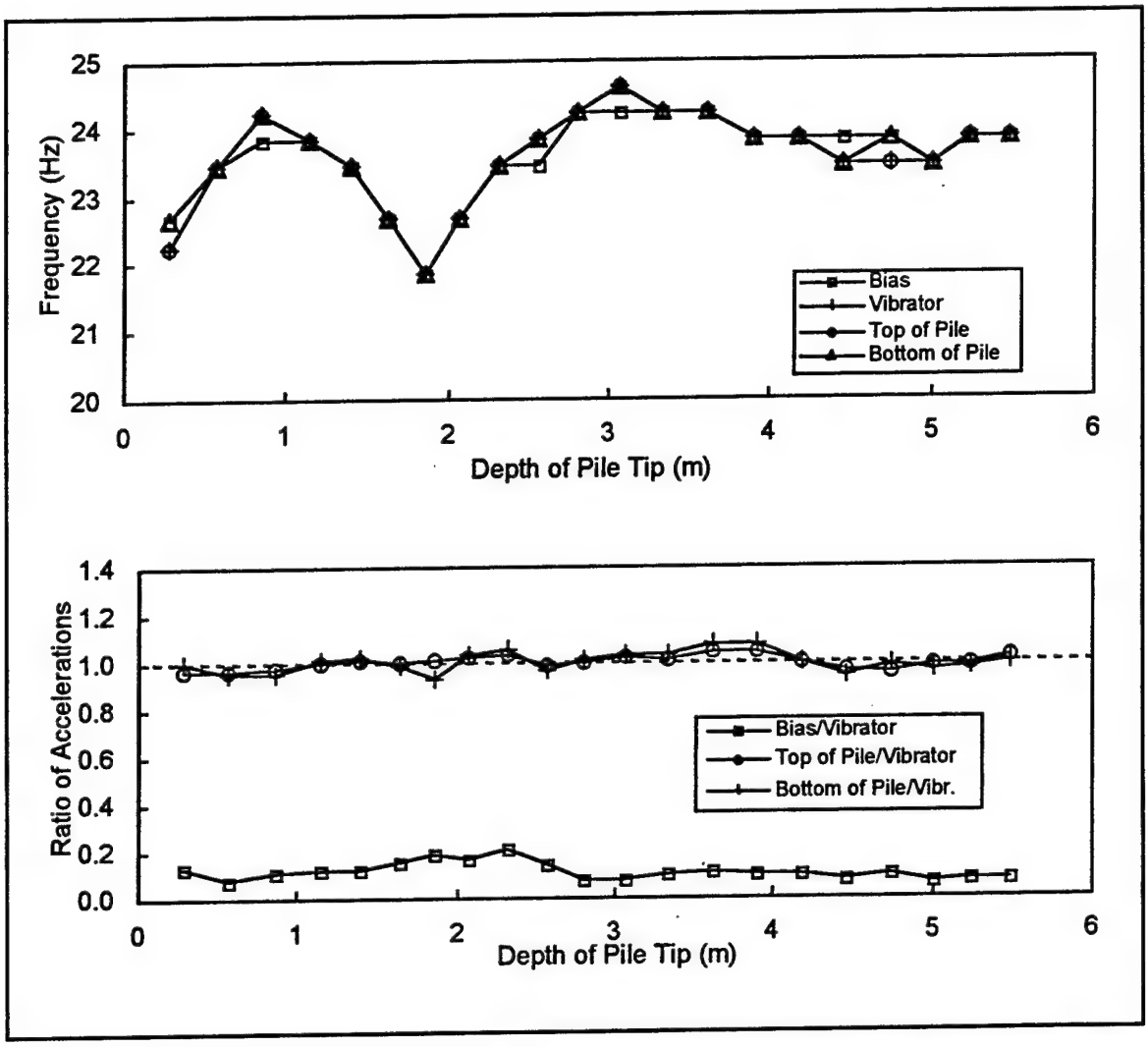

Figure 27. Typical record of frequency and amplitude for piles considered to vibrate as a rigid body (pile 10-20-H-B)

might contribute to the damping at the bottom of pile. That did not occur either for pipe piles of small diameter since the weight of soil plug was lower, nor for the H-piles, because those did not develop plugs.

The frequency and acceleration data from the pile driving operation was not always as consistent as that shown in Figure 28. For pile 8-20-P-B, the acceleration measured at the bottom of pile increased from about 20 to 100 percent of the acceleration measured at the eccentric masses at the depth of penetration about 4.5 m. However, for the other replicate pile 8-20-P-A, the acceleration at the bottom of pile decreased from 100 percent of acceleration measured at the eccentric masses to about 20 percent as shown in Figure 29. There was not a large difference between the frequency record for these two piles. Such a change in the nature of behavior during driving of the pile may be due to soil variability as the pile penetrated the soil deeper. Differences in side friction

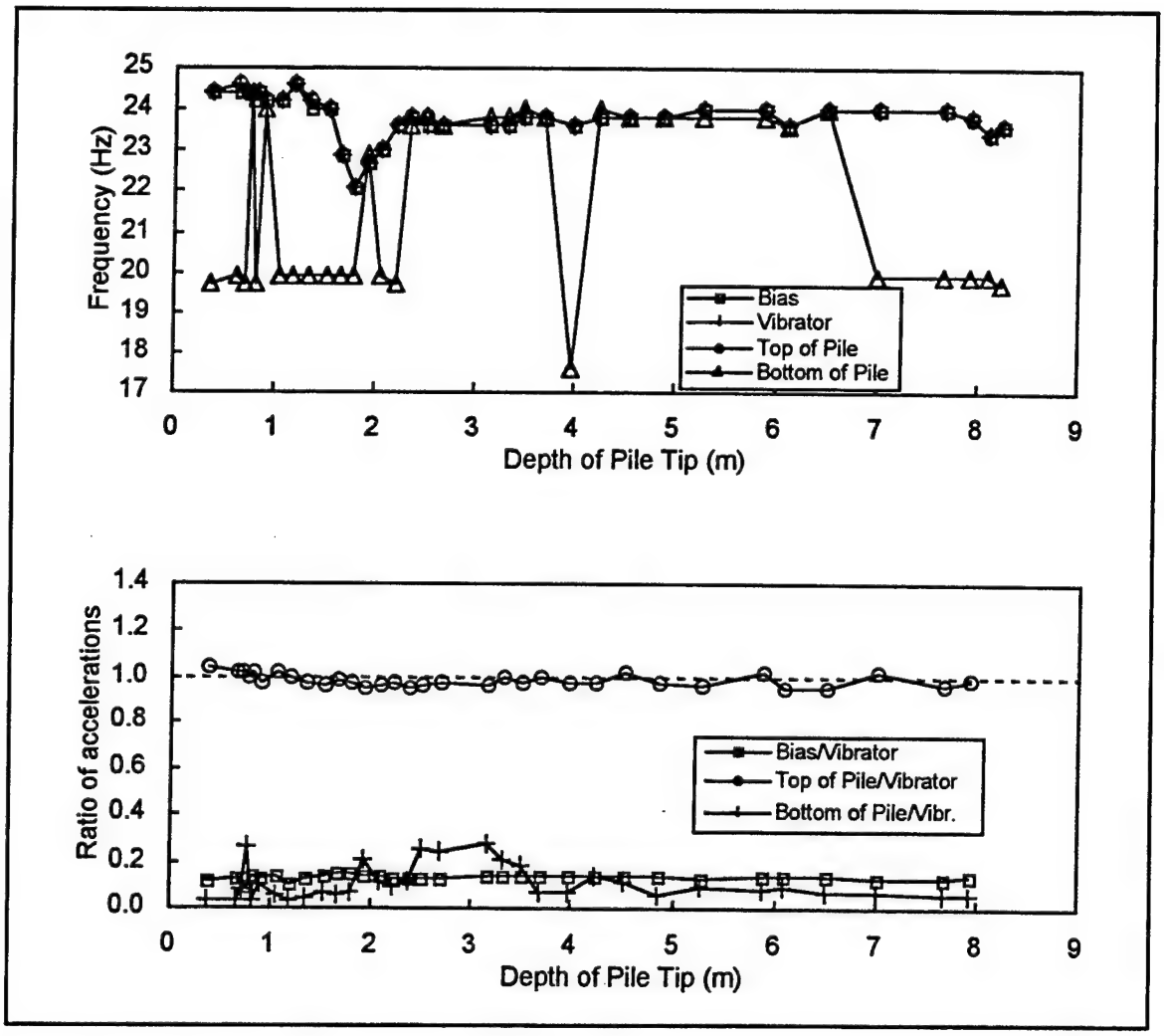

Figure 28. Effect of plugging on record of frequency and acceleration amplitude (pile 8-30-P-A)

between sand and clay may be what caused the change in the behavior of pile from rigid body to wave behavior.

The third group of pile behavior was characterized by piles that had inconsistent trends in frequency and amplitude that could not be classified in either of the first two groups. Three piles were placed into this group. For pile 8-30-B-H, the frequency measured at the top and bottom of pile dropped to about 20 Hz compared to 24.5 Hz measured at the masses for the same period of driving as shown in Figure 30. For pile 8-30-B-H, the acceleration at the bottom of pile is only about 15 percent of acceleration measured on the eccentric masses. The acceleration at the top of pile varied from about 30 to 120 percent of acceleration at the eccentric masses. The profiles of frequency and amplitude were atypical for piles 8-30-B-P and 6-30-A-P possibly due to damage of the instruments. All the profiles of frequency and acceleration are included in Appendixes D and E.

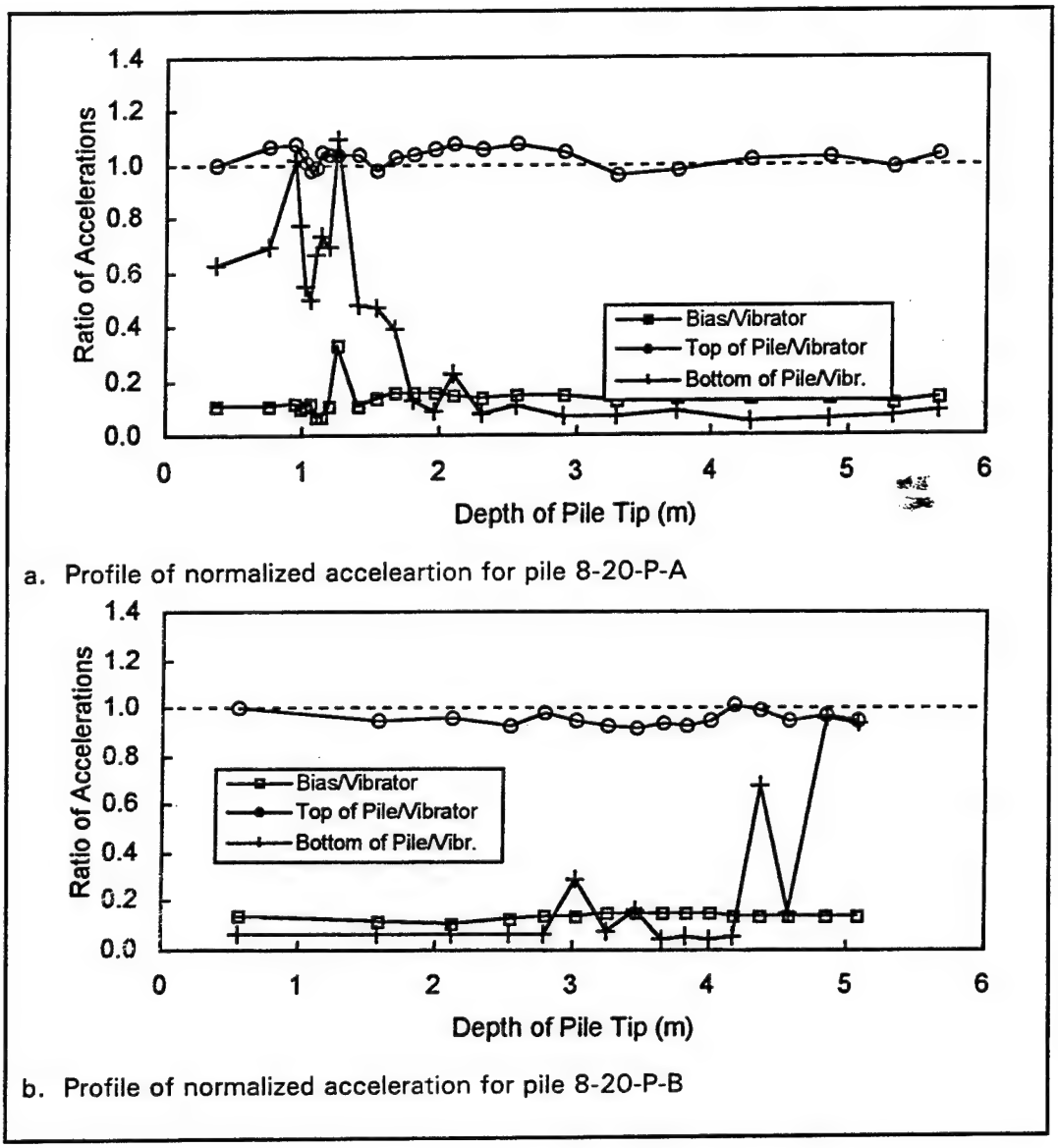

Figure 29. Comparison of acceleration record for two identical piles

Strain during driving. The strain recorded during driving was studied in terms of dynamic and static strain. The dynamic portion of strain is due to the dynamic motion of the vibrator and was measured as the amplitude of a dynamic signal. The static portion of strain was considered as a mean value of strain occurring during driving.

Dynamic strain. For most of the records, dynamic strain did not change with increasing embedded length. The behavior of the piles was divided into three groups with respect to the dynamic strain measured at the top and bottom of the pile, as shown in Table 19. For the first group of nine piles, the dynamic strain at the top of the pile was higher than the dynamic strain

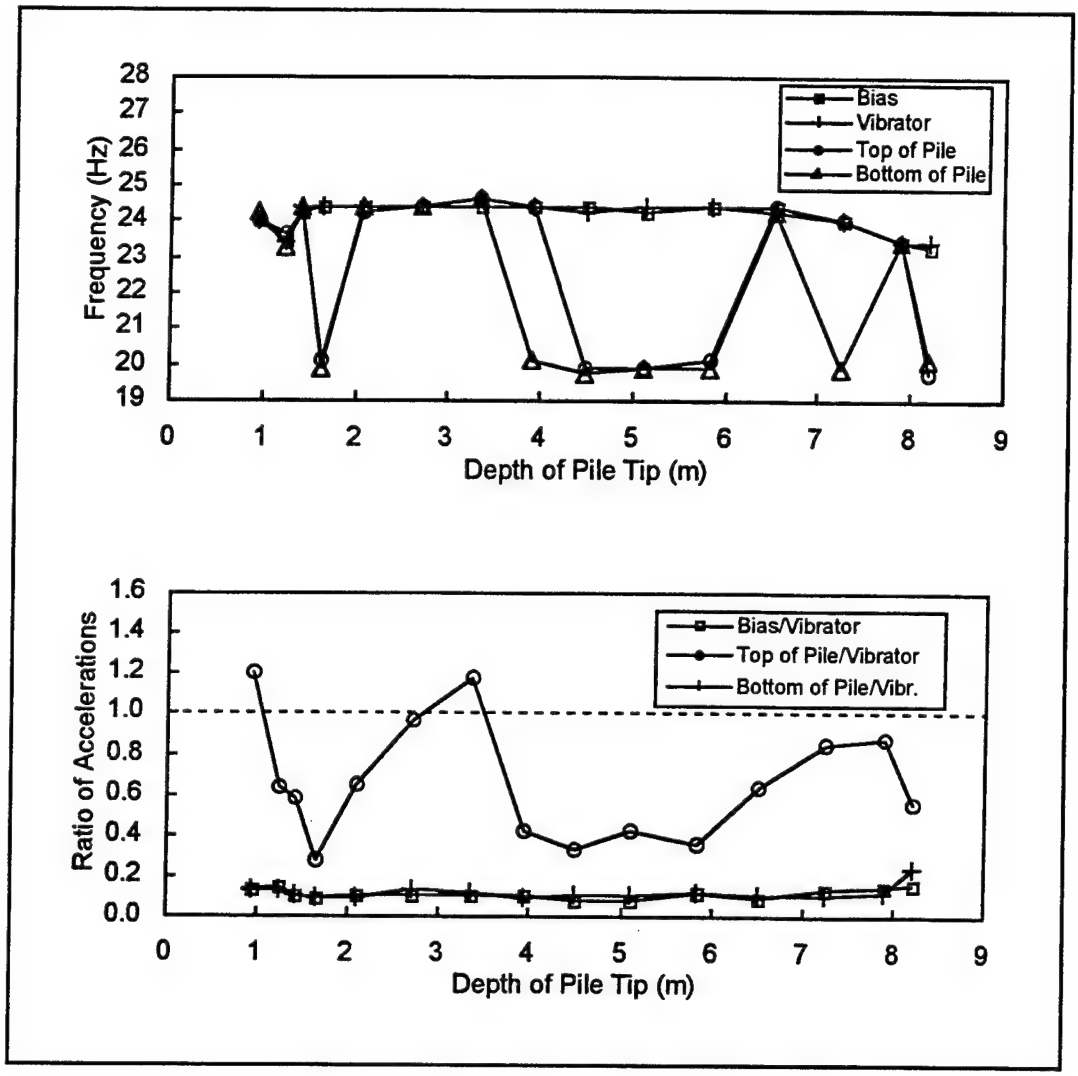

Figure 30. Atypical profile of frequency and amplitude (pile 8-30-B-H)

measured at the bottom of the pile, referring to Figure 31. The dynamic strain at the top of the pile ranged from 0.003 to 0.007 percent. At the bottom of the pile, the dynamic strain was about 0.002 to 0.004 percent. This type of behavior is expected because the skin friction resistance along the side of pile reduces the amplitude of dynamic strain measured at the bottom of the pile.

The second group of seven piles is characterized by dynamic strain that is about the same at the top and bottom of the pile (Figure 32). This type of behavior appeared during driving of both pipe and H-piles having smaller diameters of 250 and 300 mm. Piles having a smaller diameter have a smaller area for skin resistance. Thus, the reduction of dynamic strain at the bottom of the pile did not occur.

Table 19
Groups of Piles Based on Dynamic Strain Behavior

Type of Behavior	Piles	
Dynamic strain at the top higher than at bottom of pile	10-30-H-A	8 -30-H-B
	10-30-H-B	8-20-H-B
	10-30-P-B	6-30-H-B
	10-20-H-B	6-20-H-A
	10-20-P-A	
Dynamic strain at the top about the same as at the bottom	8-30-P-A	8-20-P-B
	8-30-P-B	6-30-P-A
	8-20-H-A	6-20-P-B
	8-20-P-A	
Dynamic strain at the bottom higher than at the top	10-30-P-A	6-30-P-B
	10-20-P-B	6-20-P-A

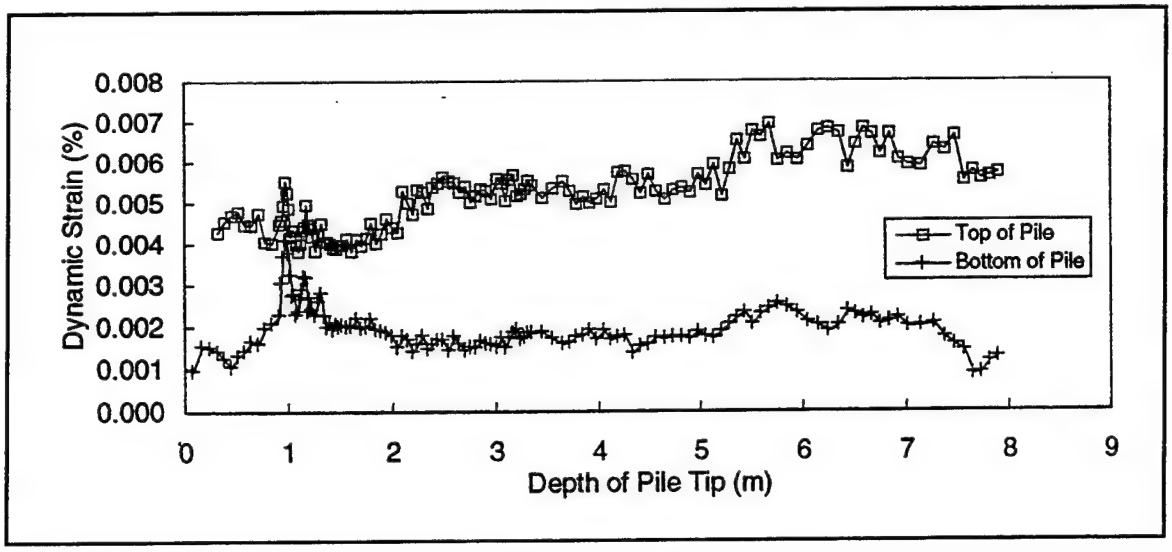

Figure 31. Typical profile of dynamic strain (pile 10-30-H-B)

For the third group of piles, the dynamic strain at the bottom of the piles is higher than that at the top of piles (Figure 33). Four piles were classified into this group. A possible explanation for such a behavior is that the oscillation occurred at the bottom of pile causing an increase in dynamic strain. The profiles of dynamic strain for all piles are included in Appendix F.

Static strain. Records of static strain were referenced to the point of zero strain defined during the calibration. This referencing resulted in strain profiles that had different levels of strain but similar relative change in level of strain. The difference may be due to the definition of zero strain during

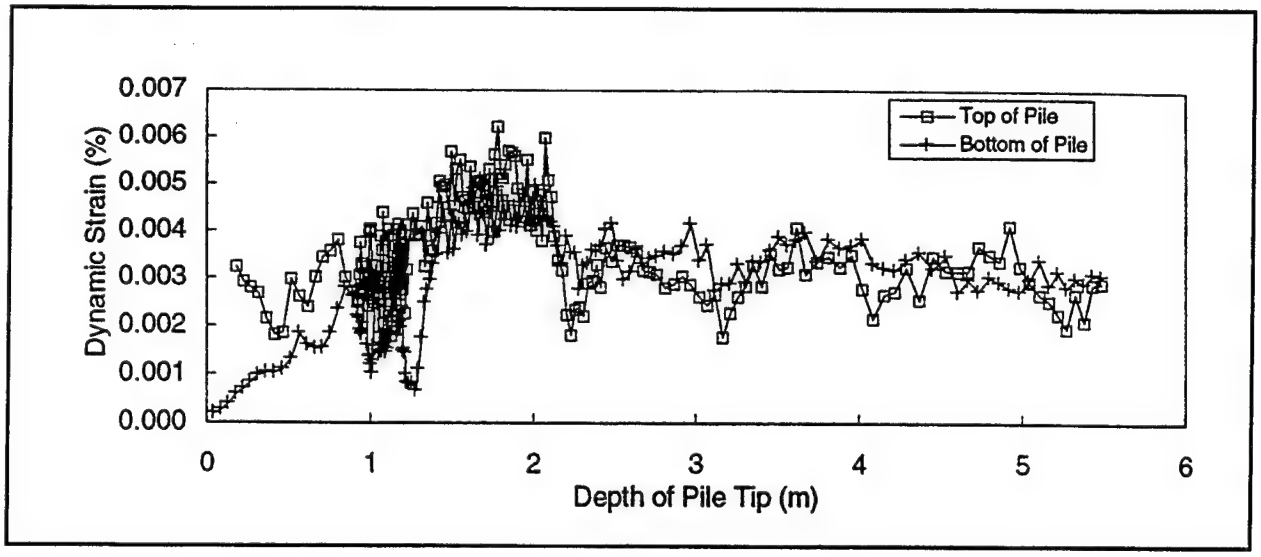

Figure 32. Typical profile of dynamic strain with same level of strain at top and bottom of pile (pile 8-20-P-A)

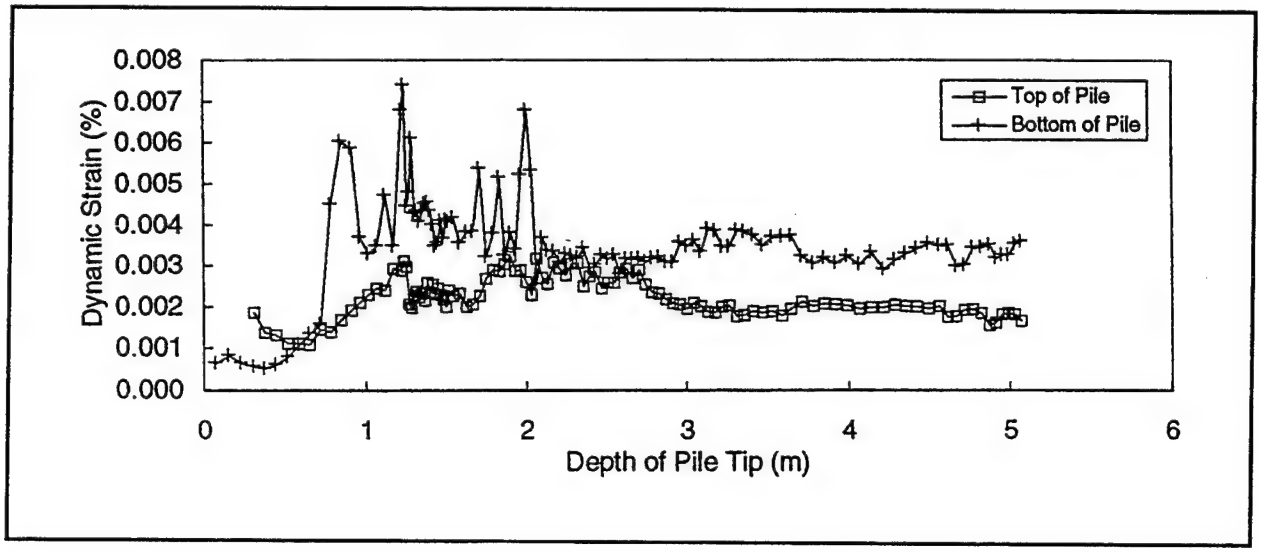

Figure 33. Atypical profile of dynamic strain (pile 10-20-P-B)

calibration. In this section, the static strain was analyzed to capture the trends occurring during vibratory driving. An increase in static strain represented an increase in compression, and the decrease in static strain represented an increase in tension. Also, the magnitude of the change of the static strain has to be evaluated with respect to uncertainty of calibration factors that were used in calculations of static strain.

The piles were divided into two groups with respect to the profile of static strain at the top (Table 20). For the first group of nine piles, the static strain

Table 20
Type of Profiles of Static Strain Measured at Top of Pile

Type of Behavior	Piles	
First increasing, then decreasing	10-30-H-B	8-20-P-B
	10-20-H-B	6-30-H-B
	10-20-P-B	6-30-P-B
	8-20-H-A	6-20-P-A
	8-20-H-B	
Small changes in static strain	10-30-H-A	8-30-P-A
	10-30-P-A	8-20-P-A
	10-30-P-B	6-30-P-A
	10-20-P-A	6-20-H-A
	8-30-H-B	6-20-P-B

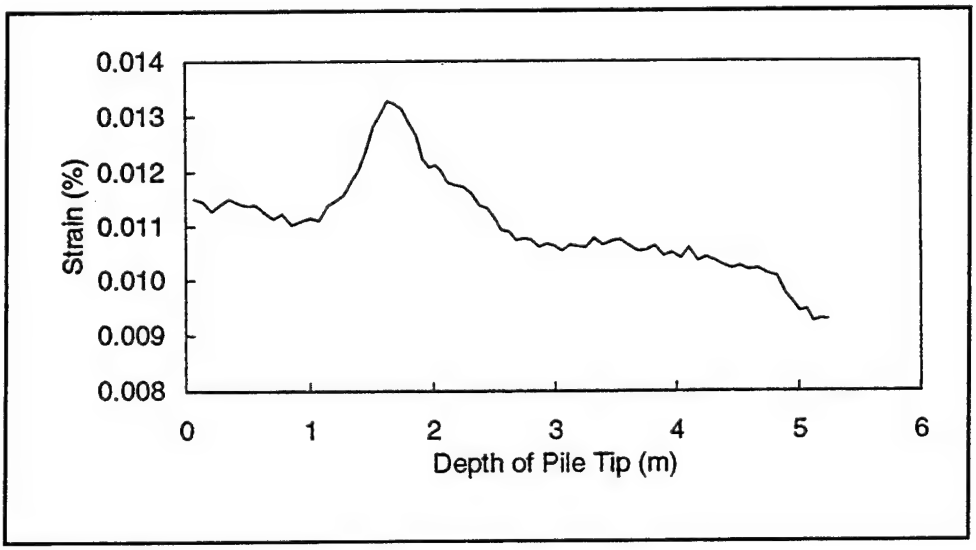

Figure 34. Trend in static strain at top of pile (pile 10-20-H-B)

increased to an embedded length of about 2 m and then decreased to about the same level as that at the beginning of driving, as shown in Figure 34. The increase in static strain corresponds to the penetration of the clay layer near the surface. The increase in static strain may correspond to more resistance of the soil to penetration at that depth and the decrease in strain may be indication that the pile was penetrating through the sand layer. For the second group of the piles, the static strain at the top of pile did not change markedly during driving. Profiles of static strain at the top of pile for all piles are shown in Appendix G.

At the bottom of the pile, the profiles of static strain were divided into four groups, as shown in Table 21. For nine piles, the static strain decreased at a

Table 21
Profile of Static Strain Measured at Bottom of Pile

Type of Behavior	Piles	
First decreasing, then constant	10-30-H-A	8-30-H-B
	10-30-H-B	8-20-H-B
	10-30-P-B	6-30-H-B
	10-20-P-A	6-20-H-A
	10-20-P-B	
First decreasing, then increasing	8-30-P-A	6-20-P-A
	8-20-P-A	6-20-P-B
Decreasing	10-20-H-B	
	8-20-H-A	
Inconsistent profiles	10-30-P-A	6-30-P-A
	8-30-P-B	6-30-P-B

depth of pile tip about 2 m and then stayed about constant for the rest of driving (Figure 35a). The second group of piles consists of four pipe piles. For those piles, the strain first decreased as in case of the first group and then started to increase (Figure 35b). For two of the H-piles, the strain was decreasing with increasing embedded length of pile (Figure 35c). The remaining piles had inconsistent trends. The profiles of static strain at the bottom for all piles are shown in Appendix G.

The static strain can be compared in terms of relative change of strain that occurred during driving. The change occurring at the top of pile were on the order of about 0.002 to 0.004 percent and at the bottom of pile about 0.01 percent.

Power and energy during driving. The power delivered to the pile from the vibratory driver was evaluated for the piles that have uncertainty in calibration factors of less than 6 percent. The power delivered to the top of the pile was relatively constant for the duration of driving. A typical relationship between power delivered to top of pile and depth of pile tip is shown in Figure 36. The average value of power was evaluated for the driving and ranged from 13 to 31 kNm/sec (Table 22). The total energy delivered to the top of pile was also calculated for those piles, as presented in Table 22.

Evaluation of bearing capacity

The bearing capacity of piles was evaluated using two theoretical methods and compared with the static load tests. Results and comparisons of the bearing capacities obtained by the different methods are presented in this section.

Predicted static-bearing capacity. Static-bearing capacities were predicted prior to load testing using the Meyerhof (1976), Vesic (1977), and Briaud et al.

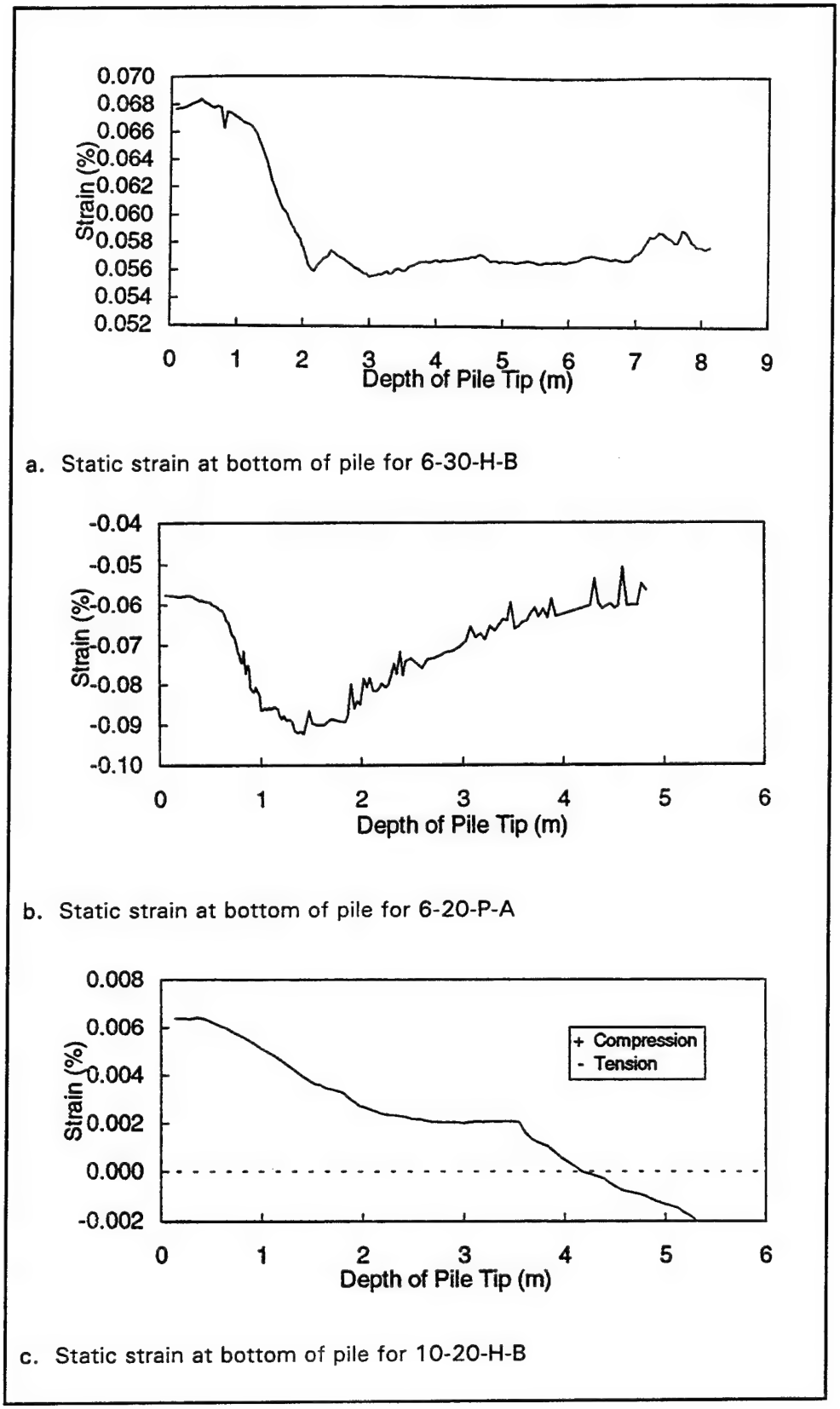

a. Static strain at bottom of pile for 6-30-H-B

b. Static strain at bottom of pile for 6-20-P-A

c. Static strain at bottom of pile for 10-20-H-B

Figure 35. Trends in static strain at bottom of pile

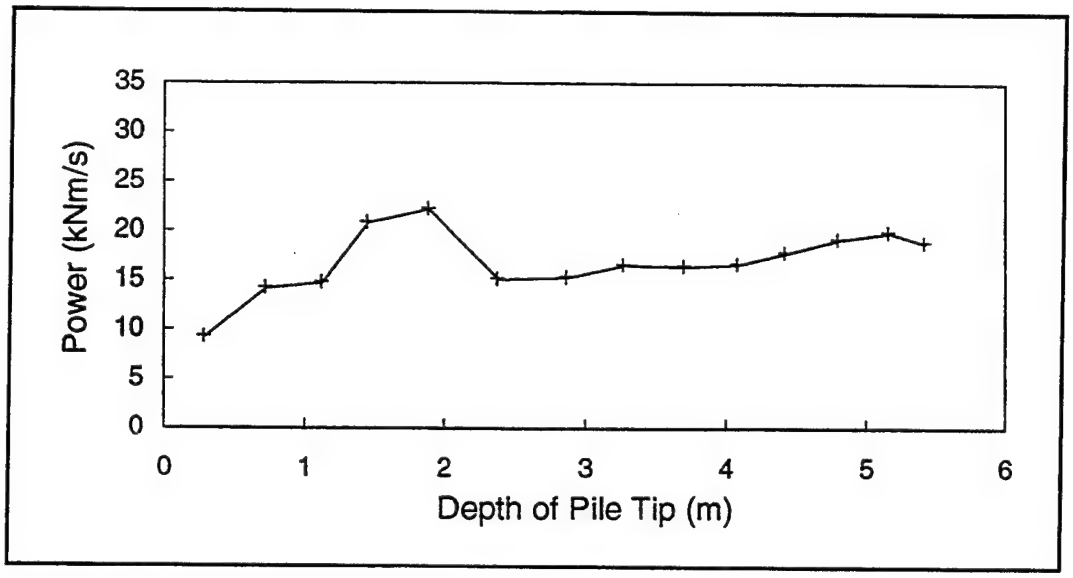

Figure 36. Profile of power delivered to top of pile (pile 8-20-H-A)

Table 22
Power and Energy Delivered to Top of Pile

Pile	Power, kNm/sec	Energy, kNm
10-30-H-A	31.13	3,497
10-30-H-B	22.84	2,069
10-20-H-B	19.08	994
8-20-H-A	17.54	659
8-20-H-B	20.86	929
6-30-H-B	20.26	2,289
6-20-H-A	13.40	804
10-20-P-B	16.07	1,018
8-20-P-A	20.96	2,756
8-20-P-B	15.08	1,345
6-30-P-B	18.03	3,231
6-20-P-A	20.44	2,078

(1985) methods described in the paragraph entitled "Static-bearing capacity." The representative soil profile with the blow counts was used for soil data inputs, as reported in Figure 1. Results of these calculations are presented in Table 23.

Capacity determined from VPDA. The bearing capacity predicted by VPDA for rates of penetration observed in the field was evaluated. The calculation was made using the parameters of ICE 416L vibratory driver (Table 4) and average values of input parameters into VPDA for the soil models

Table 23
Static-Bearing Capacity of Piles

Piles			Bearing Capacity		
Type	Size mm	Length m	Meyerhof kN	Vesic kN	Briaud kN
H-pile	254	9.14	845	875	925
		6.10	615	535	721
	203	9.14	620	625	674
		6.10	435	370	513
	152	9.14	435	430	471
		6.10	295	250	349
Pipe-pile	273	9.63	730	760	793
		6.31	535	470	623
	216	9.20	535	540	579
		6.40	375	320	444
	168	9.60	375	365	402
		6.40	260	220	299

(Table 3). The calculation was made for all sizes and lengths of piles that were driven during the field experiment.

In Figure 37, the rates of penetrations versus pile capacities predicted by VPDA are plotted for both the Smith and hyperbolic soil models. The differences between pipe piles and H-piles were small, thus the bearing capacity is estimated based only on size and length of the pile. In most cases, the rates of penetration measured during vibratory driving were much greater than rates of penetration predicted using VPDA for bearing capacities as low as 45 kN. In fact, when parameters from the driver used in the field are input into VPDA, results from VPDA report that it is impossible to achieve the motion that actually occurred in the field. This effect is shown in Figure 37. The rates of penetration in the field were on average about 150 mm/sec, and the highest rate of penetration that VPDA predicts is 130 mm/sec for the Smith soil model for pile having bearing capacity of about 45 kN.

Additional efforts were made to determine the changes in soil-structure interaction coefficients needed to produce VPDA penetration rates similar to those measured in the field. It was found that the Smith quake and damping parameters needed to be decreased by over 95 percent with the efficiency increased to 100 percent to achieve VPDA results similar to field results. These soil-structure interaction coefficients are unreasonable from the perspective of other wave equation methods based on impact hammer research.

A key finding of this research is that the common soil-structure interaction parameters used in impact hammer driving do not apply to most vibratory driving. Significantly different parameters are required. The primary reason is

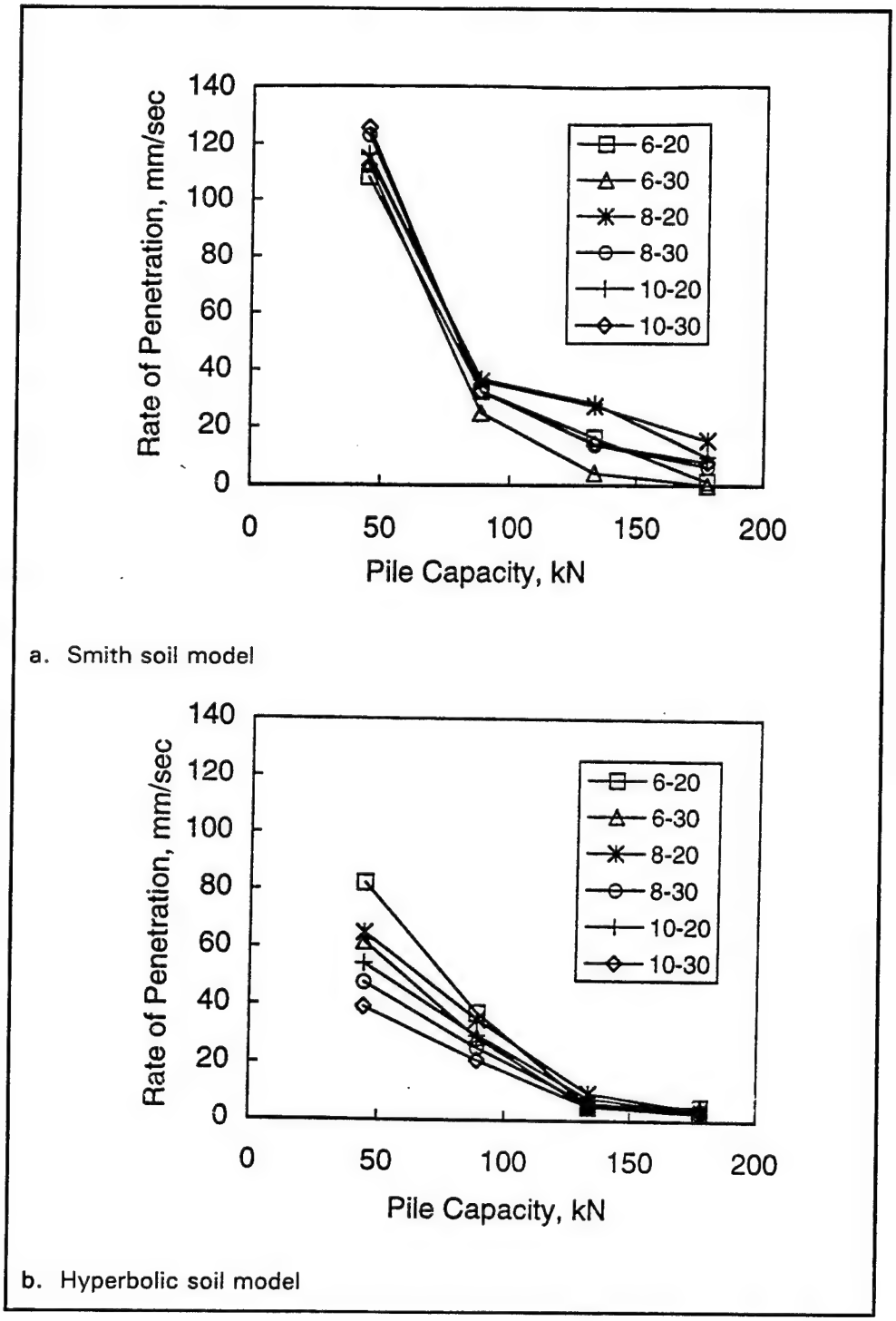

Figure 37. VPDA prediction of rate of penetration versus pile-bearing capacity

due to the dramatic increase in strain seen by the nearby soils during vibratory driving. These higher levels of strain in turn produce a dramatic reduction in shear modulus in the soils, effectively reducing the stress transfer between pile and soil. The soil and pile are acting more independently of each other during vibratory driving compared to similar piling driven with an impact hammer. Thus reductions of the Smith quake parameters by 95 percent may be reasonable during vibratory driving.

The prediction prior to driving of appropriate soil-structure interaction terms is, however, problematic. In some cases, especially in soils with greater amounts of cohesion, the interaction parameters are more similar to the suggested values for impact driving. The amount of cohesion necessary to cause this change is not known. This information will only come through the driving of instrumented piling in a variety of characterized soils so that correlations can be drawn based on index testing of soils (grain-size distribution and plasticity values). Alternatively, use of an instrumented tool to probe prospective sites could also provide an in situ test which would not require laboratory testing.

Bearing capacity determined by analysis of load tests. The ultimate bearing capacity was determined from static load tests performed on the experimental piles using three methods: (a) Davisson limit load method (Davisson 1972), (b) Brinch-Hansen method (Brinch-Hansen 1963), and (c) Chin-Kondner method (Chin 1970). Also, the load needed to result in pile displacement of 10 percent of the diameter of the pile was determined as an indicator of ultimate bearing capacity. The maximum loads reached during the load test are also shown in Table 24. In some cases, the ultimate bearing capacities predicted by methods of Brinch-Hansen and Chin-Kondner were higher than the load reached during the load test. In those cases, the ultimate bearing capacity was reduced to the maximum load reached during load test as suggested by Fellenius (1990). In most cases, the ultimate bearing capacities predicted by different methods were in good agreement. However, the ultimate bearing capacities predicted by the Davisson method were conservative (Figure 38), which is consistent with the literature (Fellenius 1990).

In most cases, the load test curves have a typical load curve shape. Figure 39 demonstrates the shape of the curve. The curves experience no sudden change in slope. However, for some piles, such as pile 10-30-P-B, an unusual load displacement relationship occurred. For pile 10-30-P-B, the displacement was increased linearly with increasing load (Figure 40). Another unusual pile was 6-20-P-B. This pile moved about 10 mm without any resistance, and after that a load curve having the usual shape developed. This may have occurred due to the final portion of driving. It is likely that the crane operator pulled the pile out of the ground after driving. During the load test, the initial load may have pushed the pile back down after which it began to take up the load in the usual way.

The results of the load tests show the variability of the bearing capacities that are achieved by piles. The variability was calculated as a change in ultimate bearing capacity for the replicate piles, as shown in Figure 41. The ultimate bearing capacity was determined by the Davisson method.

Table 24
Ultimate Bearing Capacity Determined by Analysis of Load Tests

Pile	Maximum Load Reached kN	Ultimate Bearing Capacity			
		Davisson[1] kN	Brinch-Hansen[1] kN	Chin-Kondner[1] kN	Movement of 0.1B kN
10-30-H-A	480	408	480	447	nr
10-30-H-B	552	302	552	552	421
10-20-H-A	445	330	418	445	429
10-20-H-B	320	261	276	320	318
8 -30-H-A	400	262	378	387	371
8 -30-H-B	418	297	405	374	361
8-20-H-A	240	173	240	240	219
8-20-H-B	187	164	182	178	180
6-30-H-A	222	201	206	222	216
6-30-H-B	338	302	328	338	323
6-20-H-A	80	72	81	85	78
6-20-H-B	125	92	123	125	113
10-30-P-A	471	278	471	423	409
10-30-P-B	311	116	149	311	198
10-20-P-A	383	267	374	383	358
10-20-P-B	329	178	325	329	284
8-30-P-A	151	125	146	151	144
8-30-P-B	276	187	280	276	257
8-20-P-A	205	116	205	205	188
8-20-P-B	427	294	427	427	374
6-30-P-A	71	62	67	73	62
6-30-P-B	160	98	160	160	141
6-20-P-A	249	196	247	249	239
6-20-P-B	169	89	169	169	100

Note: nr = movement of 0.1B was not reached.
[1] References are listed following main text.

Regression between bearing capacity and measured parameters

Initially, simple linear regressions were investigated between each of the parameters measured during driving and bearing capacity to identify any potential for correlation. In the second part, the stepwise linear regression was used to develop a model for prediction of bearing capacity.

Initial exploration of trends. Regression analysis was performed to determine if any relationship between bearing capacity and measured static and

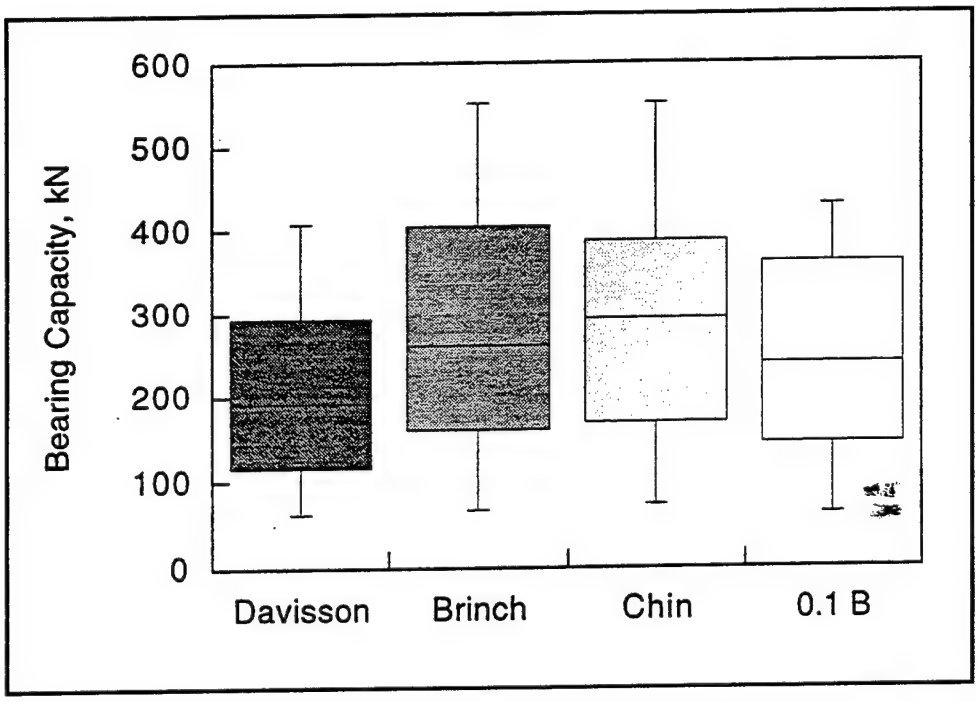

Figure 38. Comparison of average bearing capacity predicted by different methods

dynamic parameters obtained from driving records. The parameters considered in the regression analysis were:

a. Frequency of driving.

b. Acceleration.

c. Diameter of pile.

d. Embedded length.

e. Type of pile.

f. Length of plug.

g. Dynamic and static strain at the end of vibration.

h. Maximum change in static strain during driving.

i. Energy delivered to top of pile.

j. Power delivered to top of pile.

The regression analysis was made for predictions of bearing capacity using the Davisson method for evaluation of load tests. The Davisson method was

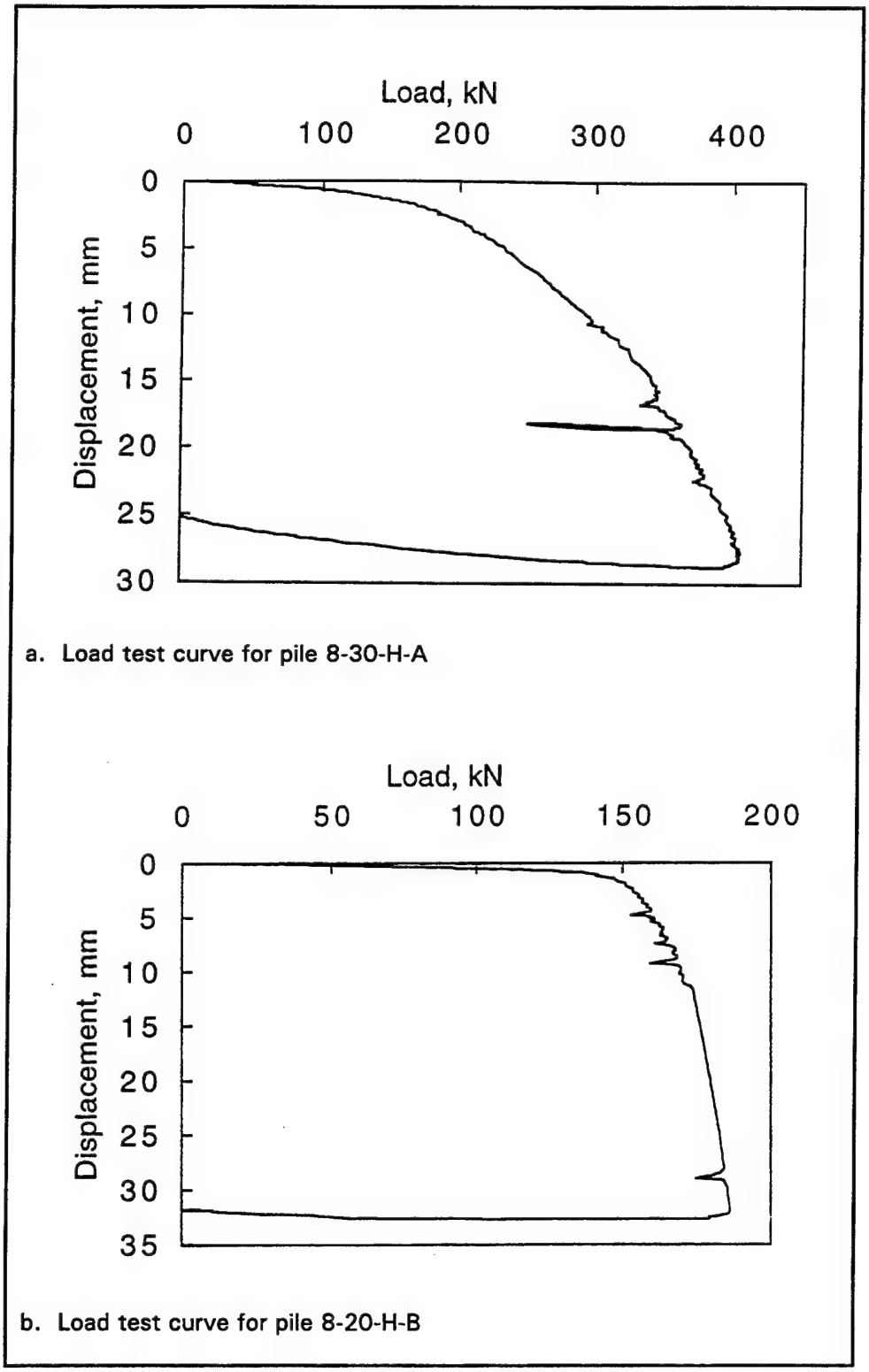

Figure 39. Sample load test curves

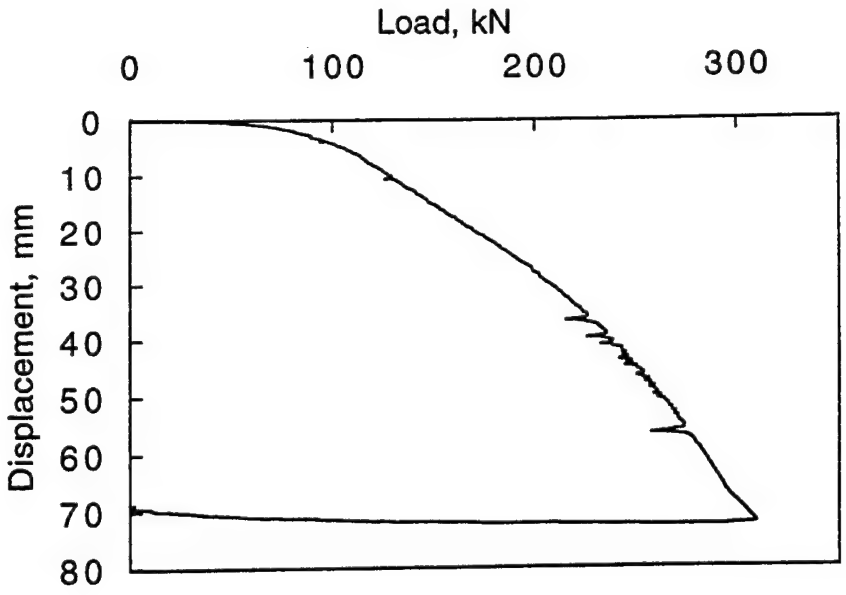

a. Load test curve for pile 10-30-P-B

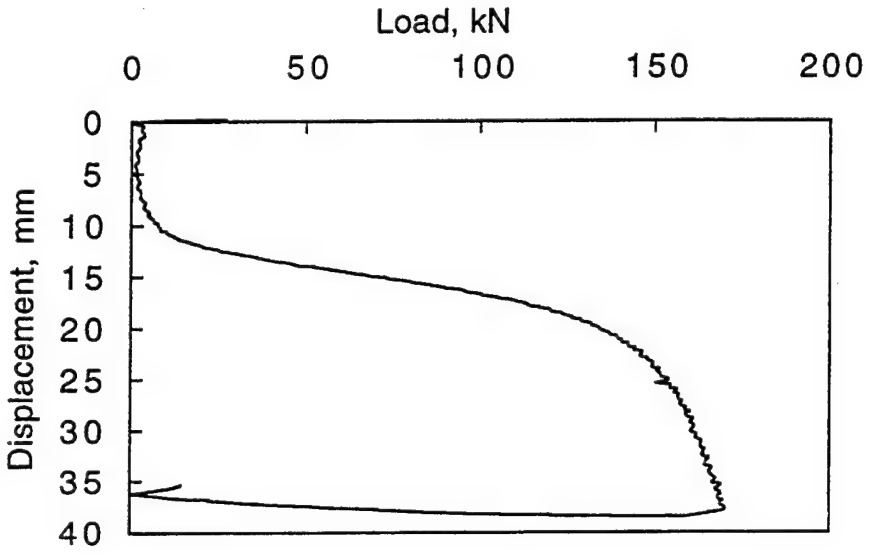

b. Load test curve for pile 6-20-P-B

Figure 40. Atypical load test curves

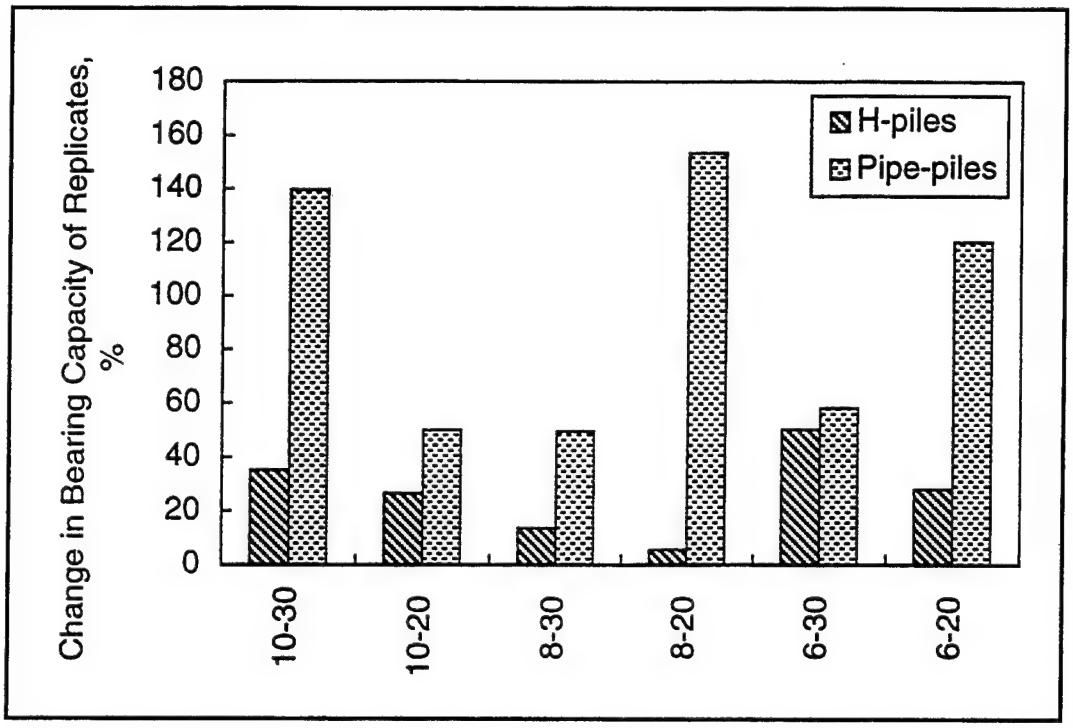

Figure 41. Change of bearing capacity of replicate piles

selected because it is the method that is most commonly used for interpretation of load test curves (Fellenius 1990).

Graphs of bearing capacity versus studied parameters were constructed and examined for both increasing or decreasing trends. For trends that appeared significant, linear regression was used to evaluate their significance. The proportional relationship between the bearing capacity and a parameter, x, was studied in the form of:

$$Q_u = \beta_0 + \beta_1 x + \epsilon \tag{25}$$

where

β_0 = intercept

β_1 = slope of the regression line

ϵ = random, independent experimental error with zero mean and constant variance

The t-ratio was used to test the significance of the slope of the regression line and statistical significance of trends. The t-ratio can be calculated as:

$$t = \frac{b}{S.E.(b)} \tag{26}$$

where

b = least-square estimate of slope

$S.E.(b)$ = standard error of slope b

To test the significance of the slope, the t-value is compared to tabulated values of t-value for a given significance level. The p-value was calculated at 95 percent confidence level (CL), which corresponds to the probability that the slope is erroneously deemed significant (Box, Hunter, and Hunter 1978). Thus, the significance of the trend is increasing with increasing t-ratio and decreasing p-value.

The ultimate bearing capacity determined by the Davisson method was used in regression analysis and the significance of trends were evaluated (Table 25). The parameters, that were found to be significant on 95 percent CL, are:

a. Perimeter of pile.

b. Cross-sectional area of pile (cross-sectional area of tip including a plug).

c. Frequency at bias mass.

d. Power delivered to top of pile.

e. Acceleration at eccentric masses.

f. Type of pile (H-pile or pipe pile).

g. Frequency at top of pile.

h. Diameter of pile, as shown in Table 25.

Trends using characteristics of piles. The characteristics of piles having a statistically significant trend with respect to the ultimate bearing capacity are:

a. Diameter of pile.

b. Area of cross section of pile including plug.

c. Perimeter of pile.

d. Type of pile, as shown in Table 25.

The diameter of the pile had a positive effect on the bearing capacity, which is expected based on bearing capacity theory (Figure 42). The lines drawn in

Table 25
Result of t-test Conducted to Test Significance of Trends

Parameter	No. of Piles	t-ratio	p-value	Significant at 95% CL
Perimeter	24	4.01	0.001	Yes
Area of Cross section	24	3.02	0.007	Yes
Frequency at bias mass	23	-2.69	0.014	Yes
Power at top	12	2.71	0.022	Yes
Acceleration at eccentric masses	23	-2.46	0.023	Yes
Type of pile	24	2.34	0.028	Yes
Frequency at top	23	-2.24	0.036	Yes
Diameter of pile	24	2.20	0.039	Yes
Rate of penetration	20	-1.73	0.100	No
Frequency at eccentric masses	23	-1.71	0.102	No
Dynamic strain at top	12	1.75	0.111	No
Change in static strain at top	12	1.75	0.111	No
Length of plug	12	1.61	0.138	No
Frequency at bottom	22	-1.40	0.176	No
Static strain at top	12	1.34	0.209	No
Static strain at bottom	10	1.32	0.223	No
Acceleration at top	23	-0.94	0.359	No
Energy at top	12	0.96	0.360	No
Embedded length	24	0.64	0.529	No
Acceleration at bias mass	23	-0.55	0.588	No
Dynamic strain at bottom	10	-0.50	0.628	No
Change in static strain at bottom	10	-0.47	0.654	No
Acceleration at bottom	22	0.08	0.934	No

Note: "Top" is referred to the top of pile and "bottom" is referred to the bottom of pile.

Figure 42 were selected by eye to represent the trend and to reasonably represent the upper and lower bounds of most data.

The area of cross section, including the soil plug and perimeter, are direct measurements of the geometry of a pile. The area of cross section of a pile, including the plug, was used to estimate the load carried by the tip of the pile as a component of static bearing capacity (e.g., Meyerhof method). The increase in the area of cross section resulted in an increased bearing capacity. This effect can be see in Figure 42.

The perimeter of the pile is used in the calculation of bearing capacity due to skin friction in the classic methods of estimating the bearing capacity of piles (e.g., Meyerhof method). The area of the pile, where the skin friction resistance is active, is calculated as perimeter times embedded length. Increases in

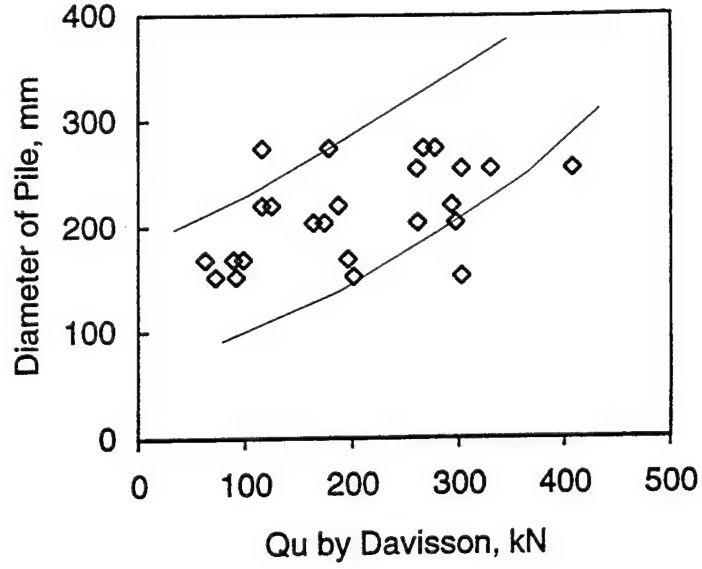

a. Bearing capacity versus diameter of pile

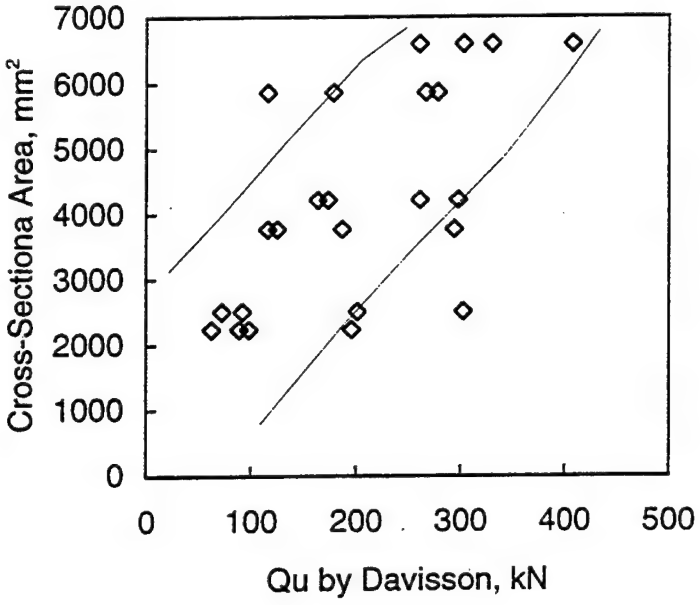

b. Bearing capacity versus area of cross section

Figure 42. Bearing capacity versus diameter of pile and cross section of pile

perimeter results in increases in bearing capacity. Again, this effect can be seen in Figure 43. However, embedded length of the pile did not show a significant trend with bearing capacity (Figure 43). This may be the result of only some of the layers contributing significantly to the skin friction resistance. At the experimental site, the clay layer having hard consistency was of variable thickness throughout the site. The friction resistance of the clay was higher than that for the sand. Therefore, the embedded length does not necessarily represent the thickness of the clay layer on the particular location of the pile and thus, does not appear significant in the analysis.

The type of pile is a general category that appears significant perhaps due to the differences in cross section and perimeters of piles for pipe and H-piles. The means of cross section and perimeters for H-pile were higher than those for pipe piles. Therefore, the mean of bearing capacities of H-piles is higher than a mean of bearing capacities of pipe piles.

Trends for dynamic parameters measured during vibratory driving. The dynamic parameters measured during vibratory driving are the key elements for prediction of bearing capacity during the vibratory driving. The parameters that showed significant trends with the bearing capacity were:

a. Frequency of driving measured at the bias mass and top of the pile.

b. Power delivered to the top of pile during vibratory driving.

c. Acceleration measured at the eccentric masses (Table 25).

The frequency of driving was evaluated for the last portion of driving. The frequency was measured at four places at the pile: (a) the bias mass, (b) the eccentric masses, (c) the top of the pile, and (d) the bottom of the pile. In most cases, changes in frequency between the bias mass, eccentric masses, and top of the pile were minimal as discussed in the paragraph entitled "Frequency and acceleration amplitude of vibratory driving." The relationship between bearing capacity and frequency measured at the various locations of the pile/driver system is shown in Figure 44. From visual comparison of the plots, it appears that the frequency of driving decreases with increasing bearing capacity for all the graphs. However, the change in frequency measured at the bias mass is only 3.5 Hz for all the piles and is even smaller for the frequency measured at the top of the pile or at the eccentric masses (Figure 44). From the results of a statistical evaluation of trend between frequency and bearing capacity, the frequency measured at the bias mass and top of the pile are significant, but frequency measured on the eccentric masses is not.

The acceleration measured at the eccentric masses toward the end of driving also seems to be a significant parameter affecting the bearing capacity of a pile (Figure 45). The bearing capacity increases with decreasing eccentric mass acceleration. A possible explanation is that because the bearing capacity is controlled by side friction, the eccentric mass acceleration would decrease with increasing bearing capacity. However, if the bearing capacity is controlled by tip resistance, one would expect that eccentric mass acceleration would not

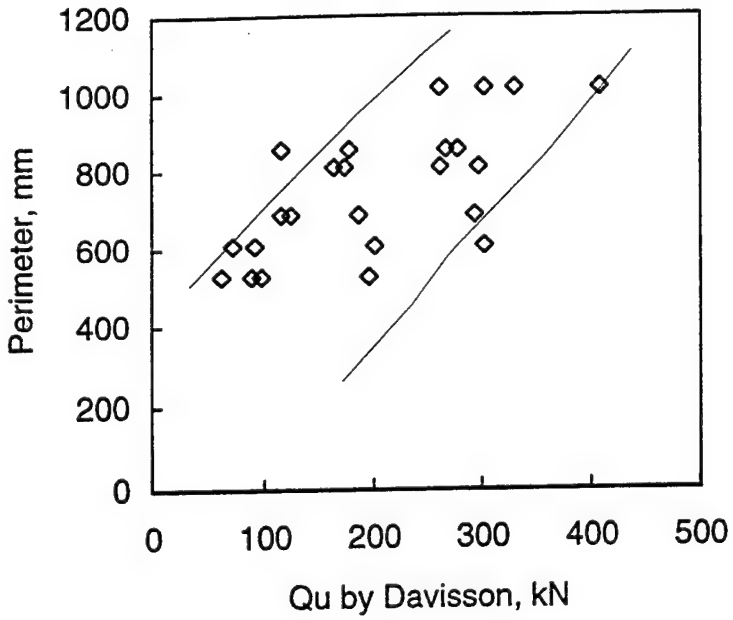

a. Bearing capacity versus perimeter

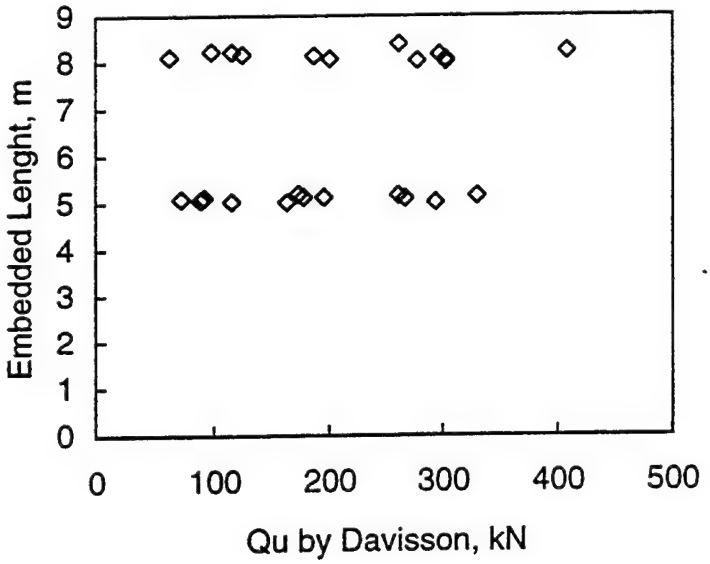

b. Bearing capacity versus embedded length

Figure 43. Bearing capacity versus perimeter of pile and embedded length

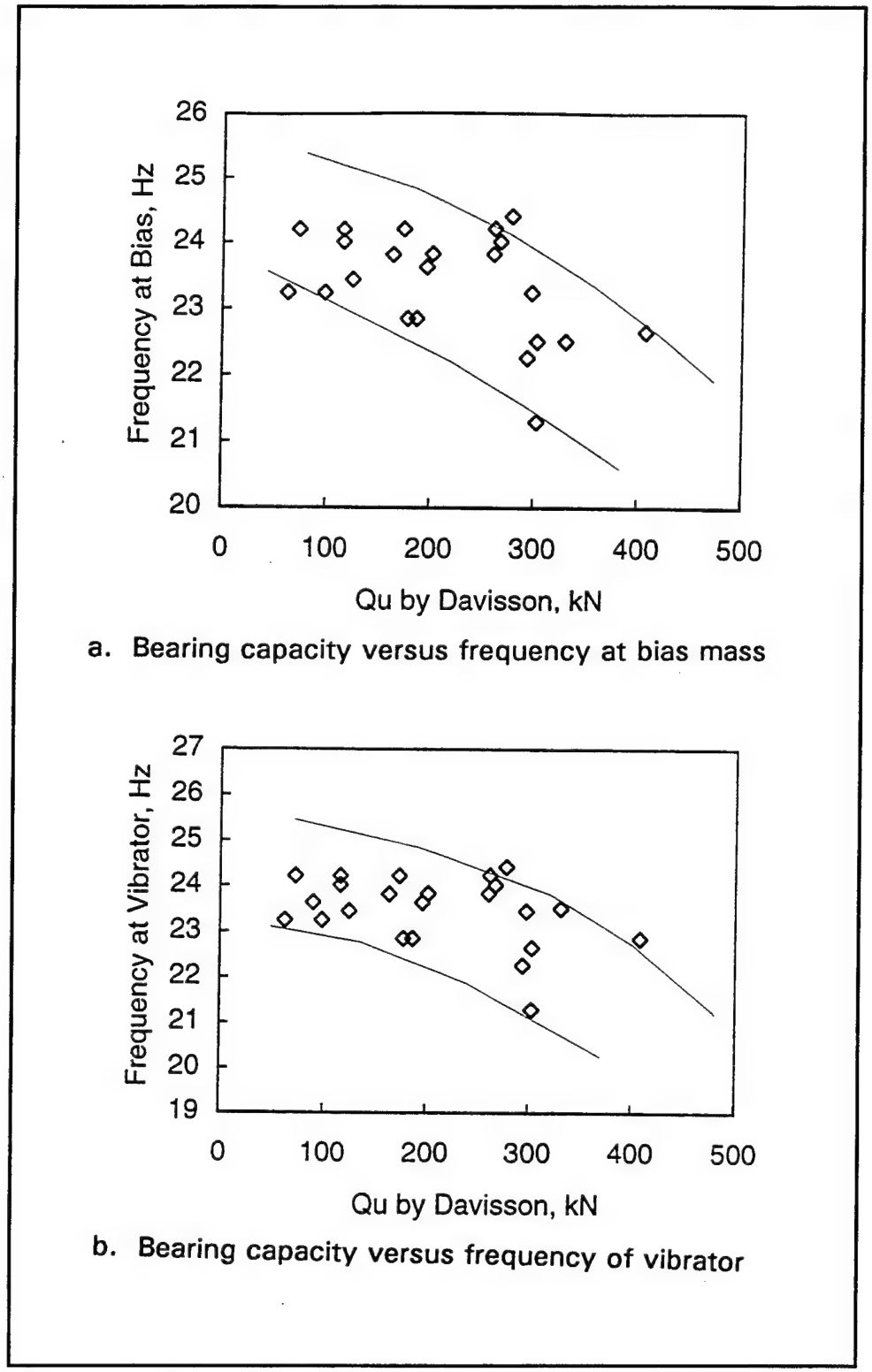

Figure 44. Bearing capacity versus frequency

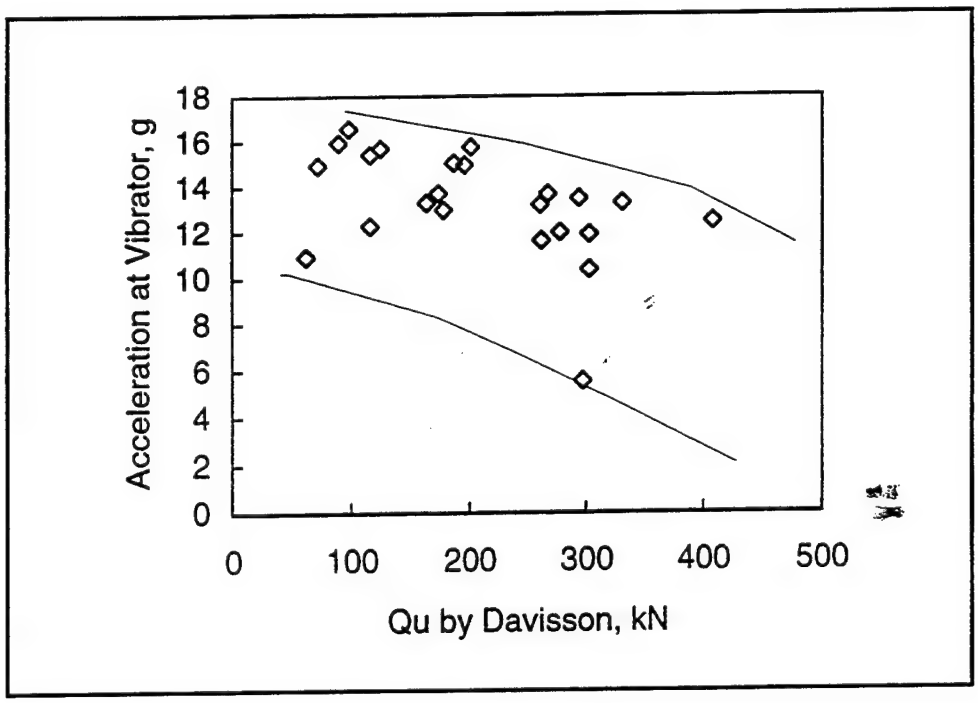

Figure 45. Bearing capacity versus acceleration

correlate to increased bearing capacity. Other factors such as pile length and frequency would affect the results.

The parameters that were identified based on measurements of strain, did not appear to have a significant trend with the bearing capacity. However, it should be noted that the number of piles for which the strain parameters were evaluated reliably, was reduced to half compared to measurements of frequency and acceleration. This is because measurements of strain were corrupted by poor calibration of the strain gauges on the pile.

Parameters that combine both measurements of acceleration and strain are power and energy delivered to the top of pile. The average power delivered to the top of the pile during the driving is a significant parameter with respect to the bearing capacity (Figure 46). However, the total energy delivered to the top of the pile is not significant (Table 25).

The fact that total energy was not significant may be due to the process of installation of the pile by vibratory driving. During driving, the penetration of the pile/driver system is often controlled by the rate of release of the crane support instead of the soil resistance. The vibrator is generating the energy to drive a pile, but the energy is consumed by the crane as well as the soil. Therefore, the actual energy required to drive a pile was less than the energy calculated from the record because the crane absorbed some of the energy. On the other hand, power to the top of the pile is an indication of the rate of energy supplied to the system with respect to time. Therefore, it may be a

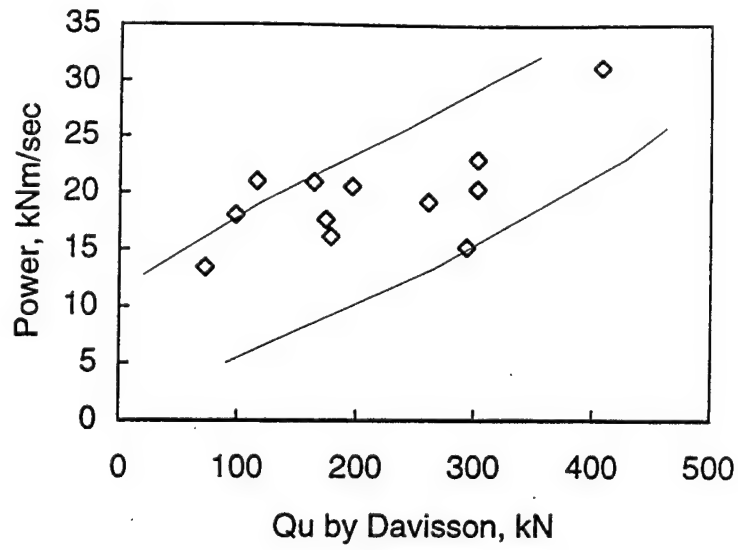

a. Bearing capacity versus power

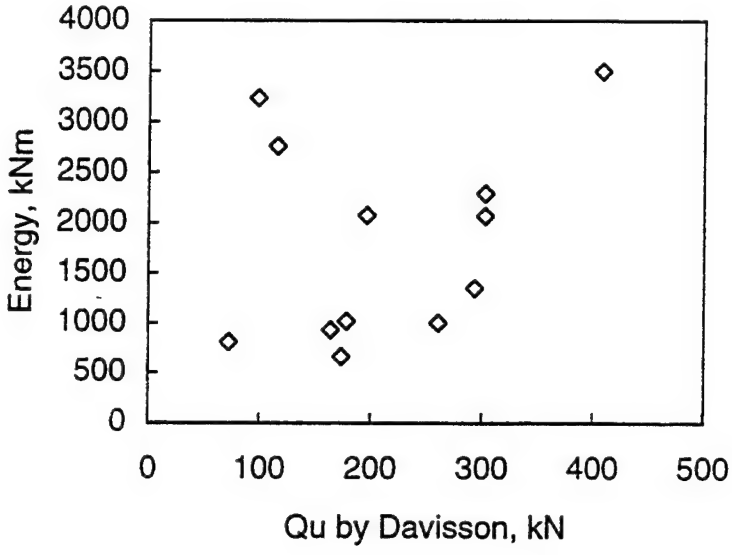

b. Bearing capacity versus energy

Figure 46. Bearing capacity versus power and energy

better indicator of the resistance the soil represents and is not dependent on the time that it takes to actually drive the pile.

The bearing capacity is plotted versus both power and energy (Figure 46). The lines on the plot were only selected by eye to represent a general trend in data. It should be noted that there are only 12 data points on which the trend is established. Again, this is the result of poor calibration of the strain gauges mounted on the piles.

Regression model. The initial exploration of trends indicated that there are several parameters correlated with bearing capacity. However, some of the variables may be correlated to each other (e.g., size of pile and area of cross section). These correlated variables were identified by multivariate regression. The regression model was developed from the measured parameters to predict the bearing capacity. The linear regression model was used in the form:

$$Q_u = \beta_0 + \beta_1 x_1 + \beta_2 x_2 + \ldots + \beta_i x_i + \ldots + \beta_n x_n + \epsilon \qquad (27)$$

where

β_i = coefficients

x_i = independent variables

ϵ = error term of a normal distribution with zero mean and constant variance

Development of model. The regression model was developed in a stepwise fashion. The variables were added to the model based on their significance determined in an initial investigation of parameters. The significance of the variables in a model were checked by a partial t-ratio and p-value. The partial t-ratio for each variable is a measure of the variance explained by the addition of a variable relative to the residual error remaining in the data. The p-value was required to be lower than 0.1 in order to keep the variable in the model. A p-value of 0.1 represents a 90 percent CL that the coefficient of the variable is not equal to zero. The CL was reduced to 90 percent due to higher overall variability in estimation of parameters.

The developed model is summarized in Table 26. The variables in the model are: perimeter of the pile, frequency measured at the bias mass, and power delivered to the top of pile. The model has R^2 of 0.83, meaning 83 percent of the variance in bearing capacity estimated by Davisson method is explained by the model.

To ensure that the model represents a good fit to actual data, the bearing capacity predicted by the model are plotted against the measured values of bearing capacity (Figure 47). Also, the standardized residuals versus predicted values are plotted to ensure that the assumption of the standard variance of the error is met.

Table 26
Multivariate Model to Predict Bearing Capacity

Parameter	Coefficient (β_i)	p-value
Intercept	1,386	0.008
Perimeter of pile	0.209	0.050
Frequency at bias mass	-63.50	0.004
Power at top	7.265	0.090

Discussion of model. The model suggests a functional relationship between bearing capacity and three variables that characterize the pile and method of installation. Other variables that appeared significant in the initial investigation of trends were not included to the model because they did not contribute significantly to the explanation of variance of measured bearing capacity.

Considering that the model was based on measurements from 12 piles, the coefficients in the model should be evaluated more for the indication of trend rather than for direct calculation of bearing capacity. The coefficient for perimeter and frequency are as expected for piles in that bearing capacity is controlled by skin friction resistance. The increase in perimeter increases the area of skin friction resistance. However, the higher skin friction resistance reduces the frequency of the vibration, such that a decrease in frequency of vibration becomes an indicator of increasing skin friction and thus higher bearing capacity. The power delivered to the pile is a measurement of performance of the driver. The power includes both the static and dynamic forces generated by the vibrator and also the response of the pile/driver system to application of those forces. The higher the power supplied to the pile, the higher the bearing capacity. It could be noted that this conclusion corresponds to conclusions of sensitivity analysis of VPDA, that parameters of the driver are important. Also, the coefficients in the model correspond to the trends observed in the initial exploration.

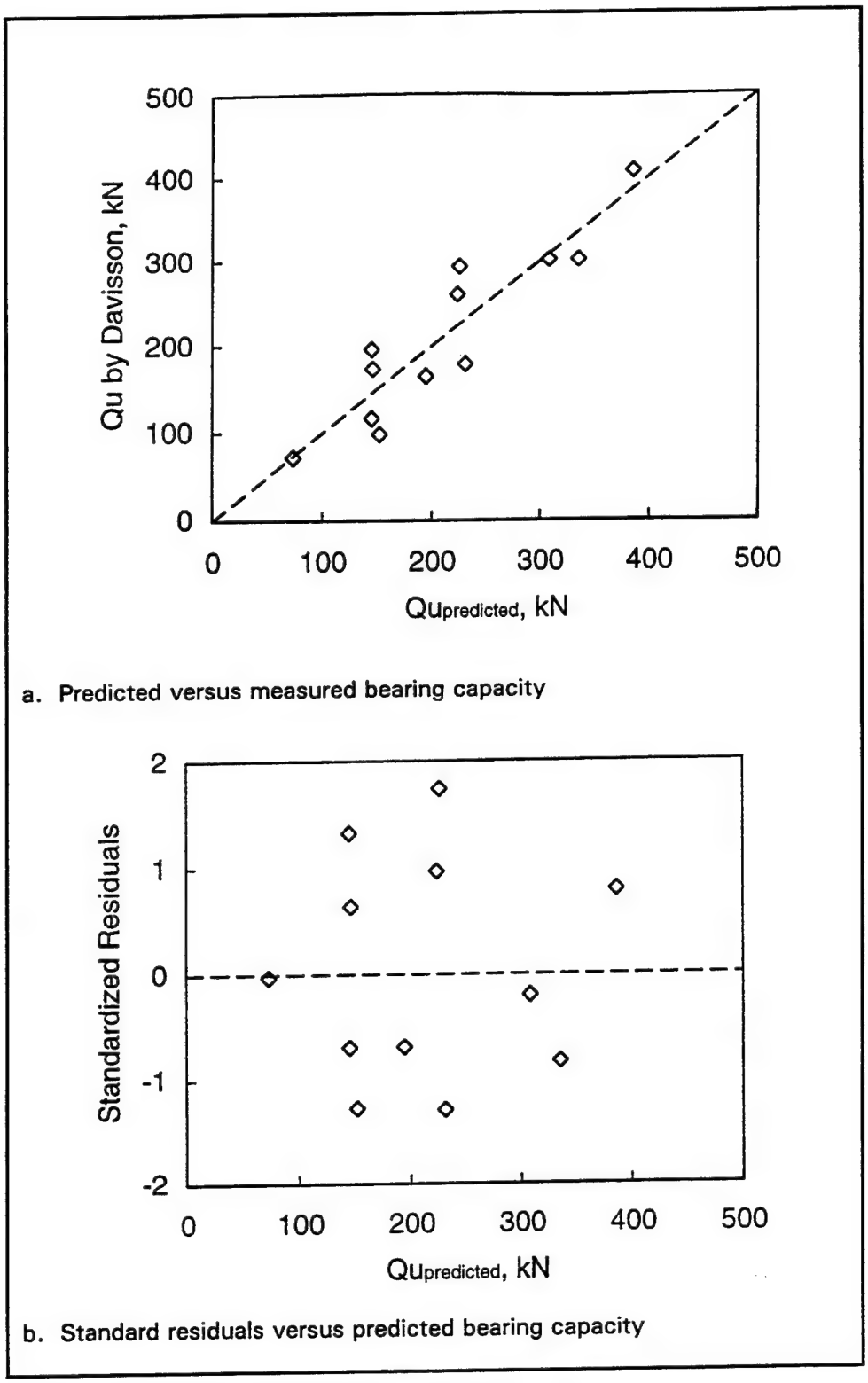

Figure 47. Model of bearing capacity

3 Conclusions

Conclusions Based on Project Objectives

The objective of this project was to develop the capability for predicting the ultimate bearing capacity of structural piling from the response of the piling during installation with vibratory driving systems. This research provided two end products that met this objective and which could be commercialized. These products are currently untested and to be successfully implemented will require additional input and support from the pile driving industry. The European vibratory driving community is currently working toward this goal (Massarsch et al. 1995).

The first product is a computer hardware-software combination (**Wisc**onsin Vibratory **P**ile **D**riving **A**nalyzer (WiscVPDA)) designed to employ a regression model developed from field testing results. The model is based on measurements of dynamic properties of the pile/driver system during driving. Records collected during vibratory driving of 24 experimental piles were analyzed to obtain profiles of the frequency and amplitude of driving, as well as static and dynamic stresses. The ultimate bearing capacity of the piles was determined by analysis of data from static load tests. Similar to the PDA, the WiscVPDA hardware records and analyzes dynamic input information and predicts the ultimate bearing capacity of individual piles driven by vibratory drivers in given soil conditions. The input consists of only measurements of frequency and amplitude of vibration at the driver and acceleration and strain at the top of the pile.

The second product, an offshoot of the first product, is a suggested tool to be employed by the vibratory driving industry to investigate a site for the potential of successful use of vibratory driving. The tool consists of a heavily instrumented pile attached to a continuously variable vibrator. Initially, this device would be used only to determine site suitability relative to driveability. Eventually, as a comprehensive data set was gathered and correlated to measured pile capacities, the device may be used to estimate the bearing capacity of vibratory driven piles on any site. Thus, vibratory hammers could be used for driving bearing piles for foundations and used on sites with a great deal of confidence in the predicted capacities.

Information about WiscVPDA

The WiscVPDA package requires hardware and software that are integrated to collect dynamic data during the pile installation, analyze the data in real-time, and output a prediction of the ultimate bearing capacity of the pile. The software is written in LabVIEW®, a virtual instrument software package sold by National Instruments. The choice of LabVIEW® for the software permits a wide variety of choices for hardware. The user can collect data from analog-to-digital (A/D) boards, GPIB equipment, serial input, or VXI equipment. The dynamic signals that are required are the strain and acceleration at the top of the pile. These are the same readings required to determine the ultimate bearing capacity for impact driving. These signals are analyzed to determine power and frequency. These quantities are then used in the regression equation to estimate ultimate bearing capacity.

Capabilities. The package just described has the ability to estimate the ultimate bearing capacity in real-time as the pile is being driven. It can also be used to record the pile-driving dynamics for subsequent, more substantial analysis such as the TAMU program described herein.

Areas of application. Driven piles are widely used to support all types of buildings, bridges, and highway overpasses throughout the United States. Consequently, the driven pile foundation installation industry is enormous and estimated to be a $1.1 billion per year industry. The technology provided by this work has the potential of increasing the efficiency of installation and thus reducing the time and installation costs by about 30 percent. Savings will be considerable when a vibratory driving system can be used to install piles instead of impact piles and could exceed $110 million per year as a result of the reduced time and effort required to install driven piles.

Limitations. This research has only been able to establish the methodology and prove the concept on one jobsite. This model is therefore currently valid only for the soil type, driver, and piling used on that site. Additional records are required to validate and extend the model to other soils, piles, and drivers.

The PDA used for impact driving utilizes "fundamental" properties of the soil-pile interaction. The approach used in this research is significantly below that level of sophistication primarily because the interactions between soil and pile are much more complicated in the case of vibratory driving. In the case of impact driving, the pile slips relative to the soil but then comes to rest prior to the arrival of the next blow. In vibratory driving, the pile is kept moving relative to the soil, making good estimation of the soil-pile interaction difficult after the vibrator has been shut off.

As the wave equation software is improved in its modeling of vibratory driving, an improvement in this model will also occur. Whereas currently the model depends on little understood empirical parameters primarily derived from impact driving, better theoretical understanding from wave equation analyses conducted on vibratory driven piles will permit these empirical parameters to be isolated and understood, yielding better results in a wider variety of conditions. Without better understanding of the soil-pile interaction during driving

relative to that after driving, the model will be relegated to regression equations and empirical data fits.

Cost. The cost of this equipment is relatively small compared to that of an impact driving PDA. This is primarily because the need for profit has been removed. It should be understood that the software is in its infancy and thus additional upgrades will be required to eliminate bugs and improve the predictive capability. The package can be used as is to record dynamic information from any instrumented pile.

The approximate costs of obtaining the capability to use the WiscVPDA package are listed in Table 27. These costs vary depending on the quality of the laptop computer desired and the amount of pile instrumentation concurrently required for several piles on the jobsite.

Table 27
Approximate Component Costs of WiscVPDA

Component	Cost ($)
Laptop or field computer	2,000 - 3,000
Data acquisition hardware	1,200
Pile instrumentation (reusable)	500 to 1,000
Software	free via website

Quantifiable benefits. The paragraph entitled "Area of application" gives details of identified benefits.

Information about proposed in situ probe

Prediction of the bearing capacity of vibratory driven piling is hampered by the wide variability in soil-structure interaction that is seen from cohesionless soils compared to cohesive soils. For this reason, additional data need to be collected from instrumented piling. These data would be collected using the WiscVPDA system. These data will be correlated to the soils, pile type, vibration parameters, and construction procedures in a similar fashion to that described in this research. Rather than instrumenting many structural piles at considerable cost, a single pile and continuously variable vibrator should be constructed and used to collect these data. This device would be used similar to "cone" rigs in probing the ground prior to construction. In the initial stages of the use of this device, potential sites would be "probed" to determine site suitability to installation of piling with a vibratory driver. Data collected from these activities would be used to generate the second, more useful capability of the device: to predict the bearing capacity of vibratory driven piles if driven in the probed site. Thus, vibratory hammers could be used for driving bearing piles for foundations and used on sites with a great deal of confidence in the predicted capacities.

Other Project Conclusions

Predictions of bearing capacity from The University of Houston VPDA were compared to the measured bearing capacity. For the vibratory driver used to install the piles in the field, analysis using VPDA with common impact driving soil-structure interaction parameters results in extremely low rates of penetrations. New parameters for vibratory pile driving must be determined and employed to permit use of the wave equation method. Also, it appears from field observations that the rate of penetration is not a reliable field measurement to predict the bearing capacity, because the crane used to support the vibratory driver during driving affects the rate of penetration of the pile. Thus the rate of penetration must be measured only after the crane "releases" the driver (with or without the use of leads). The safety of permitting the crane to let the vibrator control the rate of penetration is enhanced with the use of leads.

Based on the analysis of these data, the following conclusions are made regarding the behavior of the pile during vibratory driving and prediction of bearing capacity:

a. Based on the regression analysis between predicted bearing capacity and field measurements, the following parameters have been identified as significant at the 95 percent CL: (a) perimeter of pile, (b) cross section of pile, (c) frequency of driving, (d) power delivered to the top of the pile, and (e) amplitude of vibration measured as a peak acceleration.

b. A multivariate regression model has been proposed. Three parameters were included in the model: perimeter of pile, frequency of driving, and power delivered to the top of the pile.

c. For application of the wave equation analysis for predictions of bearing capacity, it was confirmed that most of the piles vibrated as a rigid body. However, for open-end pipe-piles having large diameters of 200 and 250 mm, damping occurred at the bottom of piles due to plugging.

Based on the results of this study, it appears that the bearing capacity can be predicted using dynamic measurements of piles during vibratory driving. The proposed multivariate model for calculation of bearing capacity has to be verified using a larger number of observations, including investigation for different types of soil and a wider range of dimensions of piles. The instrumentation of piles should include: (a) monitoring of frequency and amplitude of driving at the eccentric masses, and (b) monitoring of the acceleration and strain at the top of the pile to determine the power delivered to the pile. During the installation of a pile, an analysis of the records could be performed simultaneously to estimate the bearing capacity of the pile that could be confirmed by load tests.

4 Recommendations

A probe should be constructed and used as an in situ exploratory tool whenever vibratory driving is being considered (Massarsch et al. 1995). These data collected from the probe along with information about the soils should be recorded and analyzed relative to driveability and soil-structure interaction. The WiscVPDA could be used for this collection of data. This hardware-software product (WiscVPDA) is currently available for use. The limitations described in the paragraph entitled "Limitations" place the predictive capability of this product still in the development stage. Any use of the predictive portion should be backed up with other design methods.

The predictive portion of WiscVPDA requires additional verification and validation on a wider variety of sites and conditions to become widely useful and accepted. As additional data sets become available, updates to the product will be provided reflecting the new information.

5 Commercialization/ Technology Transfer

Production and Marketing

This report will be distributed to the U.S. Army Corps of Engineers District and Division offices. The material described herein was presented to approximately 100 engineers from Government and industry in October 1996 through a University of Wisconsin Pile Design short course in Las Vegas, NV. Nine engineers from the U.S. Army Corps of Engineers (USACE) were in attendance.

Product Availability

The software package is available via the World Wide Web (Internet) at http://bosscher.cee.wisc.edu/vibdrive/. This site contains a wealth of information about this research project and other vibratory driving information. Technical support for the package is provided via that website as well.

Technology Transfer Information

The guidance for installation of driven piles by vibratory drivers and methodology for evaluating the ultimate bearing capacity from installation records will be published in the news media of the Deep Foundation Institute and specifically the *Engineering News Record* (ENR). The news media is widely available to all deep foundation contractors. This same guidance will be available to the USACE and other Government agencies and will be published in the revision to Technical Manual TM 5-849-1 (NAVFAC DM-38.4, MARCORPS TM 3985-15/1), "Pile Driving Equipment" (Headquarters, Department of the Army 1982). Instruction on the use of vibratory driving systems has been and will be made available from training courses supported by the University of Wisconsin-Madison Engineering Professional Development Department. The computer software and technical support are available from the University of Wisconsin-Madison.

References

American Society for Testing and Materials. (1993). *Annual book of ASTM standards*. Vol. 4.08, Philadelphia, PA

a. ASTM D-1143-81, "Standard test method for piles under static axial compressive load."

b. ASTM D-4318-84, "Standard test method for liquid limit, plastic limit, and plasticity index of soils."

c. ASTM-D-2217-85, "Standard preparation of soil samples for particle-size analysis and determination of soil constants."

d. ASTM D-2216-90, "Standard test method for laboratory determination of water (moisture) content of soil, rock, and soil-aggregate mixtures."

Barkan, D. D. (1957). "Foundation engineering and drilling by the vibration method." *Proceedings 4th international conference of soil mechanics and foundation engineering*. London. 3-7.

Beckwith, T. G.,Marangoni, R. D., and Lienhard J. H. (1993). *Mechanical Measurement*, 5th ed., Addison-Wesley, Reading, PA.

Berhard, R. K. (1968). "Pile-soil-interactions during vibro-pile-driving," *Journal of Materials* JMLSA, 3(1), 178-209.

Bielefeld, M. W., and Middendorp, P. (1992). "Improved pile driving prediction for impact and vibratory hammers." *Proceedings of the 4th international conference on the application of stress-wave theory to piles*. The Hague, The Netherlands.

Box, G. E. P., Hunter, W. G., and Hunter, J. S. (1978). *Statistics for experimenters*. Wiley, New York.

Briaud, J. L., Tucker, L., Lytton, R. L., and Coyle, H. M. (1985). "Behavior of piles and pile groups in cohesionless soils," FHWA/RD-831038, Federal Highway Administration, Washington, DC.

Brinch-Hansen, J. (1963). "Discussion on hyperbolic stress-strain response cohesive soils," *American Society of Civil Engineers, ASCE, Journal of Soil Mechanics and Foundation Engineering* 89(SM4), 241-242.

Chin, F. K. (1970). "Estimation of the ultimate load of pile not carried to failure." *Proceedings of the 2nd Southeastern Asian Conference on Soil Engineering*. Singapore, 81-90.

Coduto, D. P. (1994). *Foundation design: Principles and practices*. Prentice-Hall, Inc., Englewood Cliffs, NJ.

Das, B. M. (1990). *Principles of foundation engineering*. 2nd ed., PWS-KENT Publishing Company, Boston.

Davisson, M. T. (1972). "High capacity piles." *Proceedings, soil mechanics lecture series on innovations in foundation construction*. American Society of Civil Engineers, ASCE, Illinois Section, Chicago.

Erofeev, L. V., and Warrington, D. C. (1991). "Development and improvement of impact-vibration pile driving equipment in the USSR," 1st issue, PILE BUCK, Inc., Palm City, FL.

Fellenius, B. H. (1990). "Limit-load analysis of results from the static loading test: Background to fail pile." *Deep foundation seminar*. Orlando, FL.

Forehand, P. W., and Reese, J. L. (1964). "Prediction of pile capacity by the wave equation," *Journal of the Soil Science and Foundation Division, ASCE* 90(SM2), 1-25, Proc. Paper 3820.

Gardner, S. (1987). "Analysis of vibratory driven piles," Naval Civil Engineering Laboratory, Technical Note TN-1779, Port Hueneme, CA.

Glanville, W. H., Grime, G., Fox, E. N., and Davies, W. W. (1938). "An investigation of the stresses in reinforced concrete piles during driving," Technical Paper No. 20, D.S.I.R. British Building Research Board.

Goble, G. G., Likins, G. E., and Rausche, F. (1975). "Bearing-capacity of piles from dynamic measurements, final report," Department of Civil Engineering, Case Western Reserve University, Cleveland, OH.

Goble, G. G., Moses, F., and Rausche, F. (1970). "Prediction of pile behavior from dynamic measurements." *Design and installation of pile foundations and cellular structures*. Envo Publishing Co., Inc., Lehigh Valley, PA.

Goldberg, Zoino. (1987). *Vibratory hammer study: Field measurements*. Prepared for Deep Foundations Institute, Goldberg-Zoino & Associates, Massachusetts.

Gordon, D. T., and Chapler, R. S. (1972). "Vibratory emplacement of small piles," Naval Civil Engineering Laboratory, Technical Note TN-1251, Port Hueneme, CA.

Hannigan, P. J. (1990). "Dynamic monitoring and analysis of pile foundation installations." *Deep foundation seminar*. Orlando, FL.

Headquarters, Department of the Army. (1982). "Pile driving equipment," Technical Manual TM 5-849-1 (NAVFAC DM-38.4, MARCORPS TM 3985 15/1), Washington, DC.

Hirsch, T. J., Carr, L., Lowery, L. L. (1976). "Pile driving analysis - wave equation users manual TTI program," FHWA-IP-76-13.2, McLean, VA.

Hirsch, T. J., Lowery, L. L., Coyle, H. M., and Smason, C. H. Jr. (1970). "Pile-driving analysis by one-dimensional wave theory: State of the art," Highway Research Record No. 333, Transportation Research Board, Washington, DC.

Isaacs, D. V. (1931). "Reinforced concrete pile formulas," Paper No. 370, *Transactions of the Institution of Civil Engineers, Australia*, XII, 312-323.

Kencho. (1975). "The dream island: A report on vibration pile driving at the Tokyo Waste Disposal Area," Kensetsu Kikai Chosa Co., Ltd.

Ligtering, A. (1990). "Accurate vertical pile installation by using a hydraulic vibratory hammer on the Arbroath Project," OTC 6236, 22nd Annual OTC, Houston, TX.

Mao, Y. T. E. (1958). "The Yangtze River Bridge at Hankow, China," *Civil Engineering* 910.

Massarsch, K., et al. (1995). "Frequency-variable vibrators and their applications to foundation engineering." *Proceedings to Deep Foundation Institute's 20th annual conference*. Charleston, VA, 1-14.

Meyerhof, G. G. (1976). "Bearing capacity and settlement of pile foundations," *Journal of the Geotechnical Engineering Division, ASCE* 102(GT3), 195-228.

Moulai-Khatir, R., O'Neill, M. W., and Vipulanandan, C. (1994). "Program VPDA: Wave equation analysis for vibratory driving of piles," Department of Civil and Environmental Engineering, University of Houston, Report for U.S. Army Engineer Waterways Experimental Station, Vicksburg, MS.

Novak, M. (1974). "Dynamic stiffness and damping of piles," *Canadian Geotechnical Journal* 11, 574-598.

O'Neill, M. W., and Vipulanandan, C. (1989). "Laboratory evaluation of piles installed with vibratory drivers," National Cooperative Highway Research Program, Report 316.

Paikowsky, S. G., Regan, J. E., and McDonnell, J. J. (1994). "A simplified field method for capacity evaluation of driven piles," FHWA-RD-94-042, Federal Highway Administration, McLean, VA.

Pile Dynamics, Inc. (1996). *Pile driving analyzer manual; Model PAK.* Cleveland, OH.

Press, W. H., Flannery, B. P., Teukolski, S. A., and Vetterling, W. T. (1992). *Numerical recipes example book (C).* 2nd ed., Cambridge University Press, Cambridge and New York.

Rausche, F. (1981). "A short introduction to continuous and discrete wave mechanics." *The second seminar on the dynamics of pile driving.* Boulder, CO, 1-16.

Rodger, A. A., and Littlejohn, G. S. (1980). "A study of vibratory driving in granular soils," *Geotechnique* (3), 269-293.

Satter, M. A. (1974). "Bearing capacity prediction from pile dynamics," *Transportation Research Record 1277*, Transportation Research Board, Washington, DC.

Schmid, W. E. (1969). "Driving resistance and bearing capacity of vibro-driven model piles," *Performance of Deep Foundations, ASTM STP 444,* American Society of Testing and Materials, Philadelphia, PA, 362-375.

_____ . (1970). "Low frequency pile vibrators." *Conference on design and installation of pile foundations of cellular structures. Proceedings.* Lehigh University, Bethlehem, PA, 257-265.

Smith, E. A. L. (1960). "Pile-driving analysis by the wave equation," *Journal of Soil Mechanics and Foundation Division, ASCE* 86(4), 35-61.

Smith, I. M., and To, P. (1988). "Numerical studies of vibratory pile driving," *International Journal for Numerical and Analytical Methods in Geomechanics* 12, 513-531.

Vesic, A. S. (1977). "Design of pile foundations," NCHRP No. 42, Transportation Research Board, National Research Council, Washington, DC.

Wong, D., O'Neill, M. W., and Vipulanandan, C. (1992). "Modeling of vibratory pile driving in sand," *International Journal for Numerical and Analytical Method in Geomechanics* 16, 189-210.

Appendix A
Literature and Data Review

In this appendix, the principles of vibratory driving are explained and examples of applications of vibratory driving in construction are examined. The latter portion of the section is devoted to methods of evaluating bearing capacity and computer models developed for this purpose. The computer model Vibratory Pile Driver Analyzer (VPDA), which is used for analyzing the data collected in this study, is described in detail. A brief summary of methods for evaluating the load testing of piles and methods of calculating static bearing capacity are also presented.

Principles of Vibratory Driving

Pile driving is the process of using dynamic forces combined with static forces to install piles in soil. The forces generated during pile driving must overcome the shearing resistance along the side of the pile and the reaction forces at the pile tip. To generate these forces, two types of drivers can be used: (a) impact hammers, which are most commonly used, and (b) vibratory drivers. Impact hammers generate a series of separate impacts on the pile that result in pile penetration. Conversely, vibratory drivers produce a longitudinal vibratory motion combined with a static compressive force. For vibratory drivers, the driving motion is induced by counterrotating eccentric weights in the main body of the vibrator (Figure A1).

A surcharge load, commonly called a bias mass, is attached to the top of vibrator by stiff springs designed to minimize the vibration of the bias mass during driving. To grip the pile during the driving, vibratory drivers are equipped with hydraulic clamps. Forces resisting penetration of the pile into the soil are commonly lumped into a side resistance and a tip resistance. Side resistance is a function of the friction at the interface of the soil and pile. Tip resistance depends on the bearing capacity of the soil beneath the tip of the pile.

Vibratory drivers are commonly used to install sheet-pile walls and nonbearing piles. Vibratory drivers have several advantages over impact hammers: (a) require less energy, (b) produce higher rates of penetration in cohesionless soils, (c) produce less noise, and (d) produce less structural damage to the pile

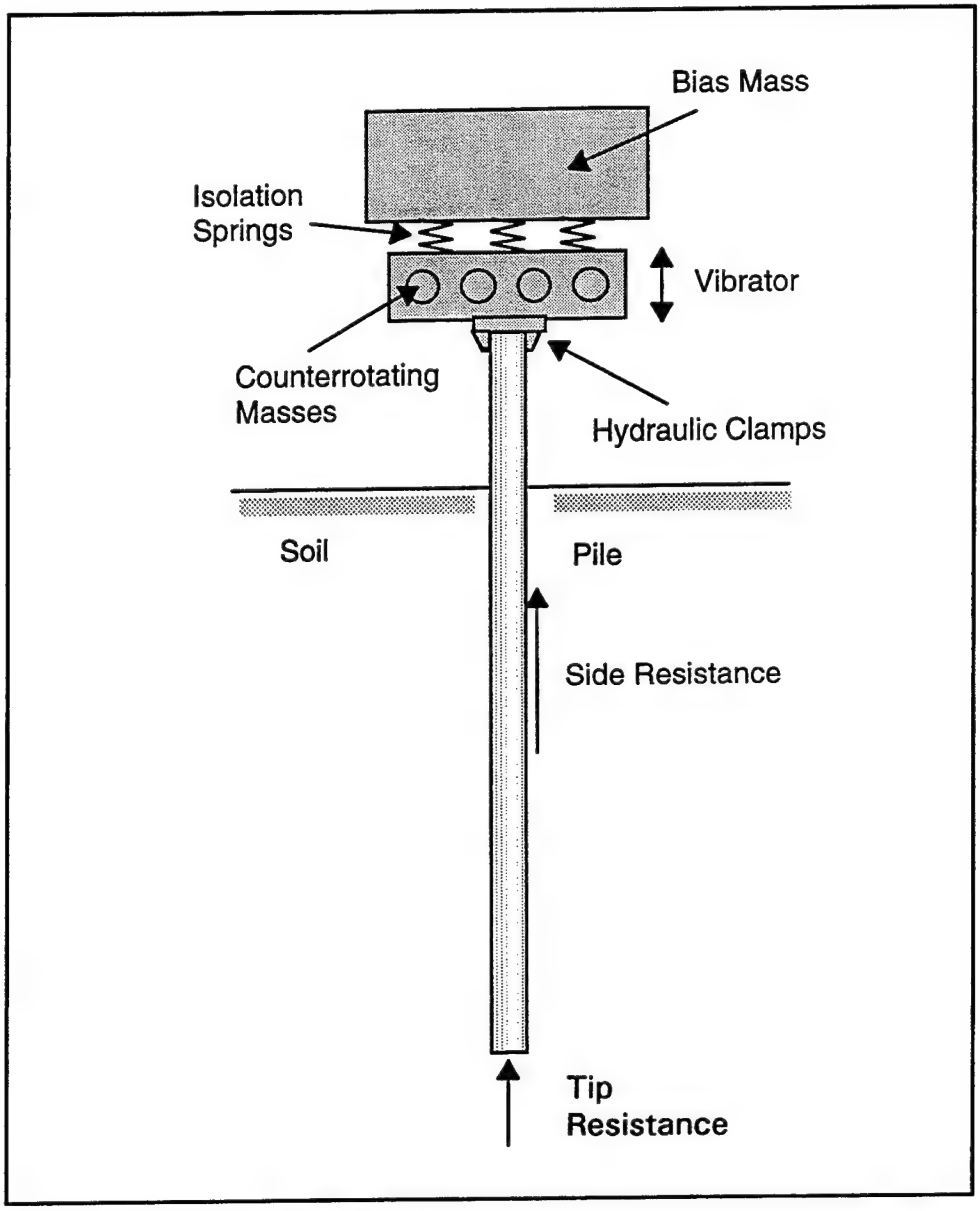

Figure A1. Schematic of vibratory driver

during the driving. However, uncertainty exists in estimating the bearing capacity of the pile during the driving operation. Commonly, the capacity of the pile is estimated by restriking it with an impact hammer. The need to restrike has negative impact on the economics of using a vibratory hammer. The type of soil is an important aspect for choosing the hammer. It has been reported by Rodger and Littlejohn (1980)[1] and O'Neill and Vipulanandan (1989) that vibratory drivers achieve higher rates of penetration and require less energy than impact hammers in granular soils.

[1] References are listed following main text.

Development of vibratory driver

Vibratory drivers have been used since the 1930s to drive and extract piles. Research into the vibratory driving of piles began in Germany, and the first commercial application was carried out by Hertwig in 1932 (Rodger 1980). The concept of vibratory driving was developed almost at the same time in the Union of Soviet Socialist Republic (USSR) as a by-product of soil dynamics research. In 1934, Barkan found that the vertical vibration of piles markedly decreases the skin friction or side resistance (Barkan 1957).

The first extensive recorded use of vibratory drivers for driving sheet piles was during the construction of the Gorky Hydroelectric Station, USSR, in 1951 (Barkan 1957). The vibratory driver, operating at a frequency of about 40 Hz, installed about 60 percent more piles in the same period of time and consumed only a quarter of the energy as compared to the impact hammer. Meanwhile, in Western Europe engineers found that the vibratory drivers with a frequency of up to 25 Hz were the optimum with respect to rate of penetration and reduced wear of motors as compare to higher frequencies (Rodger 1980). A surcharge load applied on top of the vibrator to increase driving speed and depth of penetration was first proposed by Savinov (Barkan 1957). During the 1960s, the vibratory drivers gained broader popularity. Vibratory drivers, with improved design, started to be commercially available throughout the world. Subsequently, an increased research led to the development of methods for estimating bearing capacity of piles installed with vibratory drivers (Smith 1960, Berhard 1968, Schmid 1970).

Research experiments on vibratory driven piles. One of the first experimental studies on using vibratory drivers to install small piles was performed by Gordon and Chapler (1972). They drove steel pipe piles with diameters ranging from 12.7 to 101.6 mm and lengths ranging from 0.91 to 3.35 m into uniform saturated sand in loose to medium dense conditions. The following conclusions were made from their experiment. In dense soils, lower frequencies of about 20 Hz to 40 Hz produced greater penetration rates, while in looser soils, higher frequencies produced higher penetration rates. Extensive field tests on vibratory driven piles were conducted by Gardner (1987) at the Naval Civil Engineering Laboratory in Port Hueneme, CA. In the first part of testing, they tried to relate the rate of penetration of vibratory driving to dynamic driving resistance. The piles were driven by a Foster Vibro 1000 vibratory driver with a rated driving force of 35 tons (311.4 kN). This driver was replaced every 1.2 m with an impact hammer to record the depth of penetration per blow. The piles with a diameter of 508 mm were driven to refusal at depths of 3 to 4 m in extremely dense sand having $\gamma = 20$ kN/m^2 and $\phi = 45$ deg estimated by the cone penetration test. No correlation between the measured rate of penetration and blow counts of impact hammers was found (Gardner 1987). In the second part of the testing, instrumented 220-mm-diam pipe piles were driven. Instrumentation consisted of strain gauges placed on the pile in 1.5-m intervals with the top strain gauges functioning as a load cell. In this part of the experiment, the piles with diameters of 200 mm were driven into saturated sand with a Vibro 1800 having a rated 65-ton (578.3-kN) driving force. Rates of penetration were mostly controlled by the tension in the crane cable required to keep the pile vertical.

Examples of construction projects with vibratory driven piles. In 1956, a vibratory driver was used for installation of foundation piles for a bridge spanning 1,150 m across the Yangtze River, Hankow, China (Mao 1958). Piles with lengths up to 40 m and diameters of 1,350 mm were driven with a vibratory driver that was designed so that the eccentric moment and frequency of operation could be variable.

Vibratory driven piles were used during construction of man-made waste disposal islands in the Tokyo Bay, Japan (Kencho 1975). The piles with diameters of 1,370 mm were driven to depths of up to 58 m and closely spaced around the island with a perimeter of approximately 10 km to make the interior of the island watertight. Prior to construction, trial piles were driven with impact hammers and up to 10,000 blows were required to reach the desired depth of pile penetration. Trial piles installed with a vibratory driver could be driven at a rate nearly six times greater than that of the impact driven piles. Therefore, a vibratory driver VM-50000 with eccentric moment about 50,000 kg-cm and rated energy lower than that of the impact hammer tested was chosen for the project. The success of the vibratory driver on this project was due to its higher efficiency and favorable conditions in that the piles had large side friction compared to relatively small tip resistance.

Another example of successful use of vibratory driving was installation of piles for Amoco Arbroath platform in the UK sector of the North Sea (Ligtering 1990). Piles with a diameter of 1,067 mm were installed to a depth about 25 m using an ICE-1412 vibratory driver. Due to the nature of the project, the vertical orientation of the piles was very important, and all of the piles were installed within the tolerance of less than a 0.5-deg inclination.

Mechanics of penetration initiated by vibratory driver

Modern vibratory drivers can be divided into two groups: (a) low-frequency drivers operating in frequencies up to 40 Hz, and (b) high-frequency drivers operating in frequencies between 40 to 140 Hz (Moulai-Khatir, O'Neill, and Vipulanandan 1994). Low-frequency drivers are most commonly used because they are more efficient.

Smith (1960) first described the mechanics of penetration induced by a vibratory driver. The vibrator causes the pile and all the surrounding soil to vibrate, and the excitation of soil particles near the pile results in reduced soil resistance. The forces acting on the pile are a combination of a sinusoidal excitation force and static surcharge force. Also, the vibrating pile breaks the friction between the pile and the soil, thus allowing penetration in to the ground under the action of a relatively small surcharge force. Berhard (1968) found that the displacement amplitudes are almost equal along the pile length. Rodger and Littlejohn (1980) and Smith and To (1988) confirmed in their laboratory testing the idea that the pile vibrates as a rigid body at the low frequencies. They suggested that the pile vibrates longitudinally without any nodes within the pile and the first node may exist right below the pile in the soil. At low frequencies, large damping prevails along the side of the pile. Large power input is required to break the bond between the soils grains and to

reduce interparticle and pile-skin friction. The critical frequency corresponds with the resonance of the adjacent soil combined with the pile mass system. A rigid connection between driver and pile is of primary importance to minimize energy losses, but it is a very difficult specification to be met in practice. A bias mass, which is on the top of vibrator as a static surcharge, does not participate in the vibratory motion.

For low frequencies of driving, Rodger and Littlejohn (1980) found that the pile is subject to viscous-Coulomb side resistance and elasto-plastic end resistance. In cohesionless soils with a low relative density, vibration causes a reduction in the shear strength called fluidization. The degree of fluidization is proportional to both amplitude of displacement and frequency of vibration. For piles having larger point resistance, no fluidization occurs under the tip. A large displacement and low frequency ensure maximum peak force and penetration. In cohesive soils, it is necessary to vibrate at high frequencies and small amplitudes to drive the pile.

Evaluation of Bearing Capacity

The overview of static and dynamic formulas for evaluation of bearing capacity of piles is presented in this section. The development and principles of wave equation analysis used for estimation of bearing capacity are described. Also, the evaluation of bearing capacity using the energy approach is presented in the last part of this section.

Dynamic formulas for estimating bearing capacity

Analogy to impact hammers. Schmid (1970) adjusted the pile-driving formula for an impact hammer to apply to vibratory driving using the analogy between vibratory drivers and impact hammers. He expressed the total resistance, or bearing capacity, R as:

$$R = k\frac{P}{Vp + \beta} \tag{A1}$$

where

k = nondimensional coefficient of efficiency of the energy exchange

P = power supplied by vibrator (Nm/s)

Vp = penetration rate (m/s)

β = nondimensional coefficient of correction for the rate of energy losses

The shortcoming of this approach is uncertainty in the estimation of the efficiency coefficient k. The value of coefficient k is difficult to obtain for piles driven in situ, unless a series of load tests are performed on experimental

piles. Schmid suggested using a k of 0.15, which is the average value for low-frequency driving. The change of k influences significantly the calculated value of total resistance R. The coefficient β can be evaluated as a function of the soil conditions and frequency of vibrator. The value of power input P and rate of penetration Vp can be observed during driving and a range of values for k and β can be established for a variety of conditions based on experience (Schmid 1970).

Calculation of power input. An evaluation of bearing capacity based on power input required during the last driving period was proposed by Berhard (1968). The bearing capacity R (N) can be calculated as:

$$R = \eta \frac{P_{red} * L}{v * p} \qquad \text{(A2)}$$

where

η = maximum efficiency factor

P_{red} = power input reduced by losses due to the driving mechanism (Nm/s)

L = length of pile (m)

v = average rate of penetration (m/s)

p = total penetration (m)

In this formula, soil properties are not directly included in the calculation, and it is suggested by Berhard (1968) to include them by setting the efficiency factor to 0.1. Because of the uncertainty in the estimation of efficiency, equation A2 can only be used to determine qualitative results.

Dynamic force equilibrium. Schmid (1969) identified parameters influencing vibratory driving to be the following: soil properties, characteristics of vibrator, surcharge, pile types, and type of pile-vibrator connection. Characteristics of the vibrator include frequency, eccentric mass, bias mass, maximum dynamic force, and power input. The pile could be described by its mass, length, cross section, and elastic properties. He based his conclusions on analysis of small-scale laboratory tests.

Also, Schmid suggested the evaluation of driving resistance by establishing a dynamic force equilibrium between the vibratory exciting force, the inertia forces, and the soil resistance as a function of time for a rigid body type of pile vibration. As the pile is excited by a continuous sinusoidal forcing function at the top, the pile tip experiences a series of discrete impacts interrupted by periods of separation between tip and soil. The time when the pile tip is in contact with the soil is only a fraction of the period of vibration. Based on his experimental results, Schmid suggested that the maximum dynamic resistance R_{max} (N) can be calculated as:

$$R_{max} = \frac{2B}{fT_c} \quad \text{(A3)}$$

where

B = static force due to surcharge weight (N)

f = frequency of vibration (s^{-1})

T_c = contact time (s)

The dynamic resistance corresponds to static bearing capacity of close-end pipe-piles but is smaller for open-end pipe-piles (Schmid 1969). Satter (1974) also found that the static bearing capacity could be derived from measured pile response during driving and that the dynamic response depends on the driving force, the physical properties of the pile, and the soil resistance. The accurate measurement of pile response is essential for the evaluation of bearing capacity. Satter (1974) modeled the pile as a rigid body, which is a reasonable assumption for low-frequency driving. For low-frequency driving, steady-state vibration, and viscous damping, the soil resistance can be expressed as a proportion of the cube of the pile dynamic displacement $x(t)$:

$$Mx'' + Cx' + Px^3 = F_0 \sin \omega t \quad \text{(A4)}$$

where

M = mass of pile (kg)

C = damping coefficient (Ns/m)

P = soil constant

S = bias mass (kg)

F_0 = amplitude of excitation forcing function produced by the vibrator

ω = frequency of that function (rad/s)

The soil constant P can be expressed as

$$P = \frac{4(F_0 + M\omega^2 a)}{3a^3} \quad \text{(A5)}$$

where

a = average of measured displacement over interval of maximum and zero velocities (m)

The static bearing capacity is the dynamic soil resistance Px^3 at the maximum pile velocity when the damping coefficient is small. It is necessary to

adjust the soil constant P so that the computed maximum displacement corresponds to the experimentally obtained maximum displacement.

Satter (1974) found comparable agreement between the predicted and measured values of static bearing capacity. Discrepancies in predicted and measured bearing capacity may have been caused by ground settlement, which tends to increase the damping effect on the pile. For cases in which ground settlement is a significant factor, the value of damping must be adjusted (Satter 1974).

Wave equation analysis

In 1931, Isaacs was the first to investigate the wave action occurring during driving of piles. In 1938, Glanville et al. published a solution to the wave equation applied to pile driving. However, several simplifying assumptions had to be made to find numerical solutions. Smith (1960) presented the first full numerical solution to the wave equation applied to pile driving.

The solution by Smith (1960) is based on a model of pile and soil interaction, which was further refined by Forehand and Reese (1964). The pile is divided into short elements of unit length and given mass that are connected to each other by springs and dashpots (Figure A2). The soil resistance is represented by a force R. The vibrator itself is represented as a mass with an applied sinusoidal forcing function. The time of vibration motion is divided into discrete intervals, during which velocity, force, and displacement have constant values. The proper evaluation of time increment size is important in order to obtain valid results from the discrete-element solution (Hirsch et al. 1970). Stress-wave propagation in a pile during driving can be described by the following one-dimensional (1-D) wave equation modified to include frictional resistance along the pile (Paikowsky, Regan, and McDonnell 1994):

$$E_p \frac{\partial^2 u}{\partial x^2} - \frac{S_p}{A_p} f_s = \rho_p \frac{\partial^2 u}{\partial t^2} \tag{A6}$$

where

E_p = modulus of elasticity (Pa)

$u(x, t)$ = longitudinal displacement (m)

S_p = circumference of the pile (m)

A_p = pile area (m^2)

f_s = frictional stress along the pile (Pa)

ρ_p = unit density of the pile material (kg/m^3)

The wave equation in differential form can be expressed as:

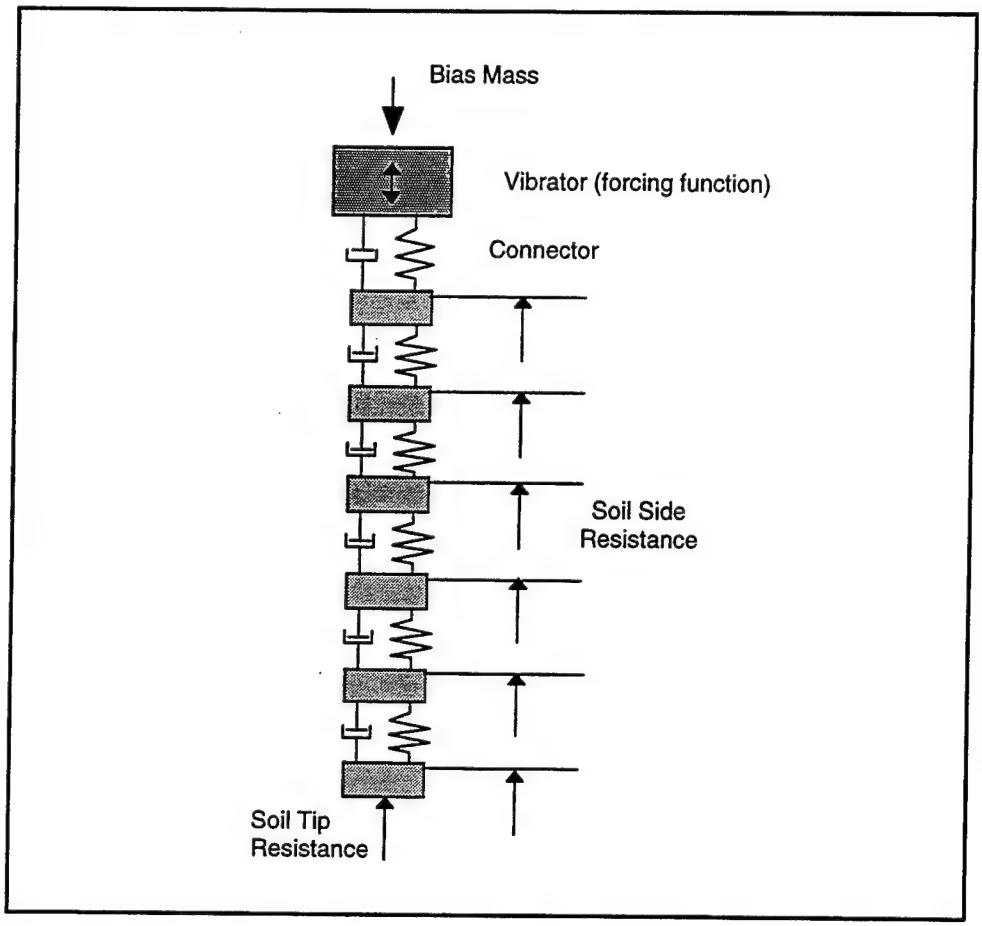

Figure A2. Pile-soil model (Smith 1960)

$$d_m^t = 2d_m^{t-1} - d_m^{t-2} + \frac{g\Delta t^2}{M_m}\left[\left(d_{m-1}^{t-1} - d_m^{t-1}\right)k_{m-1} - \left(d_m^{t-1} - d_{m+1}^{t-1}\right)k_m - R_m^t\right] \quad \text{(A7)}$$

where

d_m^t = displacement of element m at time interval t (m)

g = gravity constant (m/s^2)

Δt = size of time interval (s)

M = weight of the element m (kg)

k_m = stiffness of spring connecting element m to element $m+1$ (N/m)

R_m^t = resistance of element m at time interval t (N) (Schmid 1960)

The soil resistance is assumed elasto-plastic corresponding to Coulomb failure hypothesis (Figure A3). Starting at O, the pile moves ahead a distance of quake Q through elastic compression of the soil until resistance reaches the ultimate value of Ru. At this point, plastic failure occurs and ground resistance remains equal to Ru until point B. Elastic rebound then occurs and motion

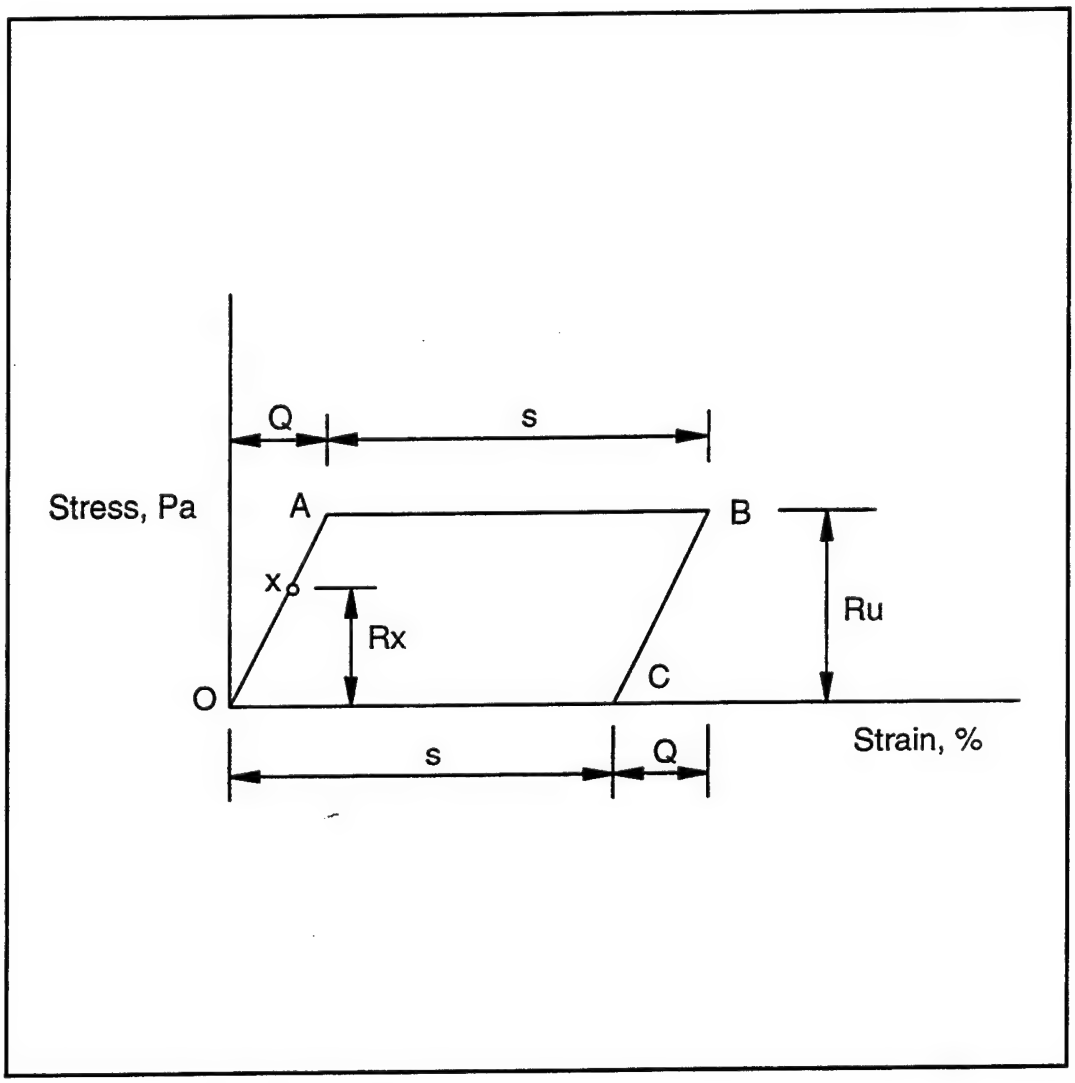

Figure A3. Stress-strain diagram (after Smith 1960)

ceases to point C, where all forces are zero. This distance s, called the permanent set, is reduced by damping, which is assumed to be viscous and proportional to velocity. For the element m, the instantaneous damping resistance is the product of instantaneous velocity v_m, damping constant C, and resistance R_x. These variables must be in consistent units. The total resistance of the element m is the sum of resistance at the point and damping resistance and can be expressed as

$$R_m = R_x(1 + Cv_m) \tag{A8}$$

Smith (1960) suggested the value of C to be 0.15 at the tip of the pile and 0.05 along the side of the pile, because the soil along the side is not displaced to the same extent as soil underneath the pile tip. The distribution of the

ground resistance along the side of pile can be specified by assigning different values to elements to accommodate for variability in the soil profile.

The ultimate soil resistance is the sum of the resistance along the length of pile. The soil springs stiffness k', connected to each of the elements, can be expressed as:

$$k' = \frac{R_u}{Q} \tag{A9}$$

where

R_u = ultimate soil resistance of the element (N)

Q = quake (m)

Smith (1960) suggests that a value of 2.5 mm can be used for the quake. In every time period Δt, the soil resistance R_m of each element along side of pile and the tip becomes:

$$R_m = (d_m - d'_m)\, k' \,(1 + Cv_m) \tag{A10}$$

where

d = displacement of the element m

d'_m = soil plastic displacement of element m

k' = soil spring stiffness

v_m = velocity of element m

C = damping constant applicable to soil either along the side of pile or the tip of pile

When the stiffness and damping constants are estimated, the bearing capacity can be calculated as the sum of R_m of each element. In cohesionless soil, the friction strength changes very little with time (Hirsch, Carr, and Lowery 1976). However, in clays, the bearing capacity of the pile increases as the remolded or disturbed clay along the side reconsolidates and gains strength, because the adhesion and friction strength of clay are generally restored with time.

The estimation of bearing capacity based on wave equation analysis depends on the determination of the soil resistance, and Hirsch, Carr, and Lowery (1976) recommended some practical value of soil resistance. The quake, Q, ranges from 1.3 to 3.8 mm and is typically 2.5 mm for average pile-driving conditions for both side and tip resistance. The damping constant, C, increases with an increase in the density of sand and effective confining stress. From laboratory tests by Hirsch, Carr, and Lowery (1976), C at the pile tip varied from 0.01 and 0.12 for saturated Ottawa sand, but for dry sand C at the pile tip

was nominally equal to zero. Along the side of the pile, the damping constant could be estimated as one-third of that for the tip of the pile.

Energy approach to bearing capacity evaluations

The energy approach for predicting static bearing capacity from pile driving requires a balance of energy in the system. The total energy that is transferred to the pile through the driving system has to equal the work done by the resisting forces during penetration.

Energy equation. Theoretical equations evaluating the total resistance of the pile are based on the work done by the pile during penetration. The force/displacement relations of the pile/soil system are assumed to be elasto-plastic. Assuming all variables are calculated in consistent units, the energy E_n (Nm) delivered to the pile can be calculated as:

$$E_n = \int V(t)F(t)dt \tag{A11}$$

where

$V(t)$ = velocity signal (m/s)

$F(t)$ = force signal (N) measured at the top of the pile during the vibratory driving

The velocity signal is obtained from measurements of acceleration $a_{cc}(t)$ (m/s^2) as:

$$V(t) = \int a_{cc}(t)dt \tag{A12}$$

and the force signal is obtained by processing the measurements of strain $\varepsilon(t)$ as:

$$F(t) = \varepsilon(t)EA \tag{A13}$$

where

E = modulus of elasticity (Pa) of the pile

A = cross-sectional area of the pile (m^2)

By inserting equations A12 and A13 into equation A11, the energy can be expressed as:

$$E_n = EA\int a_{cc}(t)\varepsilon(t)dt \tag{A14}$$

Strain in the pile can be expressed as:

$$\varepsilon(t) = \frac{\delta(t)}{\Delta L} \tag{A15}$$

where $\delta(t)$ is the deformation of the pile (m) as the wave travels a distance ΔL in the pile (m) (Hannigan 1990, Rausche 1981).

The deformation can be calculated using:

$$\delta(t) = v(t)dt \tag{A16}$$

where $v(t)$ = particle velocity (m/s) and the distance ΔL can be expressed as:

$$\Delta L = cdt \tag{A17}$$

where $c(t)$ is speed of the wave propagation (m/s).

Substituting Equations A16 and A17 into Equation A15, the strain can be calculated as:

$$\varepsilon(t) = \frac{v(t)}{c} \tag{A18}$$

Then, the modulus of elasticity can be expressed as:

$$E = \rho * c^2 \tag{A19}$$

where ρ is mass density of the pile (kg/m^3).

The total work done by the system can be expressed as:

$$W = R_u\left(S + \frac{Q}{2}\right) \tag{A20}$$

where

R_u = resistance (N)

S = permanent set or plastic deformation (m)

Q = quake denoting the elastic deformation of the pile-soil system (m)

The quake can be determined by finding the maximum displacement reduced by permanent set as:

$$Q = D_{max} - S \tag{A21}$$

where the maximum displacement D_{max} can be calculated as:

$$D_{max} = \max \int V(t)dt \tag{A22}$$

and the permanent set S can be found as:

$$S = \int\int a_{cc}dt \tag{A23}$$

The acceleration measurement has to be fairly precise, because any offset has a large effect on the displacement calculation as the second integration of the acceleration is calculated.

Assuming that the total work W done by the system is equal to total energy E_n delivered to the system, the resistance R_u can be calculated as:

$$R_u = \frac{E_n}{S + \frac{(D_{max} - S)}{2}} \tag{A24}$$

This resistance is the maximum possible resistance of the system and can be correlated to the predicted static capacity P_u by a correlation factor K_{sp} as:

$$P_u = K_{sp} * R_u \tag{A25}$$

where K_{sp} is static pile correlation factor accounting for all dynamic losses and is dependent on type of pile and soil, as well as driving resistance.

Energy losses. To develop a model of the dynamic system, the energy losses have to be correctly accounted for (Paikowsky, Regan, and McDonnell 1994). Energy losses are caused by elastic deformations of soil and the pile and the work done by the static resistance on plastic soil deformation. There are also some energy losses due to various factors associated with pile penetration such as soil damping, soil radiation, and soil inertia at the pile tip. Static soil resistance can be represented by an elasto-plastic soil model, where the viscous damping is evaluated such that it accounts for various energy losses in the system. As a result of these losses, the damping coefficients vary even for the same soil type and differ between tip and side (Paikowsky, Regan, and McDonnell 1994).

Soil inertia is major contributing factor to the energy losses during driving. The volume of displaced soil during driving is equal to the volume of penetrating pile except when plugging of the pile tip occurs (Paikowsky, Regan, and McDonnell 1994). The volume of displaced soil is a function of the pile geometry. Calibration of the energy model is not based on the soil type alone, but consideration of the pile and soil types (small versus large displacement piles), driving resistance, and installation procedure.

The classification of pile to small or large displacement can be made based on pile area ratio A_R (Paikowsky, Regan, and McDonnell 1994):

$$A_R = \frac{A_{skin}}{A_{tip}} \tag{A26}$$

where

A_{skin} = surface area of the pile that is in contact with soil

A_{tip} = area of the tip of the pile

The pile is classified as small displacement pile if A_R is greater than 350. When A_R is smaller than 350, the pile is considered a large displacement pile (Paikowsky, Regan, and McDonnell 1994).

The energy loss that occurs through the work performed by the inertia forces toward displacing the soil mass beneath the tip of the pile is directly related to the acceleration of this soil mass. The soil inertia can be multiplied by the pile displacement at the tip to obtain the energy loss. Two cases of driving resistance can be considered: (a) low resistance in loose soil, and (b) high resistance in dense soil.

In case of low driving resistance, the velocity and acceleration are high at the pile tip causing the inertia of the tip soil mass to be high, which results in high energy losses. For the case of high driving resistance, there is little if any energy loss due to low acceleration at the tip of the pile and only small mobilization of the tip soil mass occurs. Large energy losses occur when large displacement piles experience easy driving and large tip displacement takes place. Conversely, the smallest losses occur for small displacement piles driven under hard driving. Two distinct trends are observed from energy analysis of vibratory driven piles: (a) for easy driving of large displacement piles, the maximum resistance predicted using energy analysis tends to be over-predicted and has to be adjusted by K_{sp} less than unity, and (b) in hard driving of small displacement piles, the maximum resistance tends to be under-predicted and K_{sp} has to be larger than unity (Paikowsky, Regan, and McDonnell 1994).

The Case Method. The Case Method was developed by Goble, Moses, and Rausche (1970) as a procedure to estimate the bearing capacities of piles and is the principal analysis used in Pile Driving Analyzers (PDA) developed for in situ evaluation of bearing capacity of impact driven piles. The Case Method is based on the assumptions of a uniform elastic pile, ideal soil behavior, and a simplified wave propagation formulation. For the evaluation, the force and velocity measurements at the pile top and a correlation between the soil at the pile tip to a damping parameter are required.

The total soil resistance *RTL* is:

$$RTL = \frac{\left[F(t_1) + F\left(t_1 + \frac{2L}{c}\right)\right]}{2} + \left[v(t_1) - v\left(t_1 + \frac{2L}{c}\right)\right] * \frac{Mc}{2L} \quad \text{(A27)}$$

where

$F(t)$ = measured force at time, t

L = length of pile

c = speed of wave propagation in the pile

$v(t)$ = measured velocity

M = mass of pile

The expression $2L/c$ is the time it takes for the wave to travel from the top of the pile to the tip and back. There are several factors that influence the total predicted resistance such as the damping coefficient and time-dependent soil strength changes. The total resistance is the sum of static resistance which is displacement dependent and dynamic resistant D, which is velocity-dependent:

$$R = S + D \quad \text{(A28)}$$

The dynamic resistance is considered to be viscous in nature and thus a function of velocity at the toe of the pile V_{toe} and the damping constant J:

$$D = J * V_{toe} \quad \text{(A29)}$$

The velocity of V_{toe} can be calculated as a function of the velocity at the pile top V_{top} by applying wave propagation theory as:

$$V_{toe} = 2V_{top} - \frac{L}{Mc} RTL \quad \text{(A30)}$$

According to Goble, Likins, and Rausche (1975), the concentration of the majority of the damping resistance near the tip of the pile is caused by remolding effects. In most cases, the damping constant is proportional to the pile properties and dimensionless coefficient J_c as shown:

$$J = J_c \frac{EA}{c} \quad \text{(A31)}$$

where

E = elastic modulus of the pile

A = cross section of the pile

The value of J_c is a property of the type of soil at the tip and can be estimated based on the empirical recommendations in the *PDA Manual, Model PAK* (1996). If data from many load tests are available, the value of J_c can be back-calculated from static load tests and applied to the other piles nearby.

Computer Models

There have been several models developed for estimating bearing capacity of vibratory driven piles. The programs are based on either finite difference methods for the solution of the wave equation or finite element methods.

Finite difference model - Vibratory pile driver analyzer (VPDA)

Recently, a computer model called VPDA was developed for predicting the bearing capacity of vibratory driven piles (Moulai-Khatir, O'Neill, and Vipulanandan 1994). Based on the specified characteristic of the driver/pile/soil system, VPDA calculates the rate of penetration at which the desired pile capacity can be achieved. The predicted bearing capacity has to be input to VPDA, as the rate of penetration is calculated. Therefore, in the field application, the observed rate of penetration has to be compared to that calculated from VPDA until consistency is achieved, and then the bearing capacity from the calculation is the actual bearing capacity of the pile.

Principles of VPDA. The model is based on the rheological model developed by Smith (1960) and the finite difference solution of the wave equation. The pile in the soil is modeled as series of masses connected with springs and dashpots (Figure A4). The vibrator forcing function can be expressed as:

$$F(t) = \xi m_e e \omega^2 \sin(\omega t) \tag{A32}$$

where

ξ = efficiency of the vibrator

m_e = weight of eccentric mass

ω = operating frequency

t = time

For a model of a steel pile, the masses having weight of Mm are connected by the spring (assumed to be elastic) with stiffness Kp and a dashpot with viscous damping Cp. The soil resistance is modeled as springs and dashpots connected to each of the elements. The elasto-plastic characteristics are modeled with damping Cs at the side of the pile and Cp at the tip of the pile, and spring constants Ks at the side of the pile and Kt at the tip of the pile.

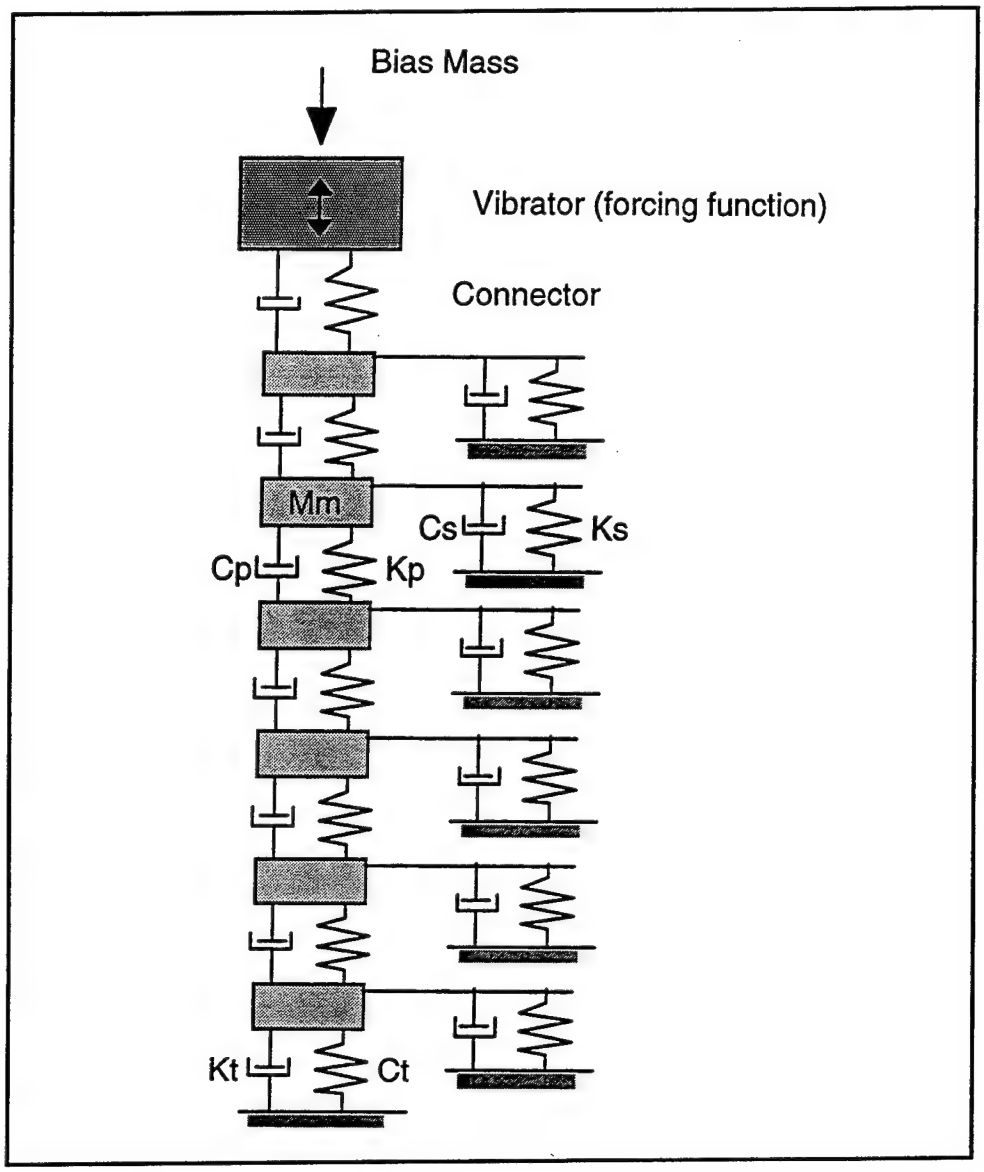

Figure A4. VPDA model

The computer model was developed in three states. First, the measured force time-history of the vibratory driver was applied as a pile-head boundary condition and the soil parameters were calculated. After the optimum soil parameters were determined, the power dissipation characteristics of the hysteric connector spring was varied until close compliance between computed and measured pile-head forces was achieved. Finally, the action of the vibratory driver was simulated by applying the static load and sinusoidal forcing function to the head of the pile and the acceleration versus time-history could be calculated for prediction of the bearing capacity. Large-scale laboratory tests were used for calibration of the model.

VPDA inputs and outputs. There are a number of input parameters (Table A1) that have to be specified for running the VPDA program. The

Table A1
Input Parameters for VPDA

Input Category	Input Variable
Driver/connector parameters	Static eccentric moment
	Weight of bias mass and vibrator
	Efficiency of vibrator
	Stiffness of connector
	Viscous and hysteretic damping of connector
Pile properties	Length of pile
	Number and length of pile elements
	Young's Modulus
	Plug height
	Weight of added mass on toe due to plugging
	Cross section of pile and pile radius
	Unit weight of soil
	Pile damping
Smith Soil Model parameters	Toe and side quake
	Toe and side damping
	Percent of load on toe
Hyperbolic soil model parameters	Side and toe stiffness for loading and unloading
	Side and toe exponent for loading and unloading
	Shear wave velocity
	External perimeter of pile
Computational capacity parameters	Predicted pile capacity
	Side shear distribution
	Side shear on 1st pile element
	Time step for output
	Pile level for output
	Computational time increment
	Driving time

parameters can be divided into several input categories: driver/connector properties, pile properties, Smith soil model parameters, hyperbolic soil model parameters, and computational capacity parameters.

For the driver/connector category, the weight of vibrator and bias as well as the static eccentric moment of the vibrator has to be specified based on the specification for the vibratory driver in use. The vibrator efficiency has to be estimated and is usually in range of 20 to 25 percent (Moulai-Khatir, O'Neill, and Vipulanandan 1994). The stiffness, viscous damping, and hysteric damping of the connector have to be specified. Some recommendations are provided in the VPDA manual (Moulai-Khatir, O'Neill, and Vipulanandan 1994).

Pile properties include length, area of cross section, pile radius, Young's modulus of pile material, and pile damping constant as well as estimated plug length and weight of added mass at the toe due to the plug. For computational

purposes, the number and length of pile elements into which the pile should be divided is also needed. The unit weight of the surrounding soil has to be specified as well.

The soil models employed in VPDA are the Smith model, commonly used for modeling of impact driving, and the hyperbolic model. As shown in Figure A5, the Smith model is an elasto-plastic soil model characterized by ultimate static resistance Ru, quake Q, and damping factor C. The quake and damping factor differ at the pile toe and the side due to the influence of pile-soil interactions to these parameters. The Smith model behaves differently at side of the pile than at the toe, where no tension is allowed. The hyperbolic soil model is a modified Ramberg-Osgood model with different loading and unloading slopes. This is shown graphically in Figure A6. The hyperbolic model is characterized by stiffnesses Kl for loading and Ku for unloading. These parameters differ for the pile side and toe. The maximum and minimum resistance fmax and fmin, respectively, are calculated in the nonlinear resistance relation using exponent μ, that must be determined empirically (Moulai-Khatir, O'Neill, and Vipulanandan 1994). The resistance fmax differs at the toe and at the side of the pile. The minimum resistance fmin for the toe of the pile is zero as no tension is allowed. The shear wave velocity and external perimeter of the pile must be used in the calculation of the resistance in the hyperbolic model.

The last input category is the predicted pile capacity. The type of side shear distribution can be chosen as triangular or uniform. Shear may or may not be specified on the first element of the pile. For computational purposes, the time step, computational time increment, and total driving time are needed. Also the predicted pile capacity, for which the calculation is made must be entered. The pile level, for which the output is given, must also be specified.

The output of VPDA consists of the rate of penetration, at which the specified pile capacity is achieved. The output also includes the displacement time-history and the velocity time-history at specified pile locations.

Laboratory experiments used for calibration of VPDA. For calibration of VPDA, 22 large-scale laboratory experiments were conducted with both vibratory and impact pile drivers and model experimental piles. Variability introduced into the testing program were soil properties, vibratory driver parameters, and soil stress conditions. The test chamber consisted of a column having diameter of 0.75 m and height of 2.5 m. The soil was submerged during all tests. The pile was instrumented to measure force and accelerations at the head and toe, total lateral soil and water pressure at the toe, and load distribution along the pile during static load testing.

For the soil properties, the grain size of sand particles and relative density were varied. Fine and coarse uniformly graded sands had effective grain sizes of 0.2 mm and 1.2 mm, respectively. The soil was placed in the chamber in two conditions: (a) isotopic stress and (b) horizontal pressure being half of vertical pressure (Ko=0.5). After initial testing, a frequency of 20 Hz was optimum for producing the highest rate of penetration and was used for the remaining tests. The effects of parameters on penetration rate are summarized

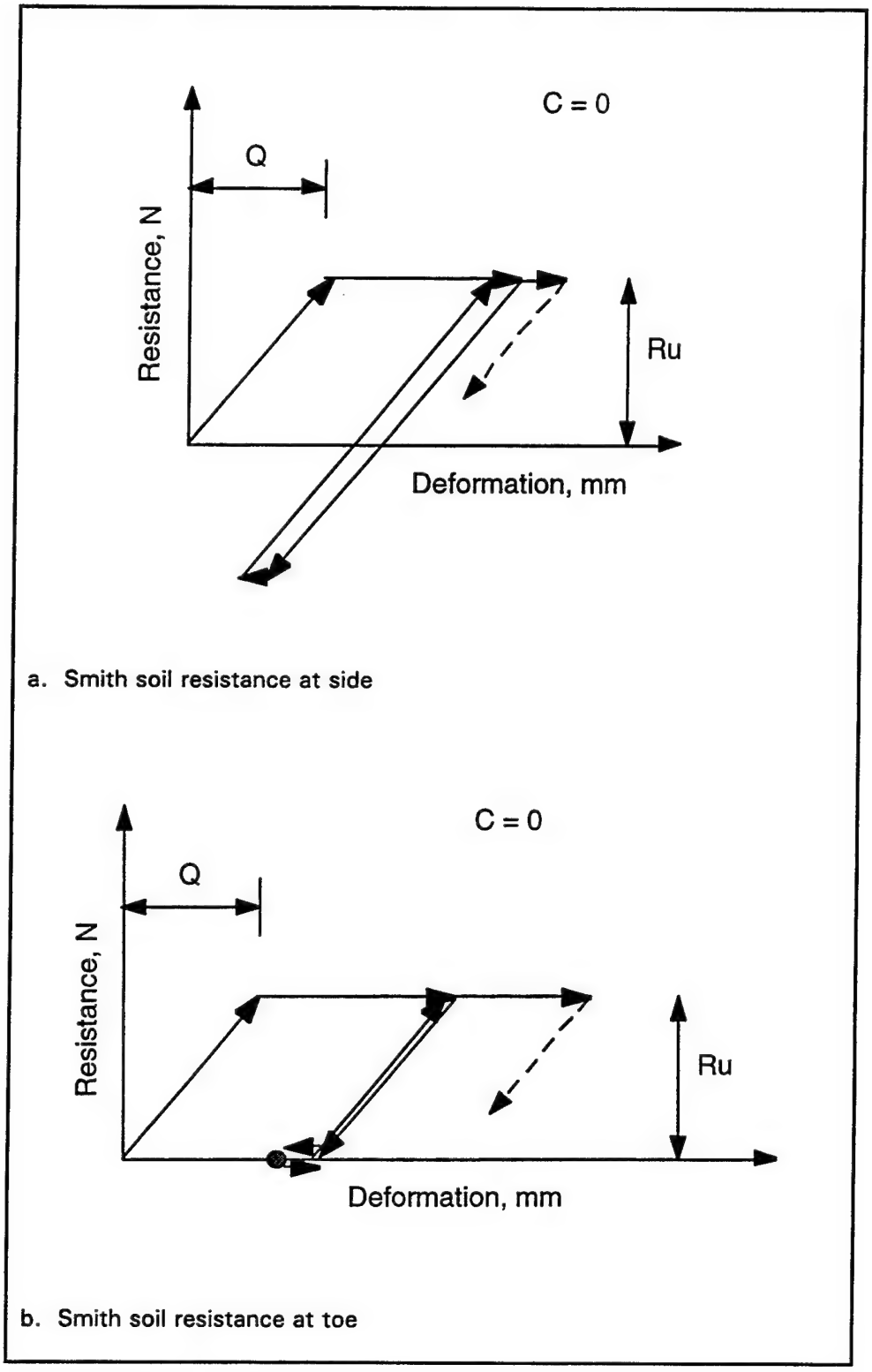

Figure A5. Smith soil resistance

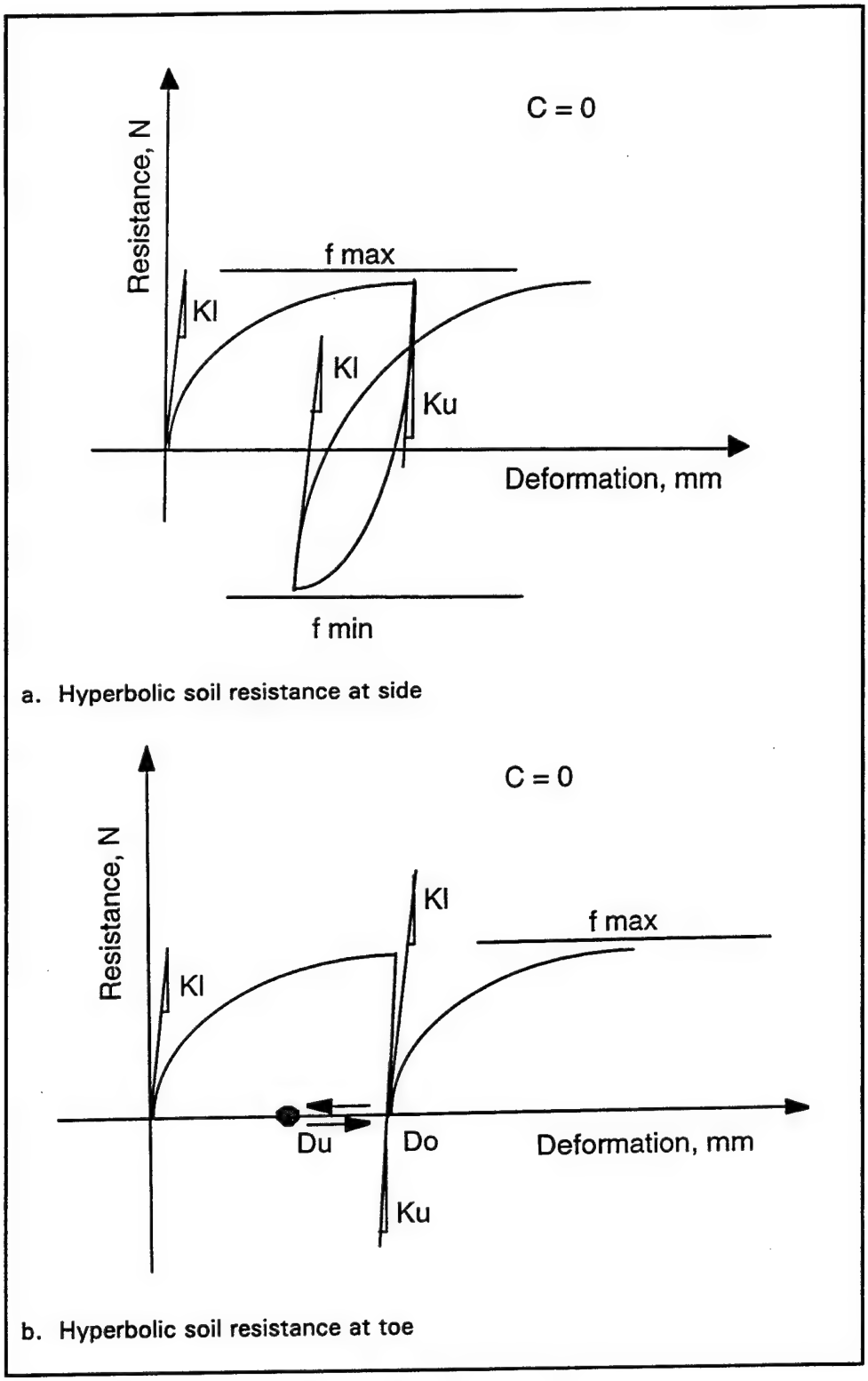

Figure A6. Hyperbolic soil resistance

as: (a) the penetration rate decreases with increasing the relative density of sand, (b) the penetration rate increases with increasing bias mass, and (c) the penetration rate decreases with increasing horizontal effective stress. The grain size had little influence on the results. The vibratory driven piles had higher capacity when driven into sand compacted to 95 percent relative density as compared to impact driven piles. However, the piles driven into sand compacted to 65 percent relative density has a lower capacity compared to impact driven piles. Restriking the vibratory driven piles did not produce a significant increase in capacity. Pile-head acceleration, velocity of penetration, and power delivered to the pile head were the major factors affecting the driving of the piles.

Programs preceding PDA - VIBEWAVE and TNOWAVE. A wave equation analysis program using the Smith pile-soil model (Smith 1960) was developed by Hirsch, Carr, and Lowery (1976). The pile-driving system is analyzed as a series of concentrated weights and weightless springs. Hirsch, Carr, and Lowery (1976) developed recommendations for improvement of the computer model to account for nonlinear behavior of isolation springs, that causes major discrepancies in the comparison.

The program, VIBEWAVE, was calibrated using field tests with pile driven into very dense sand at the Naval Civil Engineering Laboratory in Port Hueneme, California (Gardner 1987). As part of their calibration procedure, they compared the magnitudes of forces calculated with VIBEWAVE and forces measured in the field and identified which of the input parameters into VIBEWAVE significantly affected the results of analysis. Forces at different points along the length of the pile were extracted from the recorded data and were compare to calculated forces from VIBEWAVE. The VIBEWAVE calculations gave larger forces than the experimental data. Gardner (1987) identified that a proper simulation of the vibratory drive is critical for predicting correct results and suggested that the effects of the water table on driving should be defined.

Bielefeld and Middendorp (1992) developed a pile-driving prediction program, TNOWAVE, based on the solution from the wave equation. TNOWAVE can be used to analyze the performance of the vibratory driver and can predict several parameters including maximum stress in the pile, amplitude of vibration at several levels in the pile, penetration rate, and vibrations in nearby buildings. The program can analyze multilayered soil profiles and can employ different soil models. The whole driving process can be simulated from start of driving to the final depth of penetration by performing the stress wave calculation at several depths of penetration. TNOWAVE is particularly useful for selecting the appropriate driver size for given soil conditions and to determine the possibility of damaging the pile during driving due to overloading.

Finite element program

A finite element model of a vibratory driven pile was created by Smith and To (1988) by making an analogy between the response of vibratory driven pile, which is sinusoidally loaded, and an impact driven pile. The vibratory driven pile is modeled by using 1-D approximations of a simple elastic/plastic model

combined with the Mohr-Coulomb failure hypothesis of the soil. Smith and To (1988) compared their simulations with small-scale laboratory experiments on piles driven into sand for about 2 m. In their model, they assumed zero interface damping. However, from results of their laboratory study, they found that the type of soils had a significant influence and suggested the need for creating more realistic numerical models taking into account fluidization in sands, cyclic degradation, and rate effects in clays.

Static Load Test Evaluations

For a static load test, the failure load is reached when rapid movement occurs under sustained load. There are several different definitions of failure loads derived from load-movement records of a static load test, some of which are presented in this section. Pile load test data are required for the Davisson (1972), Brinch-Hansen (1963), and Chin-Kondner (Chin 1970) methods described in the following paragraphs.

Davisson (1972) proposed an offset limit method, where the limit load is defined as the load corresponding to the movement which exceeds the elastic compression of the pile by X in millimeters, where X is:

$$X = 3.8 + \frac{D}{3{,}048} \tag{A33}$$

and D is diameter of the pile in millimeters.

Graphically, the interpretation of offset limit load Q_u is shown in Figure A7.

The Davisson limit was developed in conjunction with wave equation analysis of driven piles and dynamic measurement and it is primarily intended for test results from driven piles tested according to quick methods (Fellenius 1990).

Brinch-Hansen (1963) proposed the so called 80 percent criterion that defines the failure load as that load which gives four times the movement of the pile head as that obtained for 80 percent of that load. The following relation can be derived by applying the Brinch-Hansen criteria for calculation of ultimate failure load Q_u:

$$Q_u = \frac{1}{2\sqrt{C_1 C_2}} \tag{A34}$$

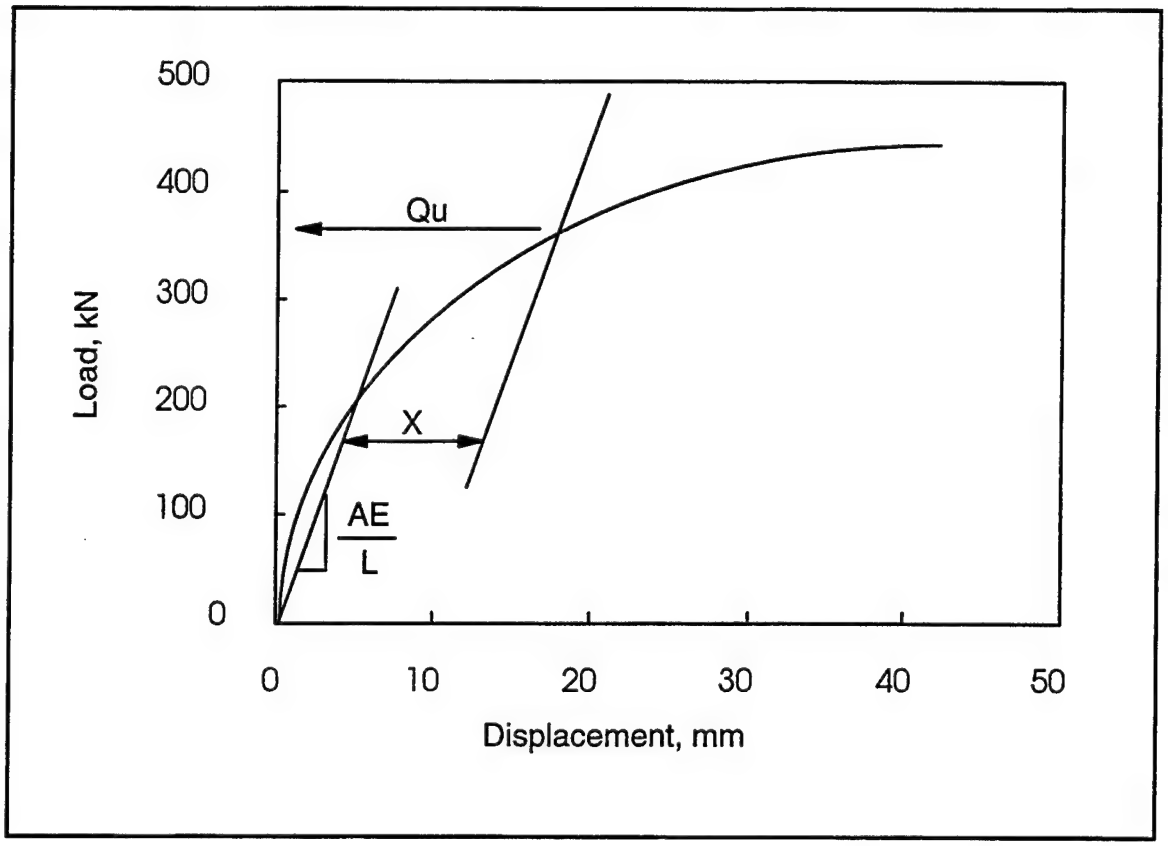

Figure A7. Davisson offset limit (after Davisson 1972)

where

C_1 = slope

C_2 = intersect of the line defined as:

$$\frac{\sqrt{d}}{Q} = C_1 d + C_2 \qquad \text{(A35)}$$

where

d = pile movement

Q = load

The values for d and Q are obtained from pile load test data.

Referring to Figure A8, the criterion determines the straight line that has to be plotted through the data so that most of the data points lie close to the superimposed line, especially near the point of the ultimate load (Fellenius 1990).

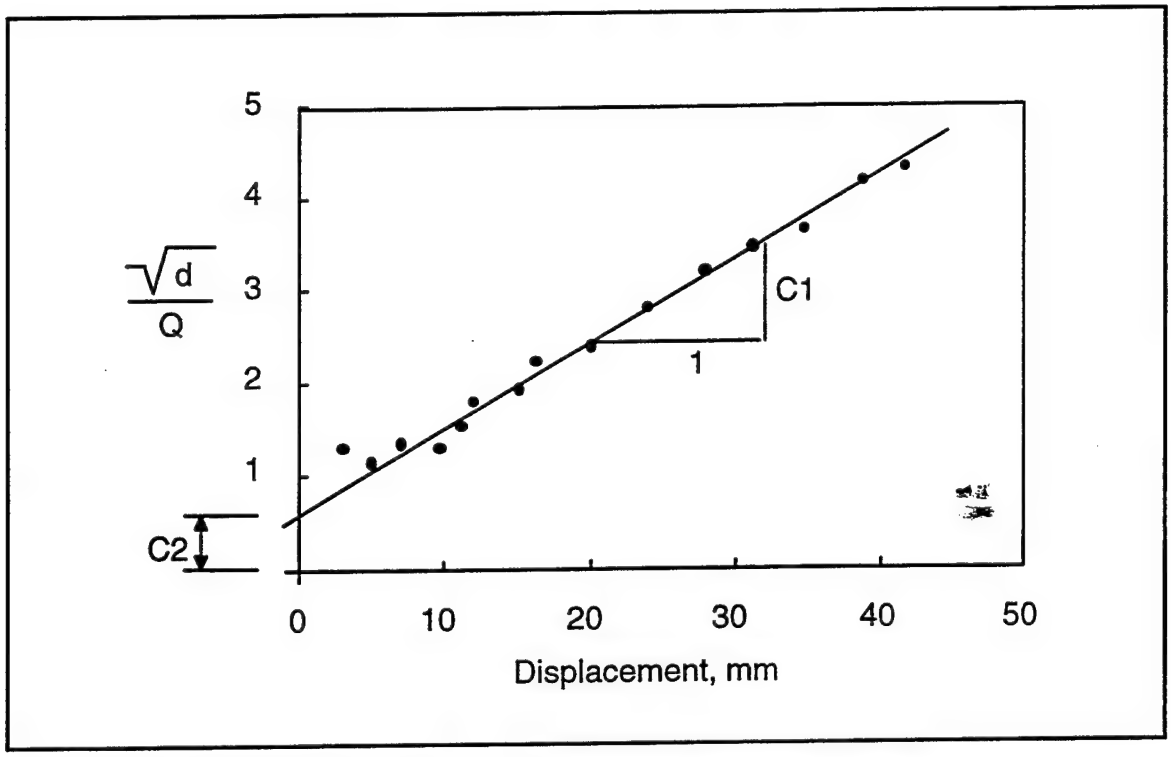

Figure A8. Brinch-Hansen method (after Brinch-Hansen 1963)

Chin-Kondner proposed a method for finding the ultimate load from load test results (Fellenius 1990). As shown in Figure A9, the plot of movement versus a ratio of movement to load is required. After some initial variation, the plotted values fall on a straight line. The inverse of the slope of this line is the Chin-Kondner failure load:

$$Q_u = \frac{1}{C_1} \tag{A36}$$

where C_1 is the slope the line defined as:

$$\frac{d}{Q} = C_1 d + C_2 \tag{A37}$$

where

d = pile movement

Q = load during the pile load test

Typically, the Chin-Kondner failure load is about 20 to 40 percent greater than the Davisson limit. The shortcoming of this method is that the straight line may not be achieved during testing and the data must be extrapolated.

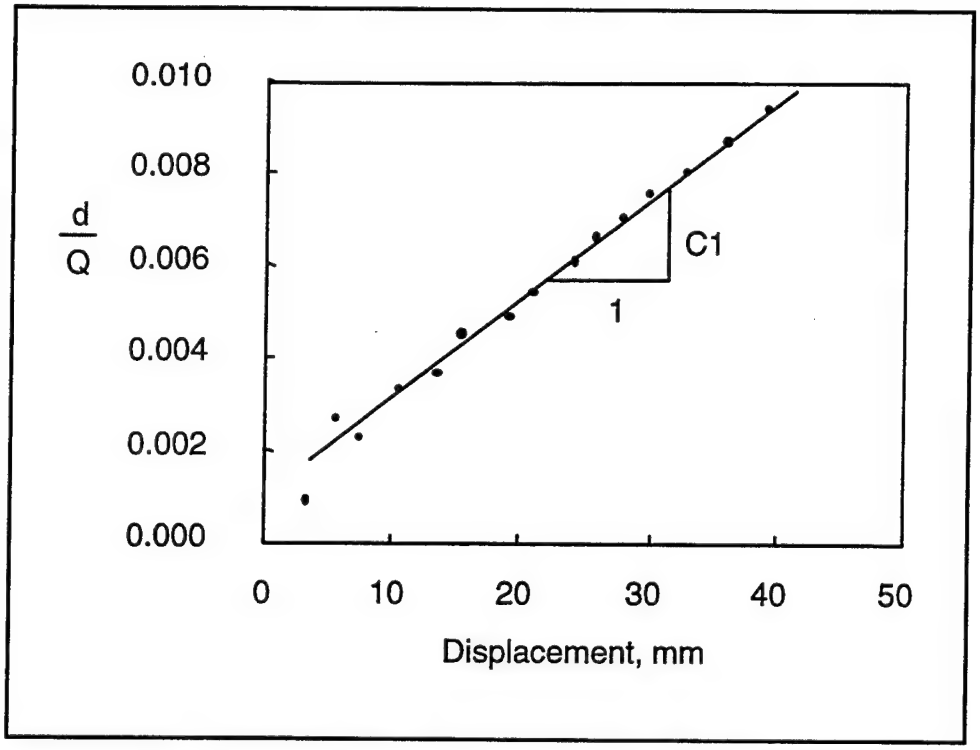

Figure A9. Chin-Kondner extrapolation (after Chin 1970)

However, Fellenius (1990) recommends that static load test data should never be extrapolated.

Appendix B
Investigation Using Fractional Factorial Design

Table B1
Fractional Factorial Design 2^{15-10} for Initial Investigation of VPDA

	Factor														
Run	EccMom	Bias	Vibrator	Freq	Type	Size	Length	Model	Effcn	Stiff	Damp	Tip	Soil	DamPile	Veloc
1	-	-	-	-	-	-	-	-	-	-	-	-	-	-	-
2	+	-	-	-	-	+	+	+	+	+	+	-	-	-	-
3	-	+	-	-	-	+	+	+	-	-	-	+	+	+	-
4	+	+	-	-	-	-	-	-	+	+	+	+	+	+	-
5	-	-	+	-	-	+	-	-	+	+	-	+	+	-	+
6	+	-	+	-	-	-	+	+	-	-	+	+	+	-	+
7	-	+	+	-	-	-	+	+	+	+	-	-	-	+	+
8	+	+	+	-	-	+	-	-	-	-	+	-	-	+	+
9	-	-	-	+	-	-	+	-	+	-	+	+	-	+	+
10	+	-	-	+	-	+	-	+	-	+	-	+	-	+	+
11	-	+	-	+	-	+	-	+	+	-	+	-	+	-	+
12	+	+	-	+	-	-	+	-	-	+	-	-	+	-	+
13	-	-	+	+	-	+	+	-	-	+	+	-	+	+	-
14	+	-	+	+	-	-	-	+	+	-	-	-	+	+	-
15	-	+	+	+	-	-	-	+	-	+	+	+	-	-	-
16	+	+	+	+	-	+	+	-	+	-	-	+	-	-	-
17	-	-	-	-	+	-	-	+	-	+	+	-	+	+	+
18	+	-	-	-	+	+	+	-	+	-	-	-	+	+	+
19	-	+	-	-	+	+	+	-	-	+	+	+	-	-	+
20	+	+	-	-	+	-	-	+	+	-	-	+	-	-	+
21	-	-	+	-	+	+	-	+	+	-	+	+	-	+	-
22	+	-	+	-	+	-	+	-	-	+	-	+	-	+	-
23	-	+	+	-	+	-	+	-	+	-	+	-	+	-	-
24	+	+	+	-	+	+	-	+	-	+	-	-	+	-	-
25	-	-	-	+	+	-	+	+	+	+	-	+	+	-	-
26	+	-	-	+	+	+	-	-	-	-	+	+	+	-	-
27	-	+	-	+	+	+	-	-	+	+	-	-	-	+	-
28	+	+	-	+	+	-	+	+	-	-	+	-	-	+	-
29	-	-	+	+	+	+	+	+	-	-	-	-	-	-	+
30	+	-	+	+	+	-	-	-	+	+	+	-	-	-	+
31	-	+	+	+	+	-	-	-	-	-	-	+	+	+	+
32	+	+	+	+	+	+	+	+	+	+	+	+	+	+	+
33	0	0	0	0	+	0	0	+	0	0	0	0	0	0	0
34	0	0	0	0	+	0	0	-	0	0	0	0	0	0	0
35	0	0	0	0	-	0	0	+	0	0	0	0	0	0	0
36	0	0	0	0	-	0	0	-	0	0	0	0	0	0	0

Table B2
VPDA Response for Initial Investigation Using Fractional Factorial Design 2^{15-10}

Run	Rate of Penetration in mm/sec Bearing Capacity in kN 67	89	111	133	156	178	200
1	61.341	24.989	1.966	0.988	0.000	0.000	0.000
2	43.144	0.000	0.000	0.000	0.000	0.000	0.000
3	44.148	49.804	52.296	41.575	25.669	23.950	31.438
4	192.339	170.584	149.865	130.119	111.206	93.088	75.656
5	74.005	53.078	36.286	22.647	11.603	2.850	1.135
6	229.837	184.470	152.443	116.048	106.744	92.055	75.385
7	143.538	37.653	10.714	0.000	0.000	0.000	0.000
8	201.910	183.177	166.733	152.116	139.012	127.155	116.368
9	36.276	20.975	7.592	4.801	4.450	4.120	3.787
10	25.573	0.000	0.000	0.000	0.000	0.000	0.000
11	116.253	105.303	105.936	85.540	72.984	98.049	90.693
12	75.314	71.138	66.860	62.522	58.163	53.792	49.449
13	50.043	43.884	38.542	33.797	29.512	25.593	21.968
14	364.480	303.273	242.014	220.033	0.000	0.000	0.000
15	110.302	13.886	0.000	0.000	0.000	0.000	0.000
16	89.530	84.089	78.516	72.829	67.089	61.270	55.402
17	71.506	78.252	71.333	14.544	0.000	0.000	0.000
18	34.455	31.890	29.210	26.444	23.625	20.785	17.950
19	19.820	9.467	2.728	0.000	1.011	0.838	0.541
20	149.408	34.153	0.000	0.000	0.000	0.000	0.000
21	52.819	4.186	0.000	0.000	0.000	0.000	0.000
22	119.642	104.320	89.438	74.191	58.227	43.198	29.042
23	79.723	69.873	62.197	54.628	47.668	41.420	35.786
24	299.400	243.655	218.247	204.737	188.813	170.815	160.533
25	69.705	56.688	36.398	11.707	7.135	11.036	3.752
26	83.528	74.163	64.778	55.364	46.012	36.670	27.407
27	96.606	78.456	61.925	45.496	29.157	14.930	4.552
28	159.301	0.000	0.000	0.000	0.000	0.000	0.000
29	74.054	9.144	0.000	0.000	0.000	0.000	0.000
30	276.875	250.297	226.916	206.131	187.508	170.693	155.346
31	102.296	88.168	64.826	45.738	29.746	16.162	4.308
32	401.549	319.717	245.387	181.864	133.154	91.735	59.172
33	221.800	187.790	147.284	101.877	88.976	74.061	83.749
34	96.116	85.895	76.180	66.949	58.174	49.789	41.697
35	217.640	184.290	140.627	94.816	72.507	62.949	49.743
36	96.251	86.111	76.492	67.363	58.699	50.437	42.502

Table B3
Fractional Factorial Design 2^{12-7} for Second Investigation of VPDA

Run	Freq	Type	Size	Length	Model	Effcn	Stiff	Damp	Tip	Soil	DamPile	Veloc
1	-	-	-	-	-	-	-	-	-	-	-	-
2	+	-	-	-	-	+	+	+	+	-	+	+
3	-	+	-	-	-	-	-	+	+	-	+	-
4	+	+	-	-	-	+	+	-	-	-	-	+
5	-	-	+	-	-	+	+	-	-	+	+	-
6	+	-	+	-	-	-	-	+	+	+	-	+
7	-	+	+	-	-	+	+	+	+	+	-	-
8	+	+	+	-	-	-	-	-	-	+	+	+
9	-	-	-	+	-	-	+	+	-	+	+	+
10	+	-	-	+	-	+	-	-	+	+	-	-
11	-	+	-	+	-	-	+	-	+	+	-	+
12	+	+	-	+	-	+	-	+	-	+	+	-
13	-	-	+	+	-	+	-	+	-	-	-	+
14	+	-	+	+	-	-	+	-	+	-	+	-
15	-	+	+	+	-	+	-	-	+	-	+	+
16	+	+	+	+	-	-	+	+	-	-	-	-
17	-	-	-	-	+	+	-	-	+	+	+	+
18	+	-	-	-	+	-	+	+	-	+	-	-
19	-	+	-	-	+	+	-	+	-	+	-	+
20	+	+	-	-	+	-	+	-	+	+	+	-
21	-	-	+	-	+	-	+	-	+	-	-	+
22	+	-	+	-	+	+	-	+	-	-	+	-
23	-	+	+	-	+	-	+	+	-	-	+	+
24	+	+	+	-	+	+	-	-	+	-	-	-
25	-	-	-	+	+	+	+	+	+	-	-	-
26	+	-	-	+	+	-	-	-	-	-	+	+
27	-	+	-	+	+	+	+	-	-	-	+	-
28	+	+	-	+	+	-	-	+	+	-	-	+
29	-	-	+	+	+	-	-	+	+	+	+	-
30	+	-	+	+	+	+	+	-	-	+	-	+
31	-	+	+	+	+	-	-	-	-	+	-	-
32	+	+	+	+	+	+	+	+	+	+	+	+

Table B4
VPDA Response for Second Investigation Using Fractional Factorial Design 2^{15-10}

Run	Rate of Penetration in mm/sec Bearing Capacity in kN			
	44	111	178	245
1	89.088	27.511	2.314	1.377
2	70.891	6.055	5.580	5.128
3	65.352	0.584	0.000	0.000
4	92.832	38.654	3.383	0.582
5	55.166	19.370	1.300	0.638
6	40.221	3.462	2.852	2.256
7	44.110	0.551	0.000	0.000
8	48.100	18.654	0.000	0.000
9	54.808	18.265	1.796	1.575
10	51.217	5.540	5.067	4.648
11	39.459	0.000	0.000	0.000
12	66.164	29.571	2.814	0.528
13	43.602	17.033	1.293	0.610
14	36.068	3.053	2.499	1.979
15	33.924	0.000	0.000	0.000
16	43.739	17.457	0.518	0.000
17	79.896	13.068	0.000	0.000
18	94.518	6.002	0.000	0.000
19	114.765	45.392	45.357	0.000
20	71.869	0.000	0.000	0.000
21	75.126	0.000	0.000	0.000
22	124.236	37.620	24.844	31.608
23	96.644	27.277	40.137	41.212
24	99.789	11.986	0.000	0.000
25	85.128	4.275	0.000	0.000
26	98.242	0.000	0.000	0.000
27	118.265	42.050	39.525	26.520
28	79.860	0.000	0.000	0.000
29	84.176	0.000	0.000	0.000
30	136.347	30.965	26.782	5.398
31	109.576	17.008	27.252	24.793
32	107.899	4.628	0.000	0.000

Appendix C
Profiles of Rates of Penetration

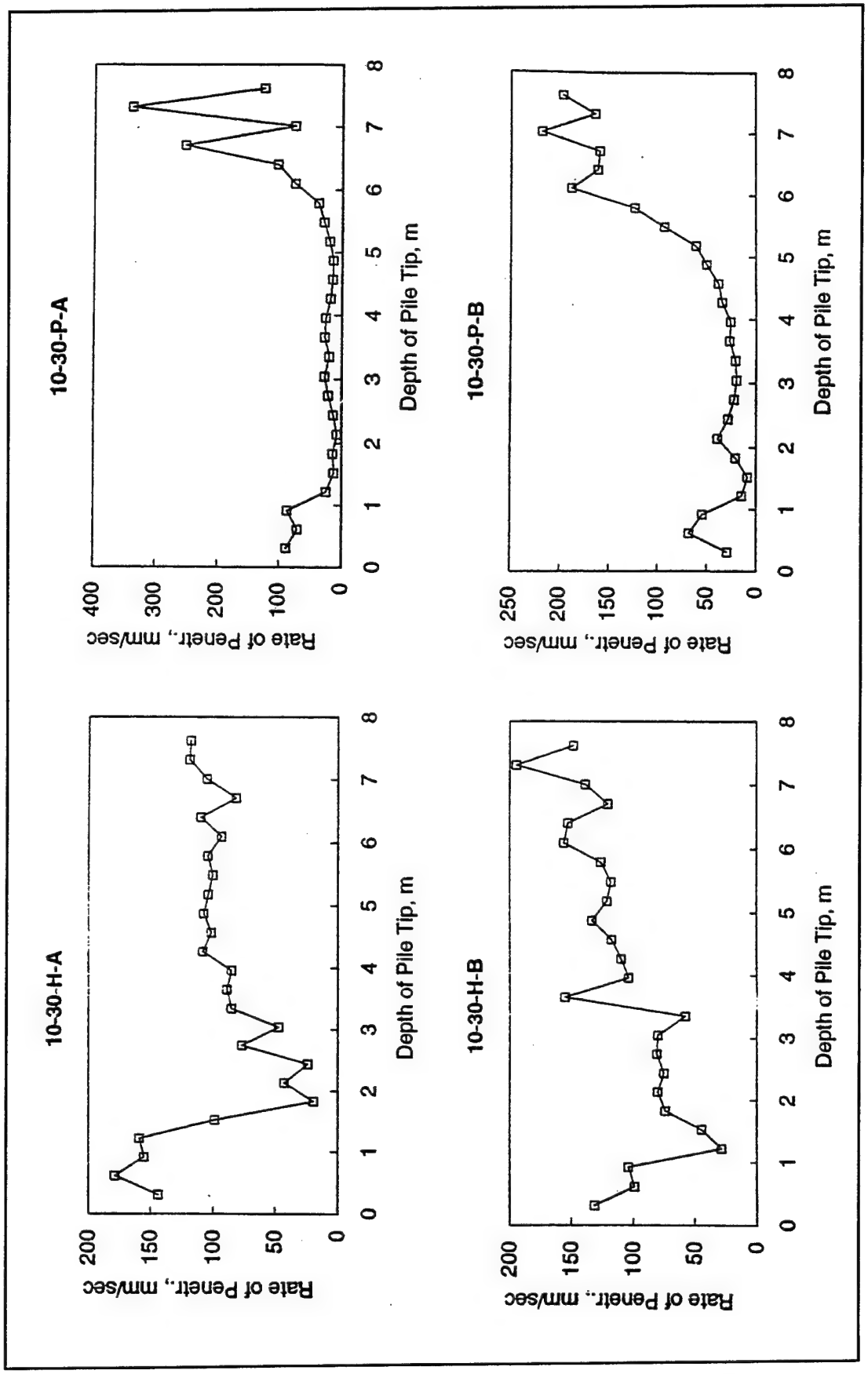

Figure C1. Rates of penetration for piles - 250-mm diam and 9-m length

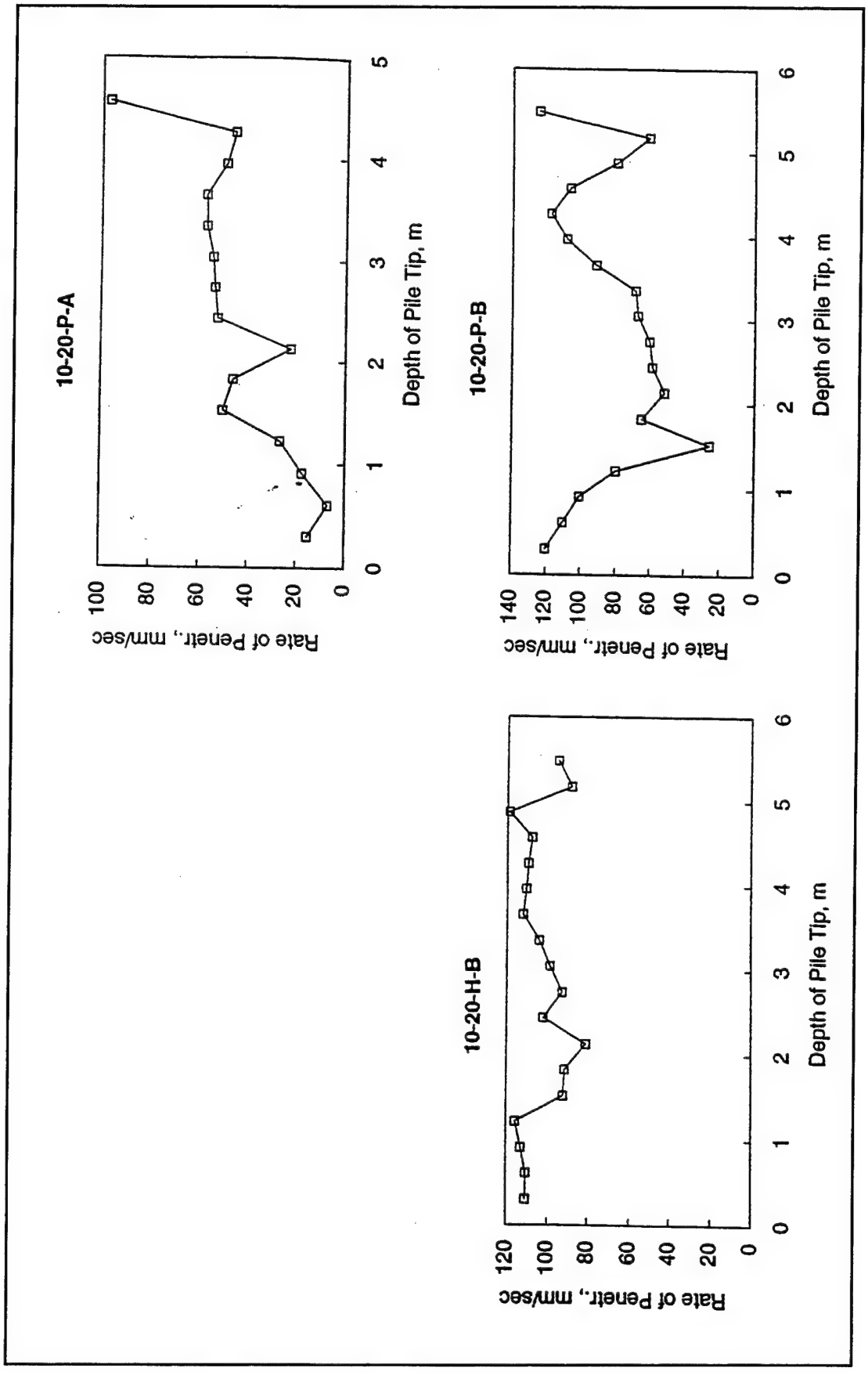

Figure C2. Rates of penetration for piles - 250-mm diam and 6.1-m length

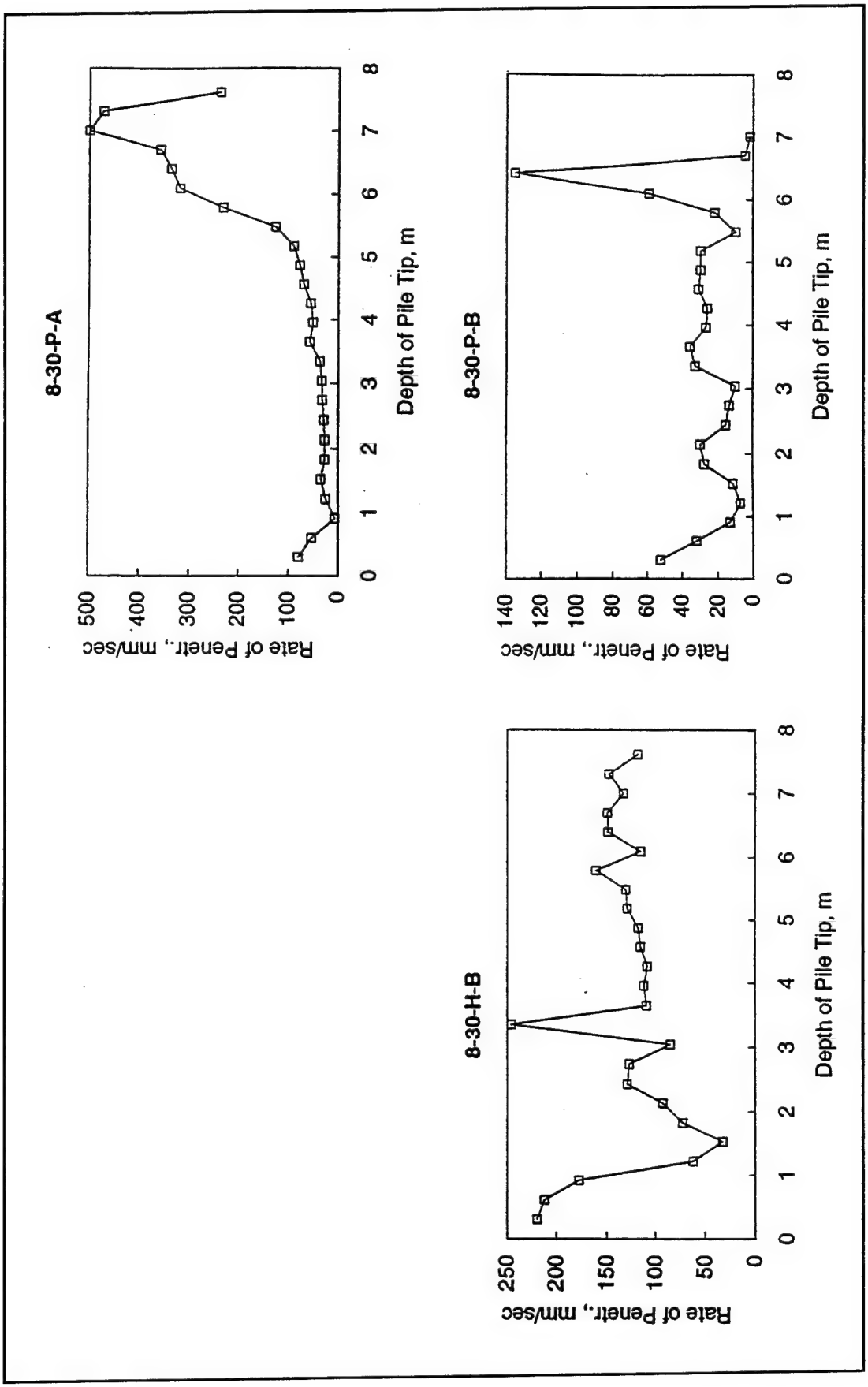

Figure C3. Rates of penetration for piles - 200-mm diam and 9-m length

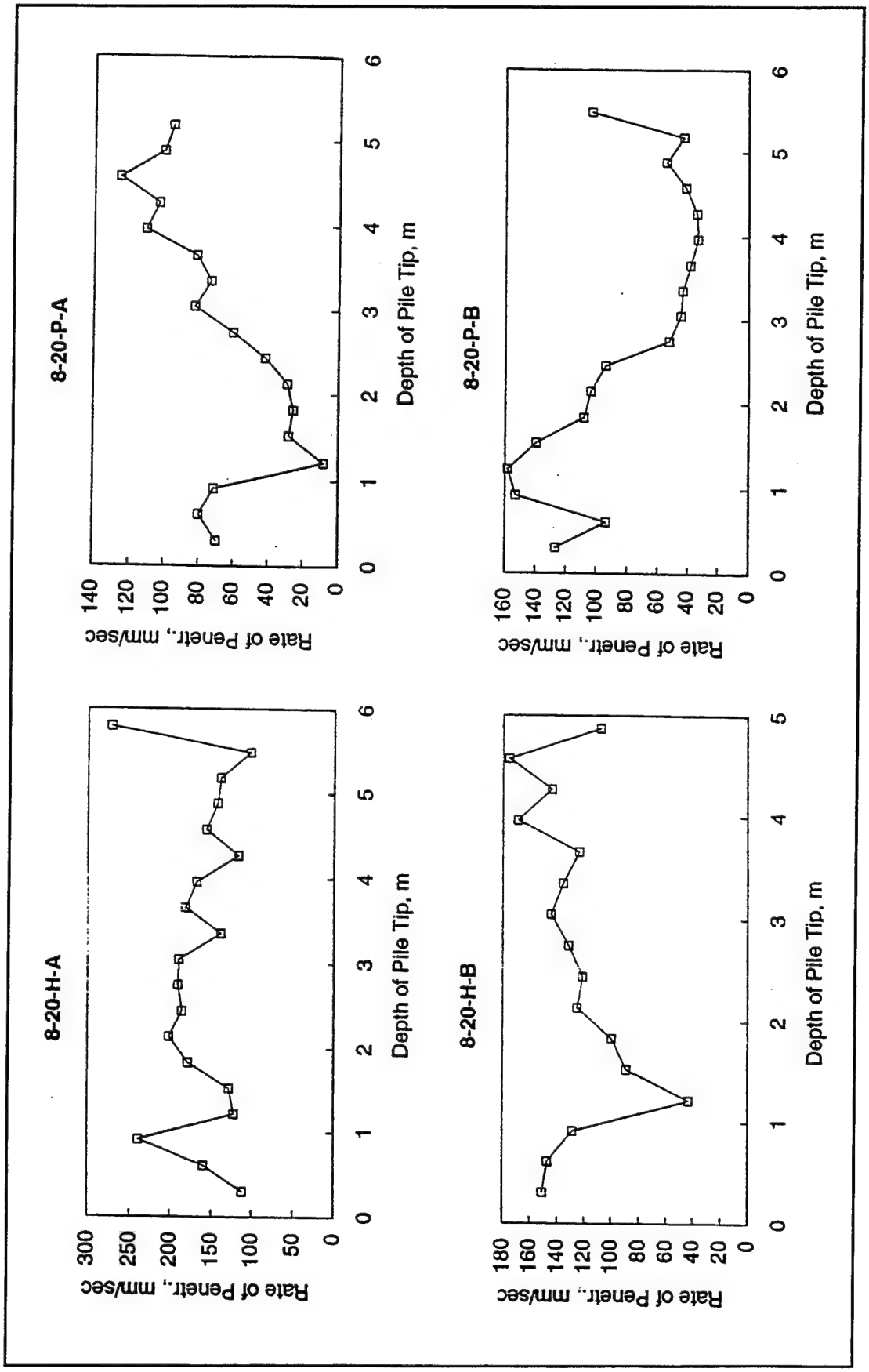

Figure C4. Rates of penetration for piles - 200-mm diam and 6.1-m length

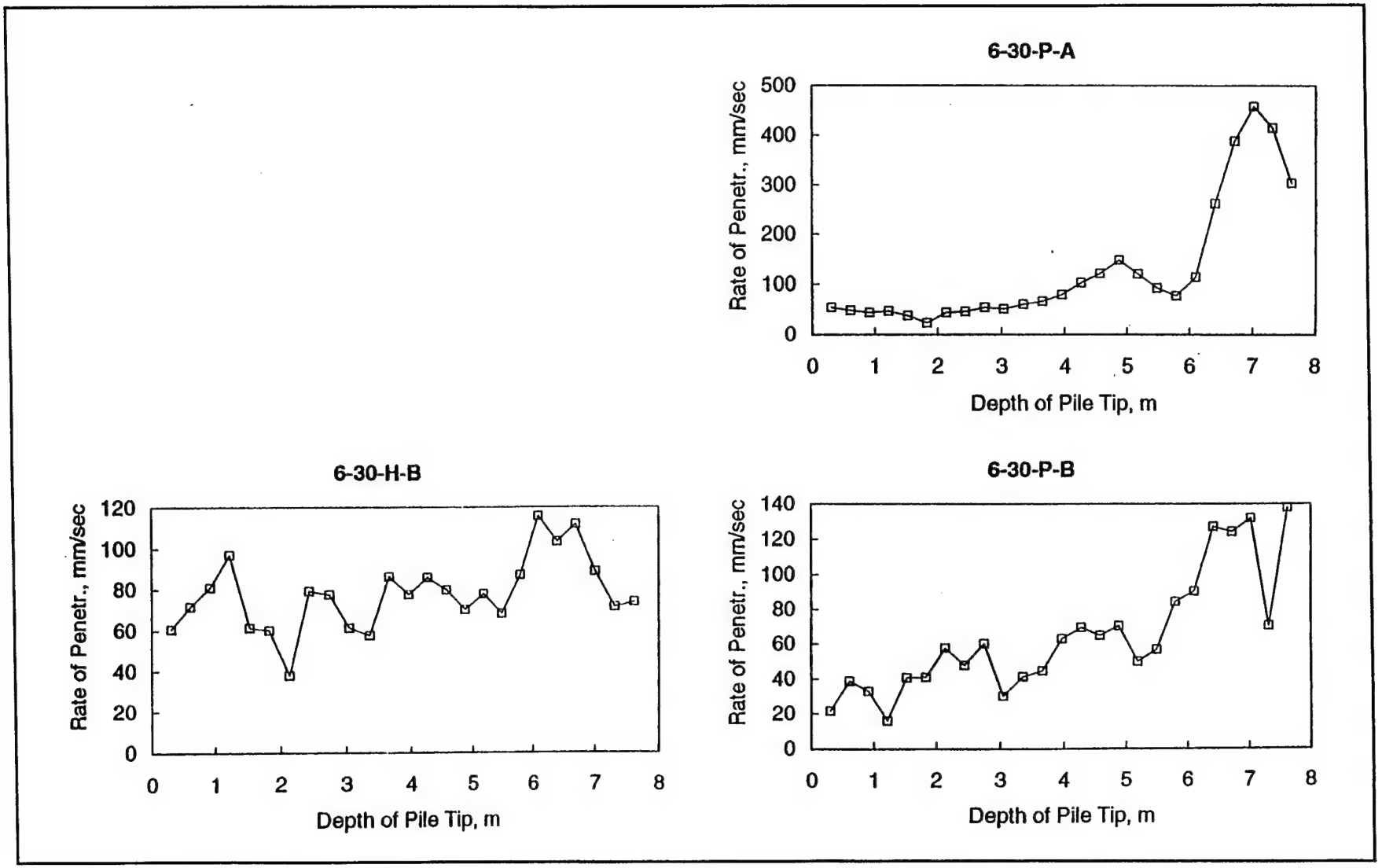

Figure C5. Rates of penetration for piles - 150-mm diam and 9-m length

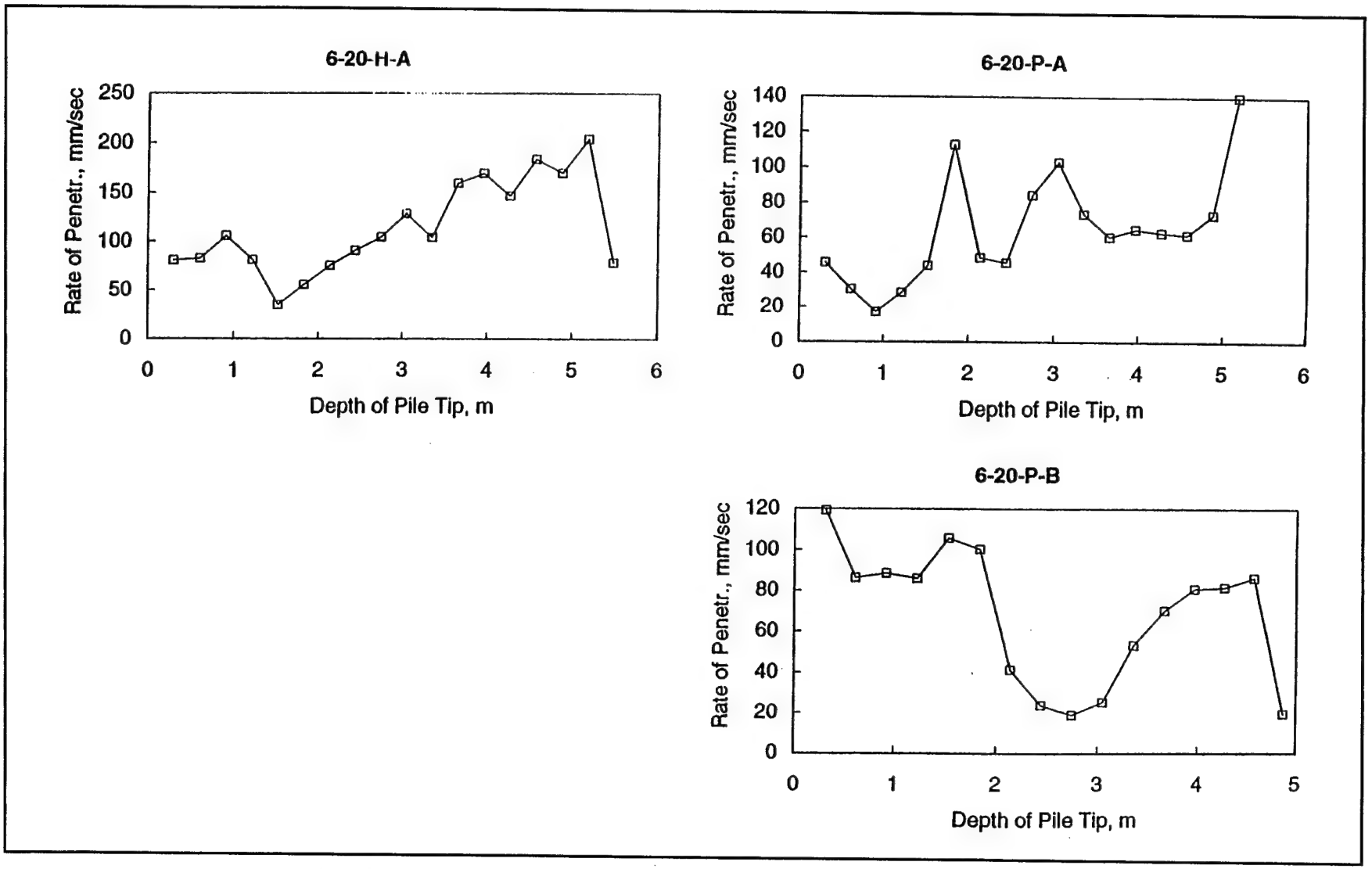

Figure C6. Rates of penetration for piles - 150-mm diam and 6.1-m length

Appendix D
Profiles of Frequency

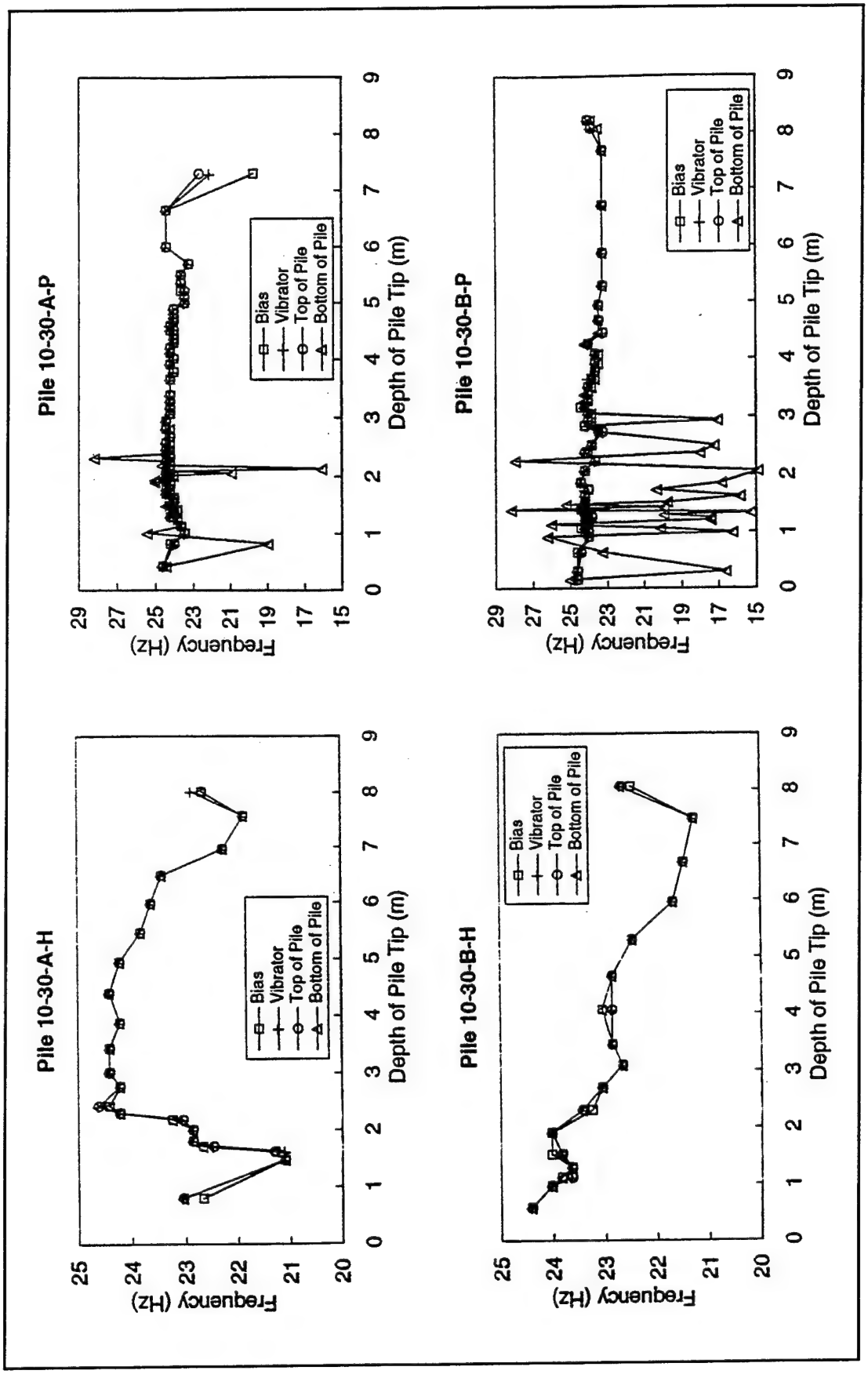

Figure D1. Frequency of vibration of piles - 250-mm diam and 9-m length

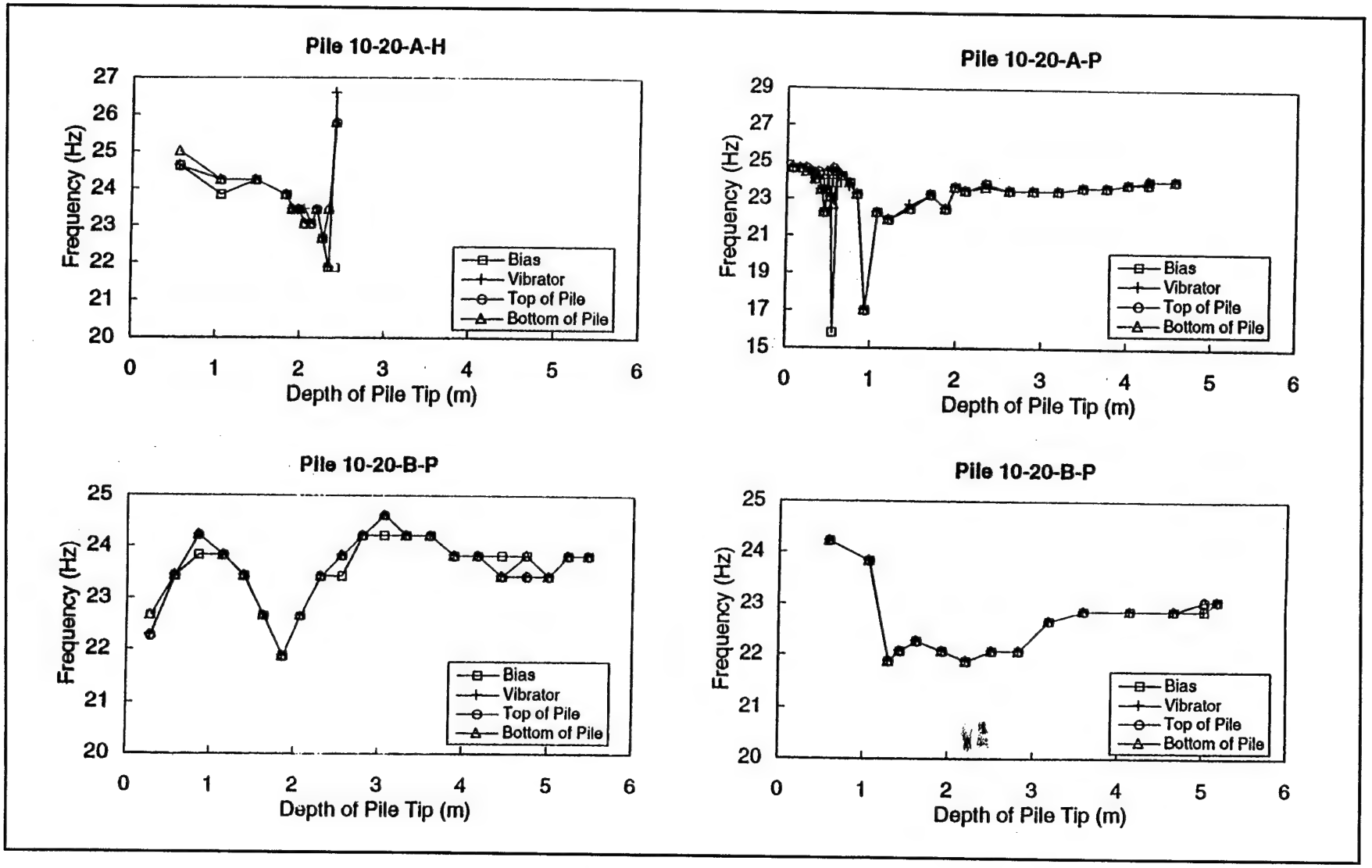

Figure D2. Frequency of vibration of piles - 250-mm diam and 6.1-m length

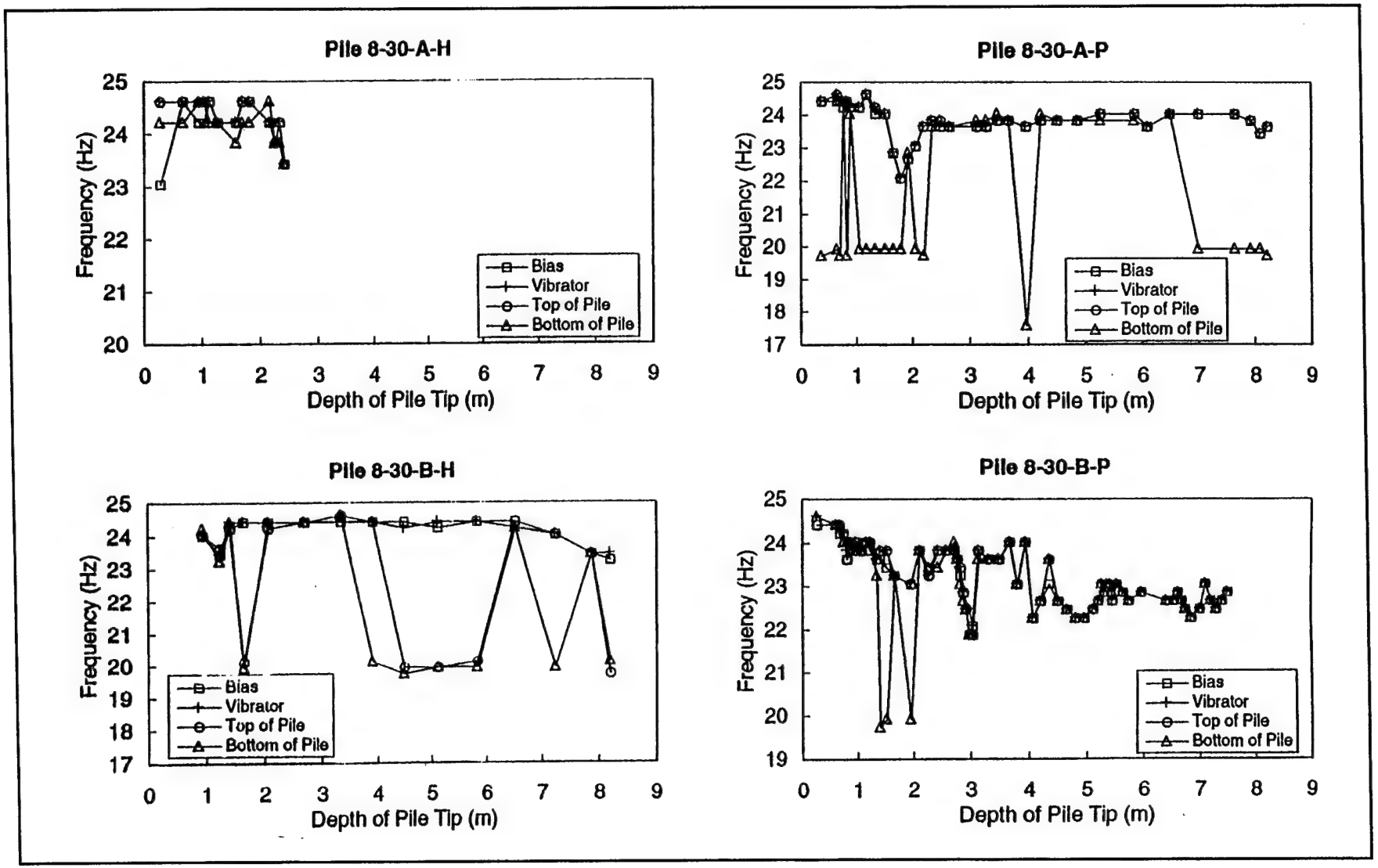

Figure D3. Frequency of vibration of piles - 200-mm diam and 9-m length

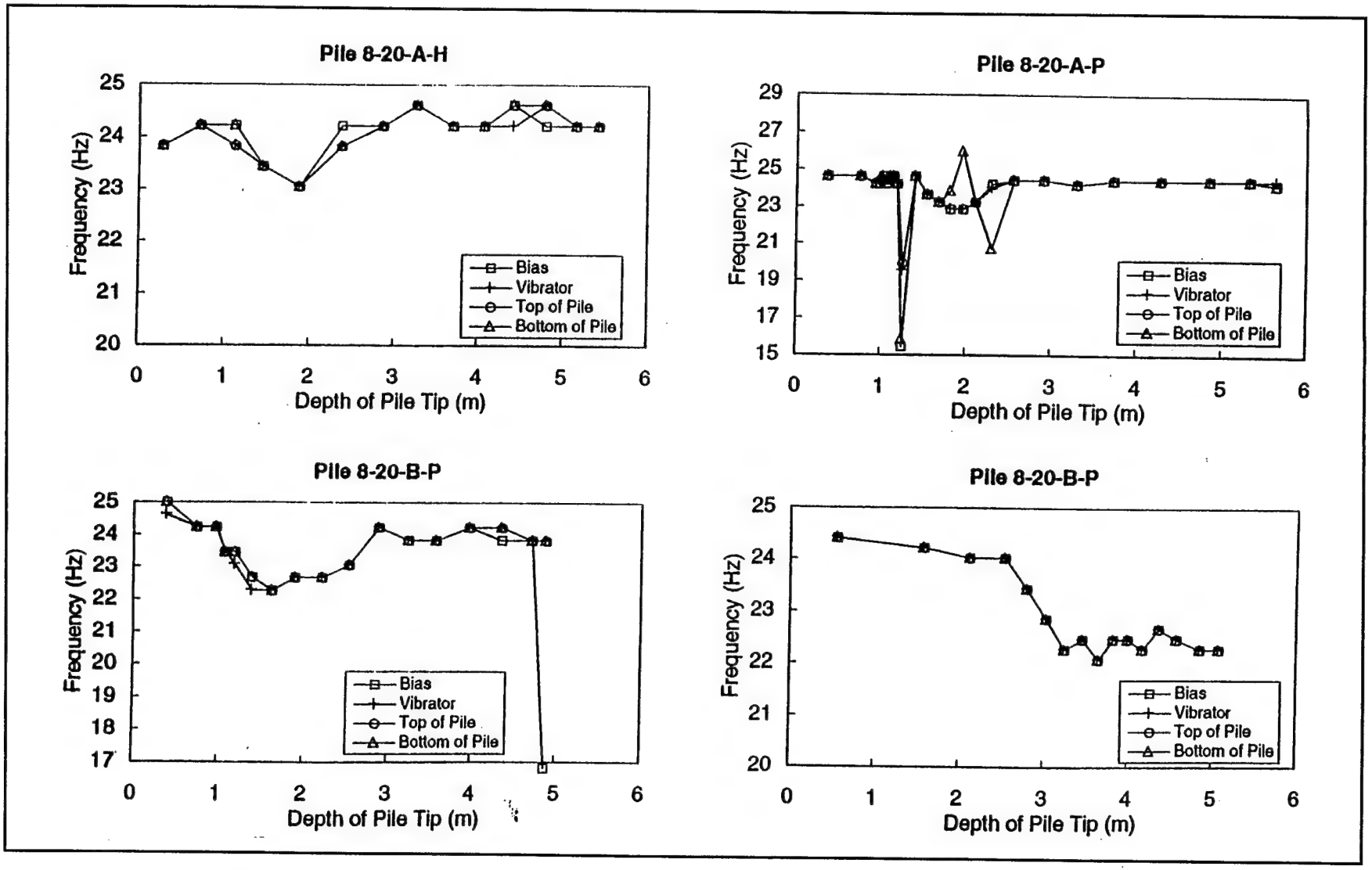

Figure D4. Frequency of vibration of piles - 200-mm diam and 6.1-m length

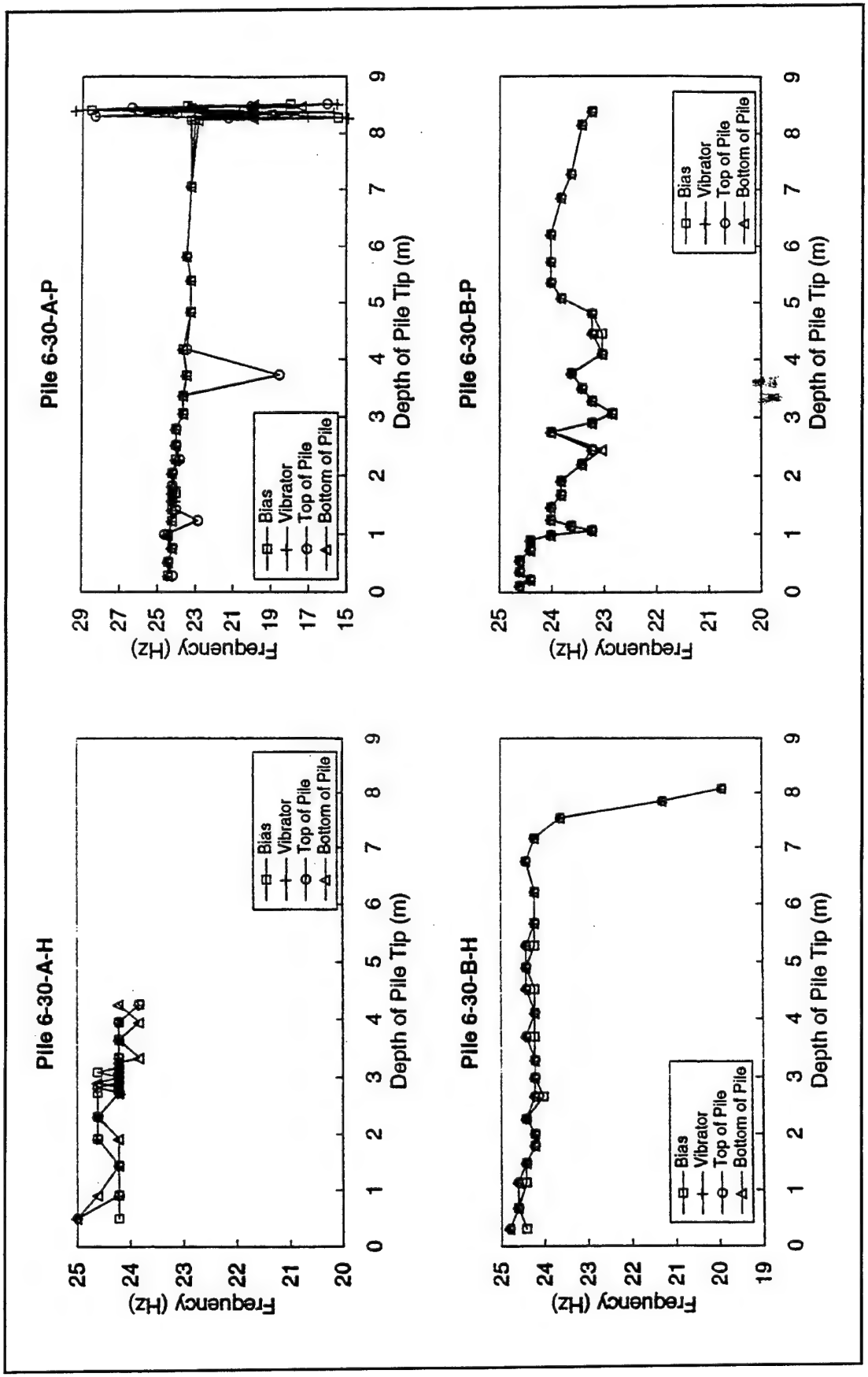

Figure D5. Frequency of vibration of piles - 150-mm diam and 9-m length

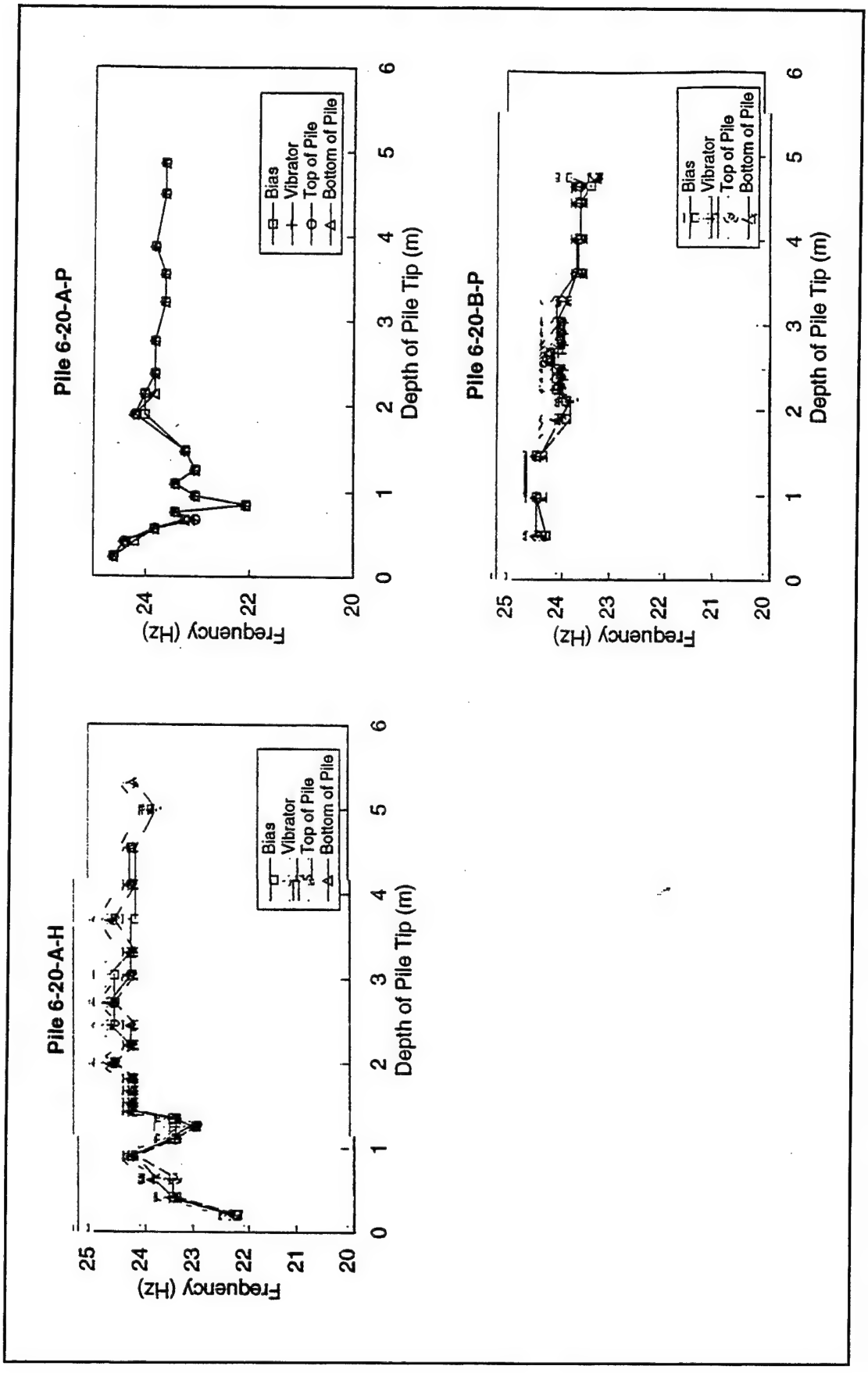

Figure D6. Frequency of vibration of piles - 150-mm diam and 6.1-m length

Appendix E
Profiles of Acceleration Amplitude

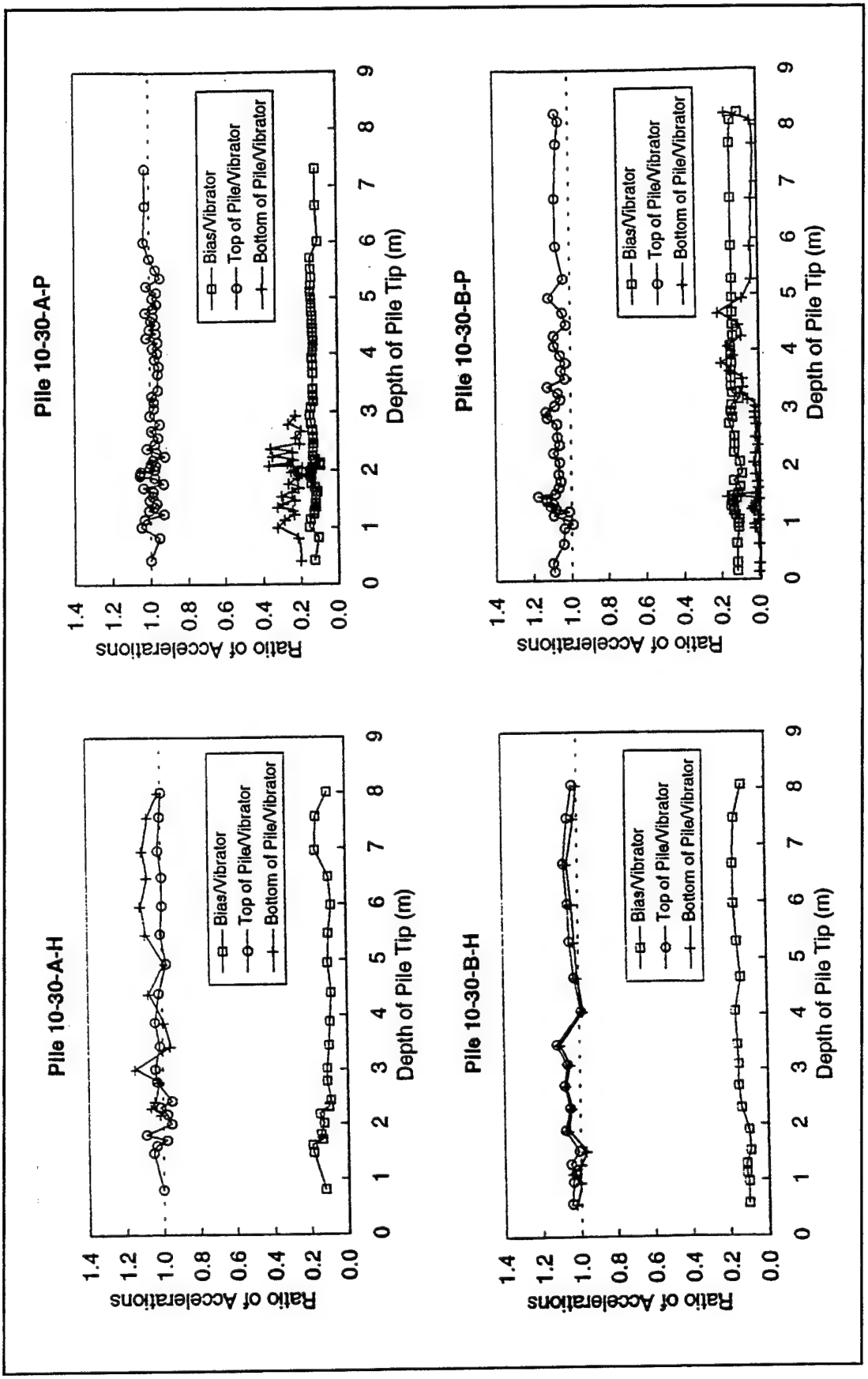

Figure E1. Amplitude of vibration as normalized acceleration for piles - 250-mm diam and 9-m length

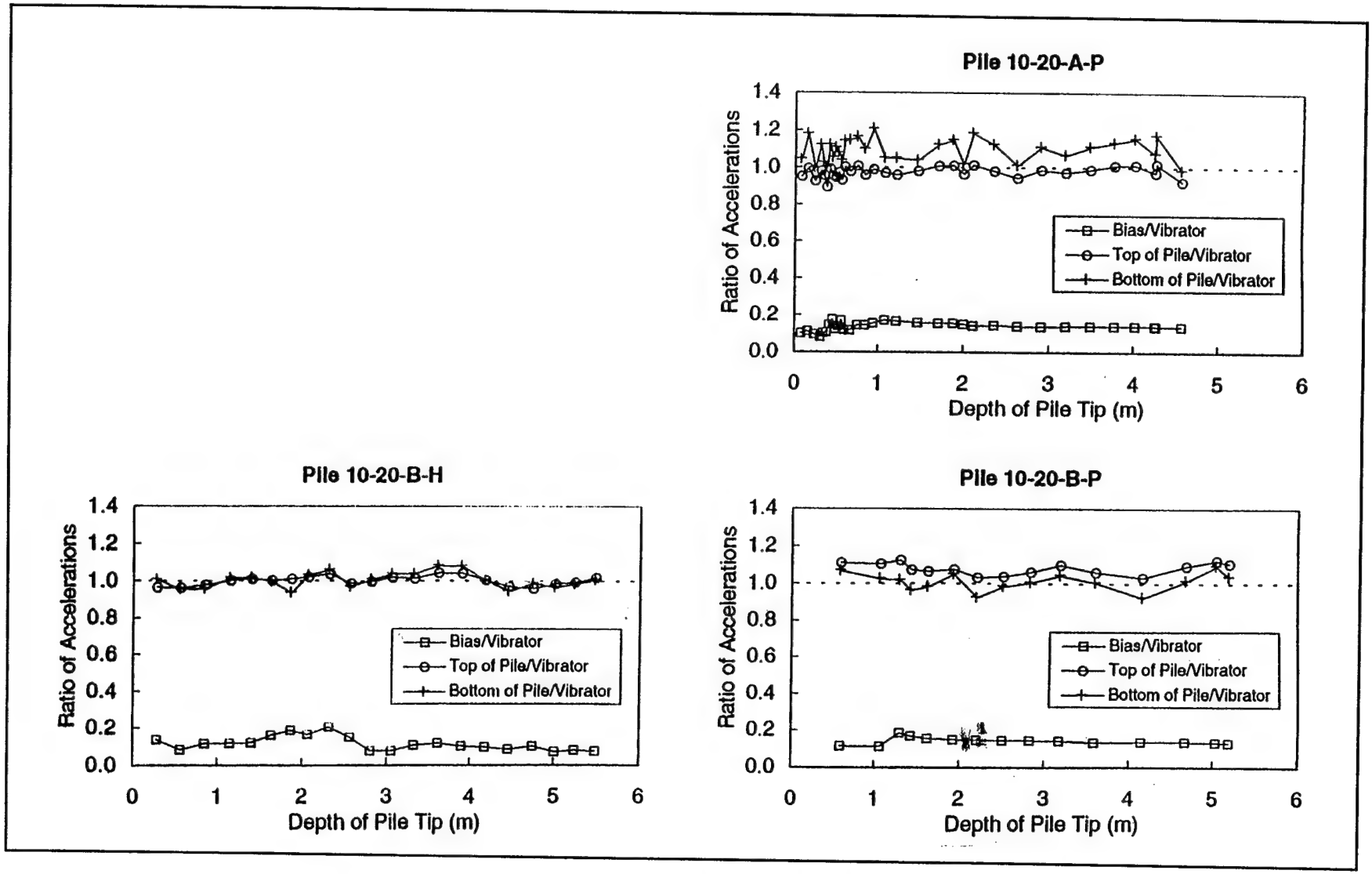

Figure E2. Amplitude of vibration as normalized acceleration for piles - 250-mm diam and 6.1-m length

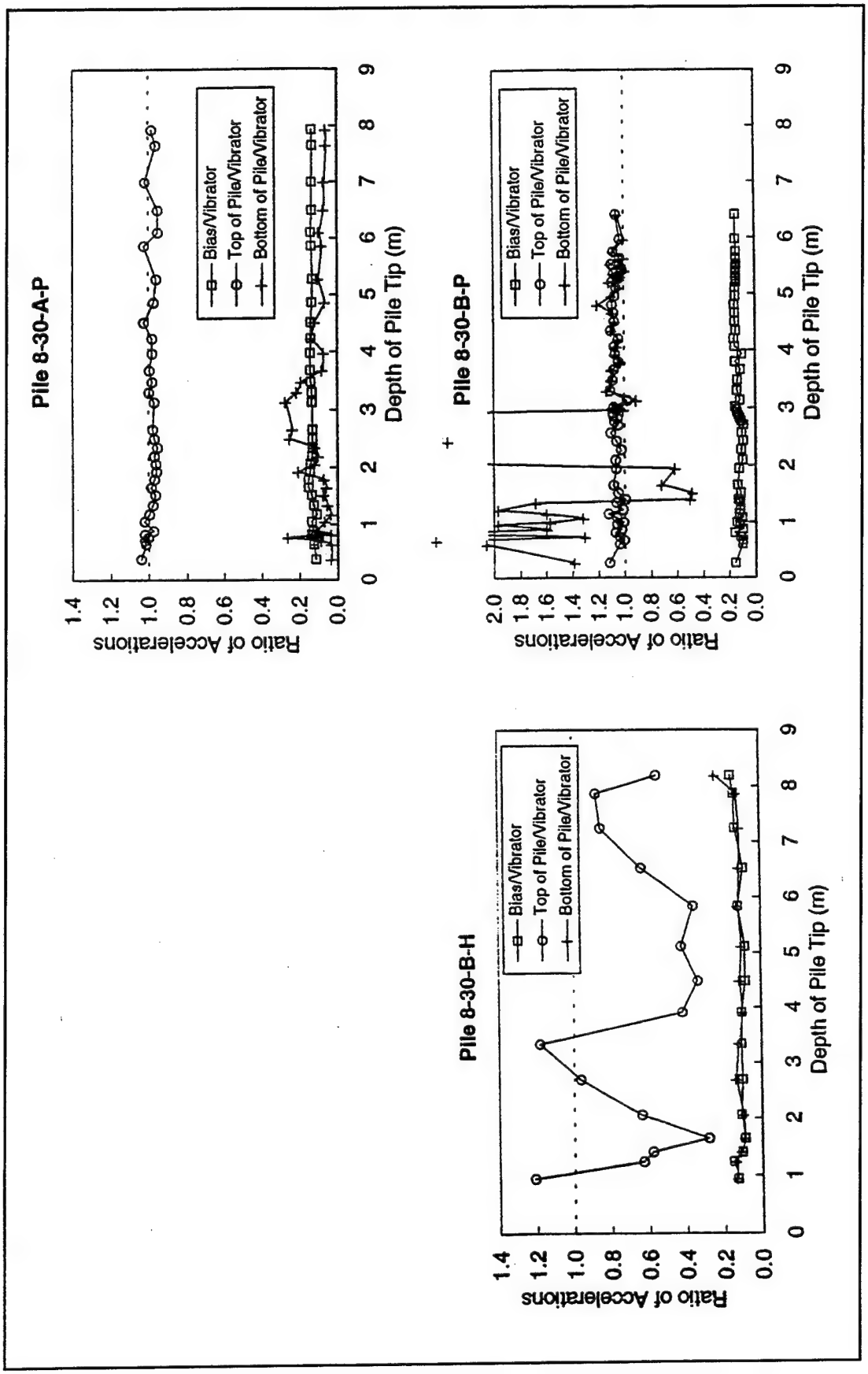

Figure E3. Amplitude of vibration as normalized acceleration for piles - 200-mm diam and 9-m length

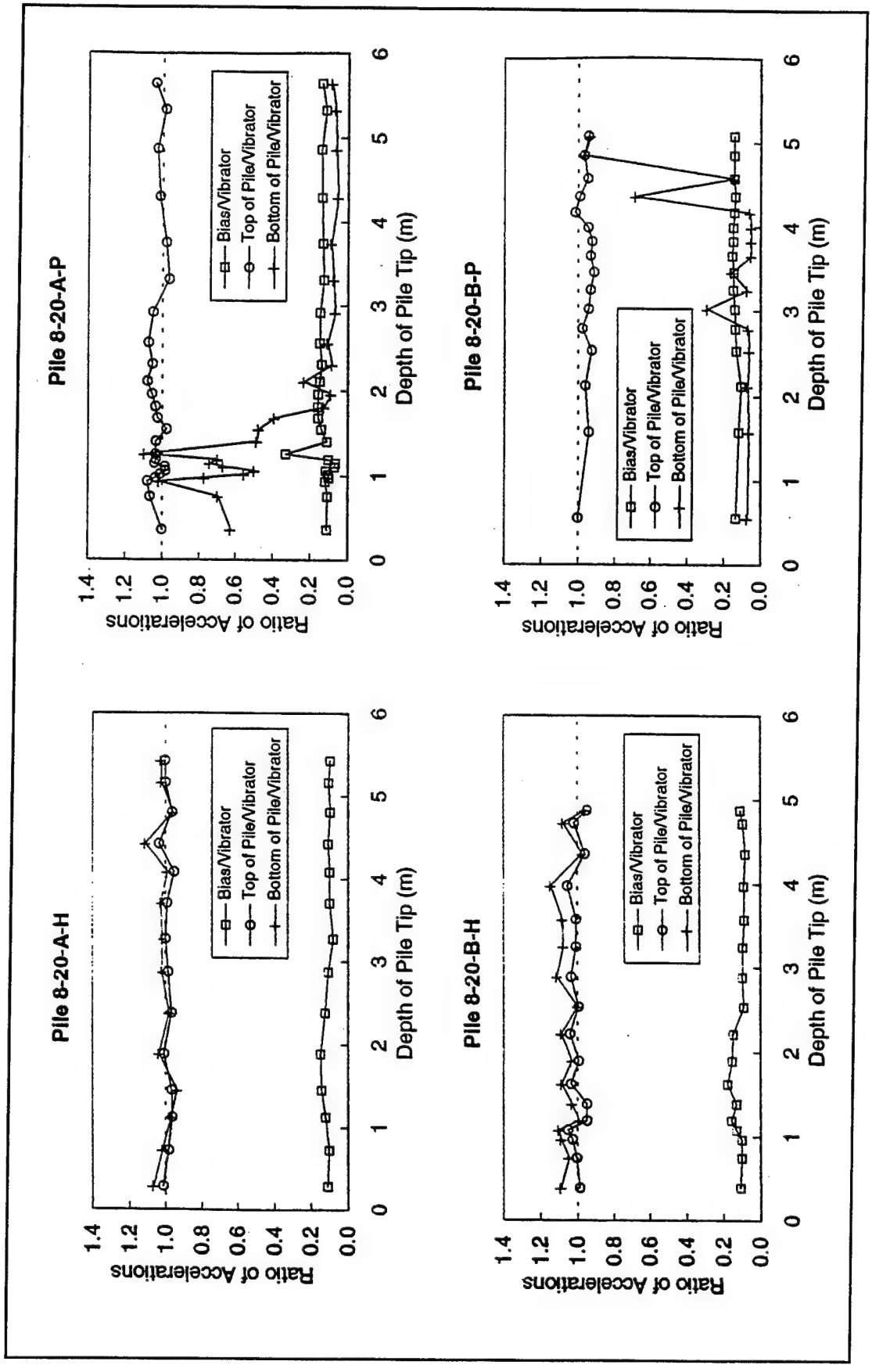

Figure E4. Amplitude of vibration as normalized acceleration for piles - 200-mm diam and 6.1-m length

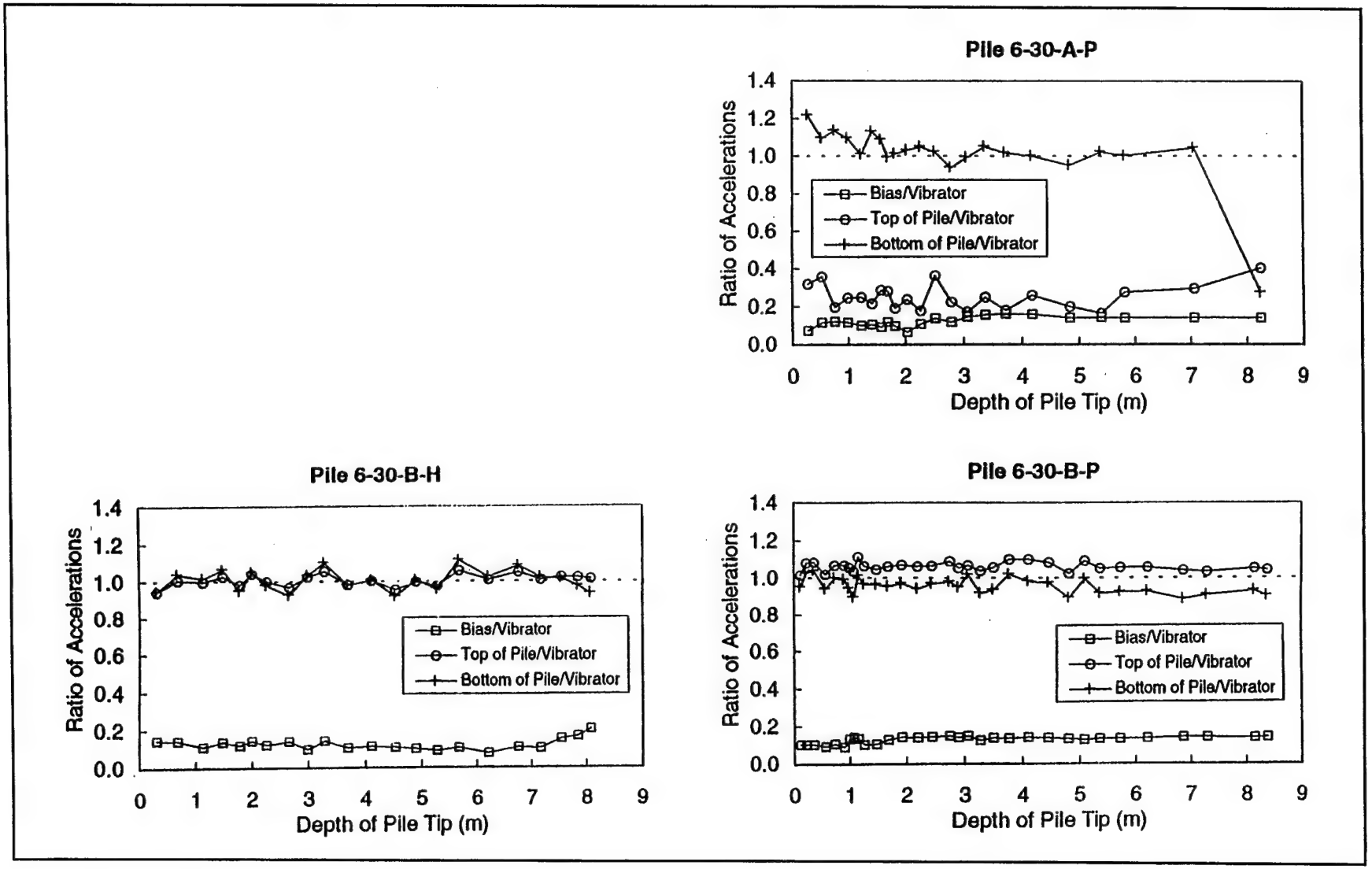

Figure E5. Amplitude of vibration as normalized acceleration for piles - 150-mm diam and 9-m length

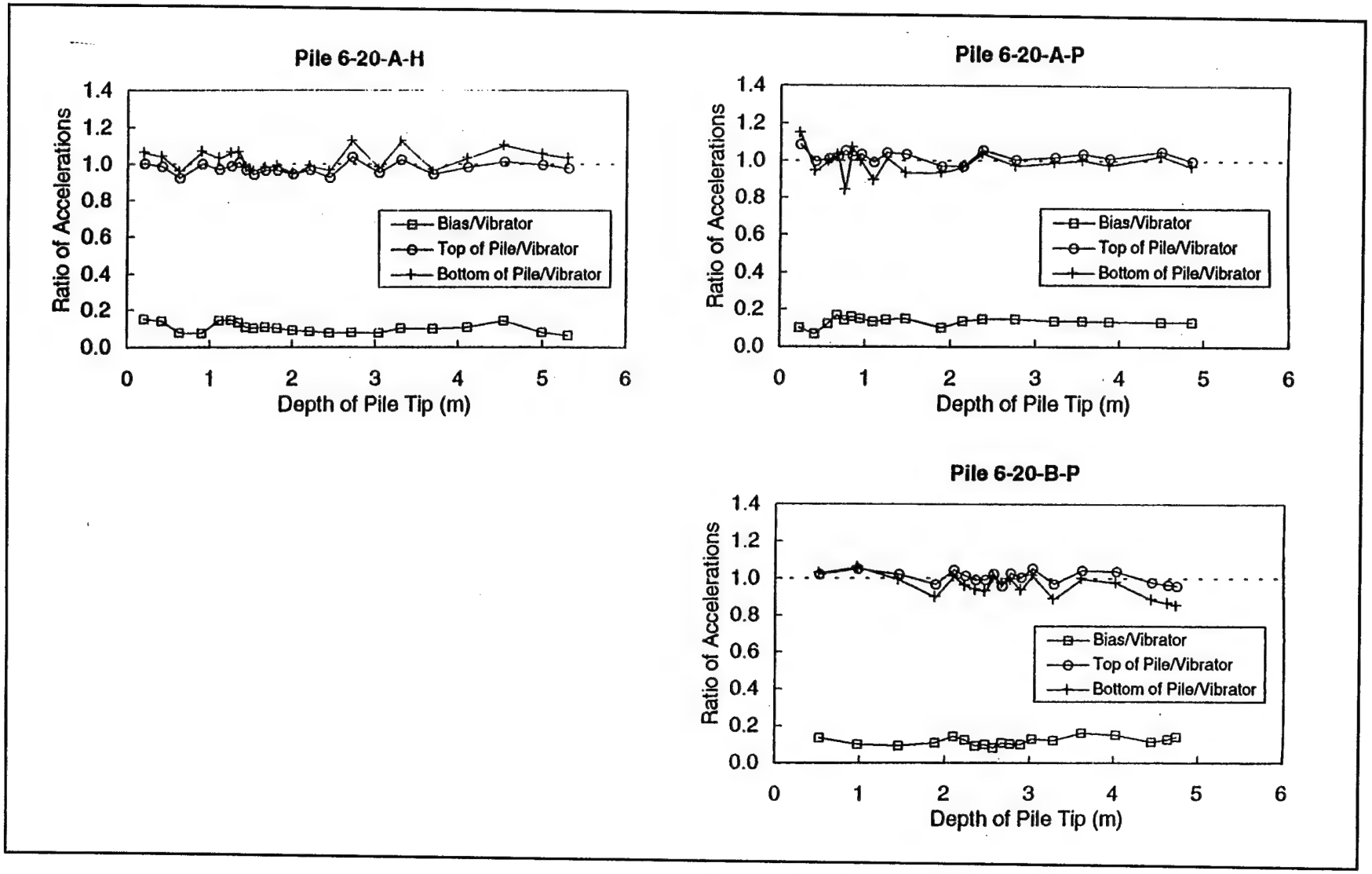

Figure E6. Amplitude of vibration as normalized acceleration for piles - 150-mm diam and 6.1-m length

Appendix F
Profiles of Dynamic Strain

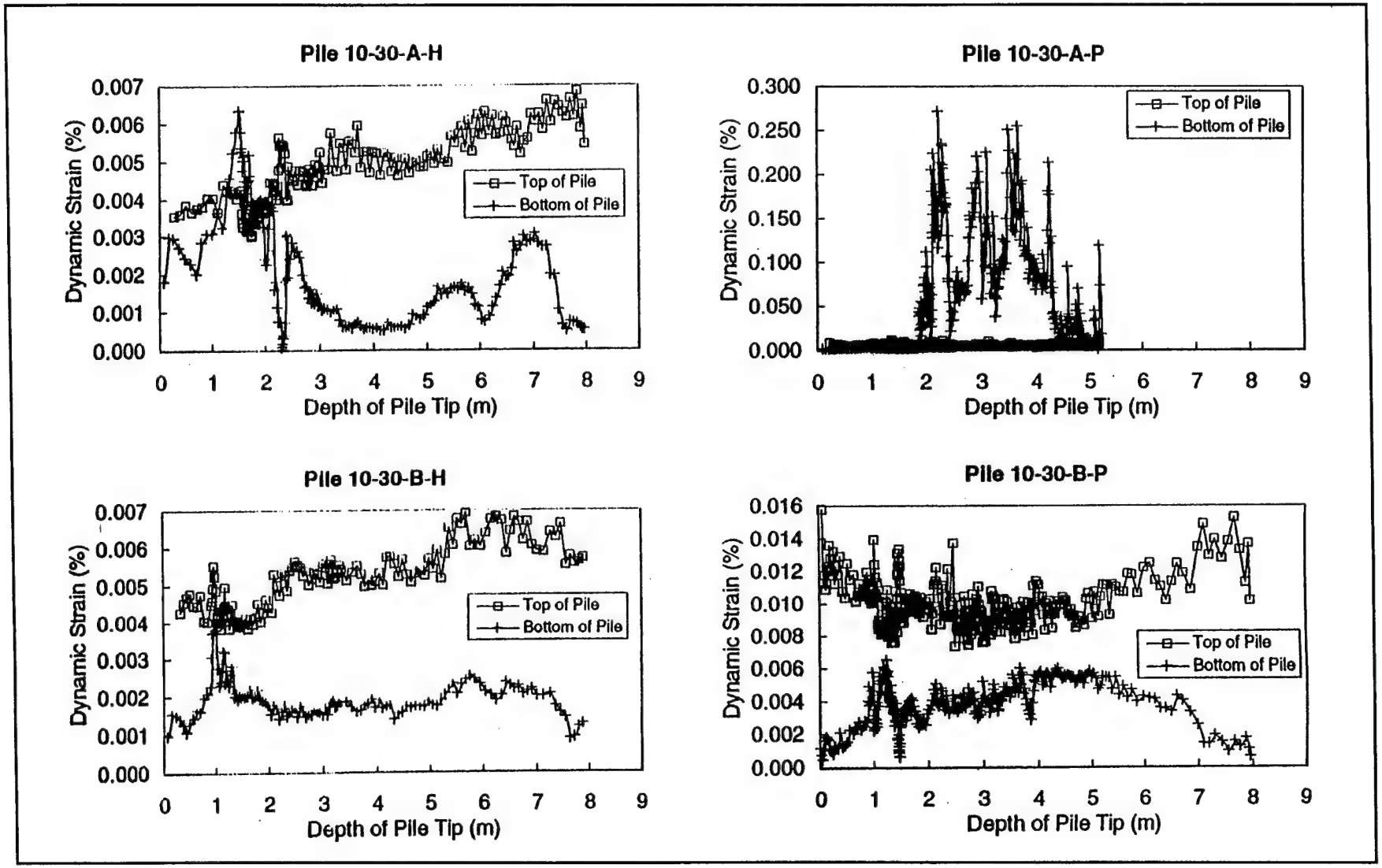

Figure F1. Dynamic strain for piles - 250-mm diam and 9-m length

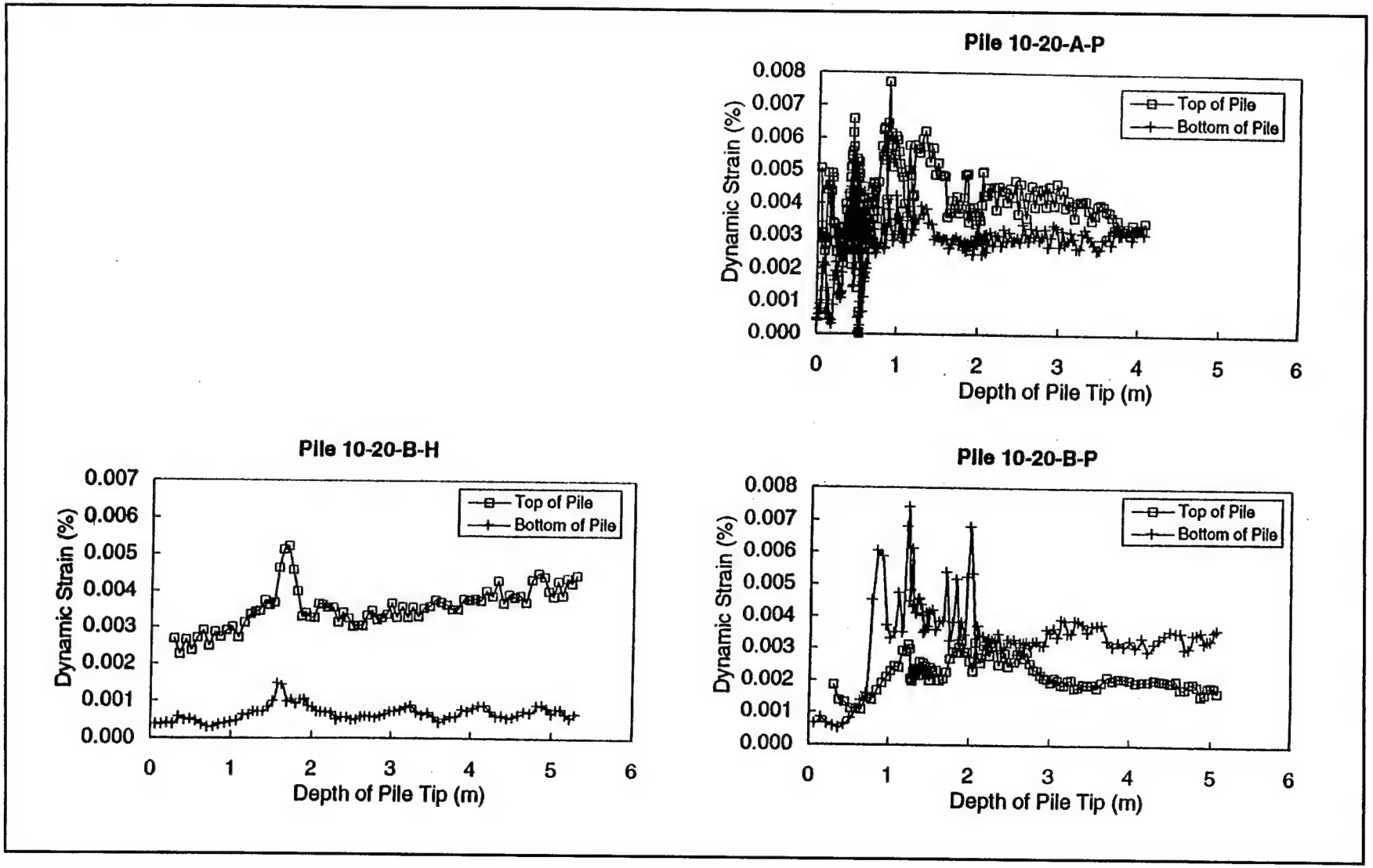

Figure F2. Dynamic strain for piles - 250-mm diam and 6.1-m length

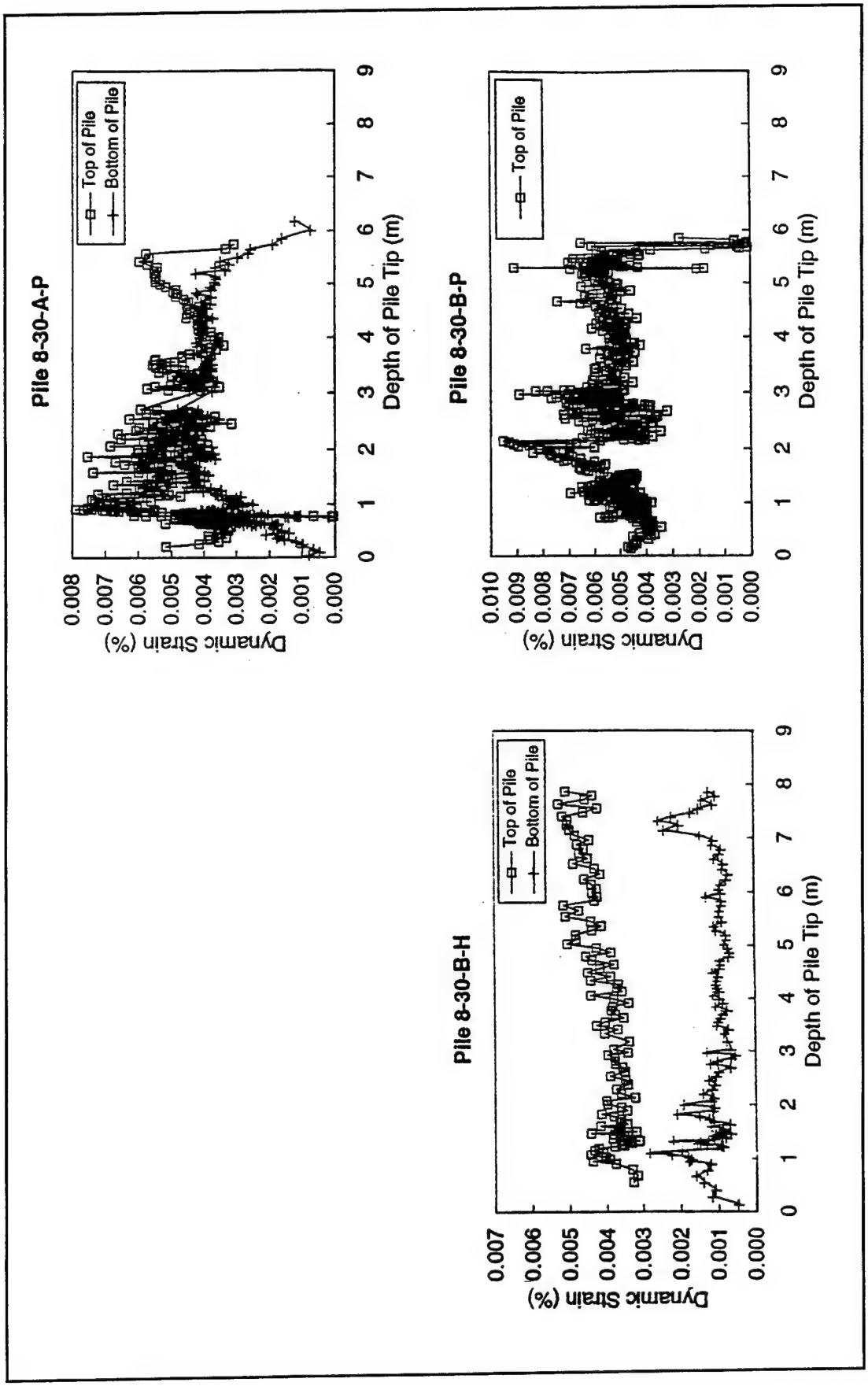

Figure F3. Dynamic strain for piles - 200-mm diam and 9-m length

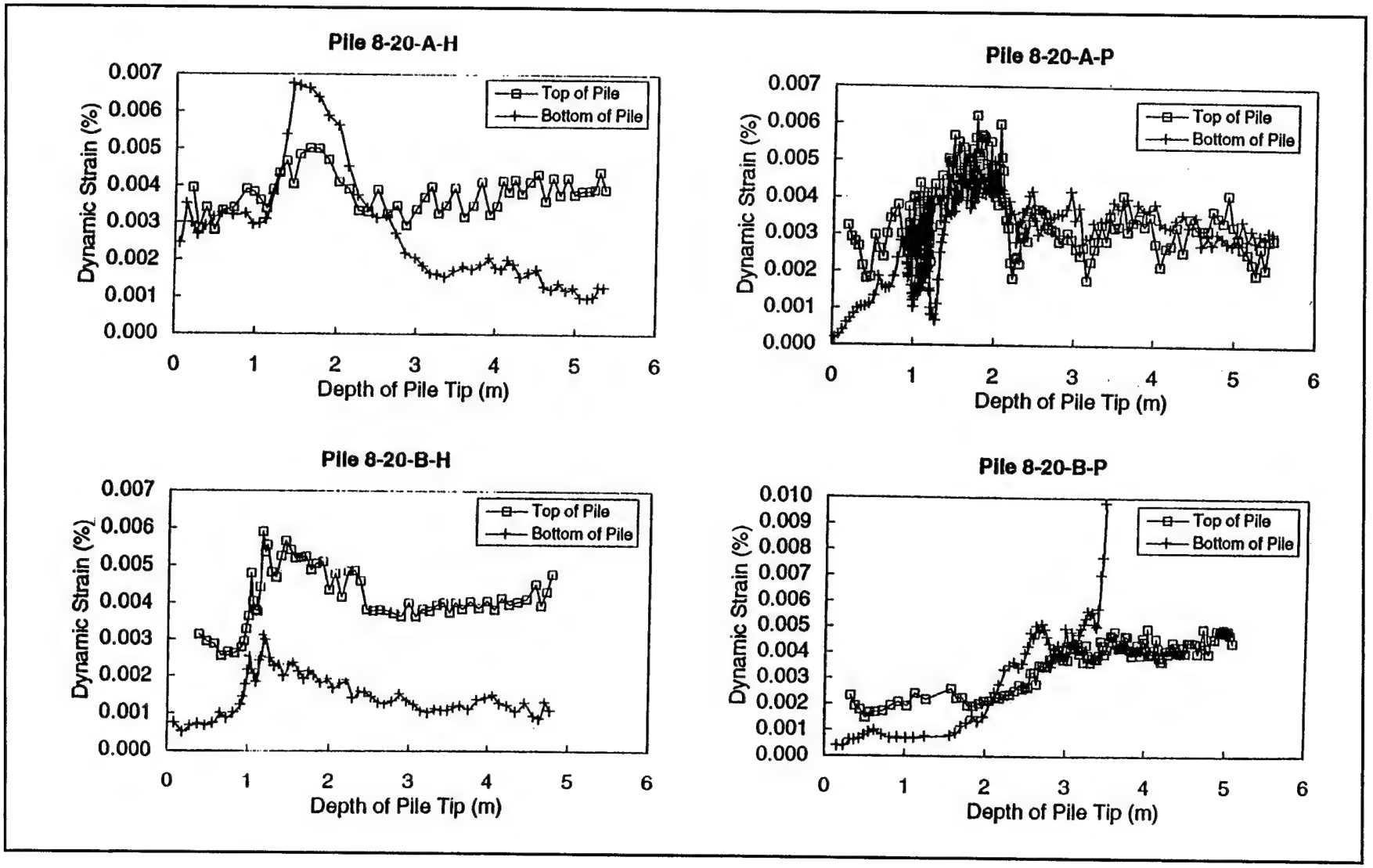

Figure F4. Dynamic strain for piles - 200-mm diam and 6.1-m length

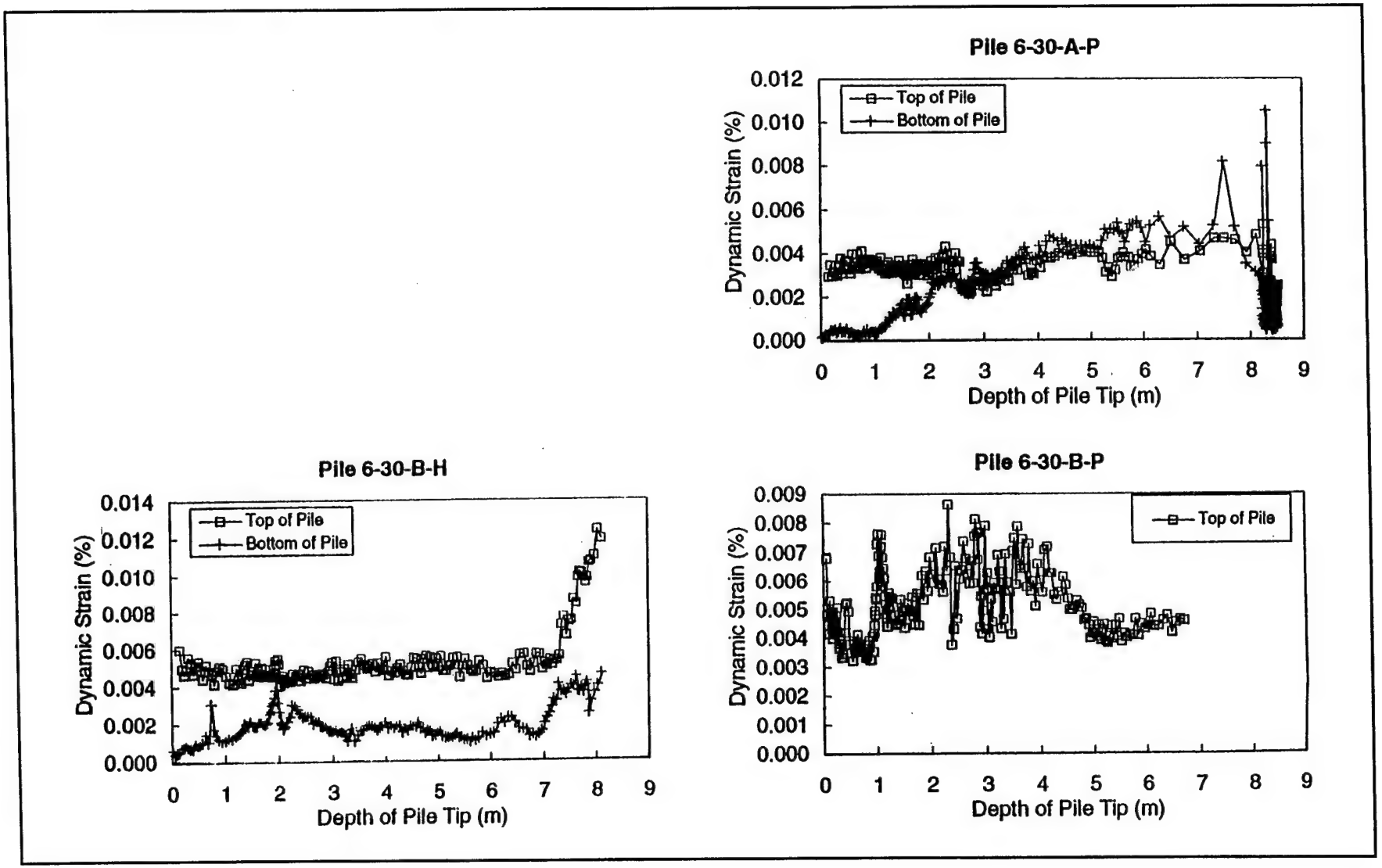

Figure F5. Dynamic strain for piles - 150-mm diam and 9-m length

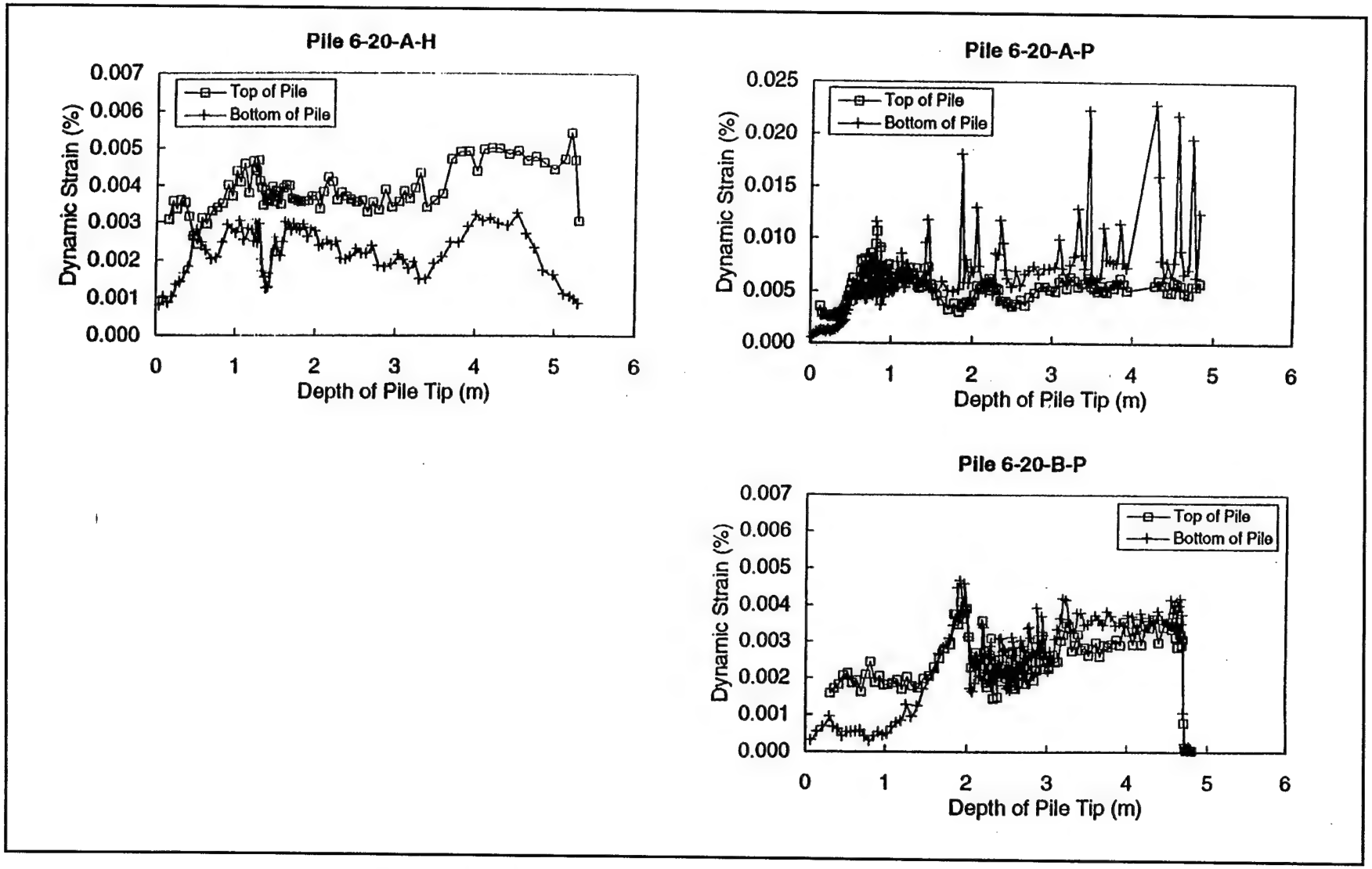

Figure F6. Dynamic strain for piles - 150-mm diam and 6.1-m length

Appendix G
Profiles of Static Strain

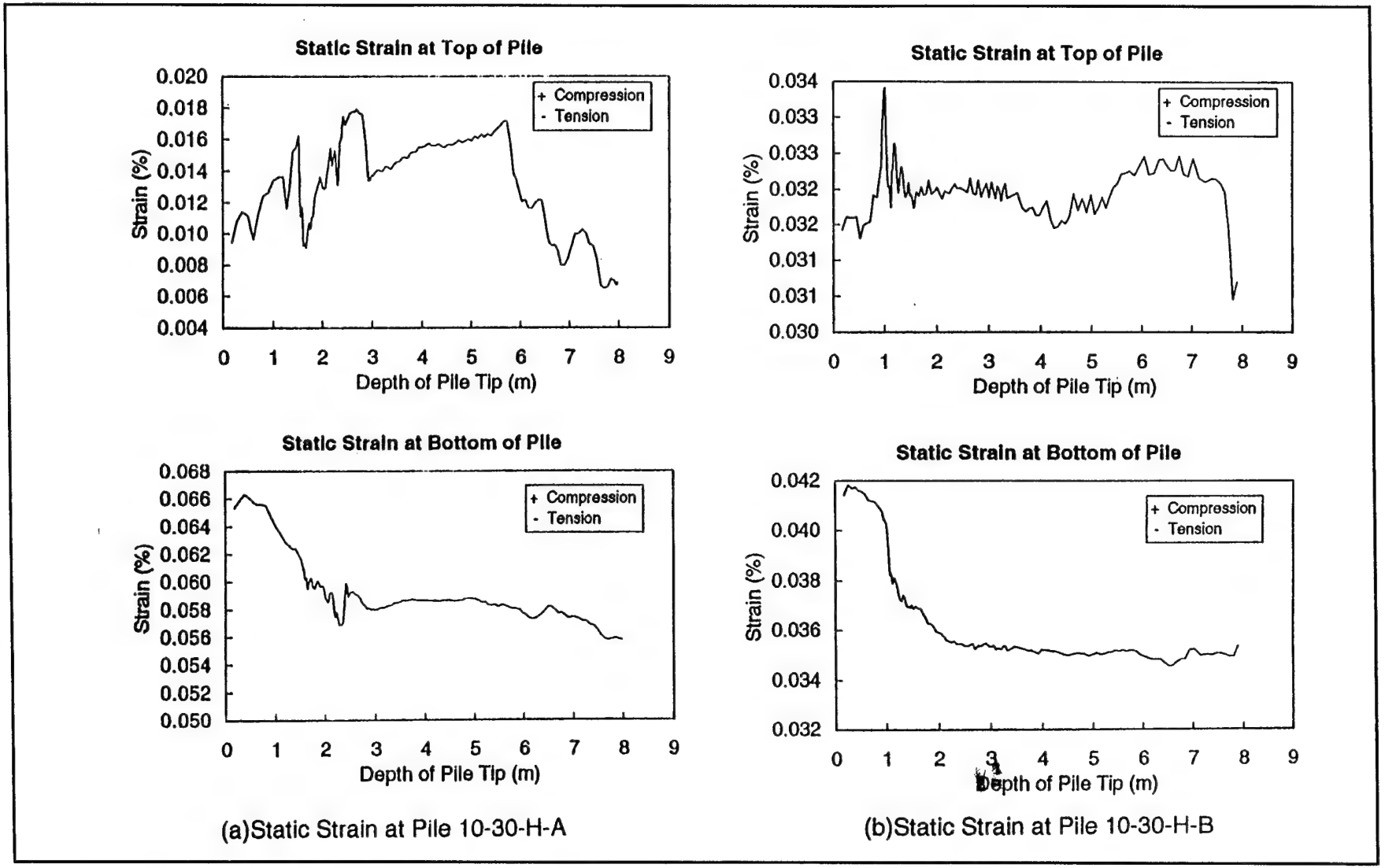

Figure G1. Static strain for H-piles - 250-mm diam and 9-m length

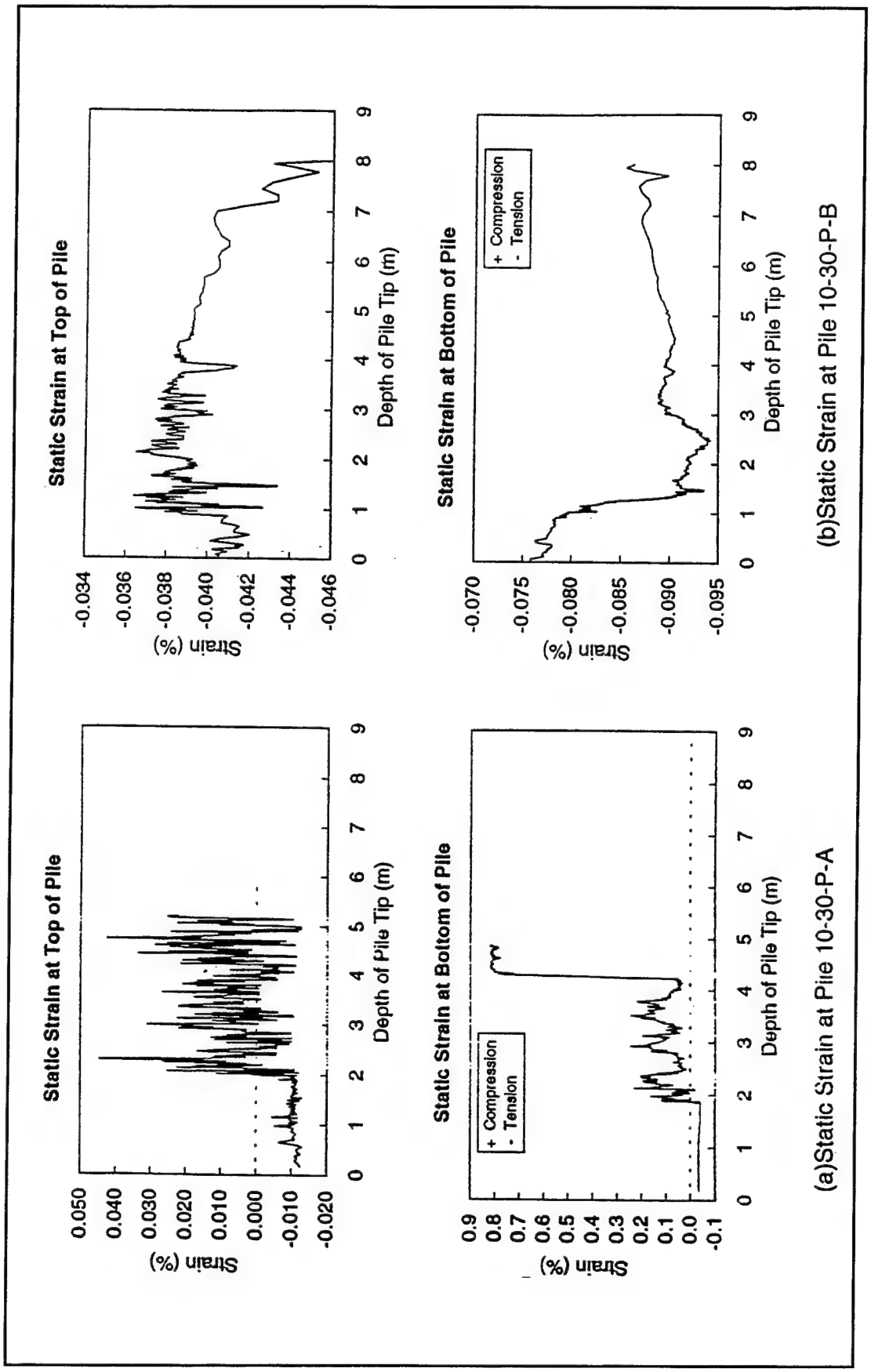

Figure G2. Static strain for pipe-piles - 250-mm diam and 9-m length

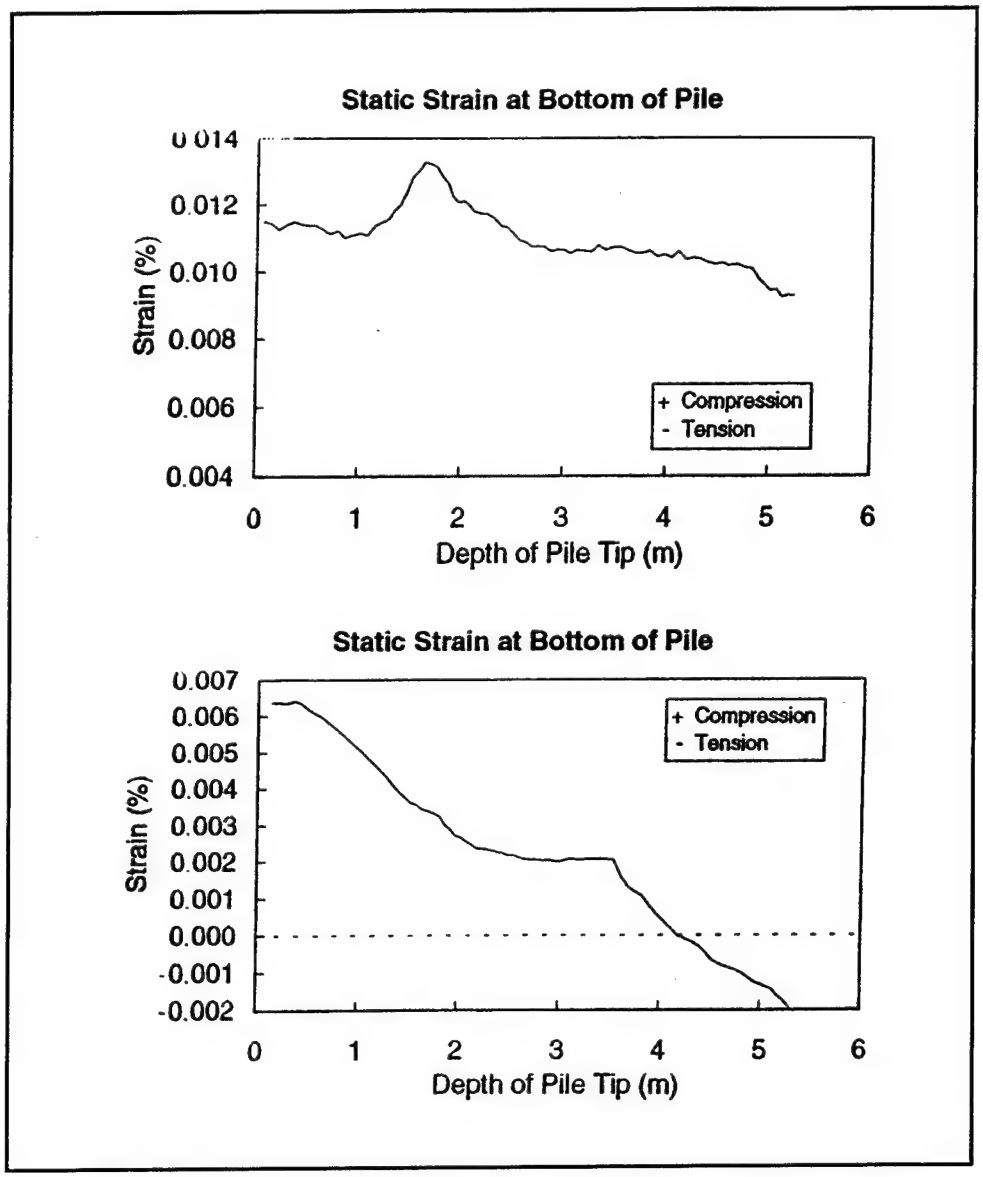

Figure G3. Static strain for H-pile - 250-mm diam and 6.1-m length (Pile 10-20-H-B)

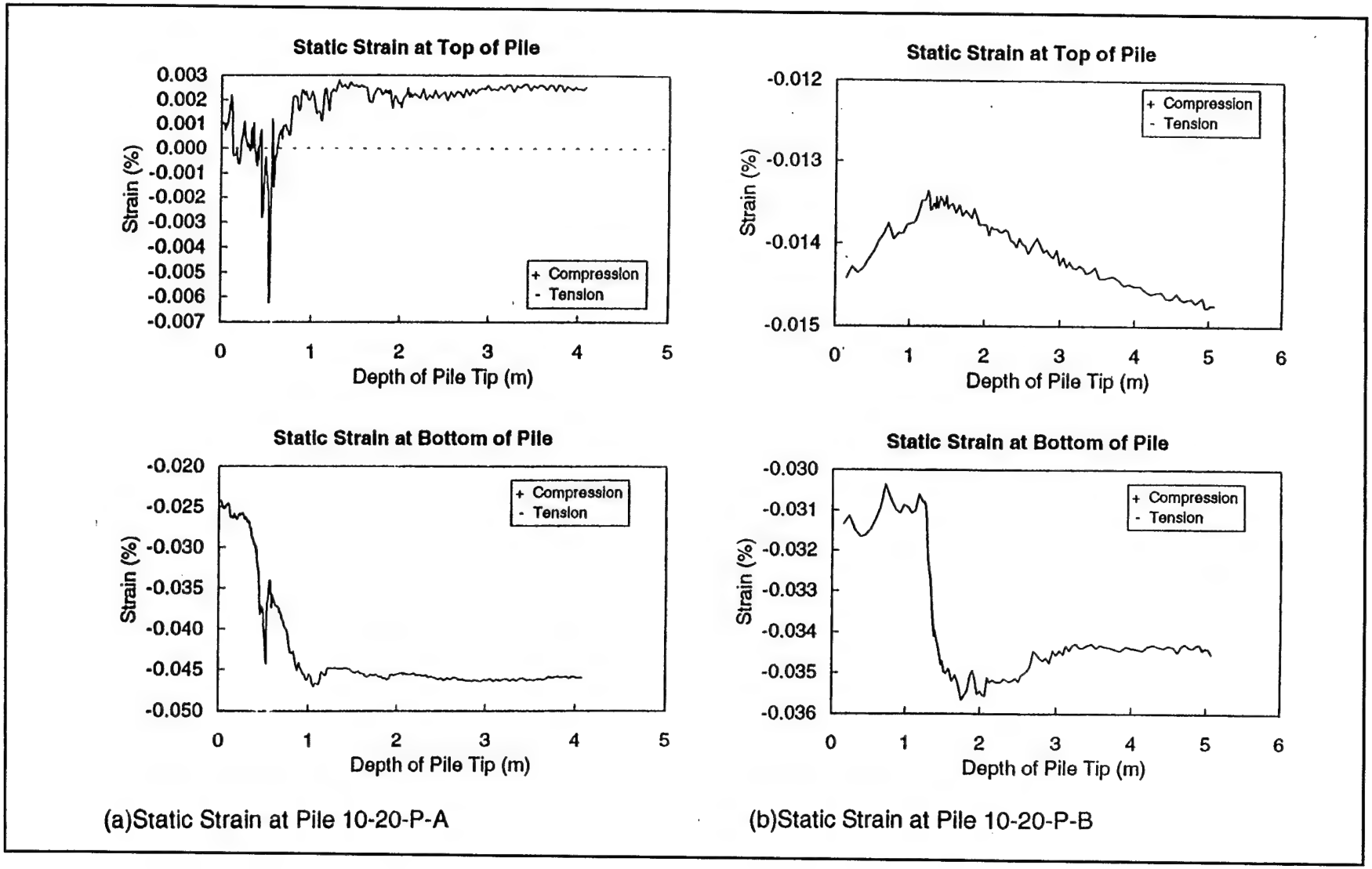

Figure G4. Static strain for pipe-piles - 250-mm diam and 6.1-m length

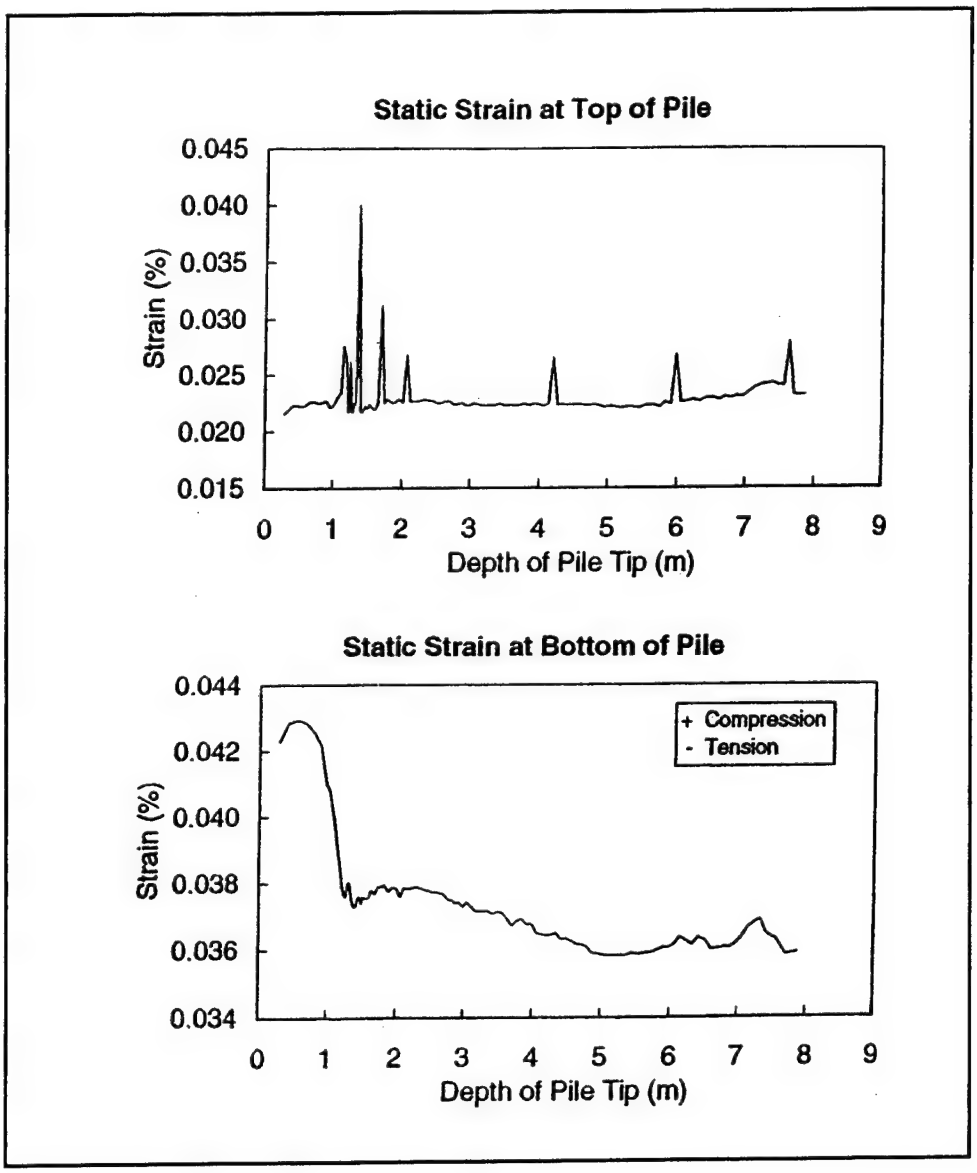

Figure G5. Static strain for H-pile - 200-mm diam and 9-m length (Pile 8-30-H-B)

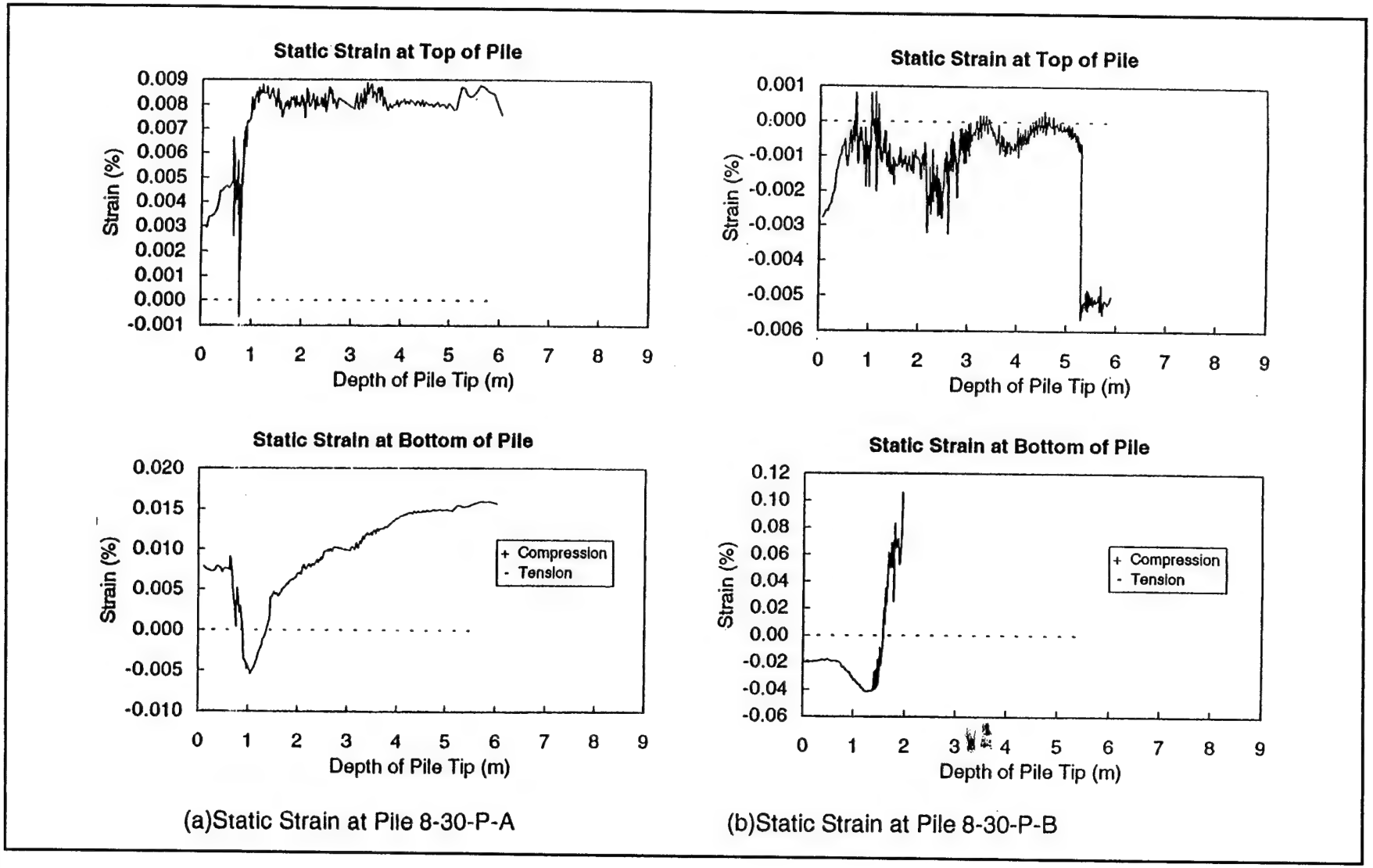

Figure G6. Static strain for pipe-piles - 200-mm diam and 9-m length

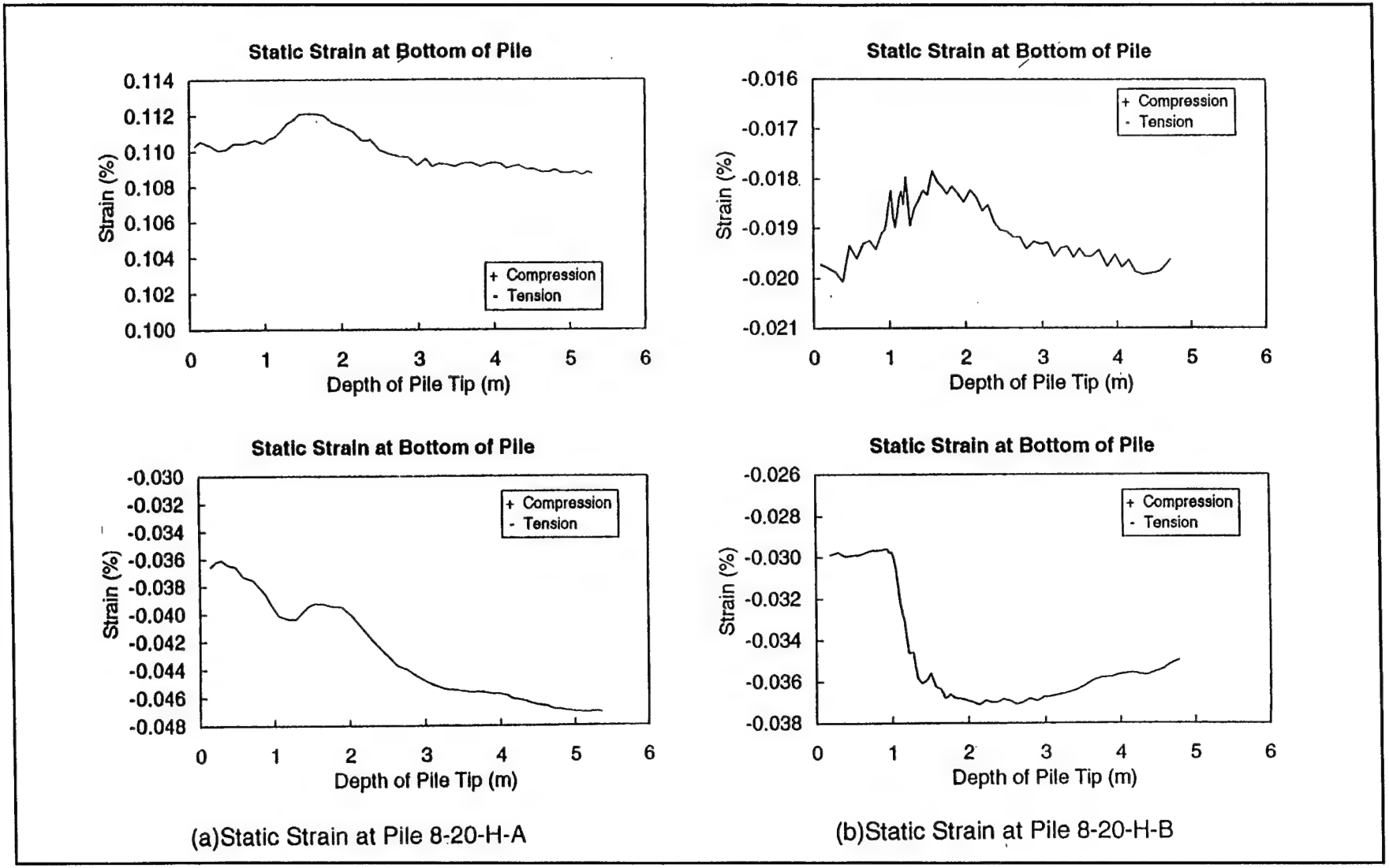

Figure G7. Static strain for H-piles - 200-mm diam and 6.1-m length

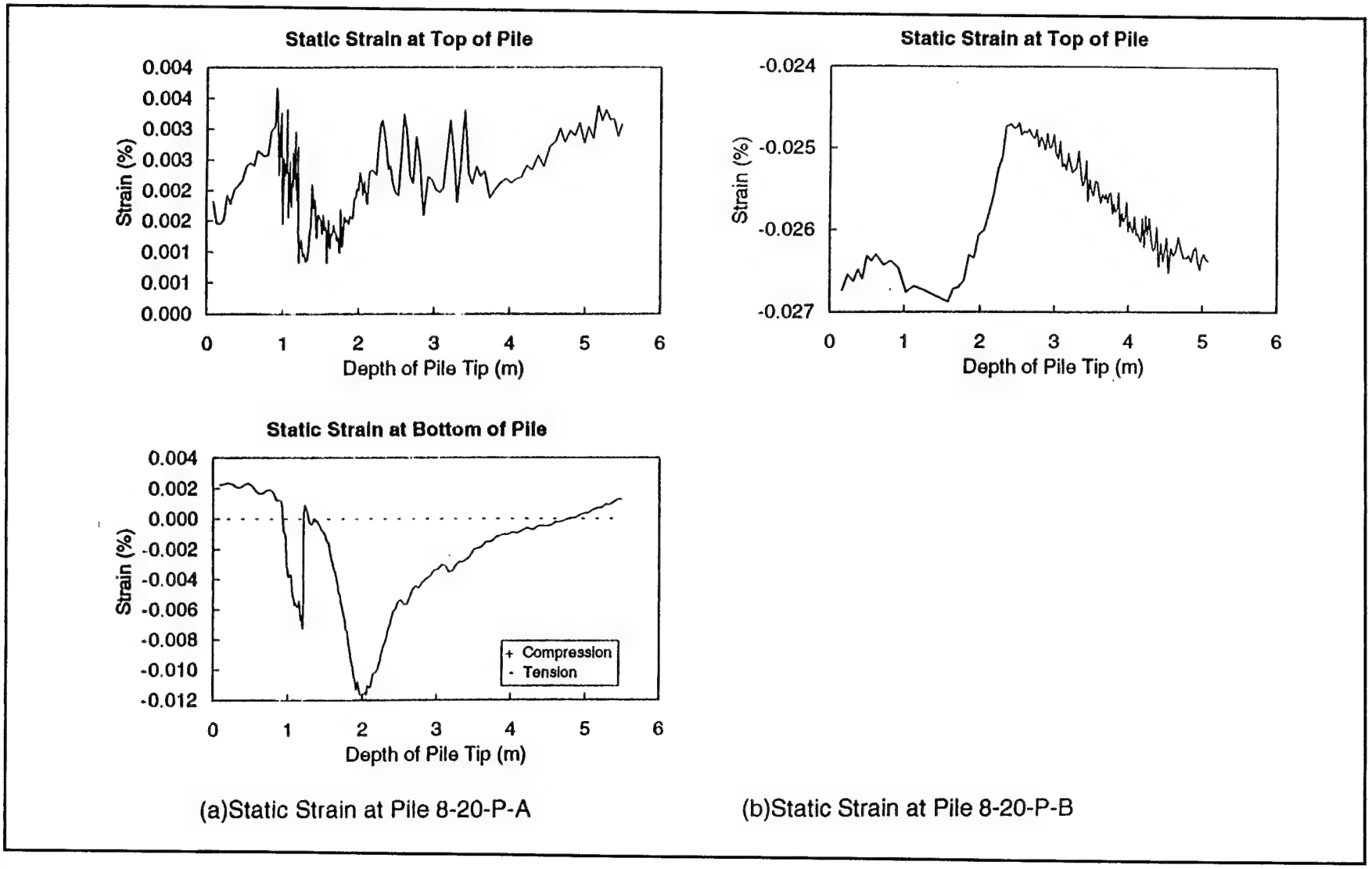

Figure G8. Static strain for pipe-piles - 200-mm diam and 6.1-m length

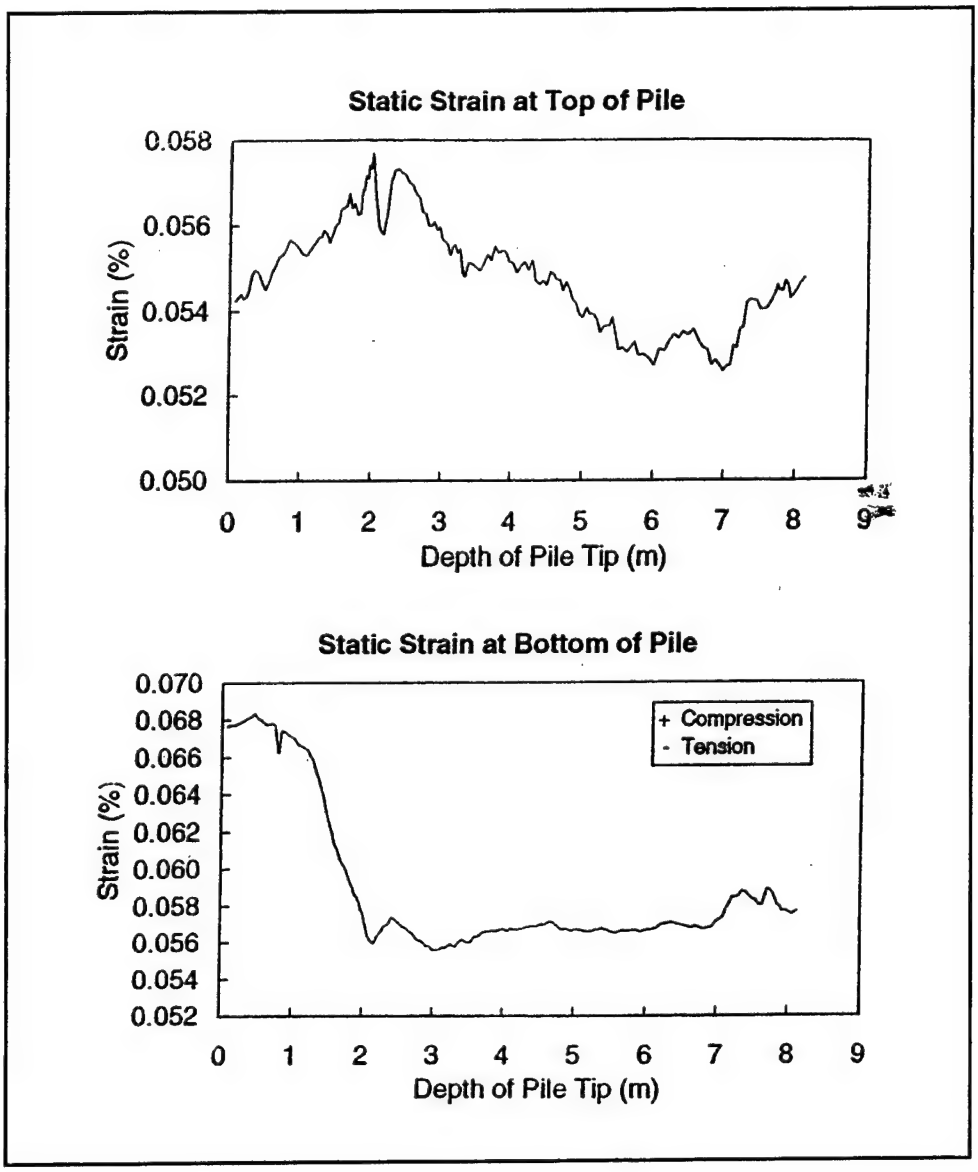

Figure G9. Static strain for H-pile - 150-mm diam and 9-m length (Pile 6-30-H-B)

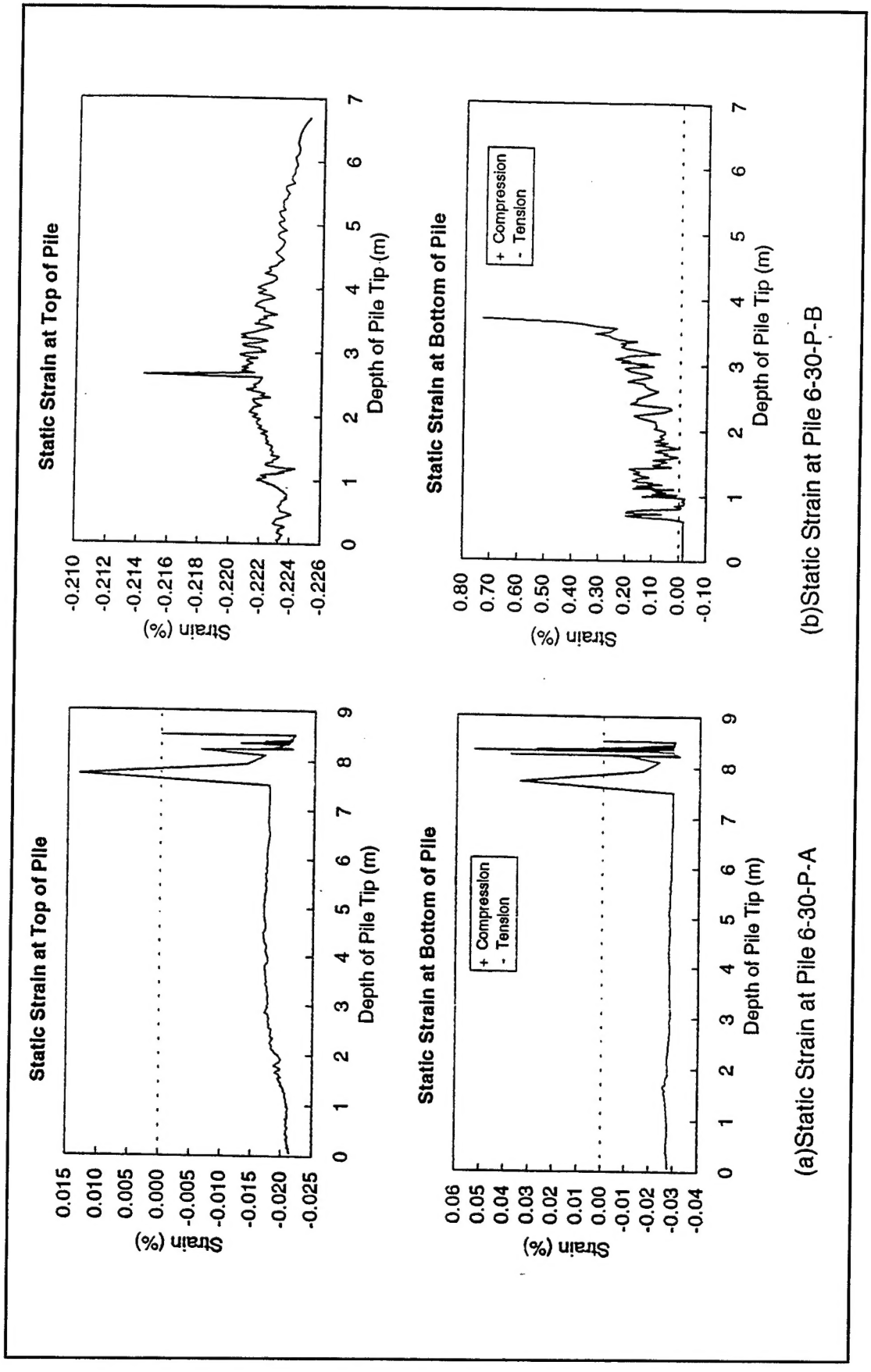

Figure G10. Static strain for pipe-piles - 150-mm diam and 9-m length

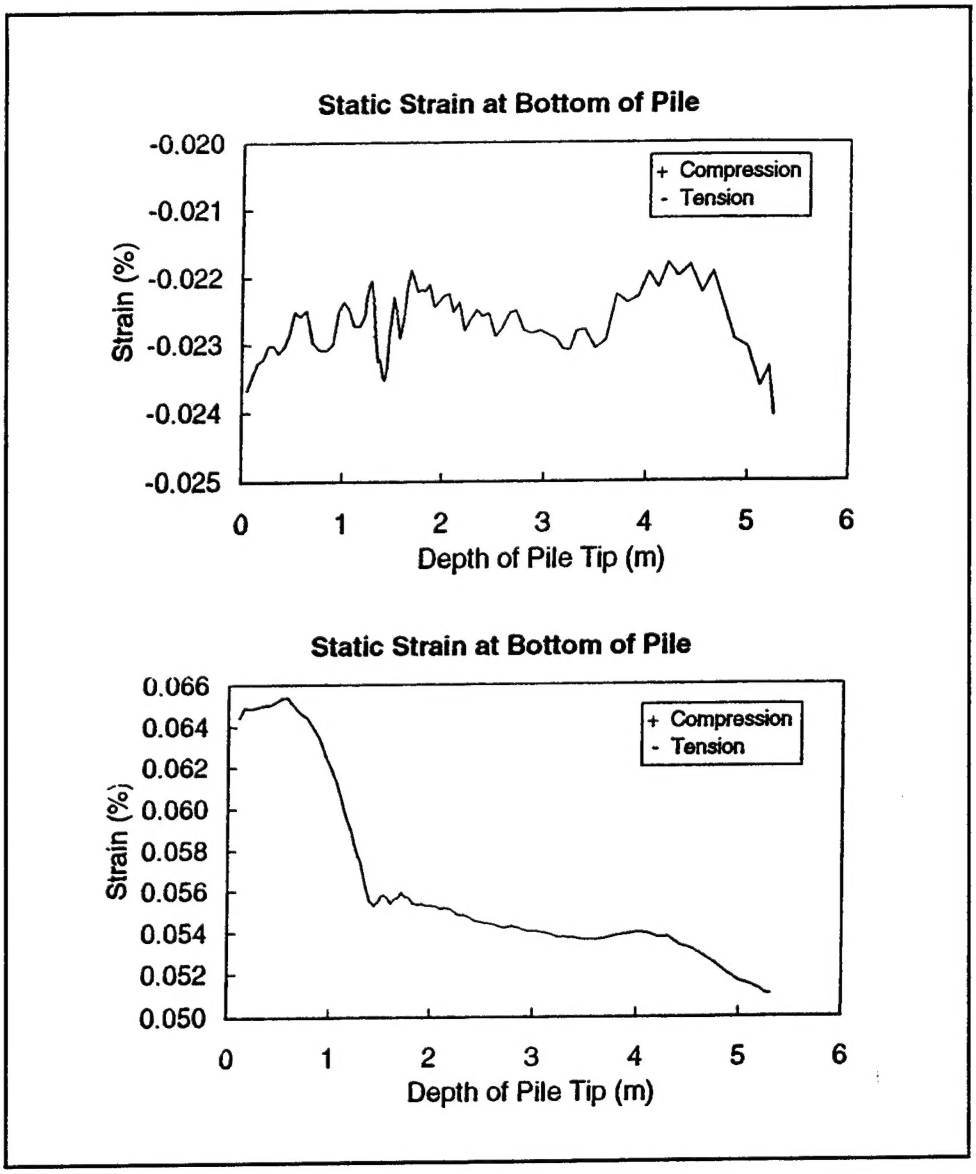

Figure G11. Static strain for H-pile - 150-mm diam and 6.1-m length (Pile 6-20-A-H)

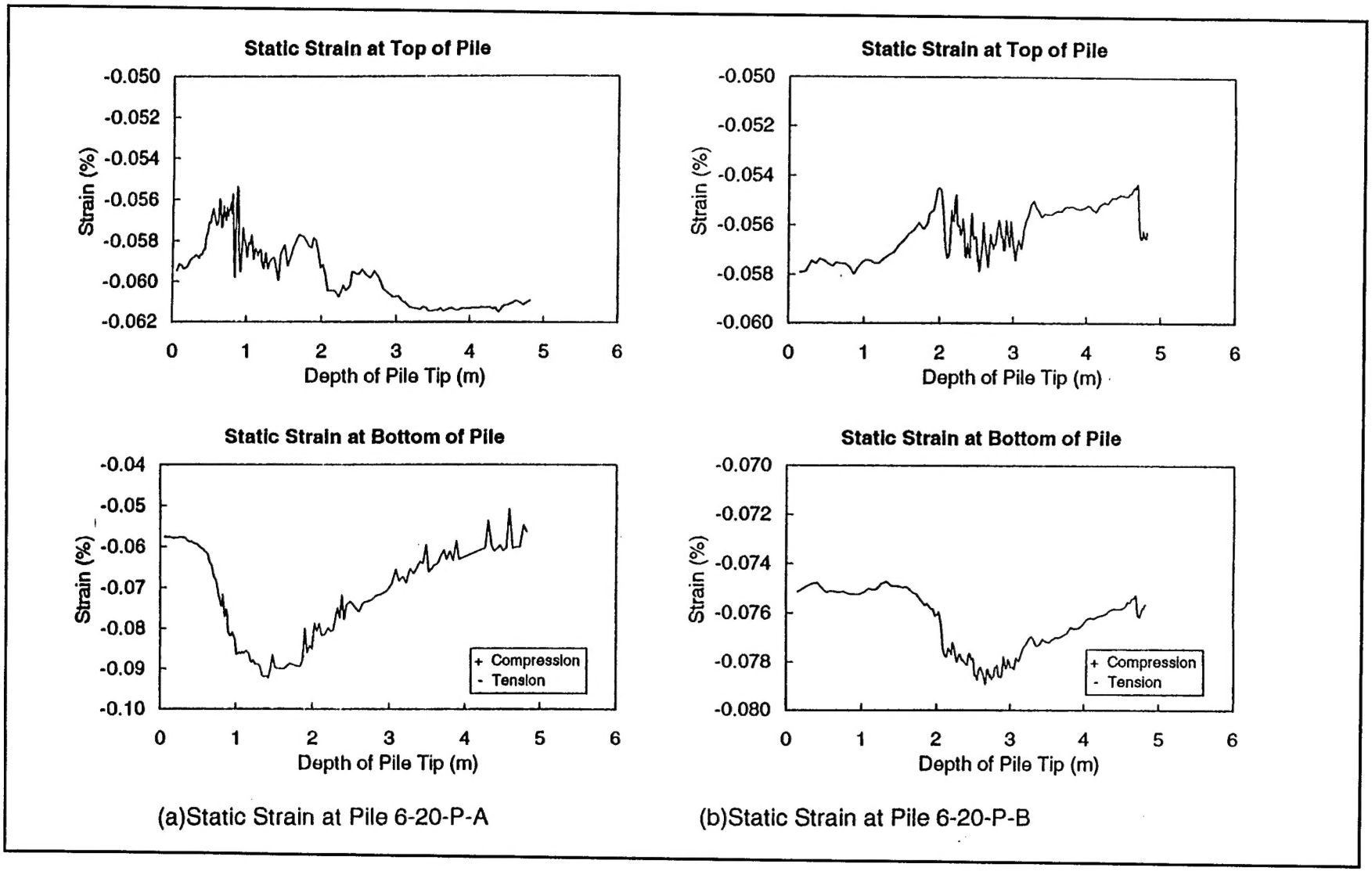

Figure G12. Static strain for pipe-piles - 150-mm diam and 6.1-m length

REPORT DOCUMENTATION PAGE

Form Approved
OMB No. 0704-0188

1. AGENCY USE ONLY *(Leave blank)*	2. REPORT DATE	3. REPORT TYPE AND DATES COVERED
	July 1998	Final report

4. TITLE AND SUBTITLE
Estimating Bearing Capacity of Piles Installed with Vibratory Drivers

5. FUNDING NUMBERS

6. AUTHOR(S)
Peter J. Bosscher, Eva Menclova, Jeffrey S. Russell, Ronald E. Wahl

7. PERFORMING ORGANIZATION NAME(S) AND ADDRESS(ES)
University of Wisconsin-Madison, Department of Civil and Environmental Engineering, Madison, WI 53714; U.S. Army Engineer Waterways Experiment Station, 3909 Halls Ferry Road, Vicksburg, MS 39180-6199

8. PERFORMING ORGANIZATION REPORT NUMBER
Technical Report
CPAR-GL-98-2

9. SPONSORING/MONITORING AGENCY NAME(S) AND ADDRESS(ES)
U.S. Army Corps of Engineers
Washington, DC 20314-1000

10. SPONSORING/MONITORING AGENCY REPORT NUMBER

11. SUPPLEMENTARY NOTES
Available from National Technical Information Service, 5285 Port Royal Road, Springfield, VA 22161.

12a. DISTRIBUTION/AVAILABILITY STATEMENT
Approved for public release; distribution is unlimited.

12b. DISTRIBUTION CODE

13. ABSTRACT ***(Maximum 200 words)***

Vibratory pile drivers are sometimes used to install sheet-pile walls, nonbearing piles, and some load-bearing structural piles. In comparison to the more commonly used impact hammers, vibratory drivers offer several advantages: (a) require less energy, (b) have higher rates of penetration of cohesionless soil, (c) produce less noise, and (d) result in less damage to the pile during driving. Presently, there are no reliable methods for estimating the bearing capacity of the pile during the driving operation. Thus, a new method for estimating the bearing capacity of structural piles installed with vibratory drivers is documented in this report. The method is based on measurements of dynamic properties of the soil-pile system during driving. The method is verified by evaluating field data collected during the driving of 24 experimental piles at the National Geotechnical Experimental Site near College Station, Texas.

14. SUBJECT TERMS
Bearing capacity
Piles
Vibratory driver
Vibratory piles

15. NUMBER OF PAGES
171

16. PRICE CODE

17. SECURITY CLASSIFICATION OF REPORT	18. SECURITY CLASSIFICATION OF THIS PAGE	19. SECURITY CLASSIFICATION OF ABSTRACT	20. LIMITATION OF ABSTRACT
UNCLASSIFIED	UNCLASSIFIED		